Terms and Conditions of Use of Digitised Theses from Trinity College Library Dublin

Copyright statement

All material supplied by Trinity College Library is protected by copyright (under the Copyright and Related Rights Act, 2000 as amended) and other relevant Intellectual Property Rights. By accessing and using a Digitised Thesis from Trinity College Library you acknowledge that all Intellectual Property Rights in any Works supplied are the sole and exclusive property of the copyright and/or other IPR holder. Specific copyright holders may not be explicitly identified. Use of materials from other sources within a thesis should not be construed as a claim over them.

A non-exclusive, non-transferable licence is hereby granted to those using or reproducing, in whole or in part, the material for valid purposes, providing the copyright owners are acknowledged using the normal conventions. Where specific permission to use material is required, this is identified and such permission must be sought from the copyright holder or agency cited.

Liability statement

By using a Digitised Thesis, I accept that Trinity College Dublin bears no legal responsibility for the accuracy, legality or comprehensiveness of materials contained within the thesis, and that Trinity College Dublin accepts no liability for indirect, consequential, or incidental, damages or losses arising from use of the thesis for whatever reason. Information located in a thesis may be subject to specific use constraints, details of which may not be explicitly described. It is the responsibility of potential and actual users to be aware of such constraints and to abide by them. By making use of material from a digitised thesis, you accept these copyright and disclaimer provisions. Where it is brought to the attention of Trinity College Library that there may be a breach of copyright or other restraint, it is the policy to withdraw or take down access to a thesis while the issue is being resolved.

Access Agreement

By using a Digitised Thesis from Trinity College Library you are bound by the following Terms & Conditions. Please read them carefully.

I have read and I understand the following statement: All material supplied via a Digitised Thesis from Trinity College Library is protected by copyright and other intellectual property rights, and duplication or sale of all or part of any of a thesis is not permitted, except that material may be duplicated by you for your research use or for educational purposes in electronic or print form providing the copyright owners are acknowledged using the normal conventions. You must obtain permission for any other use. Electronic or print copies may not be offered, whether for sale or otherwise to anyone. This copy has been supplied on the understanding that it is copyright material and that no quotation from the thesis may be published without proper acknowledgement.

Functionalised POSS for Materials Science Applications

By

Matthew Bent

A thesis submitted to the

University of Dublin

for the degree of

Doctor of Philosophy

October 2005

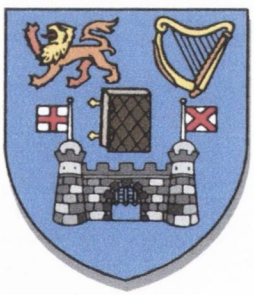

Department of Chemistry

Dublin University

Trinity College Dublin

I, the undersigned, declare that this thesis is entirely my own work, except where otherwise accredited, and it has not been submitted for a degree in any other university or institution, and furthermore, I agree that the library may lend or copy this thesis upon request.

Signed

Matthew Bent.

Summary

The main aim of this work is to develop chemistry of POSS and related materials, which might have potential applications in nanotechnology.

Chapter 1 of the thesis provides a general introduction into the area of POSS and related materials. Chapter 2 is dedicated to synthesis of different functionalised POSS.

Halogen-, amino-, allyl- and new cyclopentadienyl- functionalised POSS have been prepared in high yield by hydrolysis of appropriate $RSiCl_3$ or $RSiOEt_3$ and characterized by characterised IR mass and NMR spectroscopy.

In the chapter 3 various reactions of halogen-, amino-, allyl- and cyclopentadienyl- functionalised POSS have been studied. This include reactions of T_8Cl POSS with *t*-BuLi, $LiN[(Si(CH_3)_3)_2]$ and lithiated ferrocene, which resulted in tetra *t*-Bu- $N[(Si(CH_3)_3)_2]$ - and ferrocenyl- substituted POSS derivatives respectively. The reactions with NaI (trashalogenation) and lithiated fullerene resulted only in disubstituted species. The complete substitution of all 8 functional groups is impossible for two main reasons: sterical hinderance and limited solubility of the substituted species. C_{60} –siloxane composite demonstrated a third order non-linear optical response. Preparation and investigation of new polymeric POSS has also been explored. The Cp-functionalised POSS have been used to prepare new cross-linked 3D polymeric materials via Diels-Alder reaction.

In chapter 4 different trialkoxysilane derivatives such as (chloropropyl) triethoxysilane, (aminopropyl)triethoxysilane, allyltriethoxysilane have been used to functionalise TiO_2 nanorods. Sedimentation studies of functionalised TiO_2 nanorods have demonstrated that they have an increased solubility in organic solvents and have been used as additives for polystyrene reinforcement. Mechanical properties of the polymer composite films have been investigated by using a Zwick-100 tensile tester. The 1 % addition of functionalized TiO_2 nanorods resulted in very significant increase in tensile strength and toughness. However the concentrations of greater than one volume percent of functionalized TiO_2 nanorods would not show such good degree of reinforcement.

In the chapter 5 preparation and effective purification techniques for multiwalled (MWNTs) nanotubes have been developed. Organometallic approaches using BuLi and appropriate trichlorosilanes have also been applied to functionalise MWNTs with allyl, propyl-, hexyl- and dodecyl functionalities. The new nanocomposites have been characterised by various instrumental techniques such as: transmission electron microscopy (TEM), thermal gravimetric analysis (TGA), elemental analysis, Raman and FTIR spectroscopy. Sedimentation studies of functionalised carbon nanotubes in organic solvents have been performed to evaluate their solubility in the pure solvent as well as in the polymer solution in the solvent. Finally new polystyrene composite materials have been prepared using chemically modified multiwalled carbon nanotubes as additives. Again new polymer- carbon nanotube composites demonstrated a very significant increase in Young's Modulus, tensile strength and toughness. It was found that mechanical properties are increasing with an increase of the chain length of the alkyl functionality.

Chapter 6 contains the experimental details of the procedures and techniques described in this thesis. Finally, chapter 7 presents conclusions and the future outlook for the research performed in this project.

We believe this thesis should present an interest for materials chemistry and nanoscience.

Acknowledgements

I would like to thank the following people who have helped me complete this thesis:

Clare for her perseverance, patience and understanding, and all the endless cups of tea and sandwiches thrust under my nose; also my family for their continued encouragement and belief in me, especially my mother and my brother, Anthony.

Cassidy Knowlton and Norah Casey, who helped with the typing; Neil Leady and David John in the microscopy lab; members of the technical staff, Tom, Peggy, Brendan, Martin, Patsy, Seamus and Mark; Fred, Ed and John for all the chemical supplies and glassware; all the guys from Physics who helped with the sedimentation studies, especially Dennis, Jimmy and Kevin; John O'Brien for all the NMRs; Manuel for the GPC and countless other things too numerous to mention; all the people, past and present, who worked with me in the labs, especially Serena, Roisin, Rowen, Ian, Pierre, and Stephen. I would also like to thank the rest of the staff of the Chemistry Department, especially Corinne, Helen and Tess for all their help in the office.

Special thanks go to Professor John Kelly for all his assistance to me when I was an undergraduate, and to Professor Brian McMurray for his kindness, good humour and his exciting and informative lectures.
I would also like to thank Professor Blau and Dr. Coleman for the access to and use of the facilities in the Physics department.

Finally, of course, I wish to express my profound thanks to my supervisor and mentor throughout this project, Dr Yuri Goun'ko, for all his guidance, patience and encouragement.

Abbreviations

AFM	Atomic Force Microscopy
BTMA	40% benzyltrimethylammonium hydroxide solution
BuLi	Butyllithium
Cp	Cyclopentadiene.
CpH	Cyclopentadiene anion.
CpNa	Cp sodium. "Sodium sand".
DMA	Dynamic Mechanical Analysis
DSC	Differential Scanning Calorimetry
EtOH	Ethanol
ES MS	Electro-Spray Mass Spectroscopy
FC-POSS	Completely condensed POSS
F-MWNT	Functionalised MWNTs
F - titania	Functionalised Titania
IC-POSS	Incompletely condensed POSS
MWNTs	Multi walled nanotubes
POSS	Polyhedral oligosilsesquioxanes.
PS	Polystyrene
SWNT's	Single wall nanotubes
SEM	Scanning Electron Microscopy
T_8Cl	Octachloropropylsilsesquioxane
T_8NH_2	Octa-aminopropylsilsesquioxane
T_8(Allyl)	Octa(allyl)propylsilsesquioxane
T_8(SH)	Octa(3-mercaptopropyl)sislesquioxan
TGA	Thermal gravimetric analysis
TEM	Transmission Electron Microscopy
Titania	Titanium dioxide (TiO_2)

Contents

CHAPTER 1. General Introduction.

CHAPTER 3. Selected reactions of functionalised POSS

CHAPTER 4. Titania /Siloxane Composites

Accreditations

All illustrations, diagrams, reaction schemes and images done by the author except in the following cases:

1) Figure 1.18 (a) and Figure 1.19 were both taken from "the nanotubes site". http://www.pa.msu.edu/cmp/csc/nanotube.html

2) Figure 4.1 taken from the "Cosmo Chemical Co.Ltd" website . http://www.titanium.co.kr/tio2/class.asp

Chapter 1

Introduction

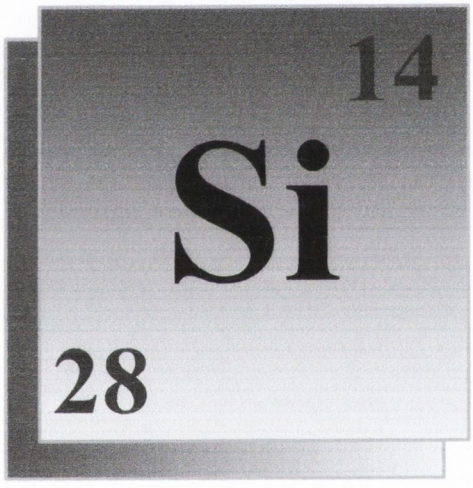

Chapter 1 Introduction

1.1 Silica

Silicon was first discovered by Jöns Jacob Berzelius (Sweden) in 1824. The origin of the name comes from the Latin word *silicis* meaning flint. It is not usually found in its elemental form but occurs mainly as oxides and silicates. Oxygen in turn was discovered by Joseph Priestly (England) in 1774. The origin of the name comes from the Greek words *oxy genes* meaning *acid* and *forming* (acid former). It is a colourless, odourless gas. It is an extremely reactive element, which forms oxides with nearly all other elements except the noble gases. It is the most abundant element in the earth's crust and makes up almost 21% of the atmosphere.

When both of these are combined we get the natural ratio of SiO_2 (Silicon dioxide), the most common form of which is silica. Silica is normally defined as a three-dimensional network of silicon dioxide, most commonly encountered as sand, and chiefly existing in crystalline or amorphous forms. Notice in figure1 below however that each Silicon is attached to 4 oxygen atoms; but as each oxygen is in turn attached to another Silicon as the lattice builds up, this means that each Silicon has a half share of each oxygen, thus the ratio of one silicon atom to two oxygen atoms still holds. By combining in this way the lattice is built up as a series of interconnected tetrahedra.

Figure 1.1 *Tetrahedral arrangement of SiO_2 in Silica.*

1.2 Siloxanes

Siloxanes or silicones (structural unit R_2SiO) are comprised of a linear polymer backbone of alternating silicon and oxygen atoms with organic side groups, such as methyl, phenyl, and vinyl etc., attached to silicon.

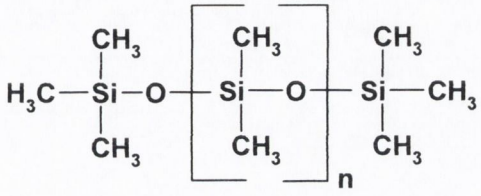

Figure 1.2 Polydimethylsiloxane, the most commonly available silicone.

The number of repeating units, "n," can range from zero to several thousand. By adjusting -Si-O- chain lengths, the functionality of the side groups and the introduction of cross linkers between molecular chains, *Silicones* can be synthesized into an almost infinite variety of useful materials .The types of organic groups attached to the silicon atoms can be controlled to create a hybrid chemistry capable of imparting important organic characteristics to the silicone. One of the simplest silicones polydimethylsiloxane is show in Figure1.2.

1.3 Silsesquioxanes

The more complex types of siloxanes (also called T- resins.) can be arranged in rings, ladders and caged structures. The structure of the caged siloxanes is simply an elaboration of the tetrahedrally arranged silica structures mentioned above. Of interest here is the class of compounds that have several rings connected together in a finite three-dimensional molecular skeleton. Such compounds are called polyhedral silsesquioxanes [1,2]. These all conform to the general formula $(R_xSi_xO_{1.5x})_n$ (n = 6, 8, 10, 12 or higher) .The term silsesquioxane is derived from the Latin *sesqui* meaning one and a half and Siloxane (explained above). If we look at the general formula for these compounds we can see the logic in the nomenclature, as the ratio of silicon to oxygen is always one to one and a half. The term polyhedral reflects the

tetrahedral network of the lattice. This term is commonly extended to polyhedral oligosilsesquioxanes, the prefix "oligo" coming from the latin *oligo* meaning short or small length which reflects the small chain lengths that these compounds commonly form. The acronyms for these compounds found in the academic and commercial literature are SSQR [3], PSSO [4,5] and most frequently, POSS [1,2].

1.4 Synthesis of Polyhedral Silsesquioxanes (POSS.)

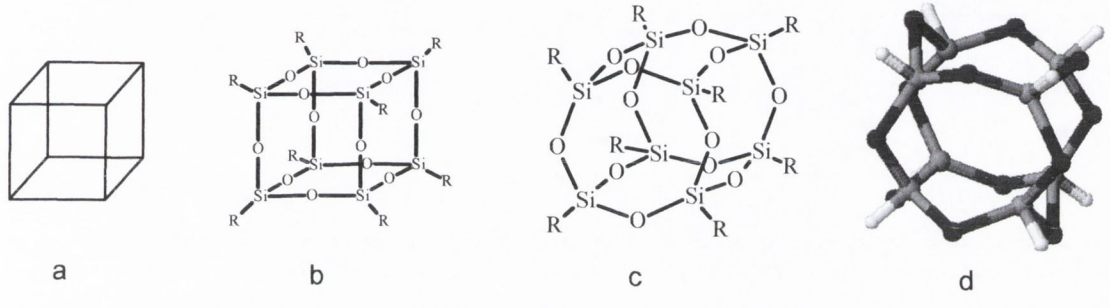

Figure 1.3 *Various representations of polyhedral silsesquioxanes used in this report. a) Simple box diagram used mostly to depict polymeric POSS each representing a monomer, can also be useful to show the hydroxyl groups in ICPOSS .b) More detailed box structure showing the Si-O-Si linkages, mostly used in the literature especially when pendant group reactions are of concern .c) More accurate representation showing the angles present in the octamer – used mostly in the literature when in reference to results based mainly on crystallography. d) Fully 3d representation used mostly in PowerPoint presentations where the three dimensional rotation of the molecule is instructive or to show basic building blocks in zeolites or other complex structures.*

POSS can be formed in three main ways: (the well documented) homo-condensation (polycondensation) [6,7] and hetero-condensation (polyaddition) [8] of organo silicon monomers, and by the more obscure route of the generation and subsequent insertion of silanones into the Si-O-Si units of the corresponding monomers (geminal fragmentation). For an in-depth discussion of this route the reader is directed to the article by Voronkov [9]. All three synthetic routes are illustrated in Scheme 1.1 overleaf.

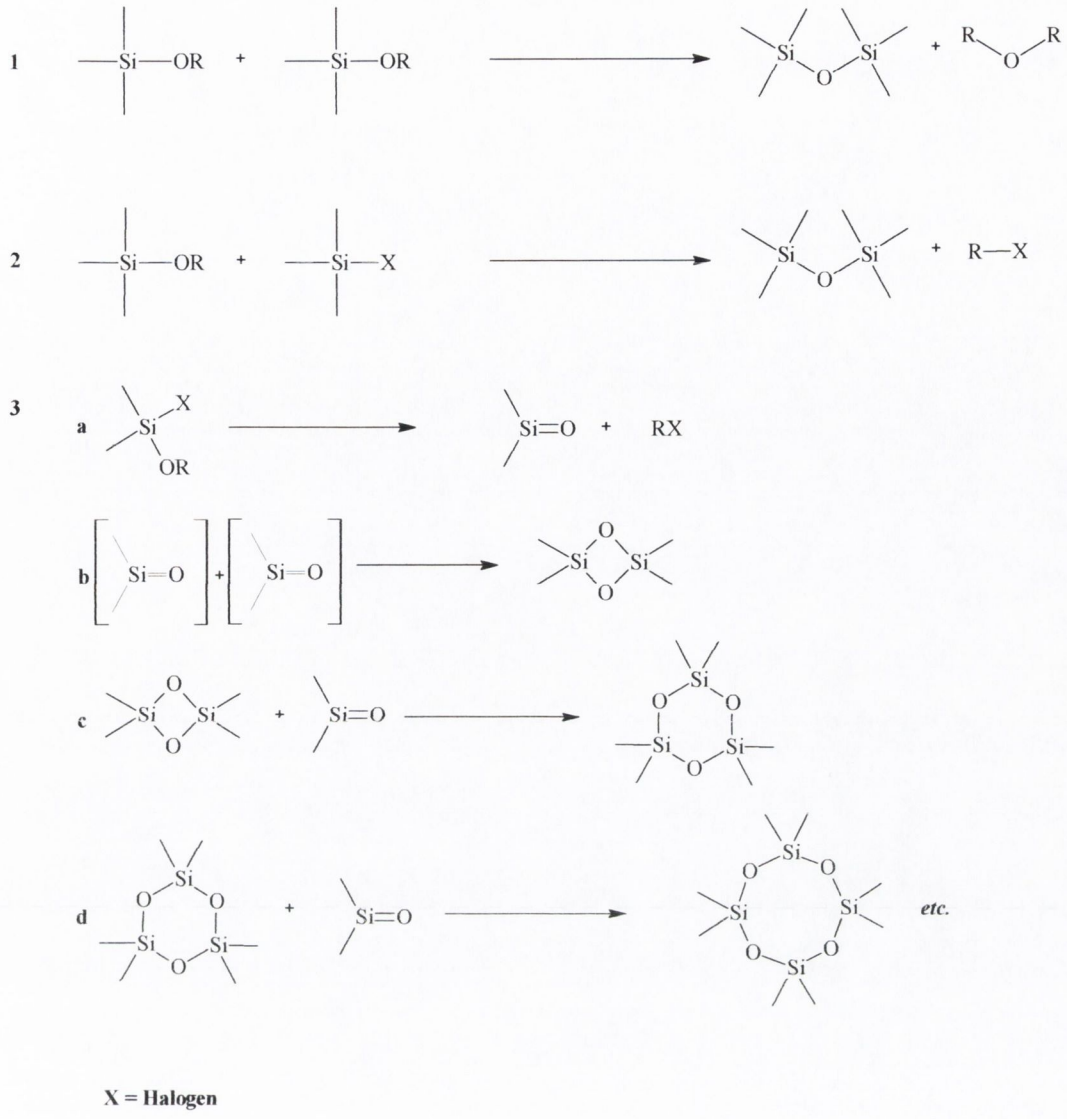

Scheme 1.1. *Main synthetic approaches for the preparation of POSS*

1.5 POSS classification.

Due to their complicated and convoluted names, various abbreviation systems have evolved for ease of writing and verbal communication on the subject of POSS. Brown [5] illustrated it elegantly when he wrote.

"According to the conventional silicone nomenclature, T denotes a trifunctional unit of Siloxane structure, i.e., a monoalkylsiloxy unit. For convenience we shall indicate the empirical composition of our polycondensates by formulas of the type where m represents the number of T units in the molecule and X_n the number and kind of uncondensed functional groups the empirical formula corresponding to T_mX_n is $(RSi)mO(3m-n)_{/2}X_n$, and the number of rings in the molecule is (m-n+2)/2".

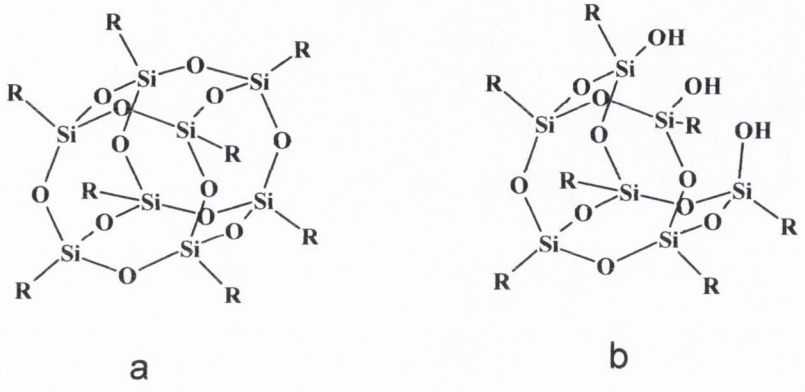

Figure 1.4 *Showing a) FCPOSS illustrating the almost perfect tetrahedral (ca.109.5°) arrangements of the 4 substituents on each silicon atom and also shows how they occupy each of the vertices. Also evident is the Si-O-Si angle open at ca.150°. b) ICPOSS (in this case a Tri-silanol) – see main text for nomenclature explanations*

To give an illustrated example we again look at figure 1.4 (a) above. This shows that the number of T units to be eight, and so having no pendant hydroxyl groups it is simply labelled "T_8" .On the other hand 1.4 (b) has seven T units and also possesses three hydroxyl groups, and therefore by convention is labelled "$T_7(OH)_3$". Other examples are shown below.

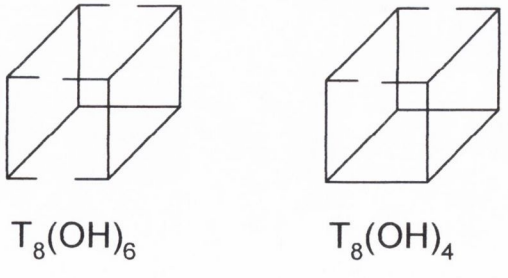

Figure 1.5 *Incomplete POSS units.*

But we can expand this point further. In many instances we may wish to make known the identity of the R groups attached to various T_8POSS frameworks; if one for instance had the 3-Chloropropyl R group (- $(CH_2)_3$-Cl) attached at each T unit, the molecule would be referred to as octachloropropylsilsesquioxane or 3-Chloropropy -octasilsesquioxane. This however can be contracted to "T_8Cl_8" or even more simply to "T_8Cl". Similarly if one had the 3-aminopropyl group attached the resultant structure -octa-aminopropylsilsesquioxane -would therefore be called "T_8NH_2". The open caged POSS are described in a similar way to the closed caged equilivant with the number of pendant hydroxyl group given in brackets for instance figure 3(b) if R equalled the 3-Chloropropyl group the structure would be referred to as $T_7Cl(OH)_3$

1.6 Characterisation of POSS

The high solubilities of some macromers and of POSS-based polymers readily lend themselves to characterization using solution NMR, GPC, Cryopscopic and IR methods. These techniques provide information relating to structure, composition, sequence, and molecular weight. The high symmetry of POSS molecules enables structural determinations to be made in a majority of cases from ^{29}Si spectra. Upon careful examination of the literature certain shifts are easily identified for the various cages, for insoluble samples MAS ^{29}SiNMR can be used in a similar manner. Table 1.1 (overleaf) gives the most common shifts. [2,8, 10, 11,12,13]

Table 1.1. Common NMR shifts for FCPOSS

^{29}SiNMR	POSS cage
δ -75ppm	T_{10}
δ -65ppm	T_8
δ -65ppm δ - 55ppm	$T_8(OH)_2$
δ -65ppm δ -50ppm	$T_7(OH)_3$

Molecular weight determinations for POSS-based polymers can be made from NMR spectra by taking ratios of end and repeat groups. GPC techniques coupled with refractive index and light scattering measurements also provide accurate determinations of number average (M_n) and weight average (M_w) molecular weights. The average Mw value obtained from successive measurements of an individual polymer sample is generally within 20-30% of the value measured by NMR. Good reproducibility for M_w ($^{+}$/- 6%) values has been observed [9]. Used in conjunction with ^{1}HNMR and ^{13}CNMR the nature of the attached pendant group can be readily assigned. Also the formation of Si-O-Si bonds can be easily shown using IR spectroscopy, as the Si-O-Si bond has a distinctive characteristic stretch between 1050-1150 cm^{-1}. SEM can also be utilised to show the nature of polymerised samples.

1.7 Sol-Gel technique.

The synthetic strategy adopted in this work relies heavily on the sol-gel technique. The sol-gel process, as the name implies, involves the evolution of inorganic networks through the formation of a colloidal suspension (sol) and gelation of the sol to form a network in a continuous liquid phase (gel). [13] . Although first discovered in the late 1800s and extensively studied since the early 1930s, interest renewed [13,14] once again in the early 1970s when at low temperatures, monolithic inorganic gels were formed and converted to glasses without a high temperature melting process [15,16,17]. Through this process, homogeneous inorganic oxide materials with desirable properties of hardness, optical transparency, chemical durability, tailored porosity, and thermal resistance, can be produced at room temperatures, as opposed to the much higher melting temperatures required in the production of conventional inorganic materials. [17]. This method sees an initial hydrolysis occurring by the nucleophilic attack of the oxygen contained in water upon the silicon atom, as evidenced by the reaction of isotopically labelled water with TEOS that produces only unlabelled alcohol in both acid- and base-catalysed systems: [18,19].

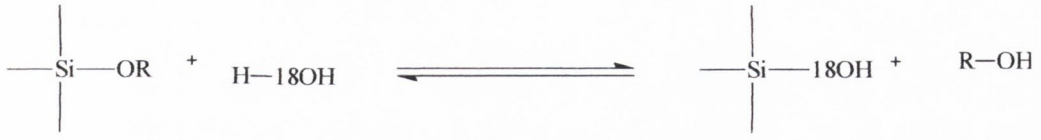

Scheme1.2. ***Showing*** *the reaction of isotopically labelled water with TEOS that produces only unlabelled alcohol in both acid- and base-catalysed systems:*

At the functional group level, three reactions are generally used to describe the sol-gel process: hydrolysis, alcohol condensation, and water condensation. This general reaction scheme can be seen in scheme 1.2. The reaction mechanism is as follows:

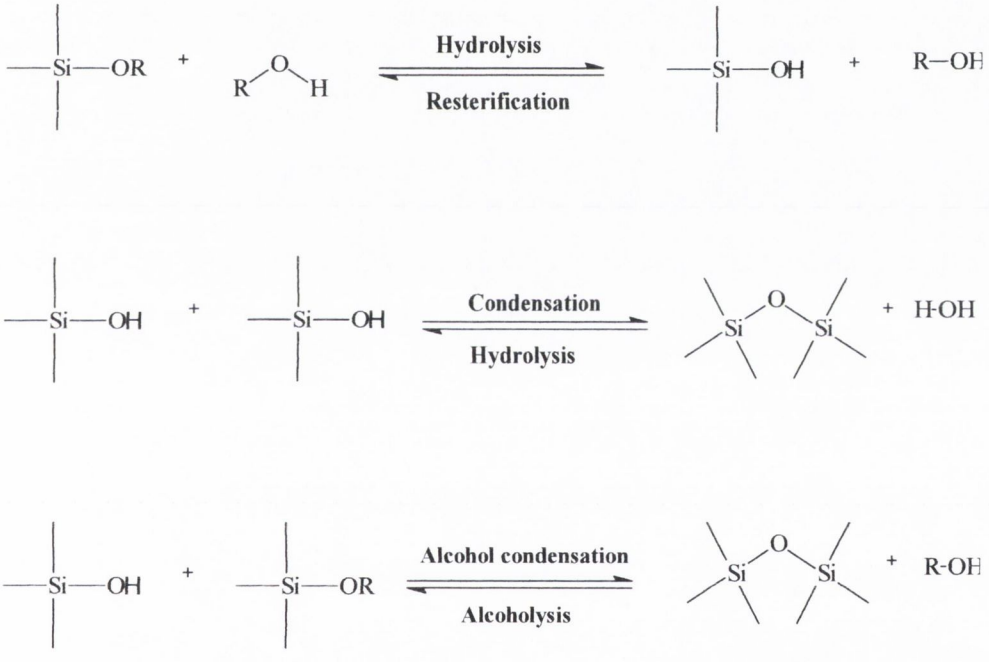

Scheme 1.3. *Showing Si-O-Si bond formation in POSS.*

Although hydrolysis can occur without addition of an external catalyst, it is far more rapid and complete when one is used. HCl and NH_3 are the most generally used catalysts, however some other catalysts normally employed are acetic acid, KOH, KF, HF and various amines [17]. In addition it has also been observed that the rate and extent of the hydrolysis is mostly influenced by the strength and concentration of the acid/base catalyst [20]. Research has shown that all

strong acids behave in a consistent manner, whereas weaker acids require a longer reaction time to achieve the same extent of reaction [21]. Compared with acidic conditions, base hydrolysis is more strongly affected by the nature of the solvent [21]. Both the acid and base reactions must now be looked at in greater detail.

1.8 Acid catalysed condensation of POSS.

Under acidic conditions, it is likely that an alkoxide group is protonated in a rapid first step. Electron density is withdrawn from the silicon atom, making it more electrophillic and thus more susceptible to nucleophillic attack from water. This results in the formation of a penta-coordinate transition state with significant SN2-type character [17]. The transition state decays by displacement of an alcohol and inversion of the silicon tetrahedron as expected for an SN2 reaction of this nature.

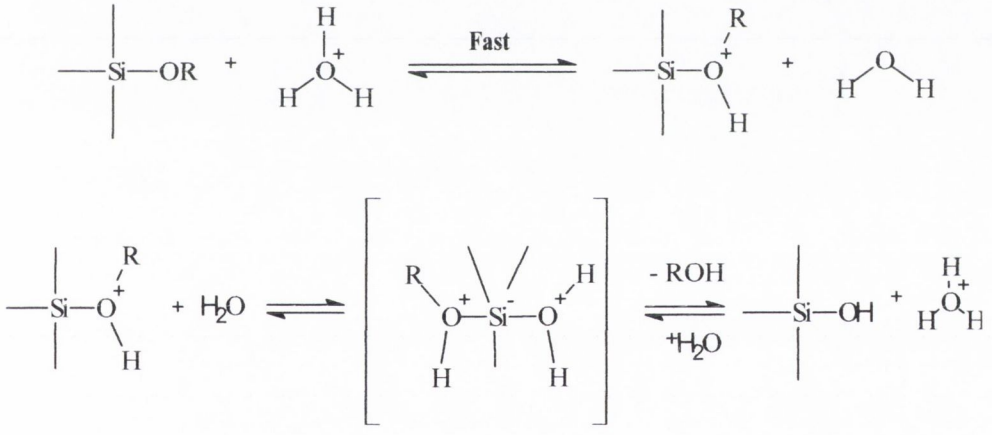

Scheme 1.4. *Showing inversion of the tetrahedron centre during acid catalysed condensation.*

1.9 Base catalysed condensation of POSS.

Base-catalysis by contrast proceeds much more slowly than the equivalent acid-catalysis concentration. The alkoxide oxygen atoms tend to repel the OH^- nucleophile. However, once the initial hydrolysis has occurred, the following reactions proceed stepwise, with each subsequent alkoxide group more easily removed from the monomer then the previous one [22]. Therefore, the more highly hydrolysed silicones are most prone to attack. Additionally, it must be mentioned that hydrolysis of the forming polymer is more sterically hindered than the hydrolysis of a monomer. Although hydrolysis in alkaline environments is slow, it still tends to be complete and irreversible [19].

Thus, under basic conditions, it is likely that water dissociates to produce hydroxyl anions in first step. The hydroxyl anion then attacks the silicon atom. Again, an SN2-type mechanism has been proposed in which the -OH displaces -OR with inversion of the silicon tetrahedron.

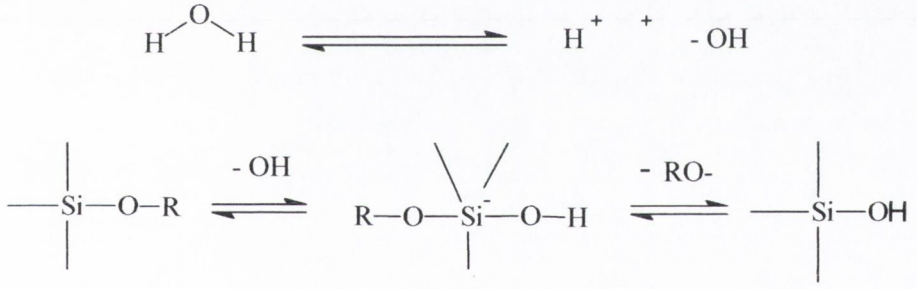

Scheme 1.5. *Showing inversion of the tetrahedron centre during base catalysis.*

1.10 Polycondensation of POSS, self-assembly and morphology.

In his 1965 paper on phenylsilanetriol Brown [5] discusses the many possible pathways for the build up mechanism of POSS cages. In this he shows how they self assemble in a series of stepwise polycondensations that begin with the initial formation of linear and then cyclic oligomers, which eventually dimerise into several closed and open caged structures.

Harrison [12] in his fascinating review on silicate cages has gone into this topic in even further and more complex detail. The following is a brief outline of both their findings. The proposed scheme of assembly of a simple closed cubic POSS is as shown in figure 1.6.

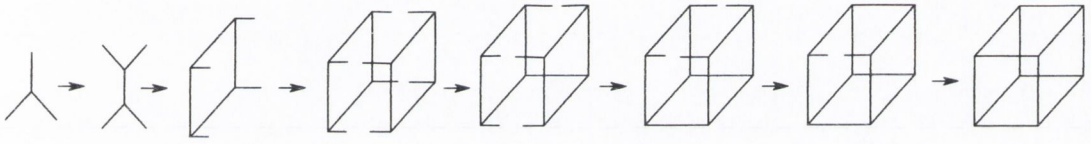

Figure 1.6 *Here we see a schematic presentation of assembly to a fully condensed POSS in this case a "cube" or "octamer" has formed, notice also the intermediate incomplete stages which can also be isolated under certain conditions.*

However other possibilities arise. In some instances three, five or six member rings, or higher are formed during synthesis. All of which can combine to form more complex intermediates which finally can end up as "octamers", six member hexamers, ten member "decamers" or twelve member "dodecamers" as illustrated below.

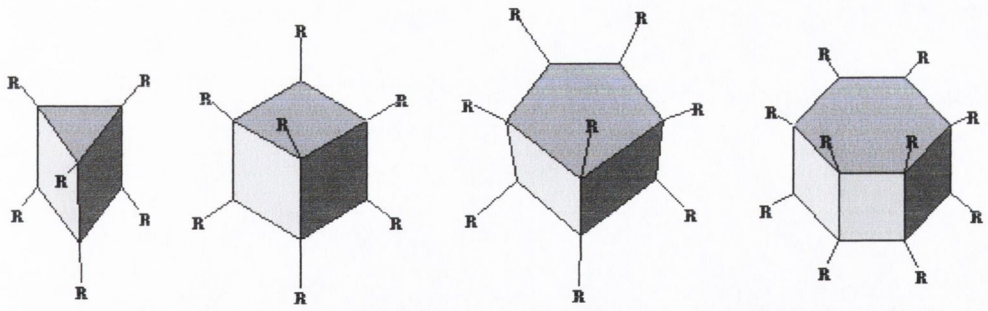

Figure 1.7 . *Various FCPOSS cage structures.*

It should now be mentioned that in all the aforementioned closed (completely-condensed) species; "incompletely–condensed POSS" forms are also possible and common. By having one or more corner uncondensed, they possess various numbers of "pendant" hydroxyl groups and hence these forms are commonly referred to as Silanol-POSS, along with the prefix Di, Tri, Tetra etc, depending on the number of hydroxyl groups attached (see figure 1.7 above). These incompletely condensed cages [23] can be further classified depending on the position of the pendant hydroxyl groups as shown in figure 1.8.

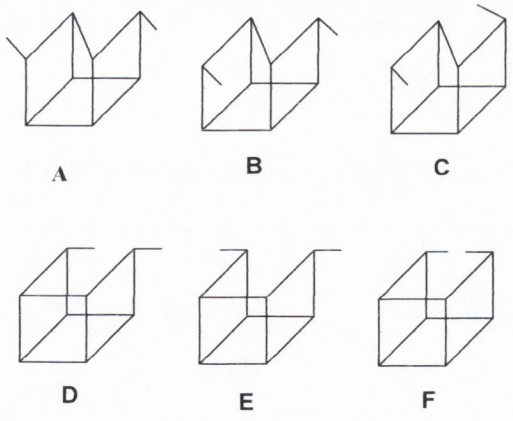

Figure 1.8 *Showing various incomplete POSS. A) "Z" type exo-exo, B) "Z" type exo-endo. C) "Z" type endo-endo. D) Regular exo-endo. E) Regular exo-exo. F) Regular endo-endo.*

Other more elaborate POSS forms are possible.

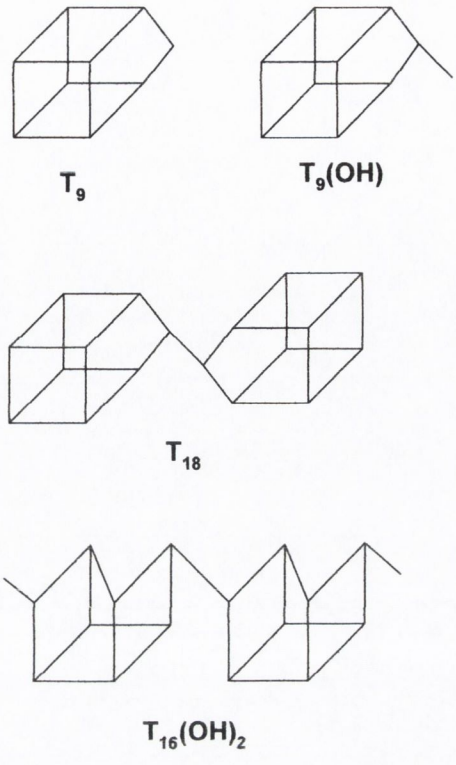

Figure 1.9 *More elaborate POSS structures*

The Polycondensation process is sensitive to many factors apart from pH. These other factors are temperature, polarity of the solvent, solubility of the products in the solvent, concentration of starting material, rate of hydrolysis, and type of catalysis used. It has been found that there is a direct relationship between temperature and degree of polymerisation i.e. the higher the temperature the more highly condensed the POSS becomes. Therefore if incomplete cages are desired, the temperature should be kept sub ambient at all times. Inversely if fully condensed POSS are required the system should be refluxed for a protracted period.

As previously mentioned the whole polycondensation process involves the formation of silanol groups as intermediaries. Clearly the stability of the polar groups depends greatly on the nature of the solvent used. Non-polar solvents such as hexane would repel the hydroxyl groups and possibly cause micelle formation, particularly if the R group at the rear were hydrophobic

itself, this would tend to favour the formation of fully condensed POSS. Conversely polar solvents such as Ethanol or Et_2O would stabilise the silanol groups via hydrogen bonding. By an analogous process the slow drop wise addition of water affects the reaction, by keeping the concentration of polar water molecules relatively low we militate against the formation of silanol groups. The nature of the solvent also affects the equilibrium of the reaction. Clearly if the product(s) are insoluble in the original solvent it will crash out of solution thus removing a factor from the right hand side of the equation. This will have the effect of driving the reaction to the right and so on to completion and high yields .If on the other hand the product proves soluble the system will remain in equilibrium and more of the incompletely condensed POSS moieties will predominate. This situation can, and often is changed, by replacement of or mixing in of alternative solvents. The solvent can have an influence over which isomers form as well. Looking at figure 1.8 above we can see that in the case of disilanols the Si-OH groups can be positioned exo or endo. Obviously – as Brown discovered [5] the "Z" type (most exposed) *exo-exo* form will favour a polar solvent whereas the regular (least exposed) *endo-endo* isomer will be more comfortable in non-polar solvents.

The natures of the R group and the X group can also have an influence. If X is a strong leaving group, such as a halogen, the rate of hydrolysis can be rapid which leads to the formation of HCl – hence the reaction autocatalyses. Other groups like EtO or MeO need acid catalysis to proceed. The nature and size of the R group is also important especially in relation to steric and inductive effects. When R is small (e.g. H, Me), fully condensed POSS structures may self-assemble. However if R is long or bulky (e.g. Phenyl, $(CH_2)_3NH_2$), self-assembly into incomplete POSS may occur. Tests by Andrianov [13] (using starting materials with the general formula for R being $Cl(CH_2)_n$ -) showed that the rate of hydrolysis is slowed noticeably when the length (n) of the hydrocarbon group is increased. By moving the halogen away from the silicon its influence diminishes and the reaction slows accordingly.

1.11 Polymerisation of POSS.

Polymerisation reactions which incorporate POSS moieties provide versatile alternative routes toward the synthesis of new polymeric and inorganic hybrid materials .For instance the use of carboranes in various polymerisations with Siloxane and acetylenic co-monomers provides a good example to show how polymerisable inorganic clusters –so called "building blocks"- can be used successfully to prepare, linear organic-inorganic hybrid polymeric systems with desirable engineering properties. ICPOSS with small numbers of pendant hydroxyl groups are ideal candidates for use in such systems, as are FCPOSS functionalised with appropriately reactive R groups such as Allylic or Cp groups. The ICPOSS have been used by Lechtenhan [1, 2] to produce graftable or polymerisable macromeres that have uses as polymer additives and linear POSS based polymeric systems. Using $R_7T_4(OH)_3$. Lechtenhan shows how the silanol functionality can be reduced from three to one by reacting it with $ClSiMe_3$ or Me_4SbOH.

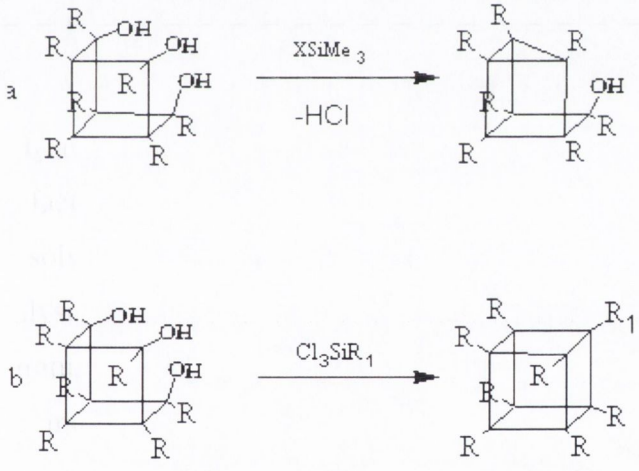

Figure 1.10 *a) Showing reduction of silanol groups in ICPOSS. B) Corner capping of ICPOSS. Both occur prior to inclusion of these units in polymeric systems.*

Alternatively, a method for controlling functionality and for the manipulation of the silicon-oxygen framework involves the use of "corner capping " This is the insertion of various silane coupling agents into a trisilanol-ICPOSS to produce FCPOSS compounds. A variety of R groups can be attached in this manner such as halogens, alcohol, olefins, Amine, epoxides etc. These groups can in turn be

further modified to give a desired functionality [11]. Such reactions give high yields especially if moisture is excluded from the system.

Well-defined FCPOSS such as these can be used as polymer additives or for the preparation of linear POSS – based systems. In general four main types are known [1, 11, 24, 25]. These are referred to as pendant, bead, triblock and star burst clusters. By careful manipulation of numerous empirical reaction variables a great deal of control over the final polymer structure can be achieved.

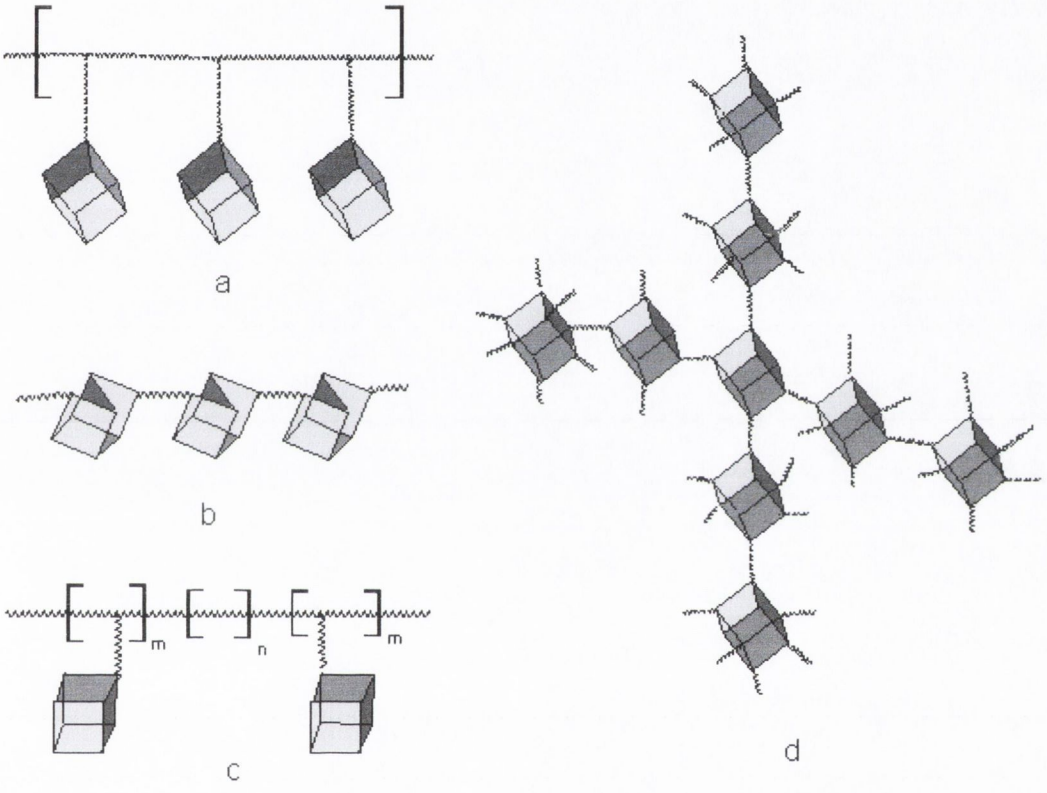

Figure 1.11 *Polymeric arrangements. a) Pendant, in pendant structures, the Polyhedrons are distributed along a polysiloxane chain. The resulting Siloxane"rakes" are used to chemically bond the polysiloxane polymer to an organic material, or to give unique orientation of the silicone on a metal or glass surface. b) Bead, notice the exo-exo Z-type ICPOSS used here. c) Triblock, showing stretches of linear polymer interspaced by pendant sections. d) Starburst, common in FCPOSS with reactive pendant groups such as Cyclopentadiene.*

A fifth, ladder type structure, based on two parallel polymer chains containing POSS groups as cross linking via Si-O-Si bonds (similar to rungs of a ladder), is also possible although mostly found in the older literature [5].

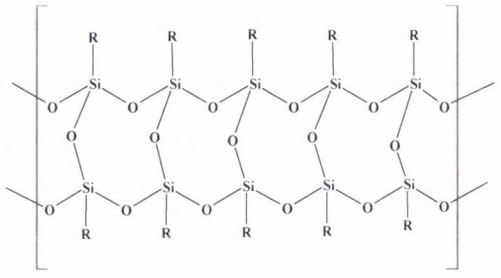

Figure 1.12 *Illustration showing the older proposed ladder structure of POSS.*

1.12 Pendant group manipulation

The number and variety of T_8POSS cages available has increased rapidly in the last few years. This is due in some part to the improvement in synthetic methods, which has led to multigram yields of easily separated versatile frameworks. More importantly, however is the increases in the number of useful pendant groups that can themselves undergo chemical manipulation.

The main challenge in pendant group manipulation is that a synthetic method has to be found that will sequentially react with all eight functional groups, which must all proceed with high conversion and must not produce any side reactions. This seems even more unlikely a goal when one considers that to fully convert T_8X_8 into T_8Y_8 there could be as many as twenty isomeric intermediates. To separate all of these would require very advanced separation equipment or techniques. Some examples do exist however of successful pendant group chemistry. Hydridosilsequioxane (T_8H_8) undergoes many synthetically useful reactions. It can be converted into T_8Cl_8 with > 98% yield. This proceeds via a radical mechanism in the presence of CCl_4. This incidentally makes the resultant molecule a good deal less reactive and therefore easier to handle than many other chlorosilanes [14]. The other reactions, such as

conversion into $T_8(RO)_8$, $T_8(MeO)_8$ involve nucleophillic attack upon the Si-H group.

Recentlty reported [26] is a new strategy utilizing dichlorocarbene addition and Friedel-Crafts alkylation reaction of a vinyl group respectively.

By far the easiest reaction to achieve is a Mono-functionalisation (see Marcolli et al [6]). This can be achieved with relative ease because the starting material has eight functional groups and so is by far the most abundant species present in reactions with low conversion.

1.13 POSS framework properties.

Except for reactions involving free fluoride or hydroxides, the skeletal Si-O-Si framework has proved to be durable and stable in most conditions necessary to convert pendant groups. However three main considerations about the framework it- self must be considered before a pendant group transformation is attempted. These are a) the framework is strongly electro withdrawing, b) strong bases generated in situ can cleave or polymerise the cage, and c) solubility can be affected by highly symmetric, highly functionalised frameworks [14].

The electron –withdrawing ability of a POSS framework has often been compared with that of CF_3 [14]. If this were the case then the frameworks are so strong that they will disrupt any form of oxidation being attempted on the pendant groups, or prevent any reaction that requires the formation of cations as transition states or intermediates. This can lead to the rates of some reactions being several magnitudes lower than their free counterparts. As mentioned above few reactions can be preformed in base that would not involve the pendant group getting involved before the framework could. However some reactions of the pendant group may cause the generation of strong bases in situ, which can lead to framework cleavage. Strong bases such as NaOH, especially in the presence of polar aprotic solvents [27], can rapidly attach to the Si-O-Si bond. Finally if the POSS framework is highly symmetric and highly functionalised with groups that can easily form intermolecular interactions, the solubility can drop drastically. This makes finding a suitable solvent difficult. The problem can be further compounded if a reaction produces such a species as

intermediates, which will then quickly proceed to crash out, leading to a poor conversion rate.

1.14 Metallasilsequioxanes.

Apart from their use in linear polymeric materials much interest has been shown also in the incompletely condensed form of T_8POSS, in particular the trisilanol forms (as outlined above). This is due in some part to their possible application as precursors to a wide range of Si-O and Si-O-M frameworks [28]. This normally involves the three Si-OH groups forming into new a Siloxane (Si-O-Si) or heterosiloxane (Si-O-M). The functionalisation of IC-POSS has led to a wide range of heterosilsequioxanes, which include main group, transition metal [29] and even lanthanide metallasilsequioxanes. The five main synthetic methods are illustrated below [8, 30, 31].

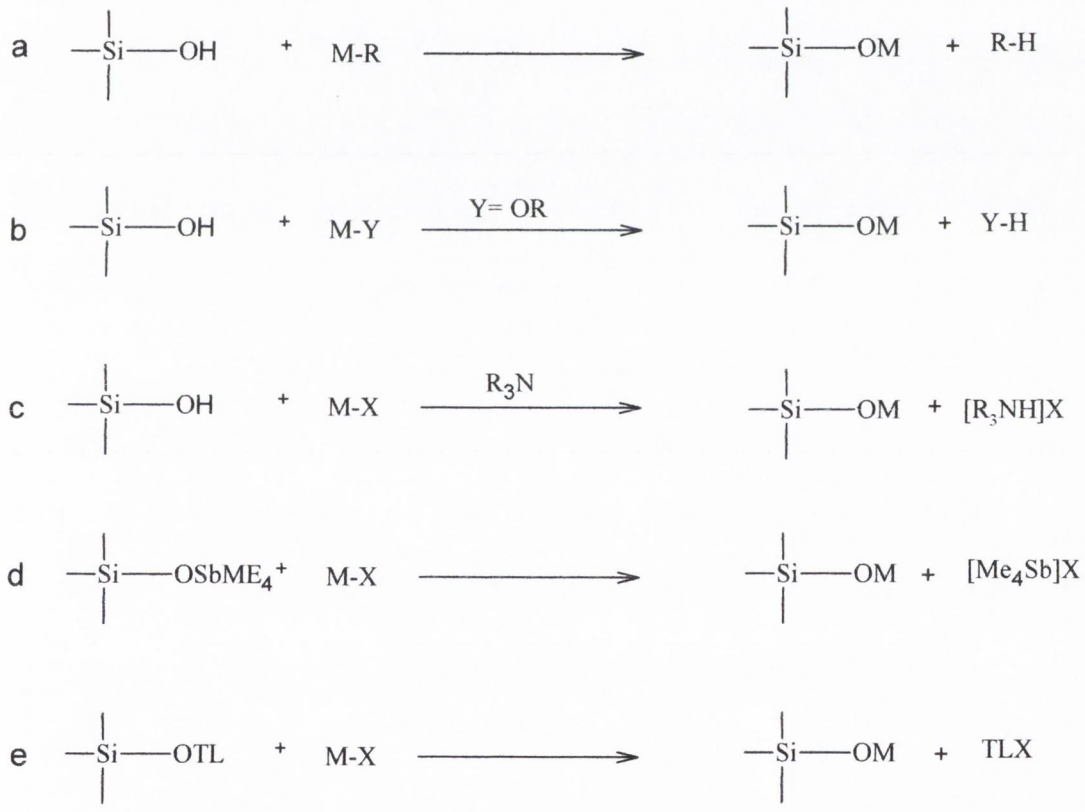

Scheme 1.5. Various methods available for production of metallasilsequioxanes.

1.15 Zeolites

Zeolites are crystalline aluminosilicates which are built from $[SiO_4]_4$ and $[AlO_4]_5$ tetrahedra that are connected by shared oxygen atoms and form channels, cages or cavities of defined size. They are composed essentially of a 3D skeleton of aluminium and silica oxides, which due to a unique configuration have a high negative charge. Positively charged cations in solution (or molecules suspended in air) can be absorbed onto the latticework and depending on pH, cation concentration and charge characteristics can later be released. The 3D-lattice work also gives zeolites another property – that of large internal surface area.

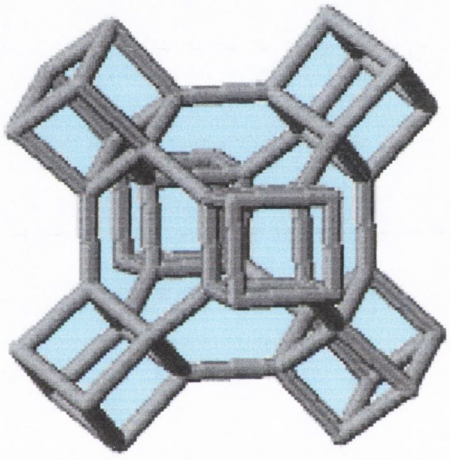

Figure 1.13 *Illustration of a Linde type A zeolite. Sodium Zeolite A is used as a water softener in powder detergent. Notice the cubicT_8 structures.*

In 1756, the Swedish mineralogist Axel Fredrick Cronstedt discovered that, on heating, the mineral Stilbite, lost water rapidly and seemed to boil. Therefore the material zeolite, from the Greek *zeo* meaning to boil and *lithos* meaning stone came into being. The overall framework charge of zeolites is negative, which can be compensated by cations like protons and alkali metals. Compensation of the negative charge by protons in some cases results in strong Brønsted acidic sites that are capable of catalysing several organic reactions with high activity. Small modifications during the preparation (*i.e.* Si/Al ratio,

temperature, pH, metal ion content to incorporate in the SiO_2 framework) result in a wide variety of zeolites. Crystalline zeolite type structures with incorporated Si, Al, P, B, Ga, Fe, Ti, Zn. Sn, etc. each have unique chemical and physical properties due to differences in adsorption properties, molecular dimensions, and electronic properties.

The loosely bound nature of extra-framework metal ions (such as in zeolite NaA) means that they are often readily exchanged for other types of metal when in aqueous solution [32,33]. This is exploited in a major way in water softening, where alkali metals such as sodium or potassium prefer to exchange out of the zeolite, being replaced by the "hard" calcium and magnesium ions from the water. Many commercial washing powders thus contain substantial amounts of zeolite. Commercial wastewater containing heavy metals, and conversely, hydrophobic silica zeolites preferentially absorb organic solvents. Zeolites can thus separate molecules based on differences of size, shape and polarity.

Nuclear effluents containing radioactive isotopes can also be cleaned up using such zeolites. The shape-selective properties of zeolites are also the basis for their use in molecular adsorption. The ability preferentially to adsorb certain molecules, while excluding others, has opened up a wide range of molecular sieving applications. Sometimes it is simply a matter of the size and shape of pores controlling access into the zeolite. In other cases different types of molecule enter the zeolite, but some diffuse through the channels more quickly, leaving others stuck behind, as in the purification of *para*-xylene by silicalite [34].

Cation-containing zeolites are extensively used as desiccants due to their high affinity for water, and also find application in gas separation, where molecules are differentiated on the basis of their electrostatic interactions with the metal ions. In powder detergents, zeolites replaced harmful phosphate builders, now banned in many parts of the world because of water pollution risks. Moreover, processes can be carried out in fewer steps, minimising unnecessary waste and by-products. As solid acids, zeolites reduce the need for corrosive liquid acids, and as redox catalysts and sorbents, they can remove atmospheric pollutants, such as engine exhaust gases and ozone-depleting CFCs. Zeolites can also be used to separate harmful organics from water, and in

removing heavy metal ions, including those produced by nuclear fission, from water.

In 1988 it was finally recognised that the T_8POSS framework bore a remarkable resemblance to sections of the Linde type A and other forms of zeolites (see figure 1.13 above). This catalyzed a renewal of interest in POSS chemistry. It was put forward that much could be learned about zeolites if these T_8POSS were subject to detailed spectroscopic analysis and it was hoped that this would yield new chemistry of related structures [35].

1.16 Silica supported catalysis

Berzelius applied the Greek *catalysis* meaning decomposition or dissolution in 1835 to describe a new phenomenon in chemistry. In 1911 Ostwald redefined this *catalytic force* that is responsible for carrying out reactions, into catalytic substances, which affect the velocities of the chemical reactions and do not influence the thermodynamic equilibrium of reactants and products. Typical in homogeneous and (enzymatic) catalysis is that catalytic processes take place in one phase [36].

This is not the case in heterogeneous catalysis. In heterogeneous catalysis surface properties, at which the catalytic reactions usually take place, are of crucial importance. The first step in a heterogeneous catalysed reaction (in the Langmuir-Hinshelwood approach), is adsorption of the reactants on the surface of the catalyst [36]. Subsequently the adsorbed species reacts (often in several consecutive steps) and finally the product desorbs from the surface while regenerating the active sites on the surface [37, 38]. To improve the properties of the catalysts (*i.e.* lifetime, robustness), catalytically active sites are often dispersed on porous supports such as silica gels (or γ-alumna). The overall catalytic activity and selectivity is determined by the composition and structure of the catalyst surface and is very sensitive to details in catalyst preparation Catalysts can be metal-oxides, metal-sulphides, metal-carbides or organometallic complexes [39, 40].

1.17 Heterogeneous catalysis

Due to complexity of the catalytic system, consisting of multiple active sites, characterization of the structure of the active site and elucidating the mechanism of the catalytic process can be most difficult. A catalyst model can provide valuable fundamental information and is obtained either from experimental or computational studies [8, 41, 42]. By using the surface organometallic chemistry approach, relatively well-defined active surface sites are synthesized with a uniform distribution and fairly high concentration, which has greatly contributed to the understanding of several heterogeneous catalytic processes [39, 40].

In surface science model systems, (usually) flat oxidized silicon wafers are used as realistic models for industrially applied catalyst supports [31]. These wafers are loaded with the active phase and a molecular level picture of the active surface is obtained by studying the properties by the usual surface science techniques [38]. Metals can be deposited on the model support by evaporation but in that case the particle size distribution is rather broad. Another method is to deposit the active phase by chemical vapour deposition or deposit the catalysts precursor via wet chemical techniques (spin coating for example), followed by drying and reduction steps. The ICPOSS cage structure can be regarded as small three-dimensional pieces of silica.

Many of these tri-silanols variants exhibit behaviour very similar to heterogeneous catalysts, and have proven to be active under conditions where similar models base on simple alcohols and silanols proved useless or ineffectual (i.e. $R_3Si\text{-}OH$, $R_3Si\text{-}O\text{-}SiR_3$, $R_2Si(OH)\text{-}OSi(OH)R_2$, $R_2Si(OH)_2$.

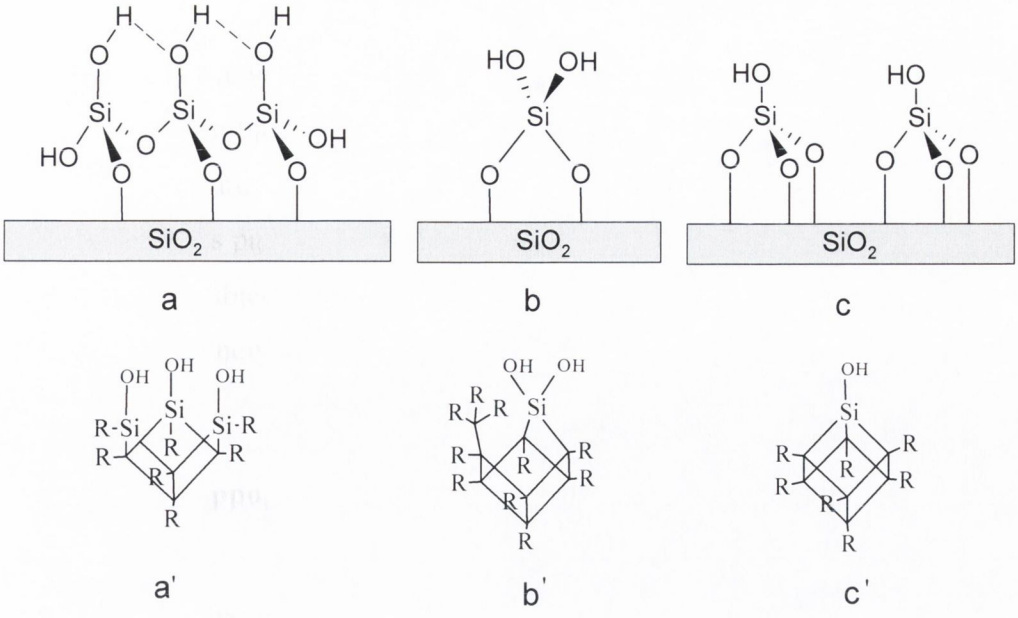

Figure 1.14 *Surface silicas,with their POSS model systems underneath. a) and a[1]) vicinal silanols which are close enough together to a hydrogen bond. b) and b[1])geminal silanols –note that two hydroxyls are attached to one silicon atom. c) and c[1]) Fully isolated silanol with at least 5 Å seperation between them.*

The leading representative of the IC- POSS is the tri-silanol $R_7Si_7O_9(OH)_3$. It is a suitable model for vicinal silanol sites, abundantly present in hydroxylated amorphous- and mesoporous silica [5, 8, 11, 14, 43, 44, 45]. The tri-silanol can model silica-grafted species or the reaction of silica with silylating agents (*e.g.* $ClSiMe_3$, $HN(SiMe_3)_2$). Also reactions with other surface modifiers and tethering groups (*e.g.* $XCH_2CH_2Si(OMe)_3$) can be mimicked. POSS tri-silanol can be partially silylated to afford vicinal disilanols which models, surface sites that are formed upon silylation of silica. A hydrophobic shell formed by bulky alkyl groups substituted at the corners of the silicate cages makes the molecules soluble in organic solvents. This enables characterisation on a molecular level with a wide range of powerful techniques. Many of these soluble models have been used to investigate what effects intermolecular hydrogen bonding has on the reactivity of Si-OH groups. This work has clearly shown that intermolecular hydrogen bonding has in fact a profound effect on the reactivity between mutually hydrogen bonded Si-OH groups. In some cases increased orders of several magnitudes have been reported for these POSS in comparison to their simple Silanol equivalents [20].

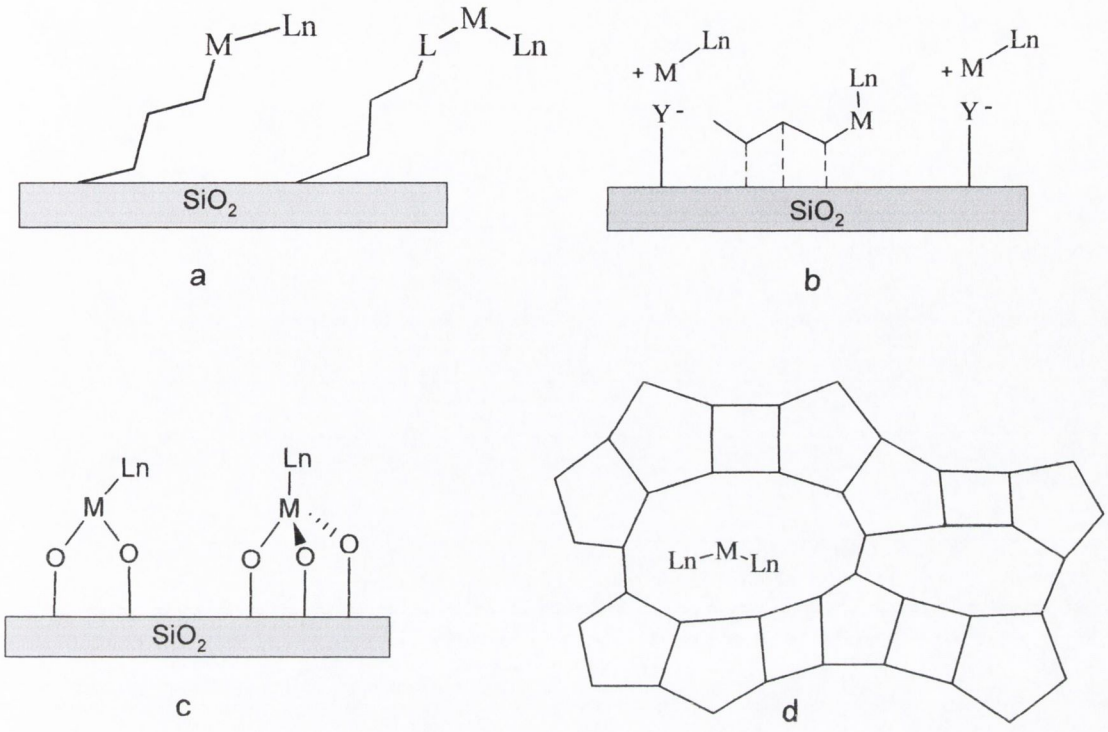

Figure 1.15 *Schematic representation illustrating the various immobilisation methods by silica supports a) Tethering, b) Physisorbtion, c) Grafting d) and Physical entrapment (e.g. zeolites).*

1.18 Homogeneous catalysis.

Most organic chemicals are often thermally unstable and their complex synthetic routes require moderate reaction conditions in the liquid phase. Well-defined homogeneous catalysts meet these requirements and ensure high efficiency in stereo-regular control of the products and reduce the formation of by-products. To facilitate the separation of the homogeneous catalysts from the products, they can be immobilized on supports [46]. When immobilization occurs via "grafting", a covalent bond between the catalyst and the inorganic support is created, which should prevent leaching of the grafted moiety. Metal complexes are, for instance, anchored by reaction with silica surface hydroxyls. For some metal complexes a more stable bond is ensured when the silanol is

first chemically modified by the introduction of alkoxysilane. A suitable linker is of the type $(RO)_3Si$-R-L, in which L is the ligand to coordinate to the metal precursor and R is a chemically inert spacer. This anchoring technique is called "tethering." Another route towards tethered species is via immobilizing a pre-synthesized catalyst precursor containing an anchorable functionality. Homogeneous complexes can be physically encapsulated in mesoporous structures that exist in, for instance, sol-gel silica or polymer structures. The host-guest interaction is neither covalent nor ionic. The guest stays in the host matrix but leaching of the complex through for instance a channel, is possible. "Physisoption" of metal complexes on a pre-treated surface is another immobilization technique. The catalytically active compounds interfered with carrier material by van der Waals interactions. Acids, bases as well as salts, oxides or complexes can be immobilized in this manner, the catalyst being held like a "ship in a bottle ". Studying immobilization strategies, stability of the supported catalyst, and electronic/steric effects of the support on the catalysts performance using homogeneous models would considerably contribute to the molecular level understanding of supported catalysts [39, 1, 40, 47].

1.19 Fullerenes

The fullerenes (60-carbons and higher order relatives) are really quite remarkable molecules that were initially discovered simultaneously by Richard E. Smalley and Harold Kroto [48] while conducting experiments aimed at understanding the mechanisms by which long-chain carbon forms molecules in interstellar space. The specific goal of the work was to explore the possibility that long carbon chain molecules such as cyanopolyynes (HC_nN, n = 5-11), which had previously been detected in the interstellar medium, could form when carbon vapour nucleates in the presence of hydrogen and nitrogen in order to carry out these experiments.

Kroto, Smalley and their co-workers developed a technique in which a laser vaporises atoms of a refractory material (such as carbon) into a carrier gas (usually helium). In the carrier gas the atoms nucleate (cluster) before being cooled by supersonic expansion, skimmed into a molecular beam, and analysed by mass spectrometry. Reactive gases such as hydrogen (H_2) or nitrogen (N_2)

could also be added to the carrier gas, and the reaction products of these gases with the carbon clusters could be also be analysed.

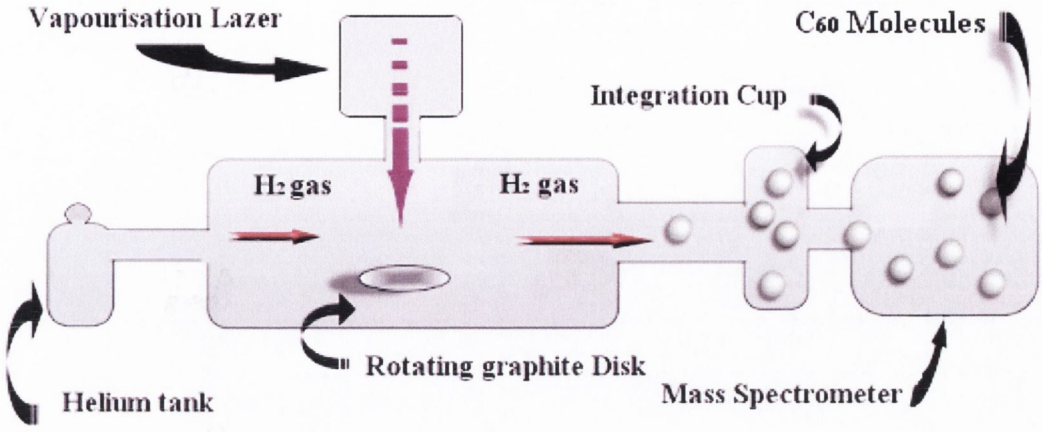

Figure 1.16 *Schematic diagram of apparatus used to generate and analyse carbon-cluster beams, which spontaneously produced fullerene molecules.*

These experiments showed convincingly that species such as HC_7N and HC_9N could, in fact, be produced in such laboratory simulations of the conditions in stars. However, even more significant was the unexpected discovery of a C_{60} Peak, which kept appearing in their mass spectra [48, 49]. Given the predominance of the C_{60} peak, Smalley, Kroto, and co-workers began to think about possible 60-atom structures that would exhibit unusually high stability.

They believed that in the laser vaporization, fragments of graphite were torn from the surface. Graphite has a planar structure composed of fused six-member rings. Each carbon is bonded to three other carbons in an infinite two-dimensional array. Small graphite fragments would contain many "unsatisfied valences" at the edges; the carbon atoms around the circumference of the fragment would be bonded to only two other carbons, rather than the more-desirable three carbon atoms. One solution to this problem of unsatisfied valences would involve curling the graphite fragment into a sphere so that atoms on one edge of the fragment could bond to atoms on the opposite edge. [48, 50, 51].

The resulting structure would take the form of a football or a "truncated icosahedrons" in which carbon atoms occupy each vertex. This structure might indeed impart unusual stability to the C_{60} cluster because all valences are satisfied.

The proposed molecule was dubbed buckminsterfullerene because its shape was reminiscent of the geodesic domes popularised by architect Buckminister Fuller, it is now more commonly called simply fullerene or C_{60} [48].

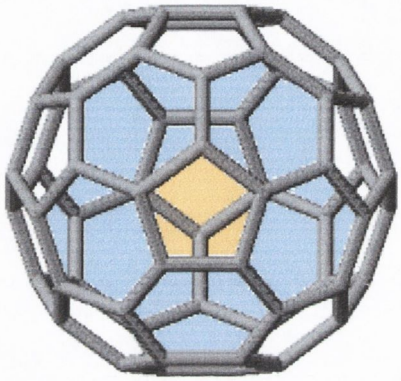

Figure 1.17 *The molecule is composed of 60 chemically equivalent carbon vertices that are connected by 32 faces, 12 of which are pentagonal (yellow) and 20 hexagonal (blue) ones as shown. Inserting a 5-sided pentagon into a sheet of 6-sided hexagons in graphite causes it to distort into a cone (12 pentagons cause it to wrap round into a ball) the bowl-shape or concavity at each sp^2 carbon centre introduces some strain into the molecule. However, the high symmetry distributes that strain evenly across the entire structure.*

Fullerenes are very robust molecules. They can survive collisions with metals and other materials at speeds, which exceed 20,000 mph, a speed that would normally tear most organic molecules apart. Recently potassium "doped" fullerenes were found to be super conducting at temperatures of 18° K[52] . These superconducting fullerenes have now been termed "dopeyballs". Unlike usual organic compounds, which possess C-H bonds and can be characterized by IR stretching vibrations, fullerenes been composed solely of carbon atoms, therefore do not have any residual infrared absorption Good solvents for

fullerene are available, these are CS_2, o-dichlorobenzene, toluene and xylene [40-50].

1.20 Carbon Nanotubes

In 1991, the NEC Corporation in Japan discovered using a high-resolution transmission electron microscope that graphitic carbon needles grew on the negative carbon electrode of the arc-discharge apparatus used for the mass production of C_{60} [53]. These needles ranged up to 1 mm in length and consisted of nested tubes or concentric cylinders of rolled graphite sheets similar to Slavic matrioshka dolls .The smallest tube observed was 2.2 nm in diameter, which corresponds roughly to a ring of 30 carbon hexagons. Some of the needles consisted of only two nested tubes, while others contained as many as 50. The separation between the tubes was 0.34 nm (3.4 angstroms), which matches the separation of the sheets in bulk graphite. Caps that were curved or cone-shaped generally closed the tips of the needles. Subsequent work at NEC optimised the synthetic procedure, allowing gram quantities of carbon needles (or "nanotubes" later referred to as multiwalled nanotubes (MWNTs)) to be isolated [Subsequently, in 1993, IBM's research centre in California independently discovered single-wall nanotubes (SWNTs)] [54]. Whereas the multiwall nanotubes were tens of nanometres across, the typical diameter of a single-wall nanotube were just one or two nanometres. The past decade has seen an explosion of research into both types of nanotubes [54, 55, 56]. Since then progress in understanding the basic physics [57, 58, 59] and chemistry [60, 61] of nanotubes has advanced at an amazing rate - and shows no signs of abating [62, 63, 64].

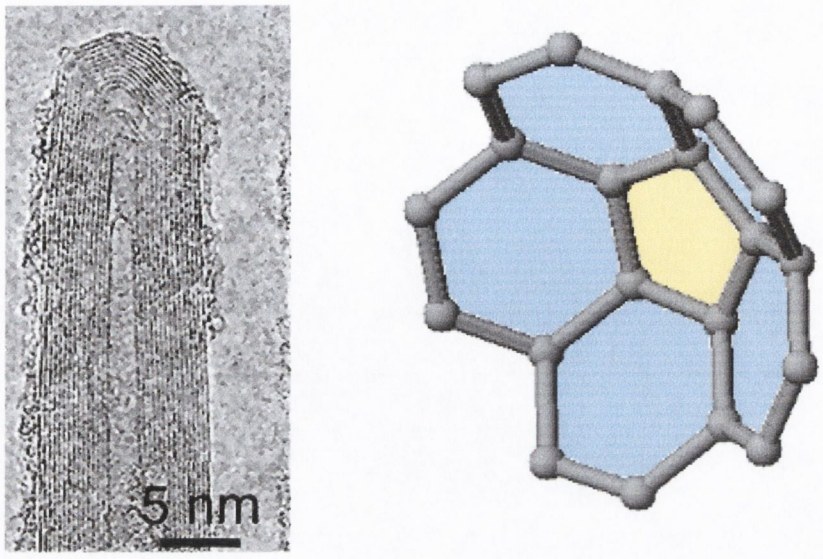

Figure 1.18 *a) TEM image show cross section of a MWNT. b) Illustration showing curvature at the tip due to the presence of a five member ring at the apex.*

Today, MWNTs can be grown efficiently by the catalytic decomposition of a reaction gas that contains carbon, with iron often being used as the catalyst [65]. This process has two main advantages. First, the MWNTs are obtained at much lower temperature, although this is at the cost of lower quality. Second, the catalyst can be grown on a substrate, which allows novel structures, such as "nanobrushes", Currently MWNTs can be grown to lengths exceeding 100 microns [65].

1.21 Mechanical properties of MWNTs

As mentioned above MWNTs can also be considered as a single sheet of graphite that has been rolled up into a tube. The electronic properties of the resulting MWNTs depend on the direction in which the sheet was rolled up. Some MWNTs are metallic with high electrical conductivity, while others are semiconductors with relatively large band gaps. MWNTs also have remarkable mechanical properties that can be exploited to strengthen materials or to act as "tips" in scanning probe microscopes. In a sheet of graphite each carbon atom is

strongly bonded to three other atoms, which makes graphite very strong in certain directions.

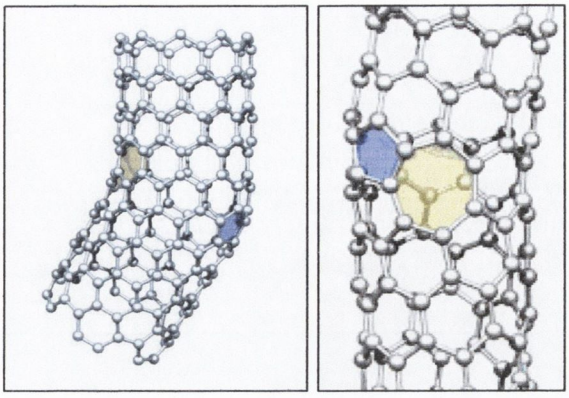

Figure 1.19 *Showing two sidewall defects in MWNTs .a) elbow defect, i.e. g a five and seven member rings on opposite sides which cause the distortion .b) a knee joint defect caused by a five and seven member rings conjoined on the same side. These defects can provide a good point of attachment for lithiated siloxnes*

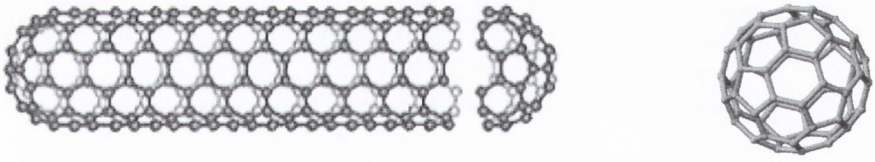

Figure 1.20 *Showing here the similarity between the C_{60} molecule and the tip of a MWNT .For this reason C_{60} is often used in reactions to model nanotube tip behaviour*

However, adjacent sheets are only weakly bound by van der Waals forces, so layers of graphite can be easily peeled apart - as happens when writing with a pencil. In contrast is not so easy to peel a carbon layer from a multiwall nanotube. MWNTs have been found to possess exceptionally high elastic strength, which per square metre is about five times the value for steel. Carbon fibre is already used to strengthen a wide range of materials, and the special durability property of MWNTs means that they could be the ultimate high-strength fibre.

It has been confirmed however that MWNTs grown by arc discharge have a high degree of stiffness; whereas the stiffness of those grown by the catalytic decomposition of hydrocarbons were one to two orders of magnitude less. These results demonstrate that only highly ordered and well-graphitised nanotubes (the carbon-carbon bonds within each layer are strong, while the interactions between layers are weak) have stiffness comparable to graphite, whereas those grown by catalytic decomposition have many more defects [66].

The high strength of carbon nanotubes makes them promising candidates in polymer reinforcement applications [67, 68] but there are some outstanding problems that must be overcome. For instance the tubes must be efficiently bonded to the polymeric material they are reinforcing (the matrix) so that they actually carry the loads. And in addition the load must be distributed within the nanotube itself to ensure that the outermost layer does not shear off.

1.22 Titanium dioxide nanorods

Titanium dioxide has attracted a growing amount of interest due to its expanding use in applications such as catalysis, photocatalysis, and dye-sensitised solar cells [69]. Research has also focused on TiO_2 nanoparticles, thin films and mesophorous solids [70]. Nanotubes entirely composed of TiO_2 have also been produced in recent years [71] using sol-gel technology. Nanotubes with diameter between 70-100 nm are reported commonly and even smaller sizes have been reported, going down in some cases to 8nm in diameter [72]. These minute nanotubes have a large surface area and possess an very higher rate of photocatalytic activity [73]. All these nanotubes consist mostly of anatase phase or anatase-rutile phase. Example of brookrite phase TiO_2 nanotubes have yet to be reported.

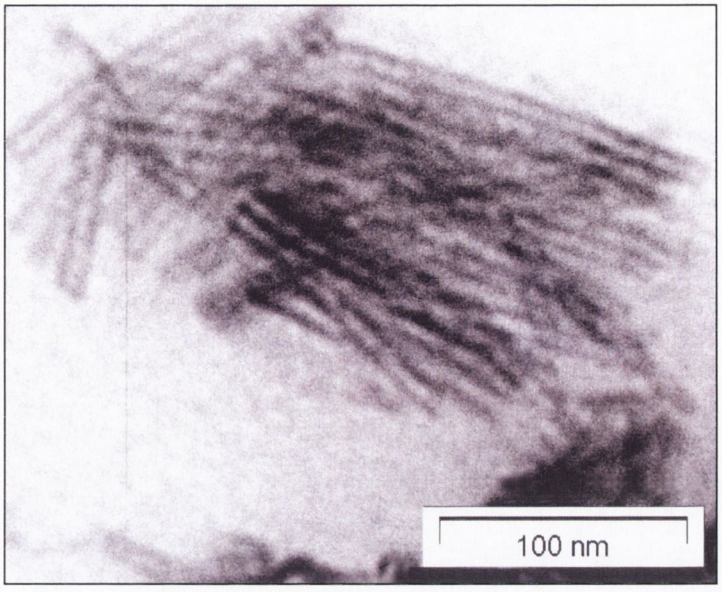

Figure 1.21 *TEM image of TiO_2 nanorods*

1.23 Sedimentation studies

The sediment studies were carried out on machines designed and built by the physics department of TCD. This machine is composed of four lasers pointers stacked vertically. The freshly sonicated sample in placed a cuvette which in turn in placed in the path of the 650 nm laser lines emitted from pointers as illustrated in figure 1.22. The four beams allow the concentrations at four different heights to be measured at 10-second intervals. The samples were left between 2-4 days and then removed with extra polystyrene added. This was continued till the percentage of Titania content to polystyrene was approximately 1-2%.

The transmittance (T) can then be transformed into local concentration using the Lambert-Beer law giving plots of local concentration as a function of time i.e.

$$\mathbf{Abs = \varepsilon_x c_x l}$$

$$\mathbf{Abs = - \log (I / I_0)}.$$

$$\mathbf{T = I / I_0}$$

$$\mathbf{Abs = - \log T}$$

Where **I** is the light intensity after it passes through the sample and **Io** is the initial light intensity.

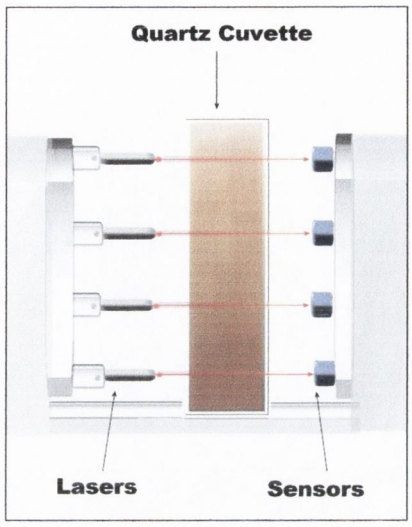

Figure 1.22 *Illustration demonstrating the basic structure of the sedimentation apparatus. The sample is placed in four laser beams, and allowed to settle for several days.*

1.24 Aims of this thesis

The main aim of this work is to develop chemistry of POSS and related materials which might have potential applications in nanotechnology. One of the first tasks is to develop an efficient synthesis of most important functionalised POSS in high yield. Then the aim is to prepare different POSS derivatives by chemical modification of their functionalities. This should involve different reactions with halogen-, amino-, allyl- and cyclopentadienyl-functionalised POSS. Preparation and investigation of new polymeric POSS is also to explored. Them we plan to use different trialkoxysilane derivatives such as (chloropropyl)triethoxysilane, (aminopropyl) triethoxysilane, allyl triethoxy - silane to functionalise TiO_2 and carbon nanotubes. Initially one of the important tasks is to develop preparation and effective purification techniques for multiwalled (MWNTs) nanotubes. Then the aim will be to functionalise MWNTs using lithium alkyls and trialkoxysilane derivatives. In our research the nanotubes are expected to serve as macromolecular ligands for organometallic

reactions. The new nanocomposites will be characterised by various techniques such as: transmission electron microscopy (TEM), thermal gravimetric analysis (TGA), elemental analysis, Raman and FTIR spectroscopy.

One of the objectives of our work is also to perform sedimentation studies for functionalised carbon and TiO_2 nanotubes in organic solvents to measure the solubility of the nanotubes in pure solvent and then with the addition of nanotubes and polymers in the solvent. DSC tests will be undertaken to analyse the thermal transitions of the nanotube-polymer composites to see if the nanotubes affect the crystallinity of the polymers.

Final important objective of this project is to prepare new ultra-strong polymer composite materials using chemically modified multiwalled carbon nanotubes and TiO_2 nanotubes as additives and as result providing an efficient bonding of nanotubes to the polymer matrix and good interfacial stress transfer. The siloxane functionalised nanotubes will be used to reinforce polystyrene (PS). This will be achieved by mixing of polymer with optimal amount of nanotubes in organic solvent with the grafted polymer chains mediating in the dissolution and by the preparation of films for nanotube-polymer composites. Mechanical properties of the films will then be investigated by using a Zwick-100 tensile tester. It is our expectation that through the interaction between the grafted polymer chain and surrounding chains, interfacial stress transfer will be enhanced.

The successful outcome of the project should contribute to the development of materials chemistry and nanotechnology.

1.25 References

1. Lichtenhan ,J.D.; Vu, N.Q.; Carter, J.A.; Gilman, J.W.; Feher, F.J. *Macromolecules* **1993**, *26*, 2141- 2142.

2. Lichtenhan, J.D. *Comments. Inorg. Chem.* **1995**,*17*, 115-130.

3. Fasce, D.P.; Williams, R.J.J.; Méchin, F.; Pascault, J.P.; Llauro, M.F.; Pétiaud, R. *Macromolecules* **1999,** *32*, 4757-4763.

4. dell'Erba, I.E.; Fasce, D.P.; Williams, R.J.J.; Erra-Balsells, R.; Fukuyama, Y.; Nonami, H. *J. Organometal. Chem.* **2003,** *00*, 1-10.

5. a) Brown ,J.F. *J. Am. Chem. Soc.* **1965**, 19, 4317-4324 b) Brown, J.F.; Vogt, L.H.; Prescott, P.L. *J. Am. Chem. Soc.* **1964**, 86, 1120-1124.

6. Marcolli, C.; Calzaferri, G. *Appl. Organometal. Chem.* **1999,** *13*, 213-226.

7. Feher, F.J.; Terroba, R.; Ziller, J.W. *Chem. Commun.* **1999,** 2309-2310.

8. Feher, F.J.; Budzichowski, T.A. *Polyhedron* **1995,** *14*, 3239-3253.

9. Voronkov, M.G. *J. Organometal. Chem.* **1998,** *557*, 143-155.

10. Gravel, M.C.; Laine, R.M. *ACS polym.prepr.* **1997**,*38,* 155-156.

11. Feher, F.J.; Wyndham, K.D. *Chem. Commun.* **1998,** 323-324.

12. Harrison, P.G.; *J. Organometal. Chem.* **1997,** *542*, 141-183.

13. Adrianov ,K.A. ; Izmailor B.A. *J. Organometal. Chem.* **1967**, *3*, 435-442.

14. Feher, F.J.; Budzichowski, T.A. *J. Organometal. Chem.* **1989,** *379*, 33-40.

15. Lev,O .*J. Anal Chem.* **1995**, 67. 22-30.

16. Hench, L.L.; West, J.K. *Chem. Rev.* **1990**, *90*, 35-40.

17. C.J. Brinker and G.W. Scherer, Sol-Gel Science: The Physics and Chemistry of Sol-Gel Processing (Academic Press, Inc.: New York, 1990).

18. a) Brinker, C.J.; Scherer, G.W. *J. Non-Cryst Sol.* **1985**, *70*, 301-322 b)Brinker, C.J. *J. Non-Crystalline Solids*. **1988**, *100*, 31-50.

19. K.D. Keefer, in: Silicon Based Polymer Science: A Comprehensive Resource; eds. J.M. Zeigler and F.W.G. Fearon, ACS Advances in

Chemistry Ser. No. 224, (American Chemical Society: Washington, DC, **1990**) pp. 227-240

20. M. Prassas and L.L. Hench, in: Ultrastructure Processing of Ceramics, Glasses, and Composites; eds. L.L Hench and D.R. Ulrich, (John Wiley & Sons: New York**, 1984**) pp. 100-125.

21. Aelion, R.; Loebel, A.; Eirich, F. *J. Am. Chem. Soc.* **1950**, *72*, 5705-5712.

22. Kelts, L.W.; Effinger, N.J.; Melpolder, S.M. *J. Non-Cryst Solids*. **1986**, *83*, 353-374.

23. Feher, F. J.; Terroba , R.; Jin, Z. *Chem. Commun.* **1999**, 2513-2514.

24. Seckin, T.; Gultek , A.; Koytepe, S. *Turk. J. Chem*. **2005**,*29*,49-59.

25. Feher, F.J.; Wyndham, K. D.; Scialdone ,M.A.; Y.Hamuro. *Chem. Commun.* **1998**, 1469-1470.

26 Dare, E.O.; Olatunji, G.A.; Ogunniyi, D.S.; Lasisi, A.A. *Polish.J.Chem* **2005**, *79*, 109-114.

27. Rikowski, E.; Marsmann,H.; *Polyhedron* **1997,** *16*, 3357-3361.

28. Feher, F. J. ;R. Blanski, L.*Makromolekulare Chemie-Macromolecular Symposia* **1993**, 66, 95-107.

29. Feher, F. J.; Budzichowski, T. A.; Rahimian, K. ; Ziller J. W.*J. Am. Chem. Soc.* **1992**, *114*, 3859-3866.

30. Murugavel, R.; Voigt, A.; Walawalkar,.M.G.; Roesky, H.W. *Chem Rev.* **1996,** *96*, 2205-2236.

31. Murugavel, R.; ChandrasekarV.; Roesky, H.W. *Acc. Chem. Res.* **1996**, *29*, 3357-3361.

32. Corma, A.*J.Catal.***2003** ,*216*, 298-312.

33. Cundy,C.S., Cox,P.A. *Chem.Rev.* **2003**, *103*, 663-701.

34. Duchateau, R.; Hamsen, R.J.; Abbenhuis, H.C.L.; Van Santen, R.A.; Meetsma, A.; Thiele, S.K.H.; Kranenburg, M. *Chem. Eur.J.* **1999**, *5*, 3130-3135.

35 Krijnen, S.; Harmsen, R.J.; Abbenhuis, H.C.L.; van Hooff, J.H.C.; van Santen, R.A., *Chem.Comm.* **1999** ,501.

36. Moulijn, J.A.; van Leeuwen, P.W.N.M.; van Santen, R.A. *Catalysis, an Integrated (Approach to Homogeneous, Heterogeneous and Industrial Catalysis,* Elsevier, Amsterdam, **1993**.)

37. Niemantsverdriet, J.W. (*Spectroscopy in Catalysis*, VCH Verlangsgesellschaft Weinheim, **1995**.)

38. Gunter, P.L.J.; Niemantsverdriet, J.W.; Ribeiro, F.H.; Somorjai, G.A. *Catal. Rev. Sci. Eng,* **1997**, *39*, 77-168.

39. Hartley, F.R. (*Supported Metal Complexes*, Reidel: Dordrecht, **1985**.)

40. Price, P.M.; Clark, J.H.; Macquarrie, D.J. *J. Chem. Soc., Dalton Trans.* **2000**, 101-110.

41. Choplin, A.; Quignard, F. *Coord. Chem. Rev.* **1998,** *178*, 1679-1702.

42. Edelmann, F.T.; Gun'Ko, Y.K.; Giessman, S.; Olbrich, F. *Inorg. Chem.* **1999**, *38*, 210-211.

43. Fink, G.; Steinmetz, B.; Zechlin, J.; Przybyla, C.; Teshe, B. *Chem. Rev.* **2000**, *100*, 1377-1390.

44. Hlatky, G.G. *Chem. Rev.* **2000**, *100*, 1347-1376

45. Feher, F.J.; Newman, D.A.; Walzer, J.F. *J. Am. Chem. Soc.* **1989,** *111*, 1741-1748

46 .Alt, H.G.; Koppi, A. *Chem. Rev.* **2000**. *100*, 1205-1221.

47. Edelmann, F.T.; Giessman, S.; Fischer, A. *J. Organomet. Chem.* **2001**, *620*, 80-89

48. Kroto, H.W.; Heath, J.R.; O'Brien, S.C.; Curl, R.F.; Smalley, R.E., *Nature* **1985**, *318*, 162

49. Krätschmer, W.; Fostiropoulos, K.; Huffman, D.R. *Chem. Phys. Lett.* **1990**, *170*, 167.

50. Haddon, R.C.; Brus, L.E.; Raghavachari, K. *Chem. Phys. Lett.* **1986**, *125*, 459.

51. Haddon, R.C.; Brus, L.E.; Raghavachari, K. *Chem. Phys. Lett.* **1986**, *131*, 165.

52. Hebard, A.F.; Rosseinsky, M.J.; Haddon, R.C.; Murphy, D.W.; Glarum, S.H.; Palstra, T.T.M.; Ramirez, A.P.; Kortan, A.R. *Nature* **1991**, *350*, 600-608

53. Iijima, S. *Nature* **1991**, *354*, 56-60.

54. Iijima, S.; Ichihashi,T. *Nature* **1993**, *363*, 603-609.

55. Kroto, H.W. *Nature* **1987**, *329*, 529-534.

56. Smalley, R.E. *Acc. Chem. Res.* **1992**, *25*, 98-101.

57. Heath, J.R.; Zhang, Q.; O'Brien, S.C.; Curl, R.F.; Kroto, H.W.; Smalley, R.E. *J. Am. Chem. Soc.* **1987**, *109*, 359-368.

58. Ebbesen, T. W.; Ajayan, P. M. *Nature*, **1992,** *358*, 220-225

59. Iacoe, D.W.; Potter, W.T.; Teeters, D. *J. Chem. Ed.* **1992**, *69*, 663.

60. Hawkins, J.M.; Meyer, A.; Lewis, T.A.; Loren, S.; Hollander, F.J. *Science.* **1991**, *252*, 312.

61. Krätschmer,W.; Lamb, L.D.; Fostiropoulos, K.; Huffman, D.R.. *Nature.* **1990**, *347*, 354.

62. Zhou, O.; Fischer, J.E.; Cousel, N.; Kycia, S.; Zhu, Q.; McGhie, A.R.; Romanow, W.J.; McCauley, J.P., Jr.; Smith, A.B., III; Cox, D.E *Nature* **1991**, *351*, 462.

63. Hebard, A.F.; Rosseinsky, M.J.; Haddon, R.C.; Murphy, D.W.; Glarum, S.H.; Palstra, T.T.M.; Ramirez, A.P.; Kortan, A.R. *Nature* **1991**, *350*, 600.

64. Bethune, D. S.; Kiang, C. H.;, DeVries, M. S.;,Gorman ,G.; Savoy, R.; Beyers ,R. *Nature* **1993**, *363*, 603.

65. Tsukagoshi K, Alphenaar B W, Ago H. *Nature.* **1999**, *401*, 572-574

66. Falvo M R. *Nature* **1997,***389* 582-84

67. Coleman J. N., Fleming A, Maier S, O'FlahertyS, Minett A I, Ferreira M S, Hutzler S.; Blau W J, *J. Phys. Chem. B.* **2004**, *108*, 3446-3450.

68. Murphy, R.; Coleman, J. N.; Cadek, M.; McCarthy, B.; Bent, M.; Drury, A.; Barklie, R. C.; Blau, W.J. *J. Phys. Chem. B.* **2002,***106*, 2210-2216.

69. Huang Q.;Gao.L. *J.Mater.Chem.* **2003,** *13*, 1517-1521.

70. Burger, R.; Evje, S.; Hvistendahl, K.; Lie K.A., *Chemical Engineering Journal* **2000**, *80* 91-104.

71. Hoffmann, M.R.; Martin, S.T.; Choi, W.; Bahnemann, D.W.; *Chem. Rev.* **1995**.*95*, 69 –75.

72. Wang, R.; Hashimoto, K.; Fujishima, A.; Chikuni, M.K.;Ojima, E.; Kitamura, A.; Shimohigoshi. M.; Watanabe T. *Nature* **1997**,*388,* 431-442

73.Sakai, N.; Fujishama, A.; Watanabe, T.; Hashimoto, K. *J. Phys.Chem. B* **2003,***107*, 1028 –1033.

Chapter 2

Synthesis of functionalised POSS

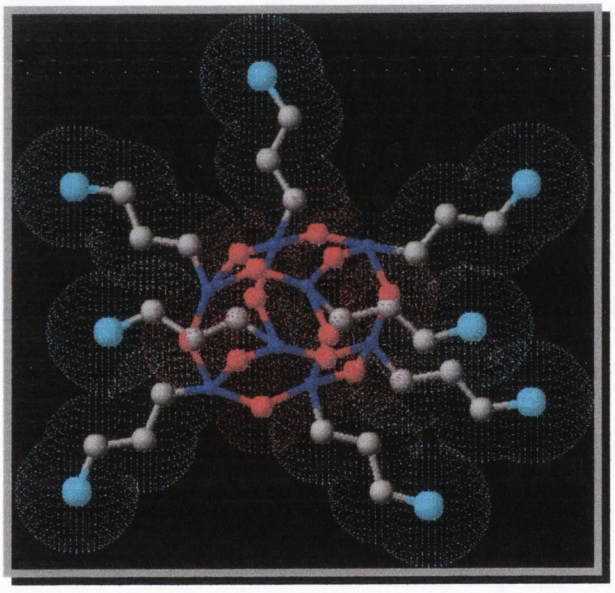

2.1 Introduction

As mentioned in the previous chapter, the most generally utilised approach in the preparation of the POSS is via kinetically controlled hydrolysis of the appropriate silicon/organic precursors [1]. Up to the recent past the chemistry of reactive functionalised POSS had remained relatively poorly developed. This can be possibly attributed to the high reactivity usually associated with pendant functional groups. This property makes the preparation of both organosilicon precursors/intermediates and their correspondent functionalised POSS very difficult with any great deal of success. Most of the approaches existing at the moment rely upon the corner capping of POSS trisilanols with various silane agents. Variation of the "R"groups on the silane, has allowed the successful placement a number of differing functionalities into the corner of POSS framework [2].

This section of the work concentrates on the development of newly functionalised POSS and explores the methods employed to optimise their synthesis. These improved methods have also being employed to improve the synthesis of some previously functionalised reported POSS, some of which might be potentially used as building blocks for new materials.

The work involves, therefore, new improved synthesis of the previously reported FCPOSS, i.e. octa(chloro-, amino- and thiol- propyl)silsesquioxane [3,4,5], and the new previously unreported compound, octa(allyl)silsesquioxane, and similarly the development of a number of new previously unknown cyclopentadienyl functionalised siloxanes. These latter compounds are of particular interest, as it is well known that cyclopentadienyls are among the most important ligands in metallorganic chemistry, since they form a wide range of stable complexes [6] whose steric and electronic properties can be easily tailored by varying the ring substitutions [7]. The η^5-cyclopentadienyl transition metal derivatives have long since played an important role in structural, synthetic and catalytic chemistry. They have found applications in many areas such as reagents in organic chemistry, Ziegler-Natta catalysts and even as cancerostatic compounds [6].

Thus the introduction of a cyclopentadienyl- siloxane hybrid, could open up fundamental new approaches in both siloxane and cyclopentadienyl chemistry.

However, there are a number of serious problems in the preparation of these materials. The Cp- fragment has been found to be quite sensitive [8,9] to temperature (*e.g.* dimerisation) and to other conditions (*e.g.* acids). This makes the work with Cp-functionalised siloxanes very difficult and challenging

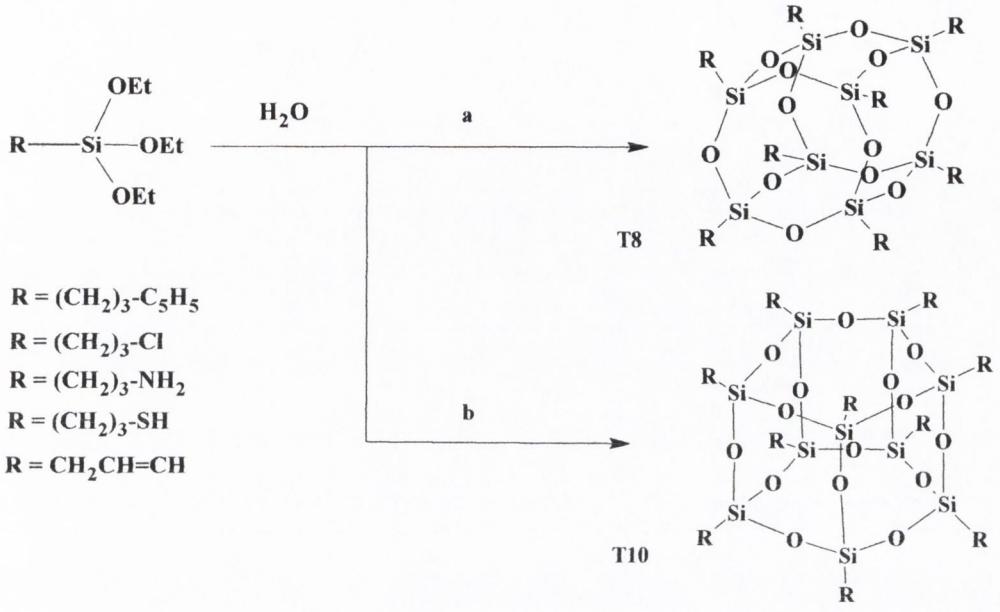

Scheme 2.1 *General Synthesis using sol-gel hydrolysis, of T_8 and T_{10} POSS cages mentioned in this chapter.*

2.2 Results and discussion.

2.2.1 Synthesis of Octachloropropylsilsesquioxane (T_8Cl). (1)

Octachloropropylsilsesquioxane was prepared by two different methods. The first procedure being followed here was taken from the literature [5], with some modifications. According to the literature this method involves a very long (five weeks) reaction of (3-chloropropyl)-trimethoxysilane and concentrated HCl at ambient temperature, which results in the modest yield of 27.6% of T_8Cl. In our modification, instead of using (3-Chloropropyl)-trimethoxysilane we used the considerably cheaper precursor, (3-chloropropyl) triethoxysilane. In an attempt to accelerate the reaction process the mixture was also heated under reflux for 35 hours. The process (after purification) gave a striking 80 % yield of the required product, T_8Cl, a white finely powdered solid. Not only does this represent a 56% improvement in overall yield but also

shows significant improvement of the existing procedure in terms of both of time and cost, the preparation of T_8Cl in good yield being reduced from 840 down to 35 hours. In a further attempt to improve the process, base catalysis was tried using differing amounts Sodium hydroxide (with carefully controlled amounts of water) added to the reaction. In all these cases, however, the resultant yields were consistently lower, the maximum achievable being 63% of impure T_8Cl .All these base catalysed products also showed a noticeable amount of impurity (in particular a range of melting points and clear shoulders visible in the ^{1}HNMR) in the product compared with the acid catalysed process.

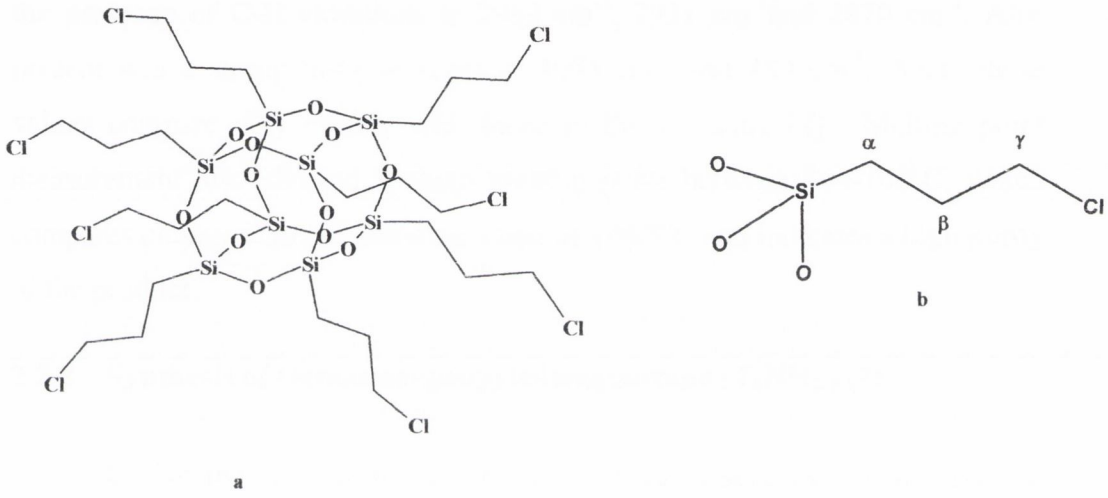

Figure 2.1. a) *T_8Cl FCPOSS, b) the locations of hydrogens mentioned in the text.*

The T_8Cl prepared by the acid catalysed condensation was characterised by ^{1}H, ^{13}C and ^{29}Si NMR and IR. The ^{1}HNMR showed all the relevant peaks for T_8Cl and were identical to those reported in the literature [4]. In the ^{1}HNMR spectrum of T_8Cl, α-protons appear as a triplet (coupling to two hydrogens) with a shift of 0.804 ppm (lit.value of 0.802ppm). The β protons appear in the spectra as a quintet (coupling to four hydrogens) at almost 1.877 ppm (1.876ppm) and the protons γ (also a triplet) falling further downfield at 3.5ppm (3.542ppm) - due to the electron withdrawing affect of the halogen. Also evident on the spectra were large signals, which were identified as ethanol, a good sign that the condensation has taken place.

The ^{13}C NMR proved to show all the appropriate CH_2 groups at 47 ppm, 26 ppm and 9.5 ppm, (referenced peaks given as 46.87ppm, 26.01ppm and 9ppm. respectively). Coupled ^{13}C NMR show each carbon as a sharp triplet indicating the presence of two hydrogens on each carbon. The ^{29}Si NMR spectrum of the T_8Cl shows a single sharp peak at –65.9 ppm, which is typical for T_8 FCPOSS and compares well with the literature value of –67.11ppm. It is important to note that ^{29}Si NMR of non-purified reaction mixture (and base catalysed products) indicated the presence of other siloxanes, with peaks at –56.08 ppm & -49.81 ppm, which are most likely attributed to lower weight POSS (e.g. $T_7(OH)_3$,T_6,$T_5(OH)_2$ etc.). The IR spectrum of the product indicated the presence of C-H vibrations at 2953 cm^{-1}, 2931 $cm^{-1}$and 2870 cm^{-1}. Also present was a strong Si-O stretches at 1093 cm^{-1} and 480 cm^{-1}. Again these values compare very closely with those in the literature [4]. Melting point measurement also showed a sharp melting point between 104-105°C, which compares closely with the literature value of 104.3°C and indicates a high purity of the product.

2.2.2 Synthesis of Octaaminopropylsilsesquioxane (T_8NH_2).(2)

Unlike the straightforward synthesis of T_8Cl, successful synthesis and purification of T_8NH_2 is considerably more complex to achieve. The compound first appears in the literature in 1991 as a patent issued to Wacker-Chemie [10], although this method, due to the use of HCl as catalyst, is now believed to have produced its octahydrochloride salt i.e. $T_8(NH_3^+Cl^-)_8$ [10]. Recently Seckin et al. [11] have reported an alternative synthesis using $PdCl_2$, although the exact role of this strong oxidising agent fails to be explained! The reaction, however, can also proceed by base autocatalysis. Due to the presence of an amino group on the precursor, the hydrolytic condensation was performed in excess THF using (3- aminopropyl) triethoxysilane with deionised water. The mixture was heated under reflux and stirred for four days. Again a slight adjustment to the published procedure [8] was made which, like the T_8Cl, required initially a gestation period of five weeks.

According to Feher et al [4], stable and fully condensed T_8NH_2 is almost impossible to prepare at room temperature. The NH_2 functionality has a

tendency to attack the Si-O-Si network, which leads to cleavage of the Siloxane cage and creation of pendant silanol groups.

Feher [4] has speculated that there are at least two pathways for decomposition of T_8NH_2. The first method probably involves the rapid formation of hydroxides *via the* reaction of water with the free amine. Support for this pathway comes from the observation that other silsesquioxane frameworks are slowly decomposed by exposure to amine bases (*e.g.* $N(Et)_3$) in wet solvents, and the fact that decomposition is found to be much slower in anhydrous solvents such as methanol .However, the fact that decomposition still occurs, even when solutions of T_8NH_2 are prepared in DMSO and stored over molecular sieves, is consistent with a second mechanism which does not require water being present . The mechanism Feher proposes, involves the attack of the amine nitrogen on Si-O-Si bond as illustrated in figure 2.2.

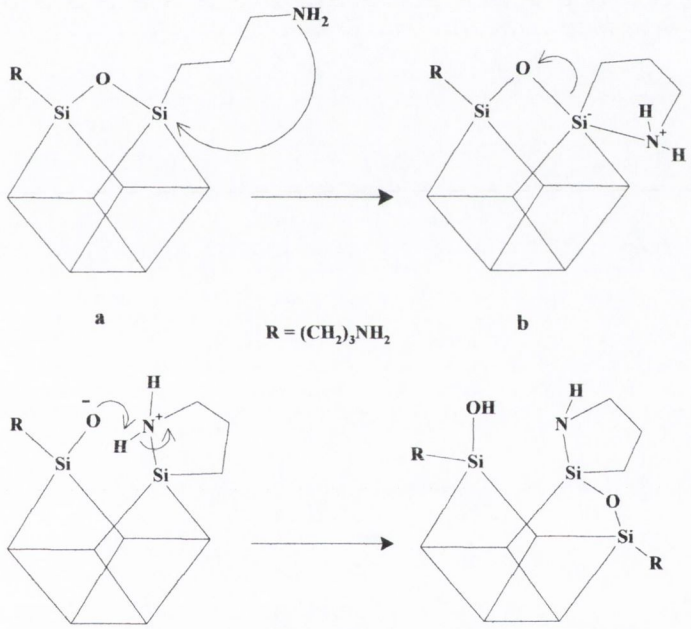

Figure 2.2. *Showing the degradation mechanism of T_8NH_2 as proposed by Feher et al .for dry samples a) the amine undergoes nucleophillic attack upon the Silicon. b) This leads to cleavage of the Si-O bond. c) The free Oxygen the deprotonates the tetravalent Nitrogen .d) this leads to the formation of one silanol group with the subsequent groups easily formed by similar reactions*

The resulting product must be stored at -35°C or lower in dilute solution to remain stable. Unfortunately it decomposes rapidly once solvent has been removed, and only lasts a few hours when raised to room temperature. For practical use in synthesis, therefore, small aliquots of a fresh T_8NH_2 sample were prepared by rapid evaporation under vacuum at –35°C, and the dried material was introduced quickly to the other reactants and stirred vigorously under inert atmosphere.

The initial samples of T_8NH_2 were quickly sent for NMR analysis. The ^1H NMR (in $CDCl_3$) spectra showed the three expected peaks due to the CH_2 groups at 2.68ppm, 1.54ppm and 0.6ppm. The literature values vary from author to author and would seem dependant on the type of duterated solvent used. The main resonance values being given in DMSO-d_6 occur at 2.75ppm, 1.71ppm and 0.71ppm [4], and in D_2O at 3.04ppm, 1.79ppm and 0.81ppm [10]. A broad signal at 2.04 in $CDCl_3$ is assigned to the resonance of the NH_2 group. The ^{13}C NMR spectrum showed the three expected propyl peaks 42.15ppm 22.9ppm and 9.9ppm, all of which compare well to the literature values taken in DMSO-d_6, and are given as 41.04ppm, 20.63ppm and 8.44ppm .The initial ^{29}Si NMR in $CDCl_3$ showed a major single peak at –65.35 ppm, which compares well to the literature values (in $C_6D_6$and DMSO-d_6, which range from 64ppm up to -69ppm), and is indicative of the presence of a T_8 FCPOSS. Subsequent samples of T_8NH_2 were also sent for NMR analysis after been allowed to stand on the bench for various lengths of time at ambient temperatures. The ^1H NMR (in $CDCl_3$) spectra showed the three expected peaks due to the protons on CH_2 groups as did the ^{13}C NMR. The ^{29}Si NMR however began to show a secondary peak at –58ppm. This was followed by another subsequent peak at –46ppm. According to the literature this is indicative of the presence of the silanol groups present on the Siloxane cage due to partial disintegration of the Si-O-Si matrix.

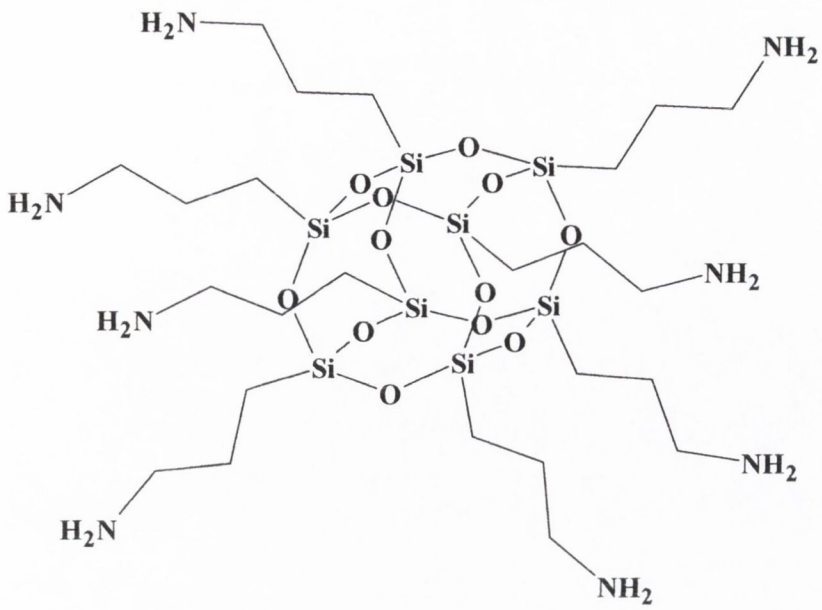

Figure 2.2. *Illustration of T_8NH_2 FCPOSS.*

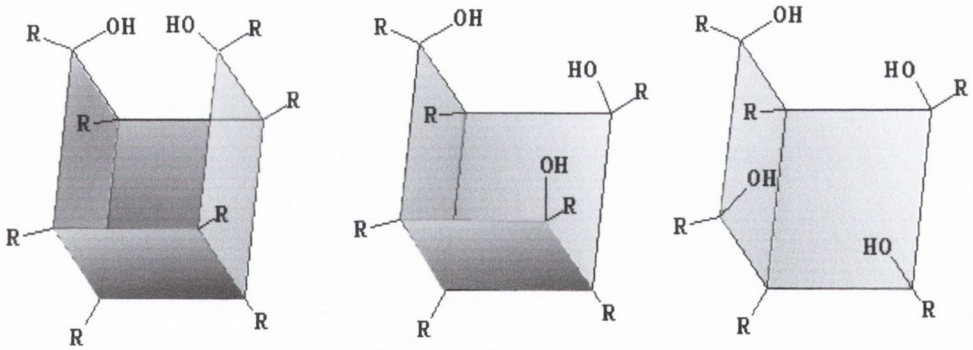

Figure 2.3. *Illustration of most common products of T_8NH_2 degradation ICPOSS T_8 NH_2 .a) $T_8NH_2(OH)_2$. b) $T_7NH_2(OH)_3$ c) $T_6NH_2(OH)_4$. R = $(CH_2)_3NH_2$.*

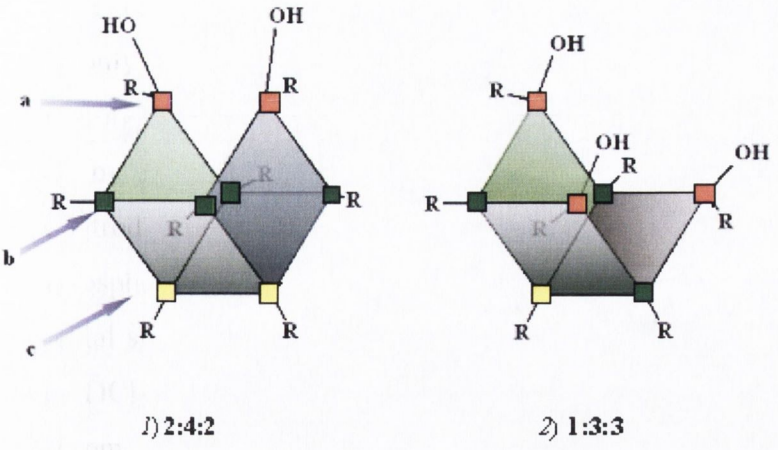

Figure 2.4. *Illustration showing the three different silicon environments and their ratios, available in both 1) $T_8NH_2(OH)_2$, and 2) $T_7NH_2(OH)_3$ incomplete cages formed as a result of cleavage by the amino functionality on the R group ($R = (CH_2)_3\text{-}NH_2$.)*

In the later ^{29}Si spectrum we find three large resonance's at –47ppm, -55.8ppm and –65 ppm with a ratio of 1:3:3. This would tend to indicate that the disintegration product formed is $T_7NH_2(OH)_3$. The Peak at –65ppm would therefore correspond to the three **b** (green) silicones depicted in figure 2.6(2) above, these being in effectively the same environment as a closed cage .The **a** (red) Silicones, being silanols, fall as well documented further down field at δ –54pm [12,13]. The solitary **c** (yellow) silicon then must be attributed to the peak at –46ppm. Further samples began to show a peak appearing at –34ppm. Feher also reported [14,15] the build up of a white resinous precipitate in the reaction vessel. This he believes is due to decomposition of the Si-O framework. The signal at δ –37ppm may be attributed to this residue. This residue is, however, easily removed by filtration via canula under argon atmosphere [16,17].

Also noticeable on the ^{1}HNMR spectra of these ICPOSS, are small shoulders to the left of the three main propyl hydrogen peaks .The presence of OH groups attached to some of the Silicones in an open cage may shift their signals downfield in the case of the α hydrogen. This would be expected to be less noticeable on the β case. The γ hydrogens may also be affected if intermolecular reactions have occurred resulting in polymerisation as reported

by Feher et al [18] however, it must also be noted that the long-standing T_8NH_2 samples show strong basic pH indicating the presence of many un-reacted NH_2 functionalities. The IR spectrum shows NH_2 bands at 1621cm^{-1} and 797 cm^{-1}and other bands at 1212 and 1174 cm^{-1} due to Si-O-Si stretching

2.2.3 Synthesis of Octaaminopropylsilsesquioxane chloride (T_8NH_3). (3)

T_8NH_3 was prepared in a very similar manner as that of T_8NH_2. The mixture of (3-aminopropyl)triethoxysilane, water excess amounts of HCl was heated under reflux for two days in methanol giving a product with >95% yield.

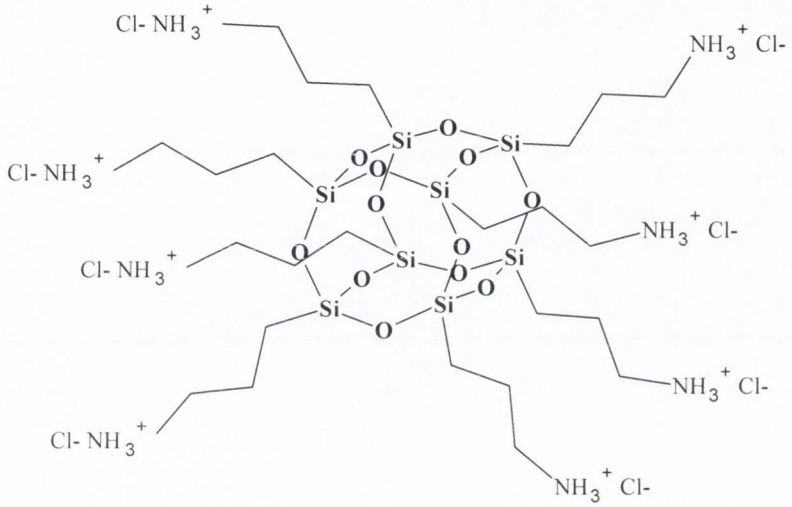

Figure 2.5. *Structure of $T_8(NH_3Cl)_8$*

Unlike the T_8NH_2, the salt version T_8NH_3 is completely stable in air and does not disintegrate or polymerise at room temperature although degeneration may occur when it is dissolved in water or strongly basic solutions [3] .In neutral or acidic media, however, it is completely stable. The white powdery microcrystalline product was analysed through ^{1}H NMR, ^{29}Si NMR, and IR.

^{1}H NMR (in $CDCl_3$) showed three main peaks at 3.39ppm, 1.9ppm and 0.86ppm corresponding to the propyl CH_2 protons. Literature values [3, 8, 9] in D_2O are given as 3.041ppm, 1.79ppm and 0.81ppm respectively. A broad shift in DMSO-d6 at 3.69ppm indicated the presence of the NH_3 groups. ^{13}C NMR spectra gave three main carbon peaks at 42.15ppm, 22.9ppm, and 9.9ppm.

These compare well with the literature values in DMSO-d_6 of 41.04ppm, 20.63ppm and 8.44ppm respectively. The ^{29}Si NMR showed a large main peak at –66.12ppm which compares very well with the –66.4ppm literature value. The IR spectra showed a stretch at 1580cm^{-1} corresponding to the N-H stretch of the NH_3^+ group and a large Si-O-Si stretch at 1068cm^{-1}.

2.2.4 Synthesis of Octa(3-mercaptapropyl)silsesquioxane (T_8SH_8). (4)

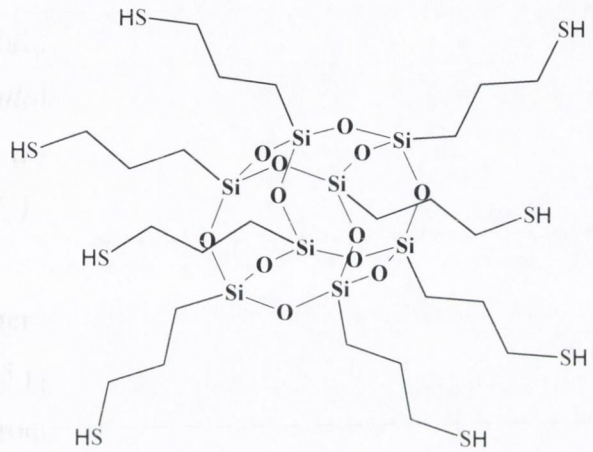

Figure 2.6. *Octa(3-mercaptapropyl)silsesquioxane.*

T_8SH was prepared following the published procedure [4] with the same modifications employed in the synthesis of T_8Cl the mixture of (3-mercaptopropyl) trimethoxysilane and concentrated HCl in methanol was heated under reflux for 48 hours. The solvent was dried under vacuum (producing an oily product, which was obtained in good yield of 70 %). The product was characterised by ^{1}HNMR, ^{13}CNMR, ^{29}SiNMR and IR analysis.

The ^{1}HNMR in $CDCl_3$ showed a peak at 1.4ppm corresponding to the SH group. Literature value [4] is given at 1.16ppm in C_6D_6. The propyl peaks fell in $CDCl_3$ at 2.6ppm, 1.7ppm and 0.77ppm. The corresponding literature values in C_6D_6 were given as 2.280ppm,1.7ppm and 0.8ppm respectivly. ^{13}C NMR values in $CDCl_3$ fell at 27.1ppm,26.9ppm and 10.4ppm .The corresponding literature values in C_6D_6 were quite similar and are given as

27.91ppm, 27.31ppm and 11.12ppm respectivly.The ^{29}Si NMR in $CDCl_3$ gave a single large peak -64.5ppm whereas the literature value in C_6D_6 was given at –66.16 ppm, this being indicative of a fully condensed octahedral POSS .Further evidence of the successful synthesis was given by the IR spectrum with a stretch at 2554 cm^{-1} corresponding to a S-H vibration, and a large Si-O-Si stretch at 1106 cm^{-1}

2.2.5 Synthesis of Octa(allyl)silsesquioxane T8(allyl) . (5)

Synthesis of Octa(allyl)Silsesquioxane was attempted by two different methods, acid and base catalysed hydrolysis of the precursor allyltrimethoxysilane in methanol. Acid catalysis resulted in colourless oily product. This product was characterised by $^{1}HNMR$, $^{13}CNMR$, $^{29}SiNMR$ and IR analysis. The $^{1}HNMR$ spectrum gave three peaks at 5.7ppm, 4.9ppm and 1.6 ppm in the ratio of 1:2:2.The $^{14}CNMR$ DEPT showed the presence of two CH_2 and one CH peak. Upon IR analysis, the characteristic Si-O-Si stretch was seen at 1117cm^{-1} and also several peaks representing C=C double bonds. The $^{29}SiNMR$ of the product showed one peak at –66.9ppm, implying that the product was one pure T_8 FCPOSS compound.

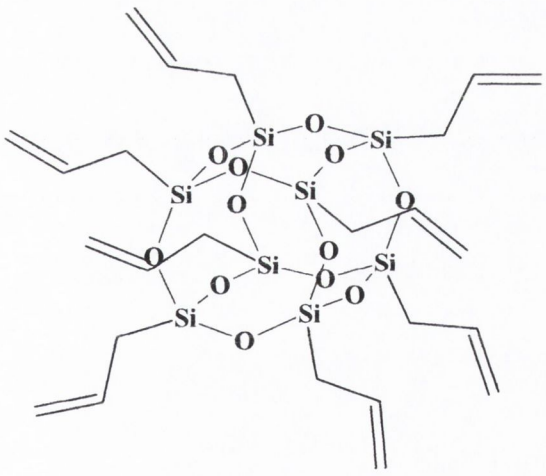

Figure 2.7. *Illustration of Octa(allyl)silsesquioxane "T_8Allyl"*

In the case of the base catalysis where the mixture of allyltriethoxysilane and tetrabutylammoniumhydroxide was heated under reflux producing a white

precipitate, the product was insoluble in many organic solvents and therefore proved difficult to characterise. It was found to be only sparingly soluble in THF and acetone. ^{29}Si NMR of the product gave only one weak peak at –72.9 ppm. This is a characteristic ^{29}Si NMR shift for a T_{10} POSS. ^{1}H NMR spectrum in d-acetone showed 3 main peaks at 5.7, 4.9 and 1.4 ppm in a ratio of 1:2:2 .According to NMR data the condensation resulted in fully condensed T_{10} POSS

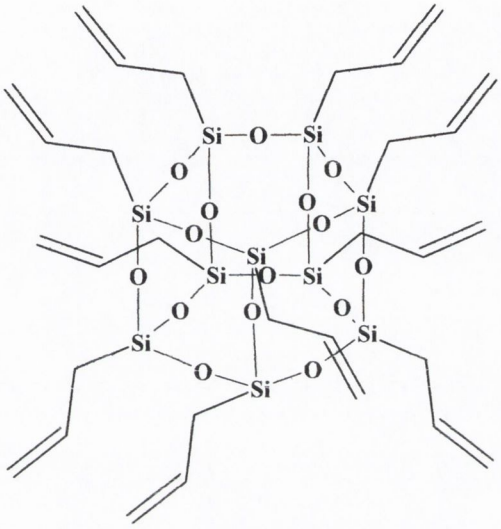

Figure 2.8. *Illustration of proposed structure of Deca(allyl)silsesquioxane T_{10}Allyl.*

2.3 Preparation and characterisation of Cp functionalised POSS.

The reactions on the preparation of Cp functionalised POSS are summarised in the Scheme 2.3 below. Most of this work involved the synthesis of precursor molecules in inert atmosphere or vacuum because many of the starting materials were extremely air and moisture sensitive.

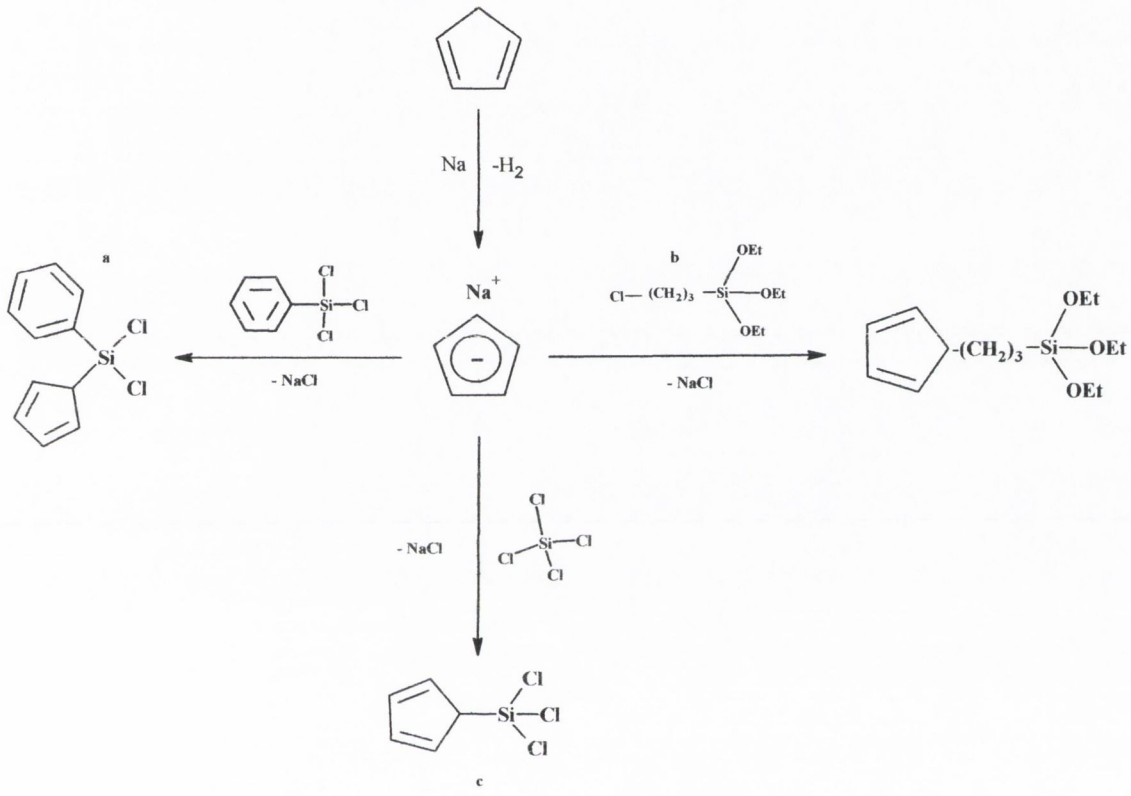

Scheme 2.2 *Schematic presentation of organosilicon precursors synthesis.*

2.3.1 Synthesis of $Cp_8Si_8O_{12}$ (6)

The first step in our synthesis was the preparation of monomeric CpNa by fractional distillation of Cp dimers under inert atmosphere, followed by the removal of an allylic proton from the cyclopentadiene molecule by the use of granular sodium metal as illustrated in scheme 2.3 below.

Scheme 2.3. *Preparation of CpNa in dry THF, after distillation of the Cp_2 dimer.*

The CpNa was reacted with an appropriate halogenosilane derivative in dry solvent resulting in the removal of the sodium halide and addition of the cyclopentadienyl group to result in new organosilicon precursors.

Thereafter $CpSiCl_3$ was synthesised by the reaction of $SiCl_4$ with NaCp in THF. Hydrolysis of $CpSiCl_3$ in THF in the presence of an excess ammonium carbonate (as shown in scheme 2.3) gave the completely condensed oligosilsesquioxane $Cp_{10}Si_{10}O_{15}$ [T_{10}] as a major product with some admixture of $Cp_8Si_8O_{12}$ [T_8]

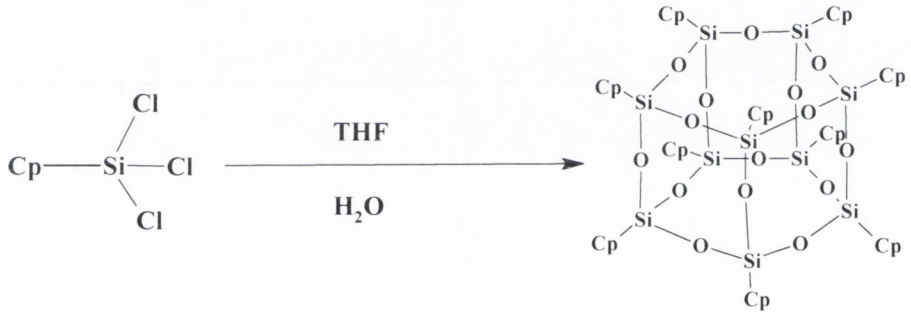

Scheme 2.4. *Synthesis of $Cp_{10}Si_{10}O_{15}$ [T_{10}]*

The compound was characterised by ^1H and ^{29}Si NMR, IR, ES MS spectra and SEM. ^1H NMR (400 MHz, d. C_6H_6, 298K) has shown very broad peaks of cyclopentadienyl group at 5.71 (H-C=) and 3.22 (H-C-) ppm with an appropriate 4:1 ratio and some residual solvent (THF and Et_2O) peaks (see Fig. 2.9). ^{29}Si NMR contained three signals at –71.50, -74.39 and –77.04 ppm. The presence of 3 signals in ^{29}Si NMR can be explained by the different positions of Si substituents in the Cp-rings (Fig. 2.10). IR spectra of the compound (in KBr) contained characteristic C-H bands and also a very broad band of Si-O-Si stretching with the maximum at 1105 cm^{-1}. The ES MS spectrum has shown a maximum M^+ peak of 1170, which corresponds to a $Cp_{10}Si_{10}O_{12}$ (T_{10}) fragment.

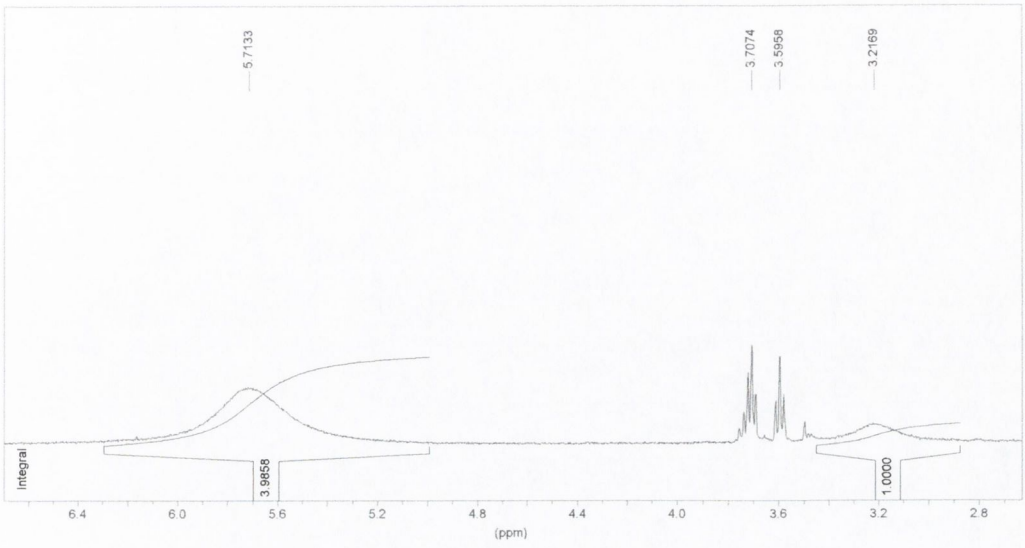

Figure 2.9. *^{1}H NMR of $Cp_{10}Si_{10}O_{15}$.*

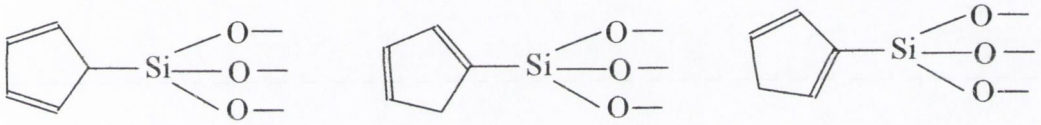

Figure 2.10 *Possible positions of Si substituents in Cp-rings.*

2.3.2 Synthesis of $PhCpSiCl_2$. (7).

A solution of CpNa in THF was added drop wise to phenyltrichlorosilane in a1:1 ratio at 0°C .The mixture was stirred and allowed to stand overnight. The cream coloured oily product was analysed using ^{1}HNMR. The ^{1}HNMR spectra showed a broad multiplet between 6.9ppm and 7.9ppm, which confirms the presence of the phenyl ring. Also present was a multiplet between 5.24ppm to 5.01 ppm, and a second one at 2.97ppm. Both corresponding to the cyclopentadiene ring.

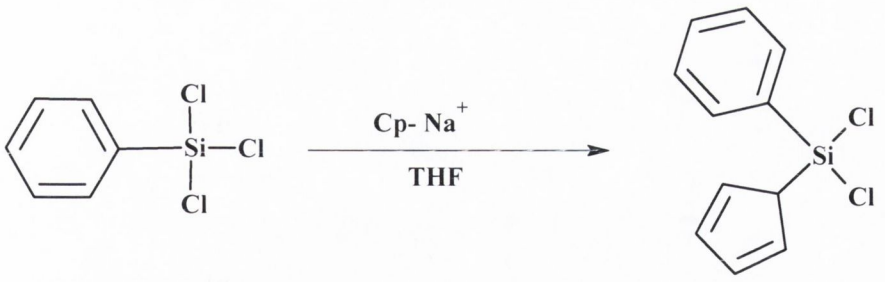

Scheme 2.5. *Synthesis of PhCpSiCl*$_2$.

2.3.3 Hydrolysis of Cp(Ph)SiCl$_2$. (8)

Hydrolysis of Cp(Ph)SiCl$_2$ was achieved by drop wise addition of water under inert atmosphere in dry THF with catalytic amounts of HCl, this resulted in the product (Cp(Ph)Si)$_n$O, which would appear to be highly acid sensitive, giving the apparent loss of Cp groups from the product. The ^{1}H NMR spectrum shows a broad signal corresponding to the Ph group at 7.82-721ppm and a broad Cp signal at 6.32-5.2 ppm. Also present is a signal between 2.81-2.11 ppm indicating again the presence of dimerised Cp. The Ph:Cp integrating ratio was 7:1. The ^{13}C NMR spectrum contained a signal between 133.72-124.85ppm indicating a combination of the Ph and Cp signals, a Cp signal at 67.43-65.36ppm and another one at 25.08ppm; presumably indicating the presence of fragments related to Cp dimer. The IR spectrum (in KBr) indicated the presence of C-H bands at 2954 cm^{-1} and 1430 cm^{-1}, and also showed a strong broad band of Si-O-Si stretching with a maximum of 1063 cm^{-1} .

The ES MS spectrum showed a M$^+$ peak at 1888 corresponding to the (PhCpSiO)$_{10}$-Ph-Cp fragments, with further peaks at 1762 -(PhCpSiO)$_9$-Cp, 1685- [(PhCpSiO)$_9$-Ph-Cp], 1153 [(PhCpSiO)$_6$-Cp].

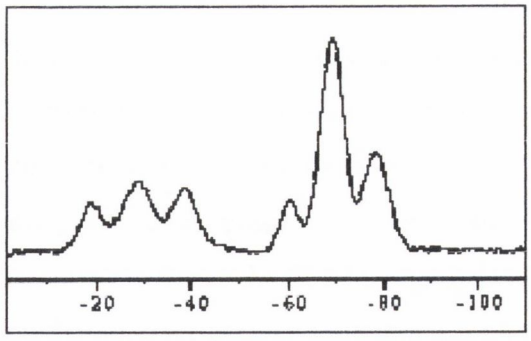

Figure 2.11 *MAS ^{29}Si NMR of compound 2 polymer. Showing six silicon peaks.*

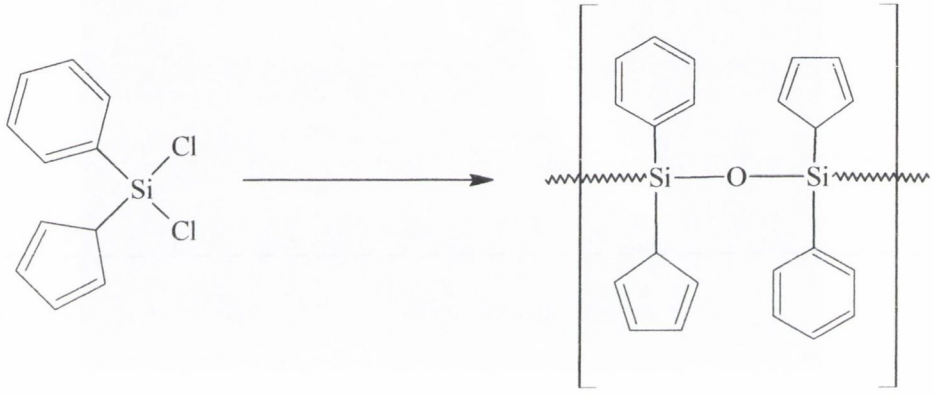

Scheme 2.6 *Showing oligamerisation of* Cp(Ph)SiO.

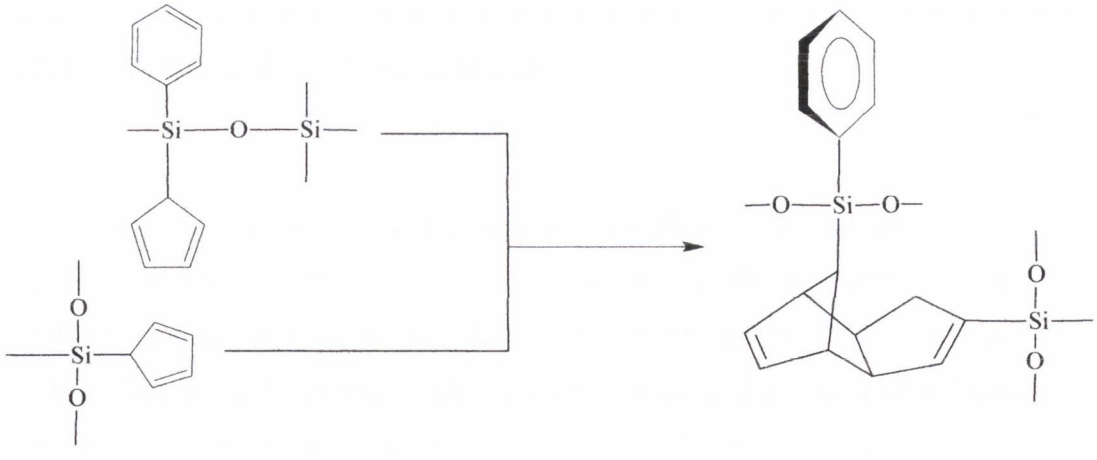

Scheme 2.7 *Showing interlinking between two Cp moieties on adjacent oligomeric strands of 2 via. Diels-Alder cycloaddition.*

Analysis of the data above indicates there is an elimination of Cp-groups in the system, presumably due to acidic cleavage of Si-Cp bond. ^{1}HNMR data also clearly show the presence of dimerised (via the Diels-Alder reaction) Cp-groups. The suggested structure of the polymeric product is shown in scheme above. The polymerisation takes place in a very random order giving six different silicon environments. From the SEM image below we see that this lack of order failed to give the polymer regular spherical morphology.

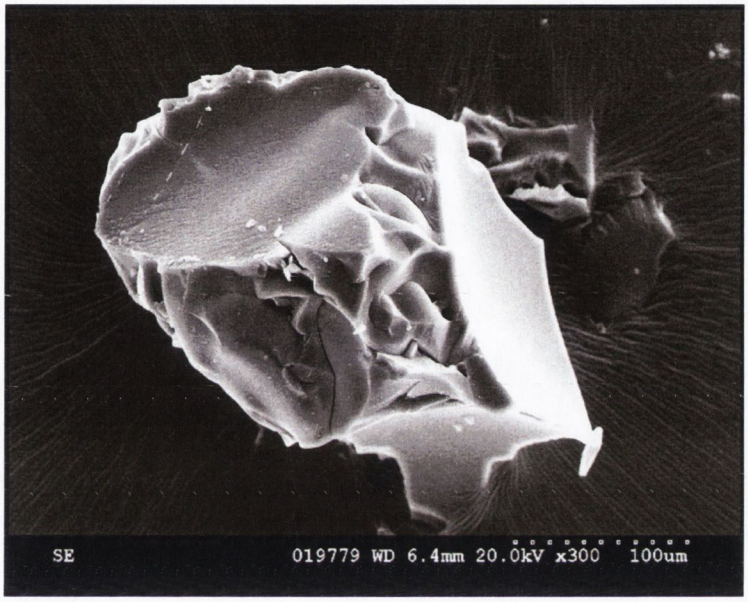

Figure 2.12. *SEM image showing the amorphous morphology of* $(Cp(Ph)SiO)_n$.

2.3.4 Synthesis of $Cp(C_3H_6)_8Si_8O_{12}$ (9).

After the synthesis of compounds **6, 7** and **8,** we have concluded that the Cp-Si bond in these compounds is quite sensitive to acids, inevitably leading to Cp-loss. For this reason we decided to investigate presumably more stable systems based on (3-cyclopentadienylpropyl)triethoxysiloxane. (3-Cyclopenta dienylpropyl) triethoxy -silane was prepared from (3-chloropropyl)-triethoxysilane and CpNa. The hydrolytic condensation of (3-cyclopentadienylpropyl)-triethoxysilane with water in acetone yielded mostly T_8 silsesquioxane $(CpC_3H_6)_8Si_8O_{12}$. The compound was characterised by ^{1}H and

^{29}Si NMR, IR and MS spectra. The ^{1}HNMR spectrum has shown very broad peaks for Cp-ligands from 6.4 to 5.99 ppm and at 3.51 ppm and CH_2 groups from 1.85 to 0.77 ppm. The ^{29}Si NMR contained only a broad signal at-76.50 ppm. IR spectra have shown a very broad band at 1155 cm^{-1} due to Si-O-Si vibrations. The MS (ESI TOF) spectrum in CH_3CN contained the $[M]^+$ peak at 1272 and peaks of several fragments formed due to Cp- or CpC_3H_6 – elimination.

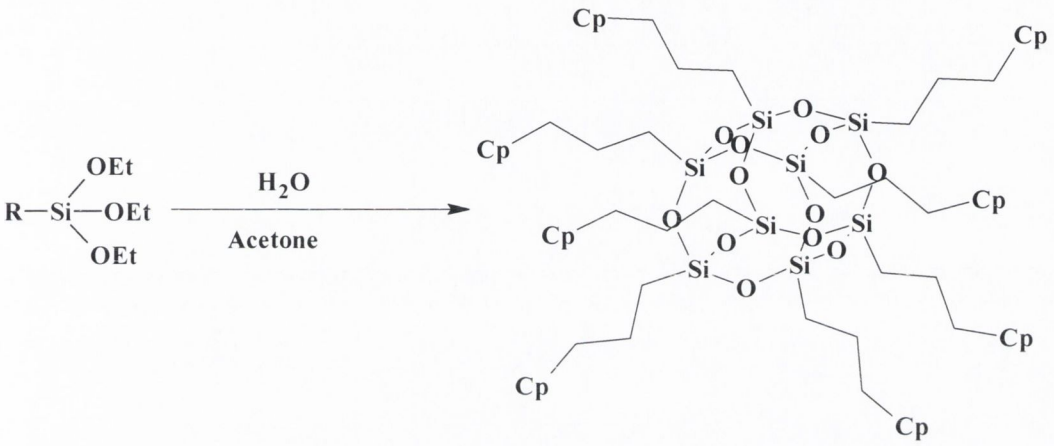

Scheme 2.8 Synthesis of $(CpC_3H_6)_8Si_8O_{12}$ T_8propyl-Cp POSS.

An alternative, but ultimately less fruitful route was also tried. T_8Cl POSS was prepared (as outlined above in section 2.2.1) in THF and was stirred until all the ligand dissolved. CpNa dissolved in THF at 0°C was then added drop wise and allowed to stir for 72 hrs. The solvent was removed by vacuum and Diethyl Ether added and allowed to stir for 3 hrs. After stirring, a white precipitate (NaCl) formed. The ether soluble component was then removed by decantation and dried under vacuum leaving a very pale yellow product (0.19 g, 84 %). The compound was characterised quickly after synthesis while still cold by ^{1}H NMR, ^{13}C NMR, and IR, and compared well to spectra as obtained by the method above. However, once the solution was allowed to warm up to room temperature the solubility began to drop rapidly due to the Cp rings undergoing dimerisation, unfortunately causing the sample to polymerise over time, and eventfully making the sample insoluble and difficult to characterise. These problems will be discussed in greater detail in the following chapter. The initial

^{1}H NMR (400 MHz, d. C_6H_6, 298K) showed very broad peaks of cyclopentadienyl group at 5.31 (H-C=) and 3.30 (H-C-) ppm . The three characteristic propyl peaks fell at 3.68 ppm, 1.52 ppm and 0.97ppm. The ^{13}C NMR spectrum showed the three expected propyl peaks 46.72ppm, 26.05ppm and 9.6ppm, all of which compare well to the T_8Cl starting material values above. The ^{29}Si NMR spectrum shows a single sharp peak at –65.8 ppm, which matches the value for the starting T_8Cl ligand very closely. The IR spectrum of the product indicated the presence of C-H vibrations at 2944, 2726 and 2671 cm^{-1}. Si-O-Si stretching at 1155 cm^{-1} and at 484 cm^{-1} was also present

2.4 Conclusions

The chloride and amino functionalised octasilsesquioxanes were produced at exceptionally higher yields compared to the literature. The introduction of the heating under reflux allowed preparing octasilsesquioxanes very quickly and with much higher yields.

Poor solubility of octaaminopropylsilsesquioxane made it difficult to work with, as it proved to be soluble in THF making reactions possible. Octa(allyl)silsesquioxane was synthesised in high yield and very high purity via acid catalysed hydrolysis. It was found that base catalysed hydrolysis of the allyltriethoxysilane results in the formation of highly insoluble decallylsilsesquioxanes (T_{10}).

New Cp-functionalised POSS have been prepared. Sol-gel condensation process revealed that Cp-Si bond is very sensitive to acidic media and the process should be performed in the presence of bases (e.g. ammonium carbonate). The new POSS compounds could also be further modified into different metal-containing products by metallation of the free C_5H_5-groups. This could be a very promising method for the preparation of new controlled pore size metal-containing materials.

All the functionalised POSS seem to be promising precursors for preparation of novel polymeric and oligomeric derivatives.

2.5 References

1. Dare, E.O.; Olatunji, G.A.; Ogunniyi, D.S.; Lasisi, A.A. *Polish.J.Chem.* **2005**,*79*,109-114.
2. Harrison, P.G.; *J. Organometal. Chem.* **1997,** *542*, 141-183.
3. Feher, F.J.; Budzichowski, T.A. *Polyhedron* **1995,** *14*, 3239-3253.
4. Feher, F.J.; Wyndham, K.D.; Soulivong, D.; Nguyen, F. *J. Chem. Soc. Dalton Trans.* **1999,** 1491-1497.
5. Dittmar, U.; Hendan, B.J.; Flörke, U.; Marsmann, H.C. *J. Organometal. Chem.* **1995,** *489*, 185-194.
6. Togni A., Halterman R.L. (1998) Metallocenes, Synthesis Reactivity, Applications, vol. 2, Wiley VCH, Weinheim.
7. Jutzi P., Heidemann T., Neuman B., Stammler H.G. *Organomet. Chem.* **1994,** *472*, 27 - 38.
8 .Čermák, J. ;Kvíčalová, M.; Blechta, V. ;Čapka, M., Bastl, .ZJ. *Organomet. Chem.* **1996,** *50,* 77 – 84.
9. Weidner.R.;Zeller,N.;Deubzer,B.;Frey,V. *U.S. pat.* **1991** ,5 047 492.
10. Gravel, M.C.; Laine, R.M. *ACS polym prep.* **1997**, *38,* 155-156.
11. Seckin, T.; Gultek , A.; Koytepe, S. *Turk. J. Chem.* **2005** ,*29,* 49-59.
12. Feher, F.J.; Wyndham, K.D.; Scialdone, M.A.; Hamuro, Y. *Chem. Commun.* **1998,** 1469-1470
13. Feher, F.J.; Terroba, R.; Ziller, J.W. *Chem. Commun.* **1999,** 2309-2310
14. Lichtenhan, J.D. *Comments Inorg. Chem.* **1995,** *17*, 115-130.
15. Feher, F.J.; Budzichowski, T.A. *J. Organometal. Chem.* **1989,** *379*, 33-40
16. Feher, F.J.; Wyndham, K.D. *Chem. Commun.* **1998,** 323-324
17. Feher, F.J.; Soulivong, D.; Eklund, A.G.; Wyndham, K.D. *Chem. Commun.* **1997,** 1185-1186
18. Feher, F.J.; Budzichowski T.A.;Blanski,R.L.;Weller,K.J.;Ziller,J.W. *Organometal. Chem* **1991**,*10*,2526-2528.

Chapter 3

Reactions of Functionalised POSS

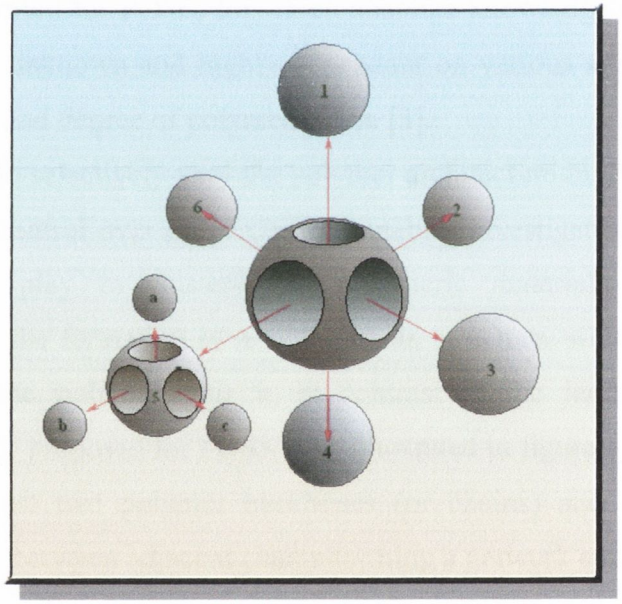

3.1 Introduction

The main objective in this section of the thesis is to develop the chemistry of selected POSS with reactive functionalities using new organic and organometallic approaches. Several silsesquioxane-based approaches to polymeric materials have previously reported especially by Lichtenhan et al [1]. Lichtenhan has shown how chemically and structurally well-defined POSS macromers can be utilised as polymer additives or for the preparation of linear polymeric silsesquioxane-based systems [2]. The distinct structure of the POSS components in such materials enables the establishment of property relationships based on chain structure and composition. This is in contrast to that previously reported for POSS, for which absolute knowledge of polymeric structure is largely unknown and highly dependant on various silane reagents, reaction conditions and degree of polymerisation [3].

The ability to selectively vary the polymer architecture in POSS systems enables additional control over properties and enables investigation on the role that polymer can play in cluster-based polymeric materials. The linear architectures allow the formation of a single chain structure, which comprises the backbone of the polymer, this is in contrast to the ladder/polycyclic structures previously proposed for POSS [4]. (Illustrated in figure 3.1, which are composed of at least two polymer backbones (or chains) and may contain covalent cross links between adjacent chains forming a network structure.

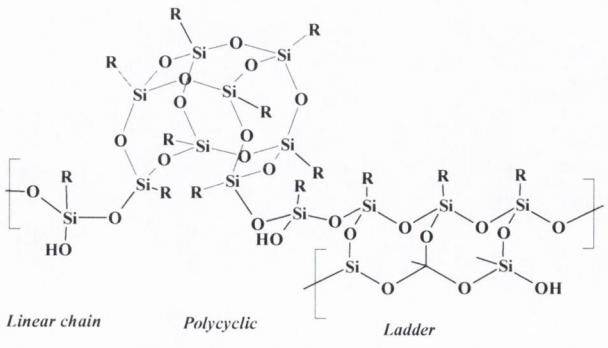

Figure 3.1 *Generalised structure for Polymeric silsesquioxanes.*

The ICPOSS component in linear systems is anticipated to behave similarly to that of a conventional hard block in hydrocarbon-based polymers [5]. Depending on the type of functionality contained on the POSS macromer and on the desired polymer architecture, macromolecular systems can be constructed which contain POSS main chain, side chain or chain terminus groups [6]. Most of these approaches are based on the reactivity of silanol groups, which enable the preparation of polymers through the formation of bridging Siloxane units [7]. However, secondary manipulations of the structure and functionality POSS are very limited. These have involved mostly standard organic manipulations such as hydrogenation, chlorination, hydrosilation, esterification, acylation and epoxydation [8]. All these manipulations and transformations occur in good yield while at the same time retaining the FCPOSS structure. Selective framework manipulations however in FCPOSS have not yet been reported, except perhaps cleavage.

3.1.1 Diels-Alder cycloaddition.

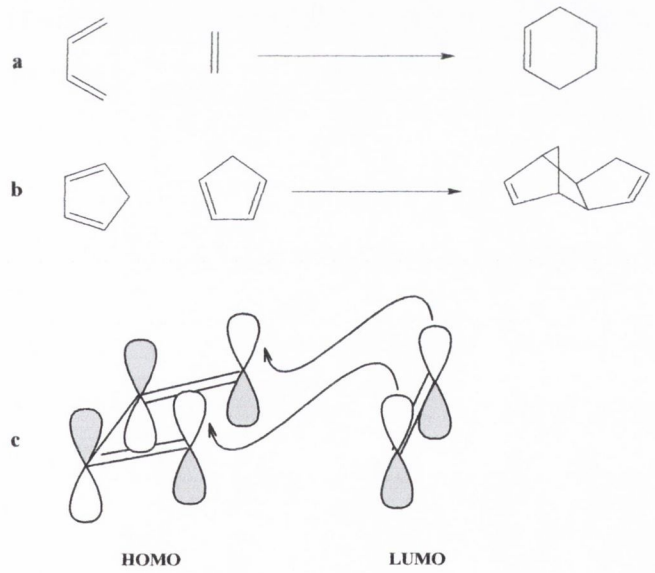

Scheme 3.1. a*) General scheme for Diels-alder reaction .b) Diels-Alder reaction between two Cp moieties .c) Showing the Suprafacial addition between the HOMO of one Cp and the LUMO of the other Cp. Notice the bonding overlap between lobes on the same face of the first Cp and lobes on the same face of the second.*

The Diels-Alder reaction plays a critical role in the polymerisation process of the molecules described in this chapter. The Diels-Alder reaction is a [4+2] π electron cycloaddition between a diene (4 π electrons) and a dienophile (2 π electrons), to yield a cyclohexane product. Typically this tends to yields a trans product due to the reaction favouring a suprafacial geometry.

3.2 Results and discussion.

3.2.1 Oligomerisation of $Cp_{10}Si_{10}O_{15}$ (10)

Dimerisation of monosubstituted cyclopentadienyl-siloxane derivatives has been noticed before as an obstacle for the preparation of Cp-functionalised polysiloxanes and gels [9]. In this work we decided to use this property for the preparation of POSS polymers. The polymerisation was achieved *via* the Diels – Alder reaction by stirring the mixture at room temperature and then by heating it under reflux The soluble products were studied by ^{1}H and ^{29}Si NMR, IR and MS spectra and Gel Permeation Chromatography The ^{1}H NMR spectrum has shown a series of very broad multiplets from 6.65 to 5.45ppm and from 3.55 to 1.7 ppm attributed to cyclopentadienyl ligands and Diels-Alder adducts. The ^{29}Si NMR spectrum contained a number of signals between –71.50 and -78.73 ppm. IR spectra of the these products (in KBr) contained characteristic C-H bands at 2962(m) and 1446 cm^{-1}, and also a very strong and broad band of Si-O-Si stretching, with the maximum at 1089 cm^{-1}. The GPC chromatogram shows a broad distribution of molar masses with M_p = 1335 g/mol and an average molar mass of the oligomer of M_w = 2761 g/mol. The average mass lies between the mass of $(T_{10})_2$ (theoretical mass 2340) and $(T_{10})_3$ (theoretically 3510). The number average molar mass ($M_{n)}$ is 1859 g/mol. The heterogeneity index M_w/M_n is 1.485.

ESI /MS has been shown to be a very good technique in the analysis of functionalised silsesquioxanes [10], certain dendrimers [11] and polymers [12]. ESI TOF MS spectra of our materials were quite informative. The MS spectrum

of products has shown several peaks assigned to doubly and triply charged oligomeric species: 1592.5 $[(T_{10})_3 - 5Cp]^{2+}$, 1517 $[(T_{10})_4 - 2Cp]^{3+}$, 1451 $[(T_{10})_4 - 5Cp]^{3+}$, 1148.3 $[(T_{10})_3 - Cp]^{3+}$, 1083 $[(T_{10})_3 - 4Cp]^{3+}$, 780 $[(T_{10})_2]^{3+}$. This data demonstrates the clear presence of $(T_{10})_2$, $(T_{10})_3$ and $(T_{10})_4$ oligomers, which is quite consistent with the GPC results.

According to this data the most plausible composition of the material is a mixture of several linked T_{10} oligomers similar to the one shown in Scheme 3.3 below. As one would expect the degree of polymerisation is not very high (4 units maximum).

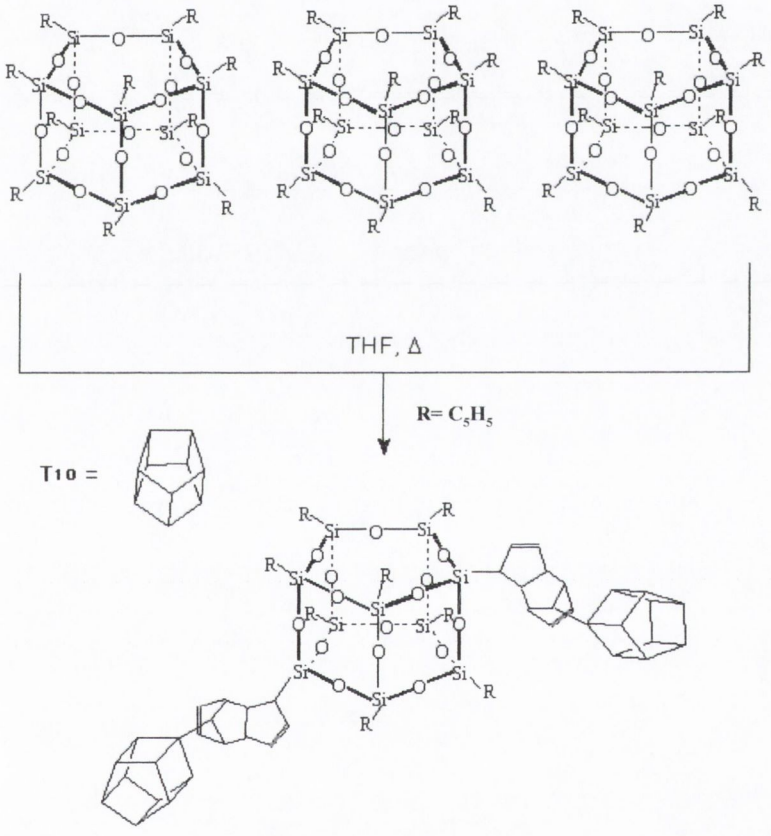

Scheme 3.2. *Schematic presentation of polymerisation of $Cp_{10}Si_{10}O_{15}$ fragments via Diels –Alder reaction. More although only two are shown here the resulting units is composed of many monomers extending in all directions*

SEM was also used to examine the insoluble main product. As can be clearly

seen from figure 3.2, the product consists of relatively uniform dice-like micro-spherical aggregates with an average diameter of 2.05 μm. These spheres in turn appear to be composed of even smaller spheres as also shown in figure 3.2. This is consistent with dendritic growth mechanism of the monomer units *via* the Diels-Alder reaction as shown in scheme 3.1.

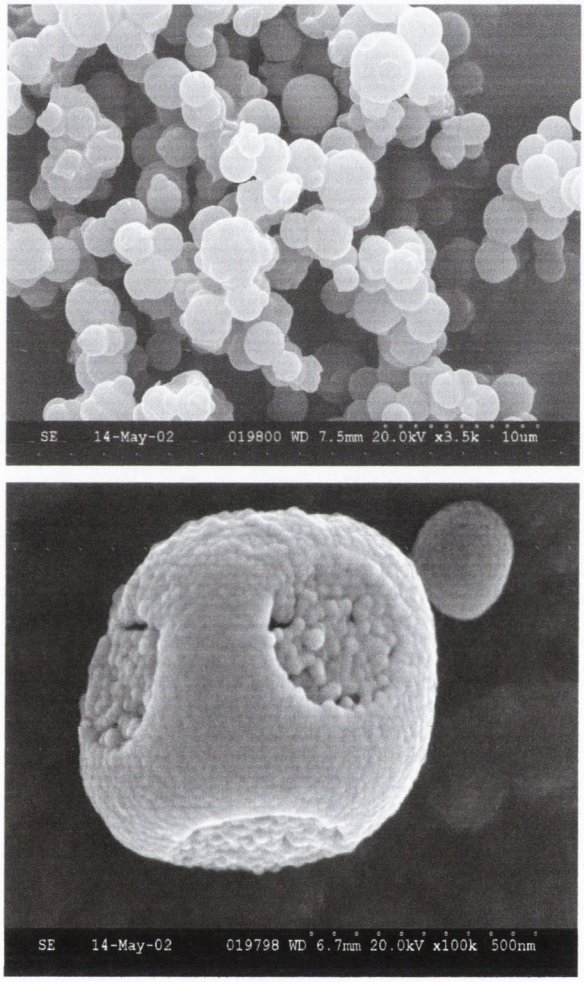

Figure. 3.2. *SEM image of polymeric product* ***10*** *showing the central "sphere" with three of the six faces visible. As can be seen from these images this material also is composed of spherical particles (with an average diameter of 2.8 μm) joined together into branched linear assemblies. Notice also the reasonably high degree of homogeneity and uniformity of the spherical oligomers*

After the synthesis and polymerisation of compound **10** it was again concluded that that Cp-Si bond in these oligomers are quite sensitive to acids, inevitably leading to Cp-loss. For this reason we decided to investigate presumably more stable systems based on (3-cyclopenta dienyl propyl)triethoxysiloxane. (3-Cyclopentadienylpropyl) triethoxy silane was prepared from (3-chloropropyl)-triethoxysilane and CpNa. The hydrolytic condensation of (3-cyclopentadienylpropyl)-triethoxysilane with water in acetone yielded mostly T_8 silsesquioxane $(CpC_3H_6)_8Si_8O_{12}$ (**11**) (Scheme 3.5). The compound was characterised by ^1H and ^{29}Si NMR, IR and MS spectra. The ^{1}HNMR spectrum has shown very broad peaks for Cp-ligands from 6.4 to 5.99 ppm and at 3.51 ppm and CH_2 groups from 1.85 to 0.77 ppm. The ^{29}Si NMR contained only a broad signal at-76.50 ppm. IR spectra have shown a very broad band at 1155 cm^{-1} due to Si-O-Si vibrations. The MS (ESI TOF) spectrum in CH_3CN contained the $[M]^+$ peak at 1272 and peaks of several fragments formed due to Cp- or CpC_3H_6 – elimination.

3.2.2 Polymerisation of $[(CpC_3H_6)_8Si_8O_{12}.]_n$ (11)

Compound $CpC_3H_6)_8Si_8O_{12}$ can be easily polymerised by heating *via* the Diels-Alder reaction in THF, giving again soluble and insoluble T_8 based products $(CpC_3H_6)_8Si_8O_{12}]_n$ (Scheme3. 7 overleaf).

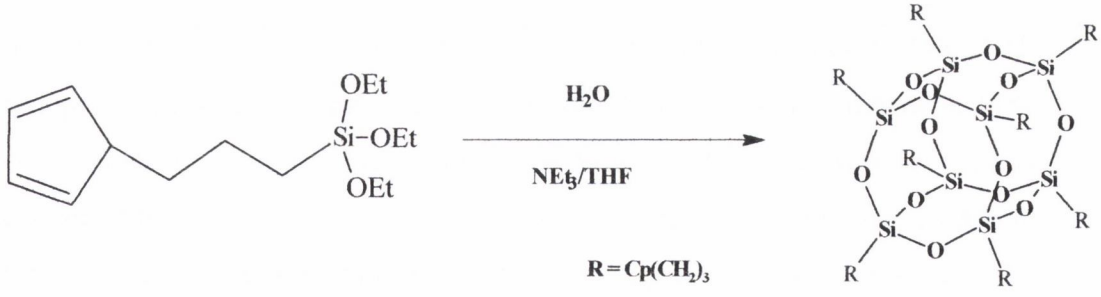

Scheme 3.7. *Showing the preparation of compound* $(CpC_3H_6)_8Si_8O_{12}$.(**11a**)

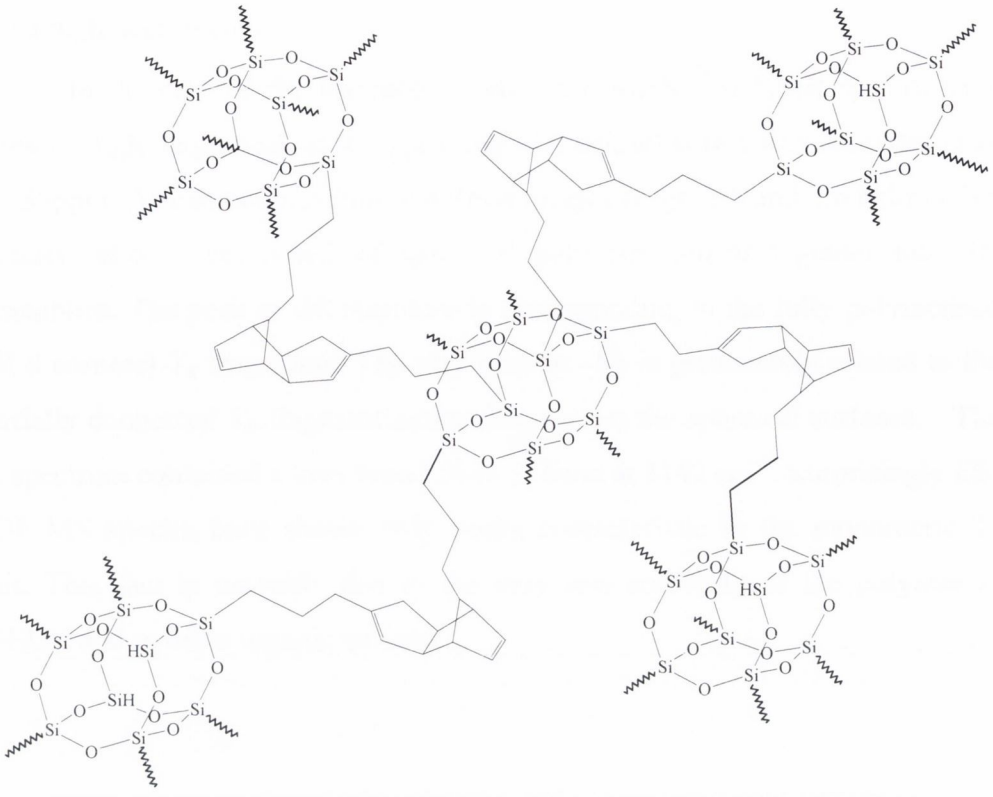

Figure 3.3. *Illustration of the starburst polymer* ***(11) form*** *of* $[(CpC_3H_6)_8Si_8O_{12}]_n$

The compound was characterised by ^1H and ^{29}Si NMR (including solid state MAS NMR), IR, and MS spectra. . ^1H NMR spectra of the soluble compounds contained very broad peaks for Cp-ligands from 6.4 to 5.99 ppm, Cp-dimer-ligands from 6.61 to 2.17 ppm and at 3.51 ppm and broad multiplets of CH_2 groups from 1.85 to 0.77 ppm. IR spectra have shown a very broad band at 1155 cm^{-1} assigned to Si-O-Si vibrations. The MS (ESI TOF) spectrum in CH_3CN contained the $[M]^+$ peak at 1272 and peaks of several fragments formed due to Cp- or CpC_3H_6 – elimination. GPC shows a very broad distribution of molar masses with M_p = 1960 g/mol. The average mass (M_w) of 5156 g/mol is close to that for the $(T_8)_4$ (theoretically 5088) fragment. The number average molar mass (M_n) is 2471 g/mol. The heterogeneity index M_w/M_n of 2.086 is quite high. After the analysis of all data we come to the conclusion that the soluble fraction is most likely a mixture based on T_8 oligomers with a broad mass distribution

and a high heterogeneity.

In the case of the insoluble product the MAS ^{29}Si NMR spectra have show a single large peak at -68 ppm (Fig. 3.6 below) with a tiny shoulder peak at –55ppm. As can be seen from the SEM images (Figs. 3.5 and 3.6 below) this material also is composed of spherical polymers joined together into 3D assemblies. The peak at -68 therefore is corresponding to the fully polymerised (all 8 corners) T_8 fragments. The tiny peak at –55 is presumably related to the partially connected T_8 fragment molecules, *e.g.* on the spherical surfaces. The IR spectrum contained a very broad Si-O-Si band at 1142 cm^{-1}. Surprisingly ESI TOF MS spectra have shown only peaks characteristic to the monomeric T_8 unit. This fact is probably due to the very low solubility of the polymer in CH_3CN and in other organic solvent.

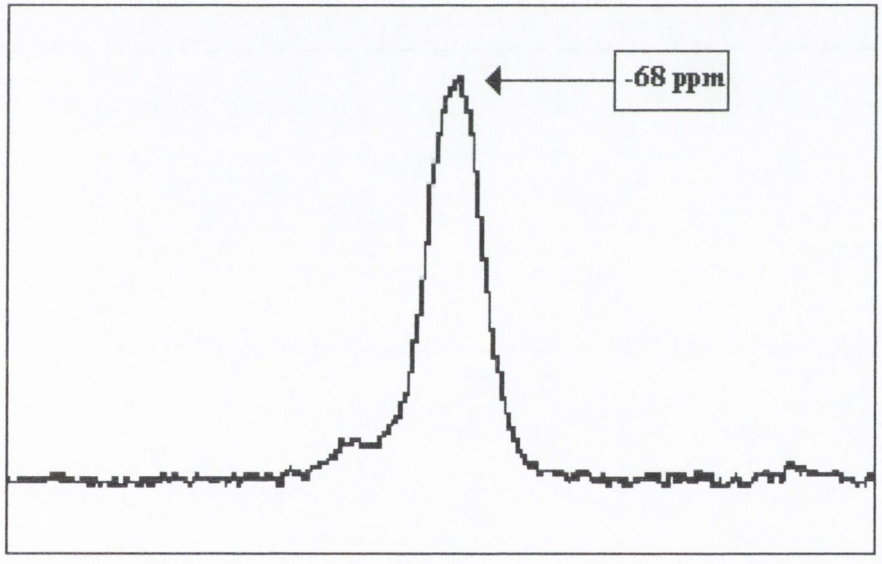

Figure 3.4. *MAS ^{29}Si NMR of polymeric compound 11.showing the predominance of the peak at –68ppm indicative if a mostly T_8 morphology.*

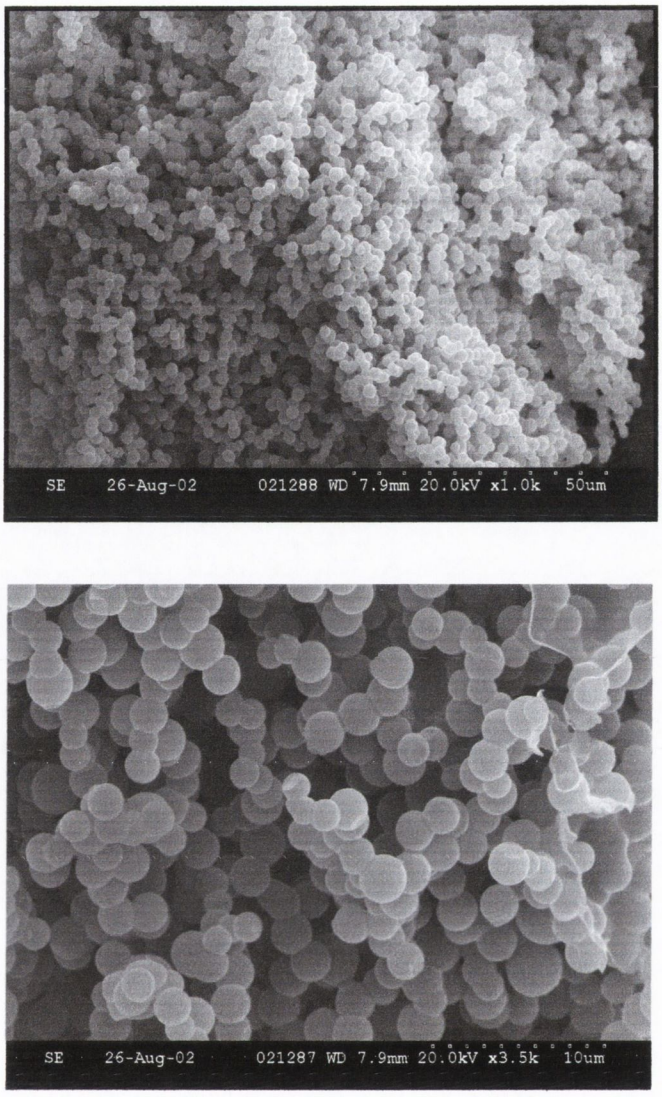

Figure 3.5. *SEM image of the polymeric product 11.This illustrates the control pore size ability of these compounds.*

SEM image of the polymeric product 11 (figure 3.5) have shown that this material is composed of spherical particles (with an average diameter of 2.8 μm) joined together into branched linear assemblies. There is the reasonably high degree of homogeneity and uniformity of the spherical oligomers homogeneity and uniformity of the spherical oligomers.

3.2.3 Reaction of t-BuLi with FCPOSS T_8Cl. (12)

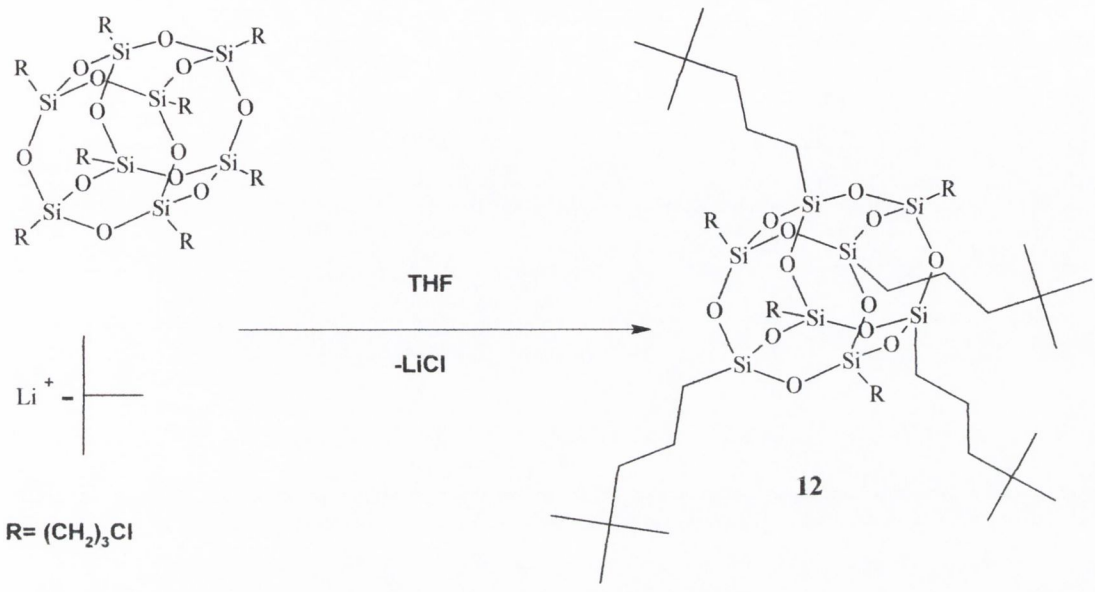

Scheme 3.9. *Showing the formation of product **12***

As would be expected with the use of t- BuLi in the presence of any halogen containing alkyl group; the halogen is readily replaced by the tert-butyl group. From the ^{1}H NMR ratios between reacted and un-reacted pendant groups, it would appear that half of the eight groups have undergone exchange. In diagram 3.9 above we have depicted the four-butyl groups spaced as much away from each other by occupying opposite vertices of the Siloxane cage. This arrangement seems a reasonable assumption when we consider the relative size and steric hindrance of the tert –butyl group.

^{1}H NMR spectroscopy of **12** revealed the unreacted propyl groups, which appear at 3.55ppm, 1.88 ppm and 0.84 ppm. The reacted propyl groups then closely follow at 3.7ppm, 2.03ppm and 0.89ppm respectively. The CH_3 groups as expected appear as a large singlet at 1.04ppm. The ^{13}C NMR proved to show all the appropriate unreacted propyl CH_2 groups at 46.57 ppm, 25.9ppm and 13.6ppm, the reacted propyl groups then follows, falling at 31.8ppm and overlaps somewhat with the unreacted signals to again give signals at 26ppm

and 13.9ppm a quaternary carbon appears at 67ppm and a strong signal corresponding to the CH_3 carbons appears at 27.1ppm. Mass spectrographic analysis in CH_3CN revealed masses at 941.9 g/mol^{-1} 888.9 g/mol^{-1} , 760 g/mol^{-}, 371 g/mol^{-1} and 245 g/mol^{-1} ,which represent the fragments $[M\text{-}2\ Bu^t]^+$,$[M\text{-}3\ But]^+$,$[M\text{-}4But\text{-}(CH_2)_3Cl]^+$, $[M\text{-}3But\text{-}2(CH_2)_3Cl]^{++}$ and $[M\text{-}3But\text{-}\ (CH_2)_3But\ \text{-}\ 4(CH_2)_3Cl]^{++}$ respectively. The ^{29}Si NMR spectrum of molecule **3** showed a broad peak at –66ppm.

3.2.4 Transhalogenation and Grignard reagent synthesis (13,14 & 15)

One of the most common reagents used in organic chemistry are Grignard reagents .The synthesis is relatively straight forward (as illustrated in schemes 3.10 and 3.11)). The initial reaction is a simple transhalogenation ,which involves replacing of chlorines with more reactive iodines this is just a modification of the classic Finkelstein [13] reaction of alkyl halides with sodium iodide in acetone. The transhalogenation product 14 was characterised by ^1H NMR, which have shown propyl peaks with shoulders with the ratio 1:3 compare to original chloropropyl derivatives. Therefore we can conclude that only 2 Cl atoms have been replaced by iodine.

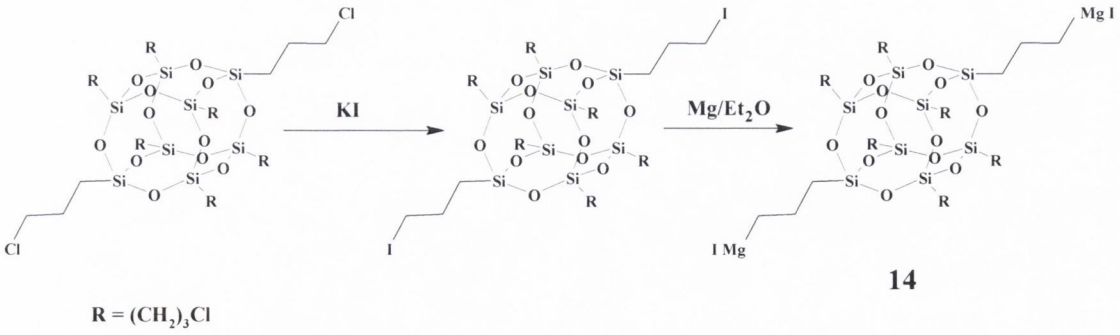

Scheme 3.10. *1) Illustration showing the four phases of the Grignard reagent synthesis.*

This is followed by the normal Grignard synthesis procedure. The product obtained was extremely air and moisture sensitive and it was not soluble in any common organic solvent, therefore it was impossible to characterise it using techniques available for us.

Clearly a molecule containing more than one Grignard functionality could be of immense use as a linker or central core in starburst polymerisation. Especially if reacted with another molecule containing C=O groups, esters etc. In this synthesis the Grignard containing FCPOSS was allowed to be hydrolysed with degassed water and evidence of hydroxyl groups looked for in the NMR as proof of Grignard formation.

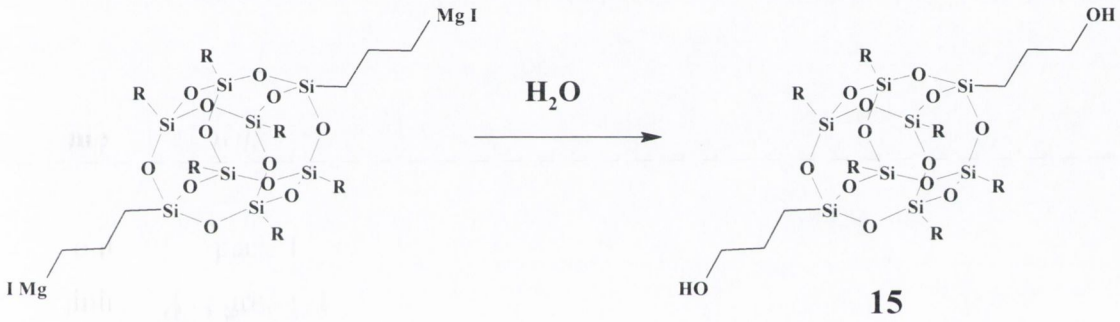

Scheme 3.11. *Hydrolysis and formation of product **15**.*

^{1}H NMR spectroscopy of **15** revealed both the reacted and unreacted propyl groups falling very tightly together, which resonate with broad signals at 3.55ppm, 1.9 ppm and 0.8 ppm. More revealing however is the presence of a broad clear singlet for an OH group falling at 3.2ppm. From the ^{1}HNMR in $CDCl_3$ ratios between reacted and un-reacted pendant groups, it would appear that only two of the eight groups have undergone the reaction. ^{13}C NMR in $CDCl_3$ showed signals at 46.66ppm, 25.8ppm, 8.9ppm, and 0.5ppm corresponding to the unreacted propyl carbons with an additional smaller signal at 12ppm, which corresponds with the two CH_2 groups attached to the hydroxyl group. In scheme 3.11 above the two-hydroxyl groups of **15** are depicted spaced as much away from each other by occupying opposite vertices of the Siloxane

cage. This arrangement again seems a reasonable assumption when we consider the steric hindrance of the intermediate MgI groups. If we assume that compound **15** to be a reasonable product then it follows that it must have come from the intermediate structure **14**. ^{29}Si NMR analysis revealed a single signal corresponding to fully condensed cage at δ –65.47ppm. Mass spectrographic analysis of in CH_3CN of unpurified product revealed masses at 391 g/mol^{-1} 609 g/mol^{-1} and 775 g/mol^{-1} which correspond to the fragments $[M\text{-}2(CH_2)_3OH - 2(CH_2)_3I - 2I]^+$, $[M\text{-}2I\text{-}CH_2]^{++}$ and $[M\text{-}2(CH_2)_3\text{-}2I - 2(CH_2)_3I]^+$ respectively. The mass spec evidence then reveals the presence of some unreacted intermediate molecule **14** and of product **15**, considering the low yield (23%) this would be expected. Also suggestive is the mass at 391a.u. which may indicates the mixture contains a small amount of a product with three reacted halogen groups. Longer reflux times may yield an even higher proportion of multiply substituted POSS Grignard reagents. IR analysis showed peaks at 3655 ppm corresponding to OH stretching as well as those described for T_8Cl in chapter two.

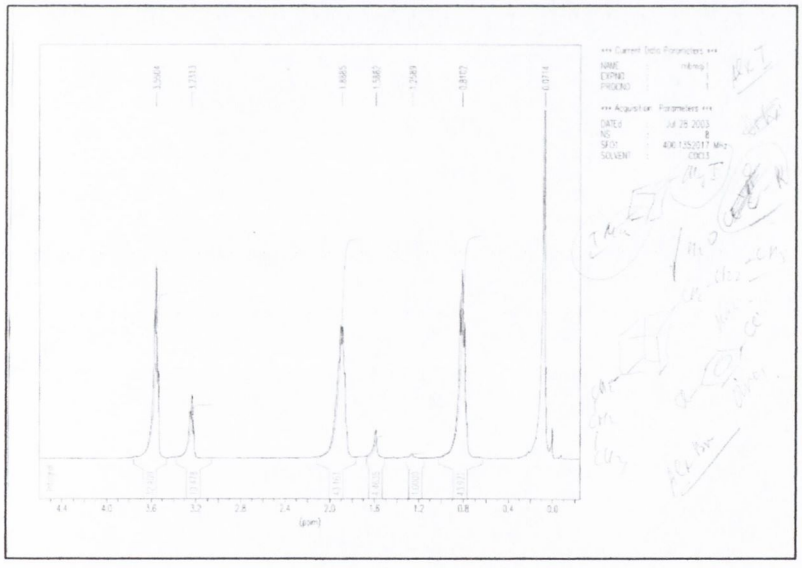

Figure 3.9 *^{1}HNMR of compound 14.*

3.2.5 Reaction of T_8Cl with $LiN[(Si(CH_3)_3)_2]$ (16).

Initially $HN[(Si(CH_3)_3)_2$ was reacted with BuLi in dry THF (Scheme 3.13). Once the reaction was complete the solvent was removed and the resulting product $LiN[(Si(CH_3)_3)_2]$ was recrystallised from hexane, dried in vacuum and then stored under argon . Thereafter T_8Cl was dissolved in dry THF and reacted with 8 equivalents of into the $LiN[(Si(CH_3)_3)_2]$.The reaction was stirred for 36 hours. The solvent was removed under vacuum and the light brown precipitate washed with THF and hexane to give 78% yield of the product. (Scheme 3.14).

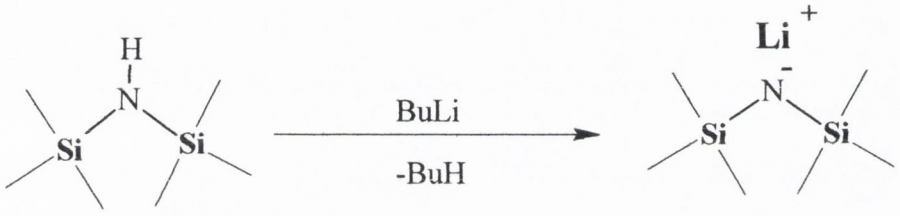

Scheme 3.13. *Synthesis of LiN[(Si(CH3)3)2]*

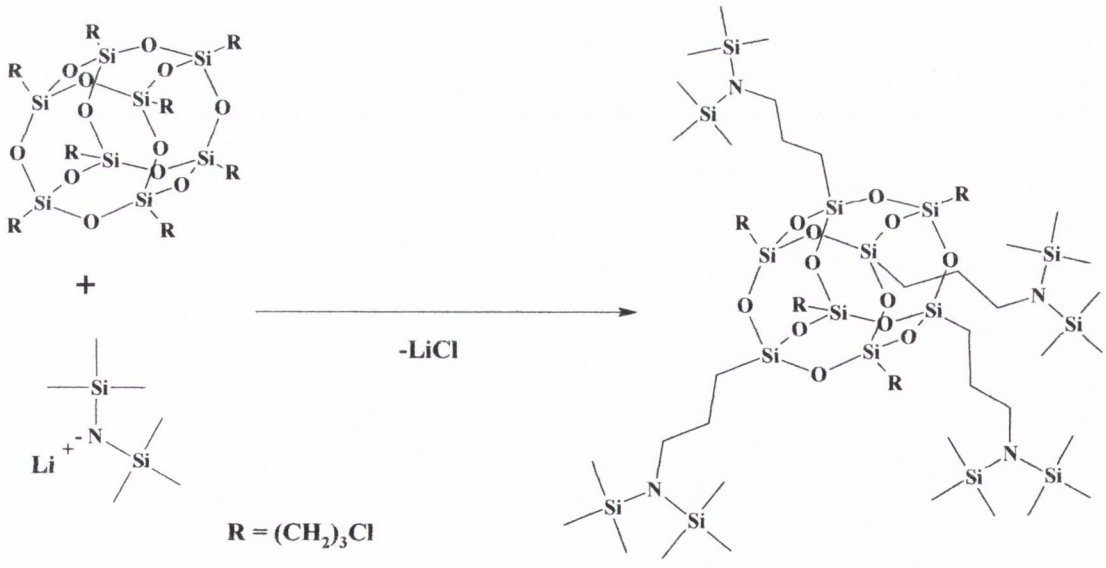

Scheme 3.14. *Showing reaction of T_8Cl and $LiN[(Si(CH3)_3)_2]$*

^{1}H NMR spectroscopy of **16** revealed the unreacted propyl groups, with resonance's at. 3.5ppm, 1.85ppm and 0.88ppm the reacted propyl groups then closely follow at 3.7ppm, 1.33ppm and 0.82ppm respectively. The CH_3 groups as expected appear as a large singlet at 0.2 ppm. The ^{13}C NMR showed a signal at 67ppm, which corresponds with the CH_2 groups attached to the Nitrogen. The un-reacted propyl CH_2 groups appear at 46.ppm, 25.8ppm and 13.6ppm,the reacted propyl groups then follow, falling at 31.8ppm, 10ppm and 8.8ppm a quaternary carbon appears at 67ppm and a strong signal corresponding to the CH_3 carbons appears at 25ppm. The ^{29}Si NMR shows two signals at –65.47ppm corresponding to the Siloxane cage and another at -61.34ppm belonging to the Silicones attached to the nitrogen. IR showed a strong signal at 1022 cm-1 corresponding to elongation of a C-N bond.

3.2.6 Reaction of T_8Cl_8 with lithiated ferrocene (17).

Ferrocene can be readily lithiated by butyllithium. This is a useful method of preparing functionalized ferrocenes. Some of the obvious variables in the lithiation of ferrocene are the choice of lithiating reagent (n-BuLi, s-BuLi, t-BuLi), the ratio of ferrocene to lithiating reagent, the choice of solvent, the reaction temperature, the addition mode, the rate of addition, the concentration, and finally, the reaction time. Some less obvious variables seem to play a role, as evidenced by variations in yield in different reactions run under identical conditions. It would seem that an excess of t-BuLi is necessary because the solvent when activated consumes some of it. The five member rings in Ferrocene undergo a wide range of substitution reactions. Once an initial proton from one of these rings is removed using BuLi the aromatic sextet is disrupted by the addition of an extra electron into its HOMO. The subsequent negatively charged ring then becomes neucleophillic in nature and readily denotes the spare electron to any molecule with a suitable leaving group. The chlorines on the T_8Cl FCPOSS are easily lost in the presence of a nucleophillic such as a negatively charged Ferrocene ring, as shown in scheme 3.15. ^{1}H NMR showed

strong evidence of the initial mono-substituted Ferrocene

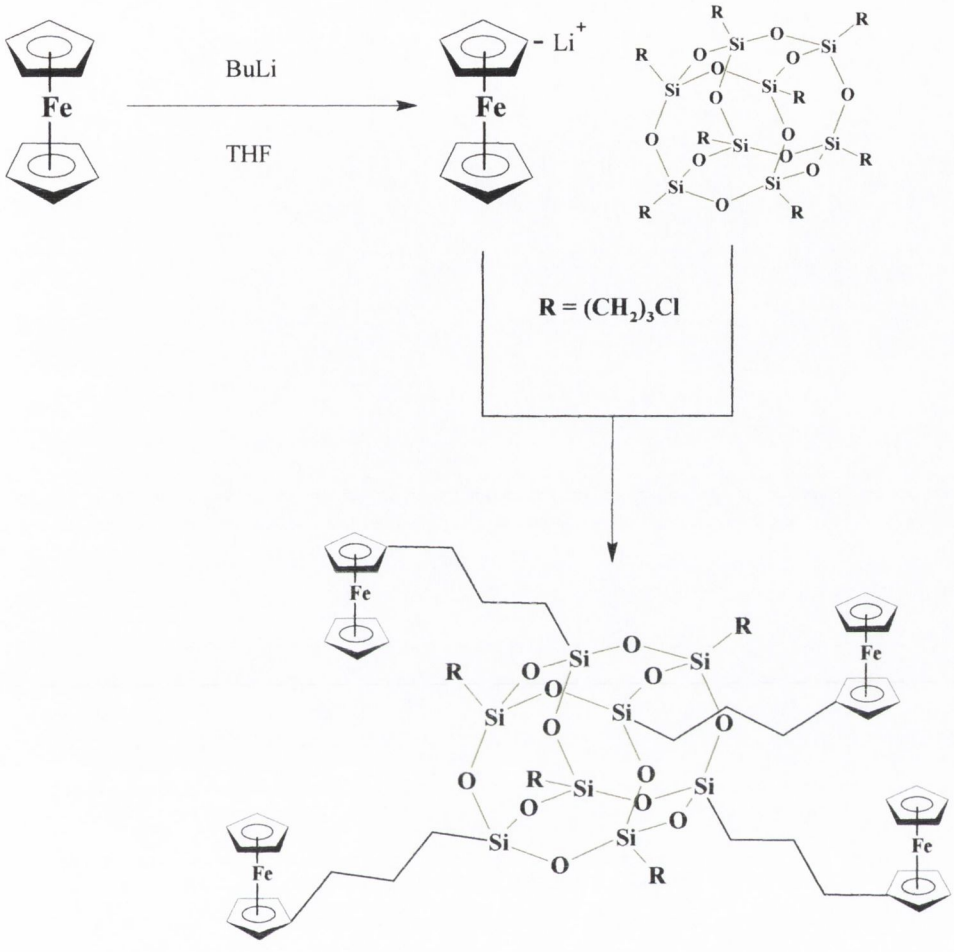

17

Scheme 3.15. *Formation of product 17 showing the four-ferrocene moieties arranged in a tetrahedral arrangement to relieve steric stress.*

A peak at 4.25ppm integrated to five hydrogens and another peak at 4.18ppm was found to integrate to four hydrogens. Both these peaks indicate the presence of an un-substituted and a mono-substituted Cyclopentadiene ring both being on the Ferrocene. Two clear sets of propyl hydrogens can be distinguished. One set with appropriate peaks 3.49-ppm, 1.98ppm and 1.17 ppm indicate the presence of un-substituted pendant groups, and another set falling at 3.2-ppm, 1.87ppm and 1.3ppm respectively which correspond to a substituted pendant groups.

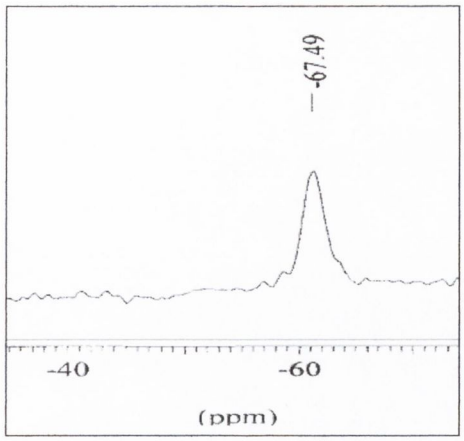

Figure 3.10 *^{29}SiNMR of compound 17.*

The ration of both these sets is 1:1 which points to the T_8Cl FCPOSS being tetra-substituted as illustrated in scheme 3.1.above. The ^{29}Si NMR showed a small peak at -67.5 ppm again indicating the presence of the fully condensed T_8 Siloxane cage. IR spectroscopy in dry KBr clearly shows a Si-O-Si stretch at 1174 cm-1. Mass spectrographic analysis in CH_3CN revealed masses of 438 g/mol^{-1} and 761 g/mol$^{-1,}$ which correspond to the fragments [M-3 (CH_2Fc)-$CH_2]^{++}$, [M- $CH_2Cl]^{++}$respectively.

3.2.7 Reaction of the lithiated C_{60} with T_8Cl. (18)

The Reaction of C60 and n-BuLi was performed according to normal procedures in dry THF. After careful washing the lithiated C_{60} was mixed with fresh T_8Cl in dry THF and allowed to reflux for seven days. The resulting brown solid was obtained in high yield 85%.^{1}H NMR spectroscopy of 18 revealed both the reacted and unreacted propyl protons falling closely together at 3.4ppm 1.7ppm and 0.83ppm with the reacted protons appearing as small shoulders off these main peaks. The Butyl CH_2 protons appeared, with their expected splitting patterns, falling at 3.5ppm, 1.4ppm and 1.03ppm with the CH_3 signal appearing as a triplet at 0.3ppm. The ^{13}C NMR clearly showed the presence of C_{60} with a large peak at 145ppm. The remaining signals proved to

show all the appropriate unreacted propyl CH_2 groups at 48.57 ppm, 21ppm and 14ppm and the reacted propyl groups again overlapping somewhat with the unreacted signals. The signals for the quaternary carbons were not distinguishable from those of those of C_{60}. ^{29}Si NMR reveals a single signal at –65.47ppm confirming the presence of a T_8 POSS cage. Mass spectrographic analysis in CH_3CN revealed three main masses at 2386 g/mol^{-1},1170 g/mol^{-1}and 781 g/mol^{-1} these corresponding to the fragments $[M\text{-}Bu^{+}\text{-}\ CH_2]^{+}$, $[M\text{-}2Bu^{+}\ ]^{+}$, $[M\text{-}\{(\ CH_2)_3\text{-}C_{60}\}\text{-}Bu^{+}\text{-}(\ CH_2)_3Cl]^{++}$ From the ^{1}HNMR ratios between reacted and un-reacted pendant groups, it would appear that only two of the eight groups have undergone the reaction. Considering the sheer bulk of two large C_{60} molecules the ration of 2:1 fullerenes to POSS seem very reasonable.

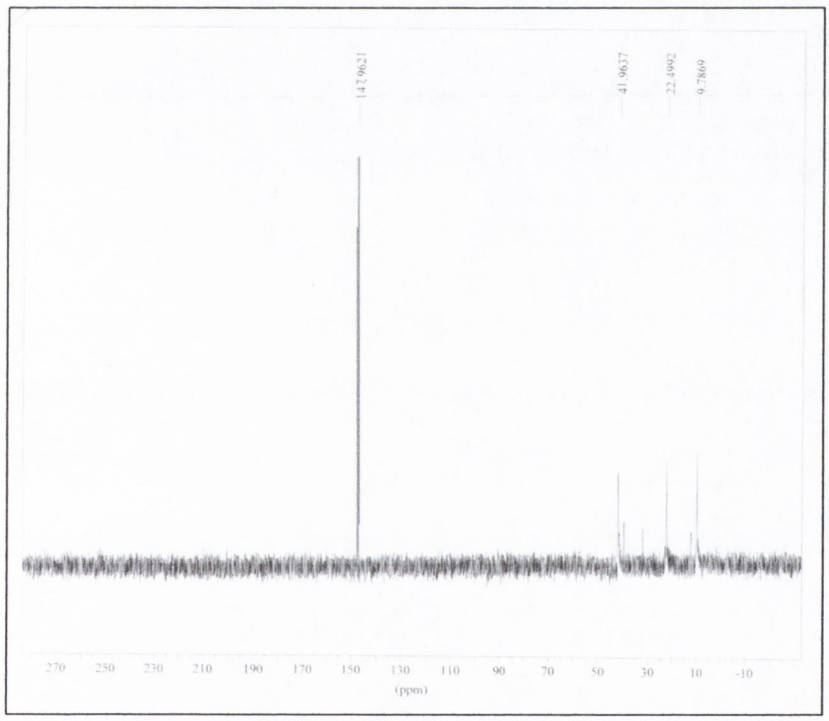

Figure 3.11 *^{13}CNMR of compound 18.*

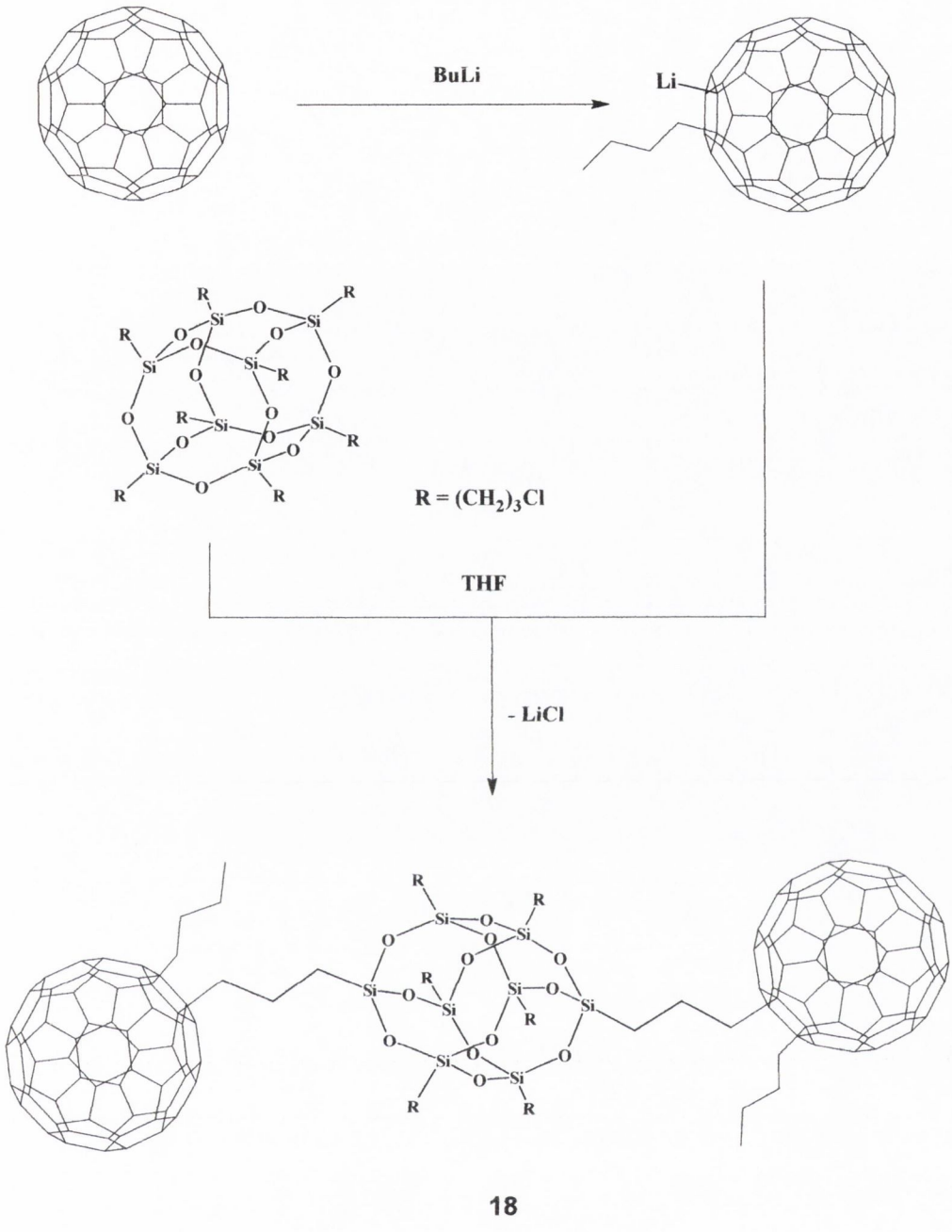

18

Scheme 3.12 *Formation of product (18) from POSS T_8Cl and lithiated C_{60}.*

3.2.8 Reaction of $PhSiCl_3$ with C_{60} (19)

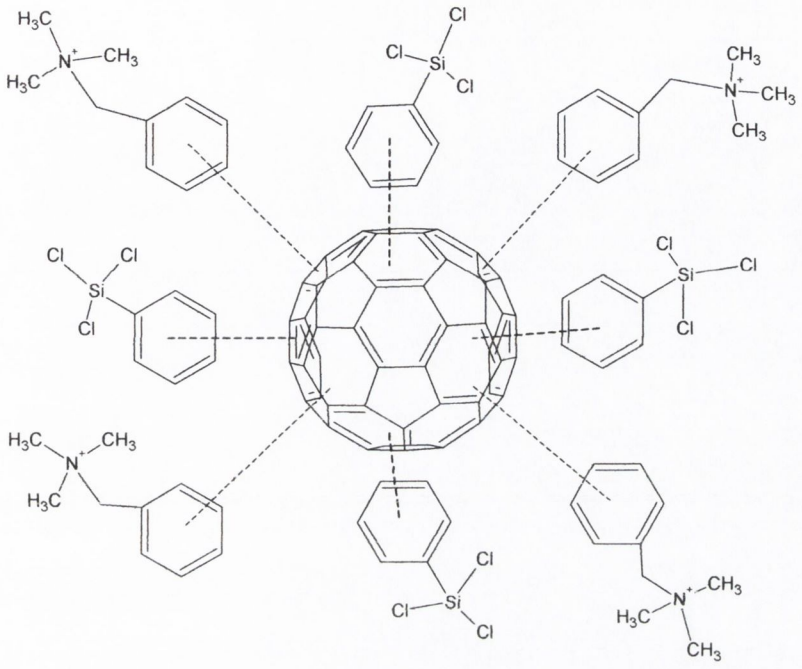

Figure 3.8. *Illustration showing the aromatic interactions between the* $PhSiCl_3$ *and* C_{60} *in the presence of BTMA .*

In an attempt at making C_{60}/siloxane composites by BTMA assisted condensation of $PhSiCl_3$ a dark brown precipitate appeared in the vessel. this compound was not soluble in the toluene solvent and the purple colour had disappeared which seemed to indicate that the C_{60} had been incorporated somehow into a complex with the siloxane. ^{1}H and ^{13}C NMR studies clearly indicated the presence of both C_{60} and the phenyl groups of siloxane. The ^{1}H NMR spectra shows three peaks between 7.2ppm.-7.6 ppm corresponding to the three different proton environments in the phenyl ring. With another (singlet) peak at 4.49ppm indicating the presence of the methyl groups on the BTMA.

The ^{13}C NMR spectrum has a strong peak at 133ppm which indicates the clear presence of fullerene. A further four peaks between 130 ppm-15ppm correspond to the four phenyl carbons and a final signal at 51ppm due to the

presence of the methyl group of the BTMA. The presence of C_{60} was also confirmed by the non-linear optical response of the sample.

Subsequent experiments showed however that the BTMA that we had assumed to be a catalyst reacted instantly with fullerene even in the absence of the siloxane component. A search of the literature [14,15] revealed some studies using primary and secondary amine compounds undergoing an addition to the 6, 6 junction of C_{60}. However there were no any data on use of the ammonium compound as we have used.

The light brown precipitate was left in contact with air for two weeks and was found to have complete solubility in water. The product was analysed using the Z scan technique and was again found to give a third order non-linear optical response,

3.3 Conclusion

In conclusion, we have prepared new Cp-functionalised silsesquioxanes and have demonstrated their possible application as building blocks for new polymeric materials. This is a fundamentally new approach for the preparation of new controlled pore size materials. Reactions of T_8Cl POSS with *t*-BuLi, $LiN[(Si(CH_3)_3)_2]$ and lithiated ferrocene resulted in tetra *t*-Bu- $N[(Si(CH_3)_3)_2]$ - and ferrocenyl- substituted POSS derivatives respectively. While reactions with NaI (trashalogenation), and lithiated fullerene resulted only in disubstituted species. Thus despite 8 equivalents or an excess of the reagents was used to treat T_8Cl POSS, full substitution of all 8 chlorine atoms have never been achieved. We believe that full substitution of all functional groups in POSS is impossible for two main reasons: sterical hindrance and limited solubility of the substituted species. C_{60} – siloxane composite demonstrated a third order non-linear optical response. This material might find a potential application in non-linear optical devices.

3.4 References

1 Angelakos, C.; Zamble, D.B.; Foucher, D.A.; Lough, A.J.; Manners, I. *Inorg. Chem.* **1994,** *33*, 1709-1718

2 Haddad T. S. and Lichtenhan J. D., *J. Inorg. Organomet. Polym.*, **1995**, *5*, 237-246.

3 Lichtenhan, . J. D. . Otonari Y. A,. Carr M. J, *Macromolecules*, **1995**, *28*, 8435-8437

4 R. A. Mantz, P. F. Jones, K. P. Chaffee, J. D. Lichtenhan, J. W. Gilman, I. M. K.Ismail and M. J. Burmeister, *Chem. Mater.*, **1996**, *8*, 1250-1259.

5 J. W. Gilman, D. S. Schlitzer and J. D. Lichtenhan, *J. Appl. Polym. Sci.*, **1996**, *60*, 591-596.

6 J. D. Lichtenhan, C. J. Noel, A. G. Bolf and P. N. Ruth, *Mat. Res. Soc. Symp. Proc.*, **1996**, *435*, 3-11

7 Lichtenhan J.D., *Comments. Inorg. Chem.* **1995**, *17*, 115-130.

8 Lichtenhan J.D., Vu N.Q., Carter J.A., Gilman J.W., Feher F.J. *Macromolecules*. **1993,** *26*, 2141- 2142

9 Togni A., Halterman R.L. Metallocenes, 1998 Synthesis Reactivity, Applications, vol. 2, Wiley VCH, Weinheim.

10 Jutzi P., Heidemann T., Neuman B., Stammler H.G. *J. Organomet. Chem.* **1994,** *472*, 27 - 38.

11 Barker P.J., Davies A.G., Henriquez R, Nedelec J-Y. *J. Chem. Soc. Perkin Trans. II.* **1982,** 745 - 750.

12 Čermák J., Kvíčalová M, Blechta V., Čapka M., Bastl Z. *J. Organomet. Chem*. **1996**,*50*, 77 - 84.

13 Hong B., Thoms T.P.S., Murfee H.J.,Lebrun M.J. *Inorg. Chem*. **1997**, *36*, 27, 6146-6147

14 Schwartz, B.L.,Rockwood,A.L.,Smith R.D., Tomalia D.A., Spindler R. *Rapid. Commun. Mass Spectrom*. **1995**, *9*,1552-1555.

15 Van Hest J.C.M., Delnoye D.A.P., Baars M.W.P.L., ElissenRoman C., vanGenderen M.H.P., Meijer E.W. *Chem. Eur. J.* **1996**, 2. 1616-1626.

Chapter 4

New composite materials based on Siloxane-functionalised Titania nanorods

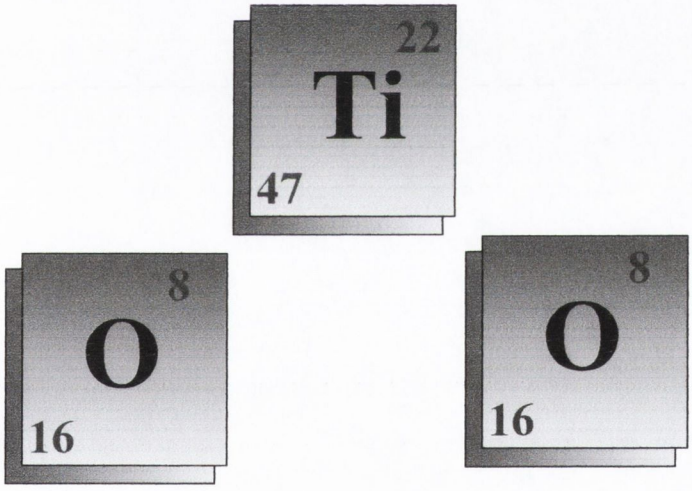

4.1 Introduction

TiO_2 is a versatile material used widely in industry, research, and environmental cleaning, for generations being used as white paint pigment and an important component in sunscreen lotions. TiO_2 has also been investigated considerably due to its unique optoelectronic and photochemical properties, such as high refractive index, high dielectric constant, excellent optical transmittance in the visible and near-IR region as well as high performance photocatalysis for water splitting and for degradation of organic molecules [1]. These properties can help cleanup the environment by utilizing photocatalytic oxidation of waste organic compounds by TiO_2 powder. There are several other compounds that have the ability to catalyse under UV light, such as Cadmium Sulphide, but unlike Titanium dioxide they are highly toxic [2]. TiO_2 has also been demonstrated as a promising electron-transport material of a dye-sensitized oxide semiconductor solar cell [3]. Nanocrystalline or porous films are used in the photo electrochemical cells due to their high surface areas. Moreover, ferromagnetic Co-doped TiO_2 films have been reported to possess a Curie temperature higher than 400 K [4]. Crystalline TiO_2 exists in three structures: rutile (tetragonal), anatase (tetragonal), and brookite (orthorhombic).

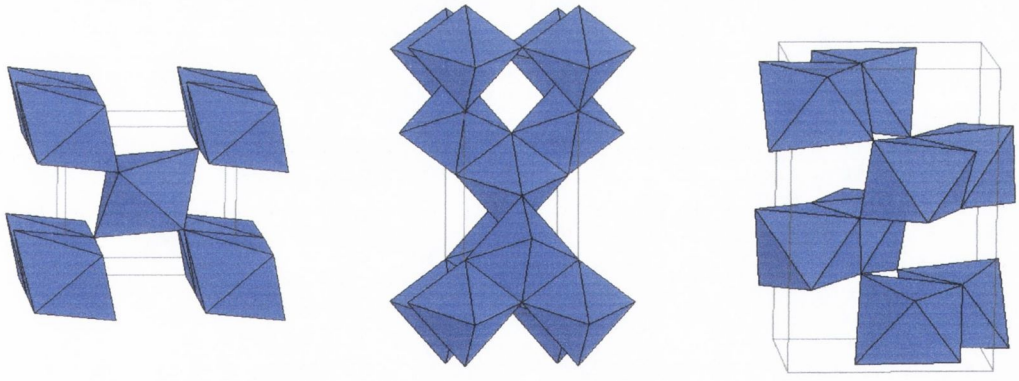

a **b** **c**

Figure 4.1 *Crystal forms of TiO_2 a) rutile (tetragonal),b) anatase (tetragonal), and c) brookite (orthorhombic).*

Among them, rutile is the most stable phase while anatase possesses superior optoelectronic and photocatalytic properties [1]. Recently, the use of one-dimensional nanostructures instead of nanocrystalline films in photo

electrochemical cells has been considered [4,5]. One-dimensional CdSe nanorods have been demonstrated to be preferable to the nanocrystalline films in solar energy conversion because of their single-crystal structures providing a directed path for electron transport [4]. In addition, a more than two-fold increase in maximum photo conversion efficiency for water splitting has been observed by replacing TiO_2 nanocrystalline films with TiO_2 nanowires [5]. Growth of one-dimensional TiO_2 nanostructures, including nanowires and nanotubes, has been demonstrated using sol-gel, electro deposition, and hydrothermal methods with or without anodic aluminium oxide (AAO) [6]. TiO_2 nanorods have also been grown on a WC-Co substrate by metal organic chemical vapour deposition (MOCVD) using titanium-tetraisopropoxide (TTIP) as the precursor [7].

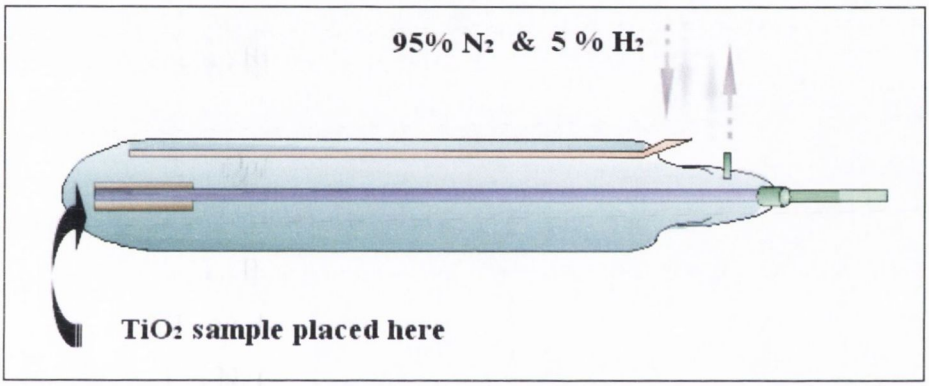

Figure 4.2 *Schematic representation of the device used in to prepare TiO_2 Nanorods [5].*

A relatively new type of hybrid is based on the FCPOSS structure, which can be regarded as one of the smallest forms of silica or even as "molecular silica" (see chapter 1). POSS compounds can be readily incorporated into polymers using simple standard methods [8,9]. In contrast to clay nanocomposites, incorporation of POSS can actually lead to a reduction in the polymer melt viscosity, also by increasing the concentration of the POSS structures in polymers has a dramatic effect in increasing the glass transition of the polymer. Which represents a distinct advantage for many applications [10].

POSS chemical technology has two unique features firstly the chemical composition ($RSiO_{1.5}$) is a hybrid, intermediate between that of silica (SiO_2) and silicone (R_2SiO). Secondly POSS molecules are physically large with respect to

polymer dimensions and nearly equivalent in size to most polymer segments and coils. Unlike polymer hydrocarbons POSS-based polymers typically possess very high decomposition temperatures and are very resistant to combustion. This property is thought to be associated with the pre-ceramic nature of the POSS component, which forms a glassy layer of $SiOC_x$ during pyrolysis that may prevent or retard the diffusion of oxygen through the surface. POSS nanocomposites occupy the performance region indicated as "hybrids properties" in Figure 4.3. By manipulating the relative amounts of POSS copolymers, control over thermal and mechanical properties can be achieved and used to establish thermoplasticity.

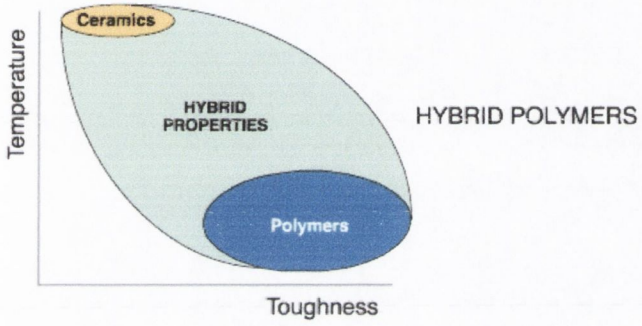

Figure 4.3 *Illustration showing the "hybrid" nature of POSS nanocomposites molecules [4].*

4.2 Tensile strength and Young's Modulus

The tensile strength of a material (or ultimate tensile strength) is the maximum amount of tensile stress that it can be subjected to before it breaks. Tensile strength is an important concept in engineering, especially in the fields of material science, mechanical engineering and structural engineering. Once past the elastic limit, the material will not relax to its initial shape after the force is removed. The tensile strength where the material becomes plastic is called *yield tensile strength.* This is the point where the deformation (strain) of the material is un-recovered, and the work produced by external forces is not stored as elastic energy but will lead to contraction cracks and ultimately failure of the construction. On the stress-strain curve below this point is in between the elastic and the plastic region.

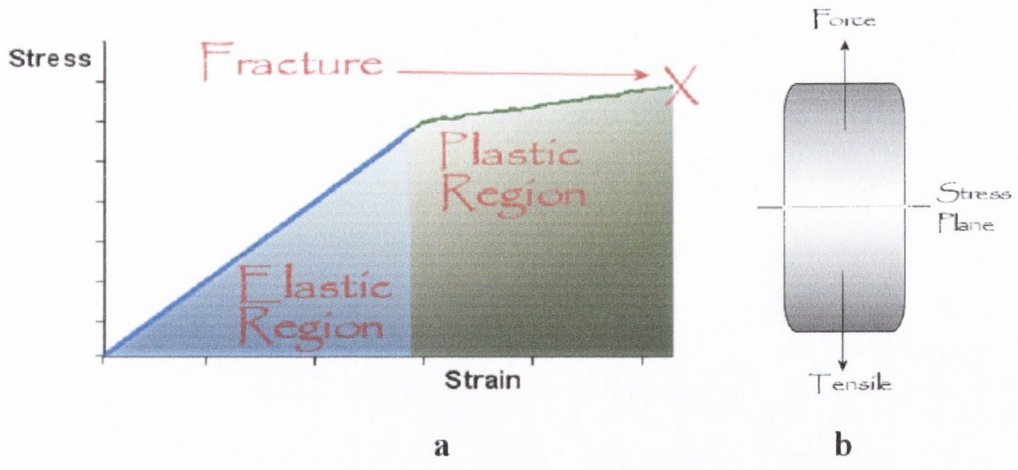

Figure 4.4 *a) Idealised Stress strain curve, the height of the curve when the sample breaks is the tensile strength b) diagram showing the forces at work in mechanical testing, the plane of a tensile stress lies perpendicular to the axis of operation of the force from which it originates.*

To measure the tensile strength of a polymer sample, we take the sample and we try to stretch it just like in the picture above. We usually stretch it with a machine (DMA). This machine simply clamps each end of the sample, and stretches the sample. While it is stretching the sample, it measures the amount of force (F) that it is exerting. When we know the force being exerted on the sample, we then divide that number by the cross-sectional area (A) of our sample. The answer is the *stress* that our sample is experiencing.

$$\frac{F}{A} = \textbf{stress}$$

Then, using this machine, we continue to increase the amount of force, and stress naturally, on the sample until it breaks.

There is more however to understanding a polymer's mechanical properties than merely knowing how strong it is. All strength tells us is how much stress is needed to break something. It doesn't tell us anything about what happens to our sample while we're trying to break it. Another interesting property is "elongation behaviour" of a polymer sample. Elongation is a type of deformation. Deformation is simply a change in shape that anything undergoes under stress. When talking about tensile stress, the sample deforms by stretching, becoming longer. We call this elongation, usually we talk about

percent elongation, which is just the length the polymer sample is after it is stretched (L), divided by the original length of the sample (L_0), and then multiplied by 100.

$$\frac{L}{L_0} \quad \text{x} \quad 100 \quad = \text{\% elongation}$$

There are a number of things we measure related to elongation. Which is most important depends on the type of material one is studying. As mentioned above the tensile strength is important for any kind of material. The yield tensile strength is also of importance if your material is an elastomer. Elastomers have to be able to stretch a long distance and still bounce back. Most of them can stretch from 500 to 1000 % elongation and return to their original lengths without any trouble. But for some other types of materials, like plastics, it usually better that they not stretch or deform so easily. If we want to know how well a material resists deformation, we measure something called tensile modulus, or Young's modulus. This is the measure of stiffness of a given material. It is defined as the limit for small strains of the rate of change of stress with strain. Young's modulus can also be thought of as the spring constant for solids. When we pull or press on a solid bar its length changes. The relative length change (longitudinal strain) is given by

$$\mathbf{e = \Delta L/L}$$

this is proportional to the applied stress:

$$\mathbf{S = Ye}$$

The **Y** parameter is therefore classed as Young's modulus. [11,12,13,14]

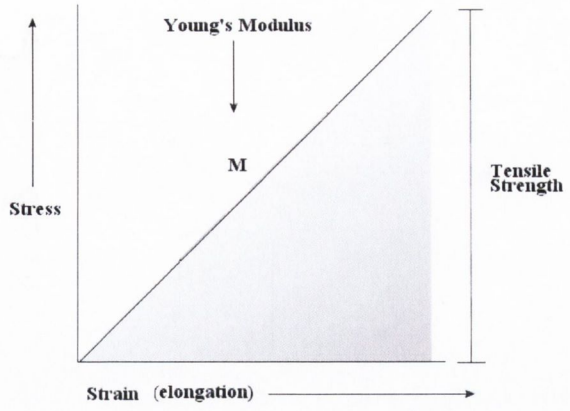

Figure 4.5 *Idealised Stress strain curve, and Young's modulus is the slope of this plot. If the slope is steep, the sample has a high modulus, which means it resists deformation. If the slope is gentle, then the sample has a low modulus, which means it is easily deformed. The shaded area beneath the plot represents toughness.*

Single-walled carbon nanotubes have the highest tensile strength of any material yet measured, with the highest single measurement of a nanotube being 63 GPa. As of 2004, however, no macroscopic object constructed using a nanotube-based material has had a tensile strength remotely approaching this figure, or substantially exceeding that of high-strength materials like kevlar.

4.3 Toughness

The plot of stress versus strain (as illustrated in figure 4.5 above) can also give another very valuable piece of information. If one measures the area underneath the stress-strain curve, coloured red in the graph below, the number you get is something we call *toughness*.

Toughness is really a measure of the energy a sample can absorb before it breaks. Since the height of the triangle in the plot is strength, and the base of the triangle is strain, then the area is proportional to strength time's strain. Since strength is proportional to the force needed to break the sample, and strain is measured in units of distance (the distance the sample is stretched), then

strength times strain is proportional is force times distance, therefore force times distance is energy. [11,12,13,14]

4.4 Mechanical properties of POSS

POSS molecules can be thought of as the smallest particles of silica possible. However unlike silica or modified clays, each POSS molecule contains covalently bonded reactive functionalities suitable for polymerization or grafting POSS monomers to polymer chains. Each POSS molecule contains non-reactive organic functionalities for solubility and compatibility of the POSS segments with the various polymer systems. POSS chemical technology is easy to use with monomers available in both liquid and solid form and they are soluble in most common solvents. Use of POSS additives often eliminates the need to use common (dense) fillers such as silica. Depending on loading level, bulk density reductions of up to 10% have been observed with viscosity reductions of up to 24% relative to silica. POSS incorporation increases modulus and hardness while maintaining the stress and strain characteristics of the base resin. Additionally since POSS is a chemical nanotechnology, processing and mould ability is maintained.

4.5 Aims of this work

The main aim of this part of our work is to investigate reactions between TiO_2 nanorods and different alkyl and allyl derivatives of trialkoxy- or trichlorosilanes. It is expected that OH groups and water on the surface of TiO_2 nanorods will react with trialkoxy- or trichlorosilanes resulting in covalent boding of these species to the surface and functionalisation of the nanorods. The prepared TiO_2 nanorods composites will be investigated by FTIR spectroscopy and TGA. Sedimentation studies will be performed in order to evaluate the solubility of functionalised nanorods in an organic solvent. The functionalised nanorods are expected to be more stable in an organic solvent, e.g. THF, which could be used for preparation of nanorods solutions and their further modification. Finally, we plan to use functionalised TiO_2 nanorods as additives for polymer (polystyrene) reinforcement. We believe that that the alkyl functionalised TiO_2 nanorods should have an increased solubility in polymer solution and will intertwine and entangle with the polymer molecules in the polymer matrix. It was expected that the shorter alkyl chains attached to

the nanorods should have less effect on polymer reinforcement than the longer chains.

4.6 Preparation and characterisation of functionalised TiO_2 nanorods.

Initial IR studies have shown the presence of hydroxyl groups in abundance on the surface of the TiO_2 nanorods (figure 4.6). By reacting halogenated ($RSiCl_3$) silanes (or triethoxy- ($RSiOEt_3$)) silanes with the TiO_2 nanorods in dry solvent, binding of halogenated silanes or triethoxy- silane occurs readily with the loss of HCl or ethanol (Schemes 4.1 and 4.2). The reaction was performed in the following manner. The TiO_2 nanorods samples were placed under vacuum for one hour at the ambient temperature and then flashed with argon. Dry THF was then added via canula under argon. The resultant mixture was then stirred vigorously for 24 hours. Halogenated silanes or triethoxy- silane precursor was then added drop wise via insulin syringe. The mixture was stirred for 48 hours. Thereafter the solvent was removed in vacuum and the dry precipitate washed with dry ether to remove any un-reacted silane derivative. All samples were then washed with wet THF and stirred over night. The samples were then allowed to settle for ten minutes until any non-functionalised nanorods settled out. The solution was decanted and the solvent was removed in vacuum. The functionalised nanorods were then washed with diethyl ether and dried in vacuum. This process was performed for a series of halogenated silanes or triethoxy- silane precursors (figure 4.7) giving TiO_2 nanorods functionalised with different alkyls. The products were characterised by TEM, IR and Raman spectroscopy.

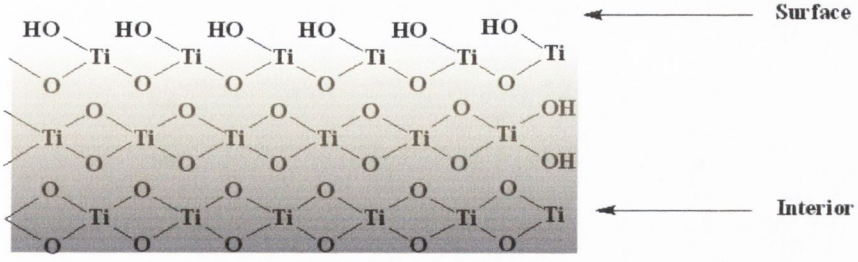

Figure 4.6 *Illustration showing the Hydroxylated surface of TiO_2.*

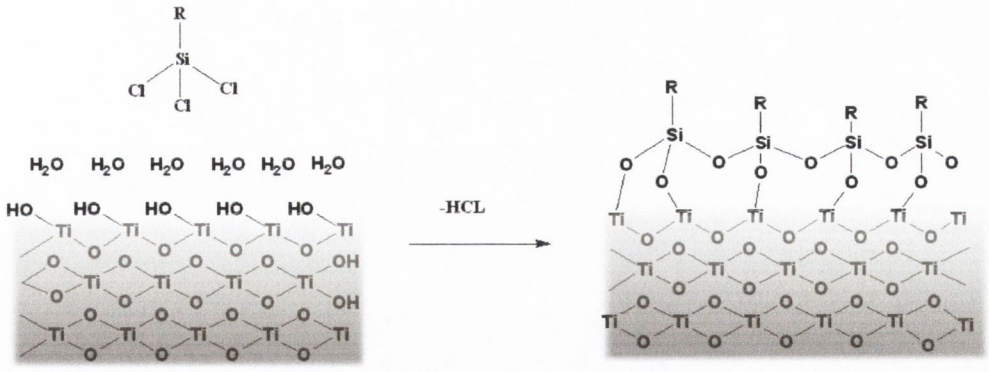

Scheme 4.1 *Schematic presentation of binding of $RSiCl_3$ to TiO_2 surface. The presence of H_2O to the surface of TiO_2 is necessary as the OH-groups on Ti are not acidic enough to replace HCl on their own.*

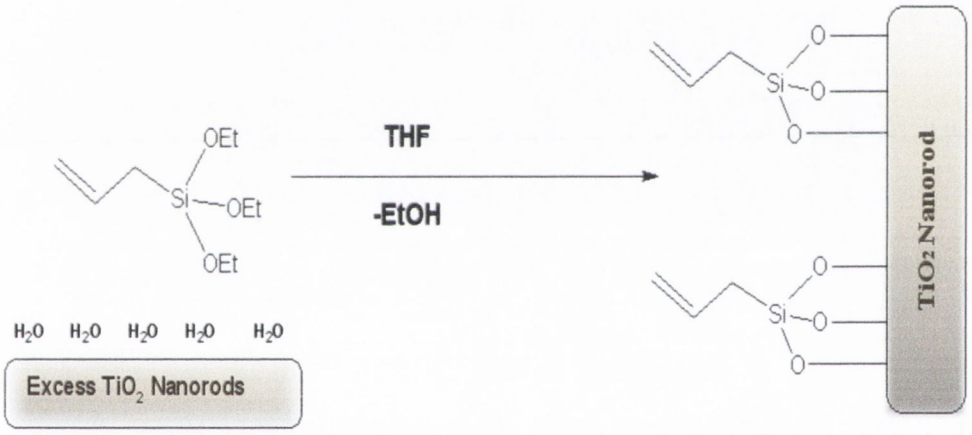

Scheme 4.2 ***Schematic presentation of binding of allyltriethoxysilane to TiO_2 surface.***

IR spectroscopy of all TiO_2 functionalised nanorod samples showed the presence of siloxane Si-O-Si stretches at 1148 -1198 cm^{-1} and a Si-O-Ti bands at 989-997 cm^{-1} as well as other characteristic peaks, these results are shown in table 4.1.

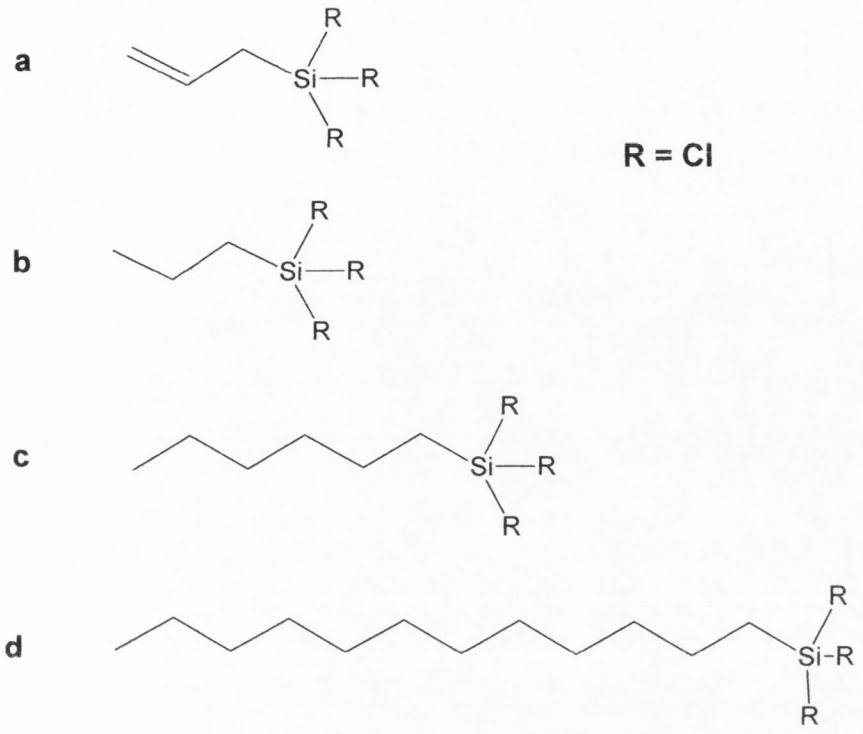

Figure 4.7 *Showing all precursor molecules that were mixed with TiO_2 rods.*

Table 4.1 *Summary of IR signals or all TiO_2 composites used in this section of the work*

Sample	Si-O-Si	Si-O-Ti	OH /H_20/CH_2
Allylic	1152 cm^{-1}	997 cm^{-1}	3045 -3584 cm^{-1} 1927 cm^{-1}, 1942 cm^{-}
Propyl	1159 cm^{-1}	997 cm^{-1}	2800-3600 cm^{-1} 3450 cm^{-1}
Hexyl	1148 cm^{-1}	989 cm^{-1}	2980-3645 cm^{-1}
Dodecyl	1198 cm^{-1}	995 cm^{-1}	3100-3045 cm^{-1}

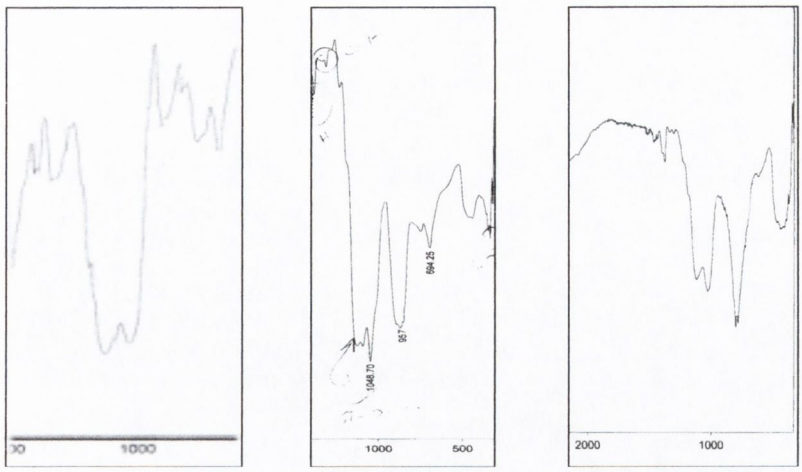

Figure 4.8 *IR showing the emergence of the Si-O- Ti signal.*

The functionalised TiO_2 nanorods were also examined using TEM. TEM images of non-functionalised TiO_2 nanorods and functionalised TiO2 nanocomposites are shown in figures 4.9 and 4.10 respectively. From the images it is clear that there is a thin ~ 5 -10 nm siloxane coating on the functionalised TiO_2 nanorods. The coating is certainly thicker than one monolayer due to the formation of multilayered siloxane structure hold together by Ti-O-Si and Si-O-Si bonds.

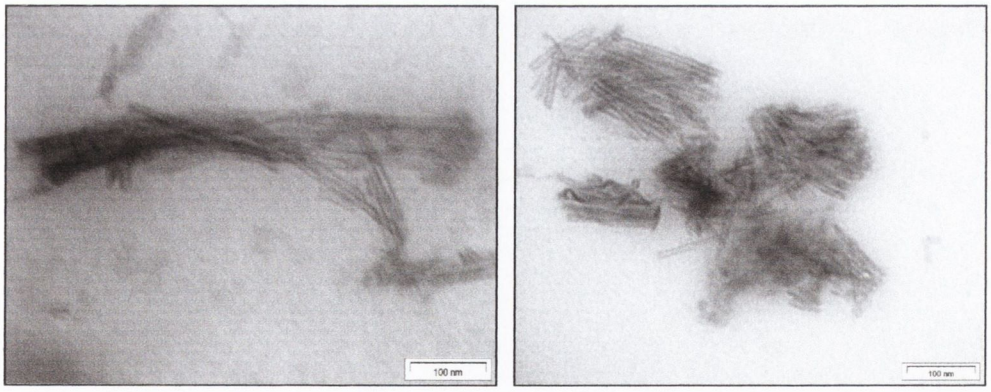

Figure 4.9 *TEM of initial non-functionalised TiO_2 nanorods*

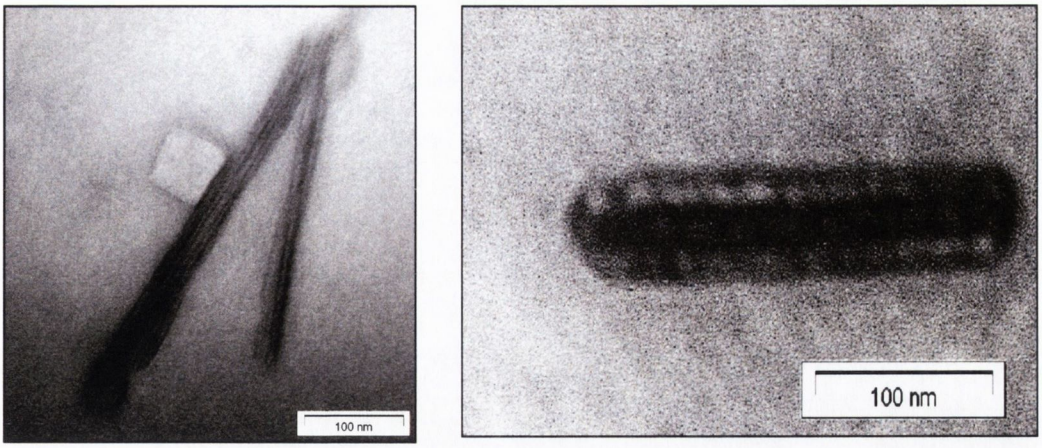

Figure 4.10 *TEM images showing allylic siloxane functionalised TiO2 nanorods.*

4.7 Sedimentation studies

Sedimentation studies were necessary to examine the solubility and stability of the alkyl and allyl functionalised TiO_2 nanorods in a selected organic solvent. The selected solvent was THF, because this solvent was most promising for the preparation of nanorods doped polymer films. Initial non-functionalised TiO_2 nanorods are not soluble in this solvent. To perform the sedimentation studies a sample of functionalised TiO_2 nanorods was taken and sonicated using a high power ultrasonic tip (120W, 60kHz) for five minutes. This was then transferred as quickly as possible to a 1 cm quartz cuvette. The sample was then placed in a sedimentation machine and the transmitted light was recorded. Then similar dispersions and sedimentation studies were performed with an addition of polystyrene for a range of concentrations. It was expected that polystyrene molecules should have quite strong interaction with the functionalised surface of TiO_2 nanorods (Scheme 4.3).

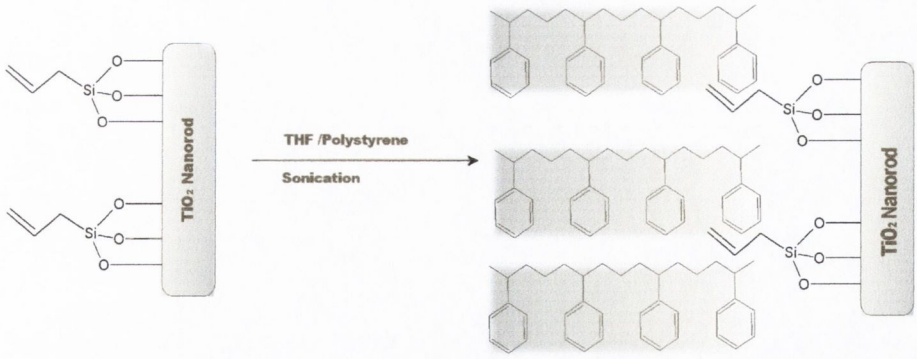

Scheme 4.3 *Schematic presentation of interaction between allyl-functionalised to TiO_2 surface and polystyrene molecules.*

4.7.1 Sedimentation of TiO_2 functionalised using (CH_2CHCH_2) $SiOR_3$

Sedimentation curve of allyl-functionalised TiO_2 is illustrated in figure 4.10. As we can see the concentration of functionalised TiO_2 begins to remain more stable in THF after twenty hours of sedimentation. This picture changes

somewhat upon the addition of polystyrene in measured amounts. The average curve fits well to the second order decay curve–apart from a bump at 5h –with accuracy (R^2) of 0.997. The stable dispersion concentration can be easily determined visually from this curve as approximately 0.1 g/l. This is confirmed by the A2 value of 0.18537 g/l.

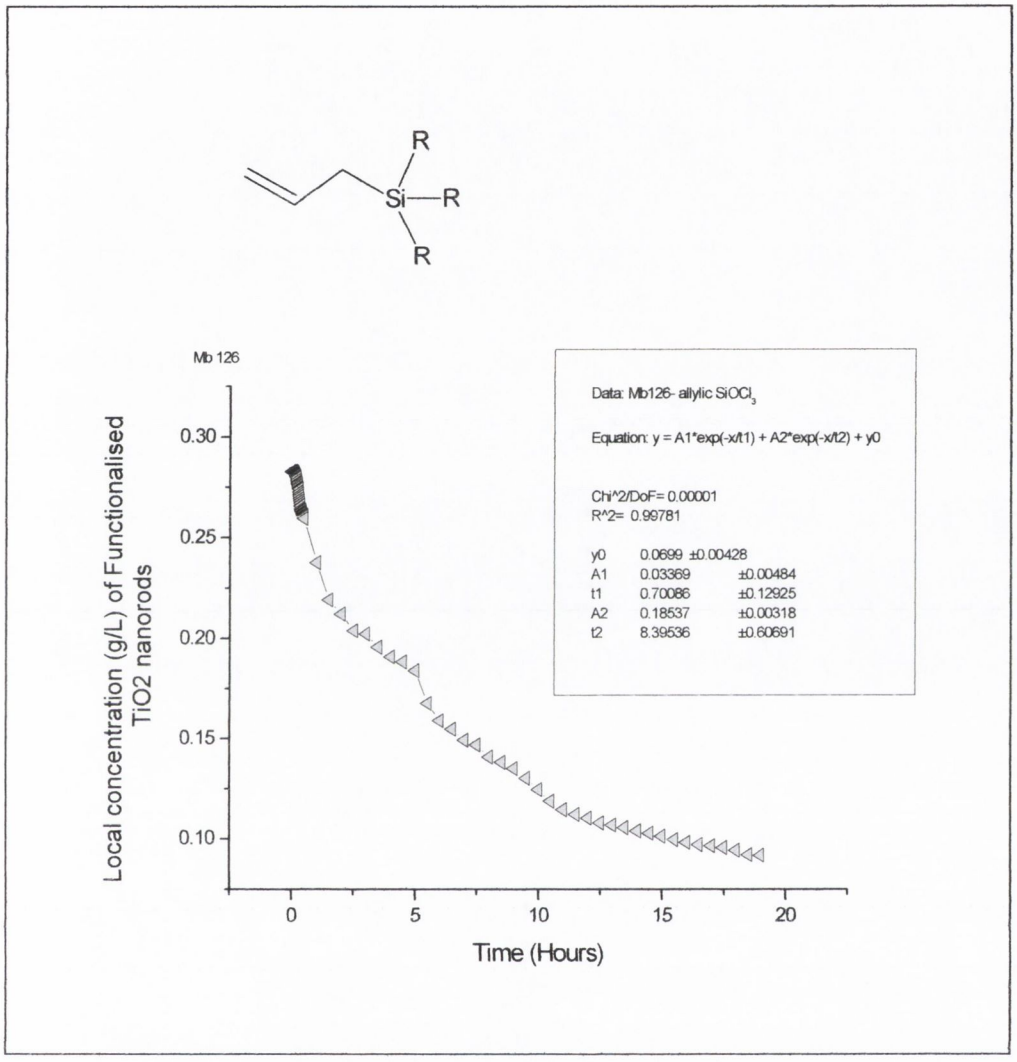

Figure 4.11 *Average sedimentation curve of allyl-functionalised TiO_2 nanorods. Concentration of TiO_2 nanorods as measured as a function of time in THF by light scattering.*

From figure 4.11 we can see that the addition of polystyrene immediately increases the amount of nanorods that remain stable after twenty hours In THF alone 33% of the functionalised rods remain in suspension after twenty hours. This increases to 44% upon addition of 12.6 g/l. this increases again to 52% and finally to 56% with further additions. In addition to this the

amounts that remain stable after five hours have increased substantially as well. This also is shown in table 4.2. Figure 4.12 shows that concentration of functionalised TiO_2 nanorods increases linearly with an increase of polystyrene concentration in solution.

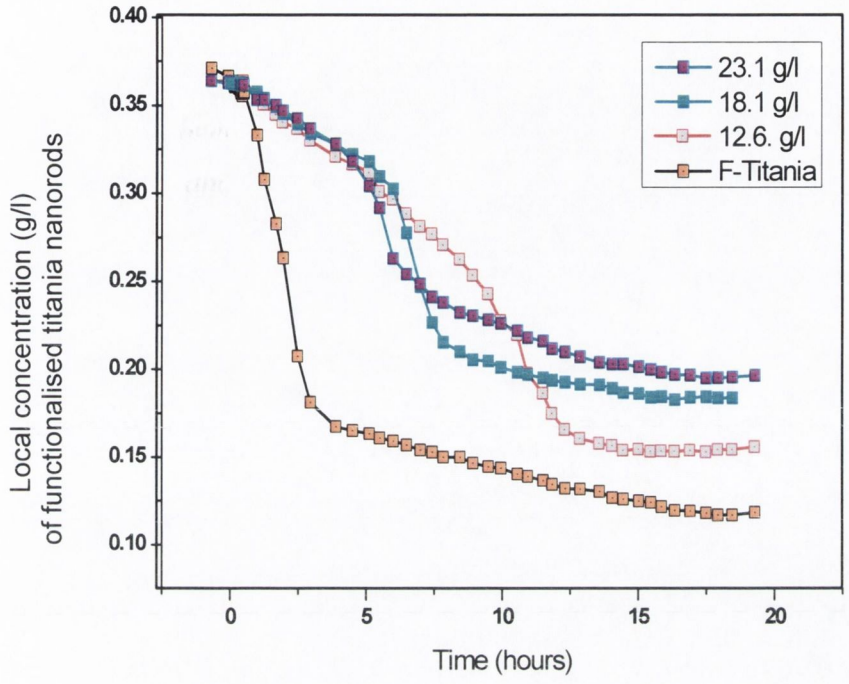

Figure 4.12 *Local concentration of allyl- functionalised TiO_2 nanorods in THF and polystyrene as measured as a function of time.*

Table 4.2 showing the percentage of F-titania remaining in suspension after time.

	0 g/l	***12.6 g/l***	***18.1 g/l***	***23.1 g/l***
20 hours	33%	44%	52%	55%
5 hours	46%	88%	90%	86%

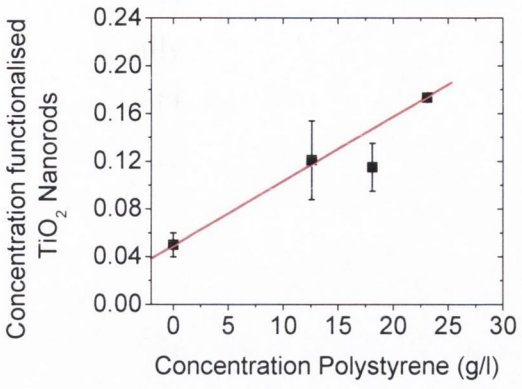

Figure 4.13 *Graph illustrating the increase in stability of allylic- POSS functionalised TiO_2 nanorods the increase in stability with increasing concentration of polystyrene added.*

4.7.2 Sedimentation of TiO_2 functionalised using $CH_3(CH_2)_2SiOR_3$

Sedimentation curve of propyl-functionalised TiO_2 is illustrated in figure 4.13.

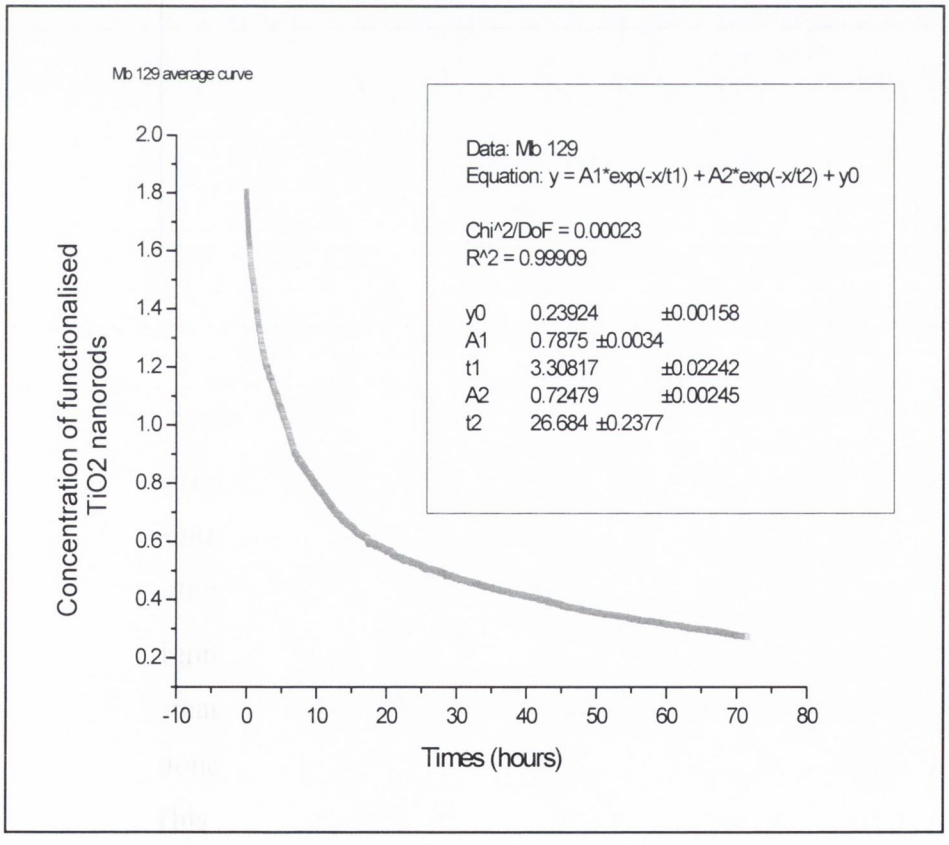

Figure 4.14 *Local concentration of propyl- functionalised TiO_2 .*

This time stable concentration of nanorods of 0.3 g/l was achieved after 70 hours of sedimentation. As measured as a function of time by Non-soluble material falls out after about 50 hours. An addition of polystyrene resulted in almost linear increase of solubility of propyl-functionalised nanorods (see figures 4.14 and 4.15).

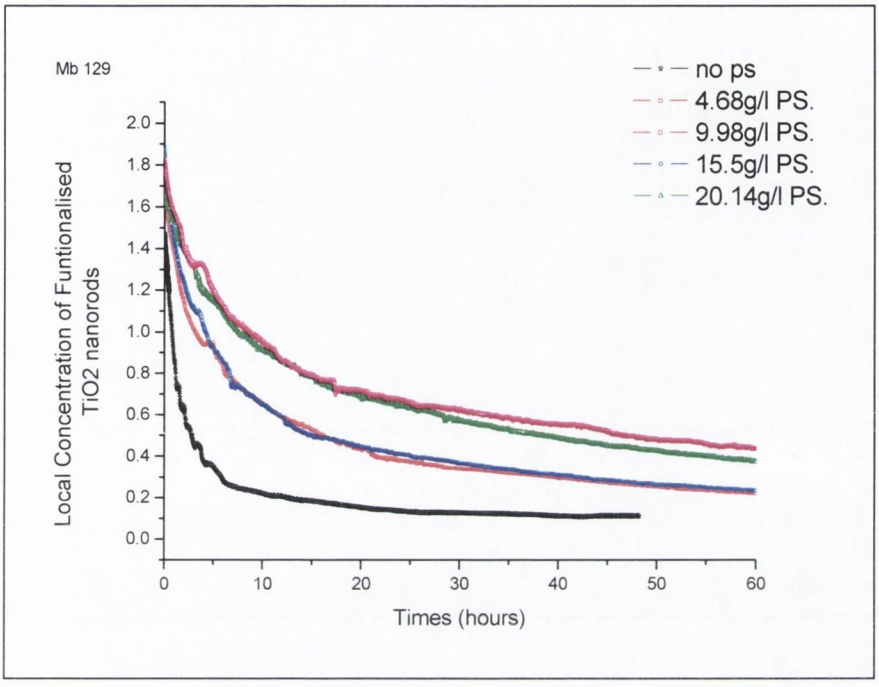

Figure 4.15 *Local concentration of propyl- functionalised TiO_2 .*

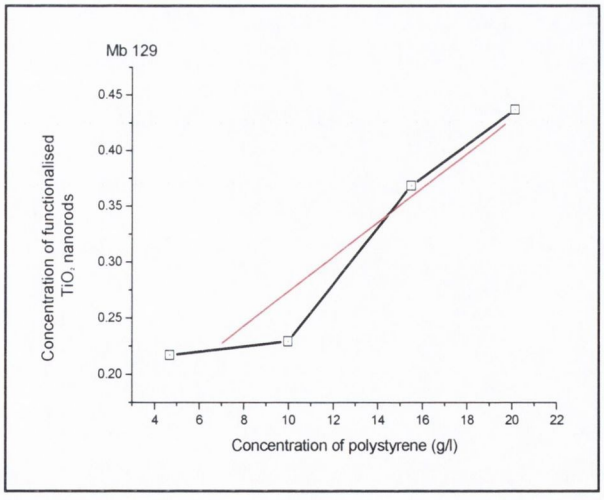

Figure 4.16 *Graph illustrating the increase in stability of propyl-functionalised TiO_2 nanorods the increase in stability with increasing concentration of polystyrene added.*

4.7.3 Sedimentation of TiO_2 functionalised using $CH_3 (CH_2)_5 SiOR_3$

The sedimentation curve of hexyl-functionalised TiO_2 is shown in figure 4.16. The stable suspension of functionalised TiO_2 nanorods was achieved after 20 hours at the concentration of 0.4 g/l. This represents ~33% of the initial concentration. It is important to notice that this curve is quite different from the propyl- functionalised Titania nanorods, which precipitated for longer time and at a bit more steady rate to reach to the stable suspension.

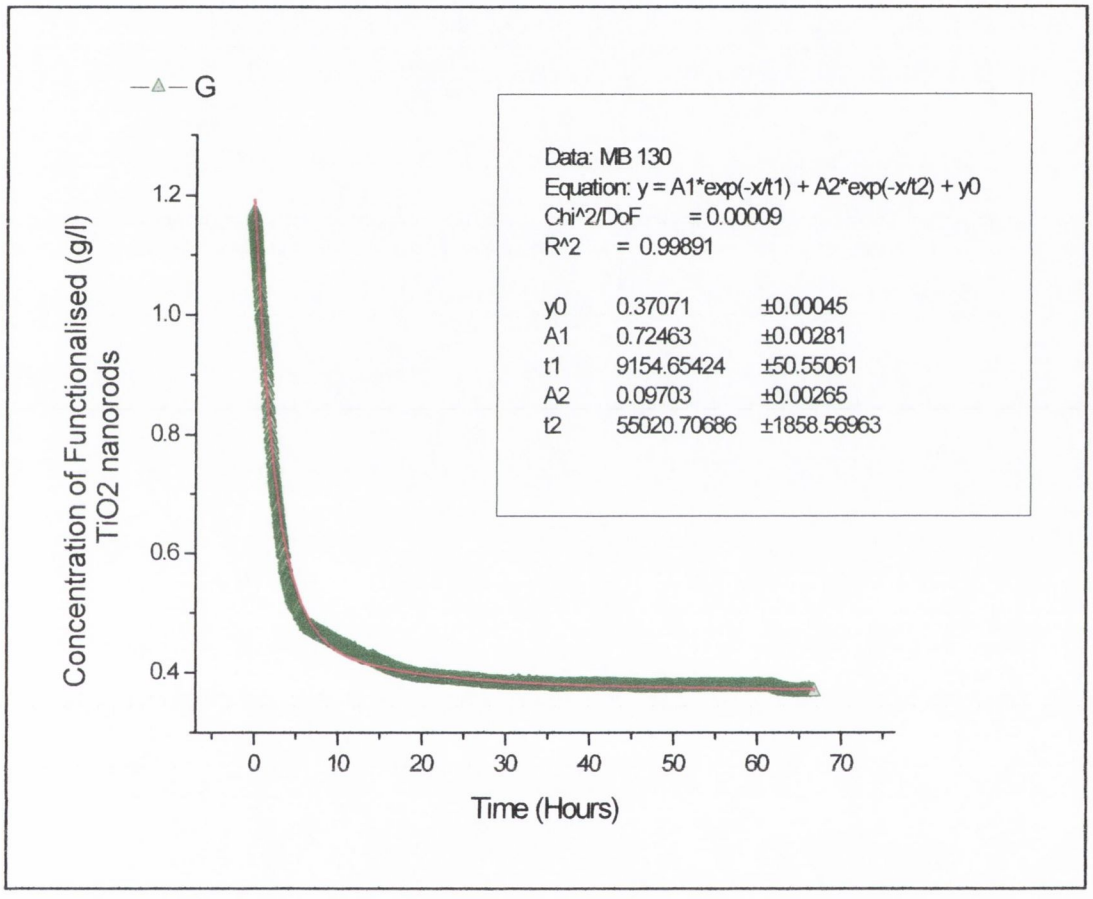

Figure 4.17 *Average Local concentration of hexyl- functionalised TiO_2.*

An addition of polystyrene again resulted in increased solubility and stability of functionalised TiO_2 in THF solution (figures 4.17 and 4.18). These samples were left on the bench for one month and were still very stable.

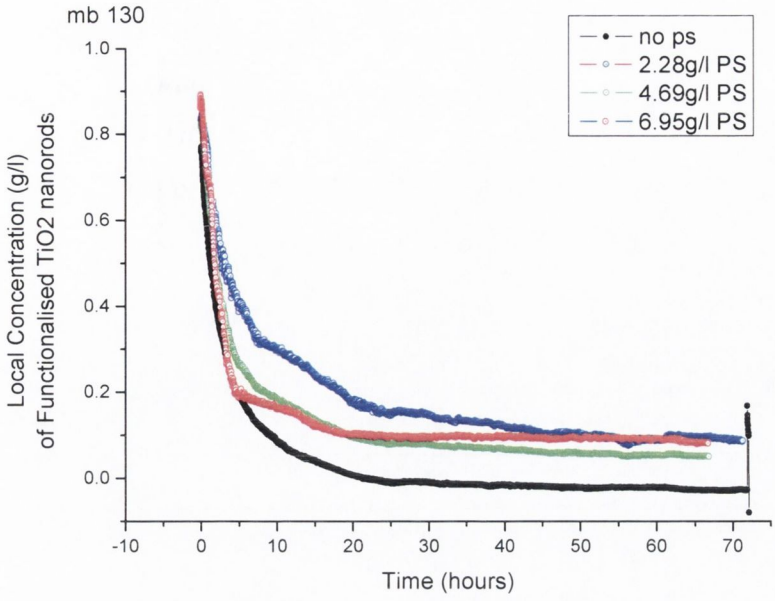

Figure 4.18 *Local concentration of Hexyl- POSS functionalised TiO_2 nanorods as measured as a function of time by light scattering any remaining non-soluble material falls out after about 20 hours.*

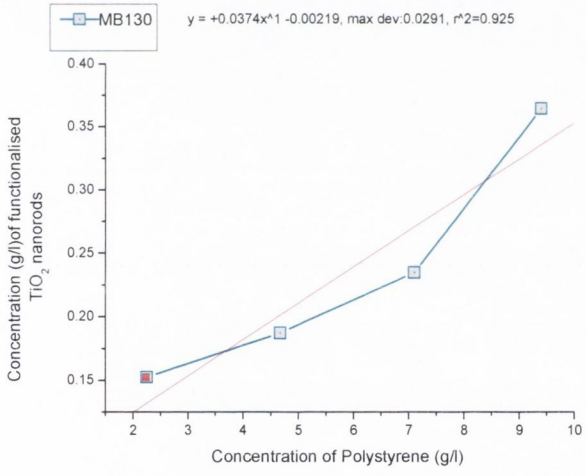

Figure 4.19 *Graph illustrating the increase in stability of Hexyl-POSS functionalised TiO_2 nanorods the increase in stability with increasing concentration of polystyrene added.*

4.7.4 Sedimentation of TiO_2 functionalised using $CH_3(CH_2)_{11}$ $SiOR_3$

The sedimentation curve of dodecyl-functionalised TiO_2 is shown in figure 4.21.

The stable concentration of 0.3 g/l was reached after 75 hours. This implies that 16% of the initial weight contains Titania nanorods that are functionalised sufficiently to remain stable for long periods. As seen from the curve illustrated in figure 4.19 above the curve for dodecyl functionalised - Titania has a gradual change from vertical to horizontal, implying that the sample is composed of particles with a large variation in the degree of functionalisation, the hexyl sample show previously had a much more rapid drop to the horizontal suggesting that the sample containing a narrower range of functionalised material that the dodecyl sample. However, overall dodecyl-functionalised TiO_2 nanorods are less soluble and stable in THF suspension, than correspondent hexyl-functionalised nanocomposites. We believe this occurs mainly due to the thermodynamic reasons.

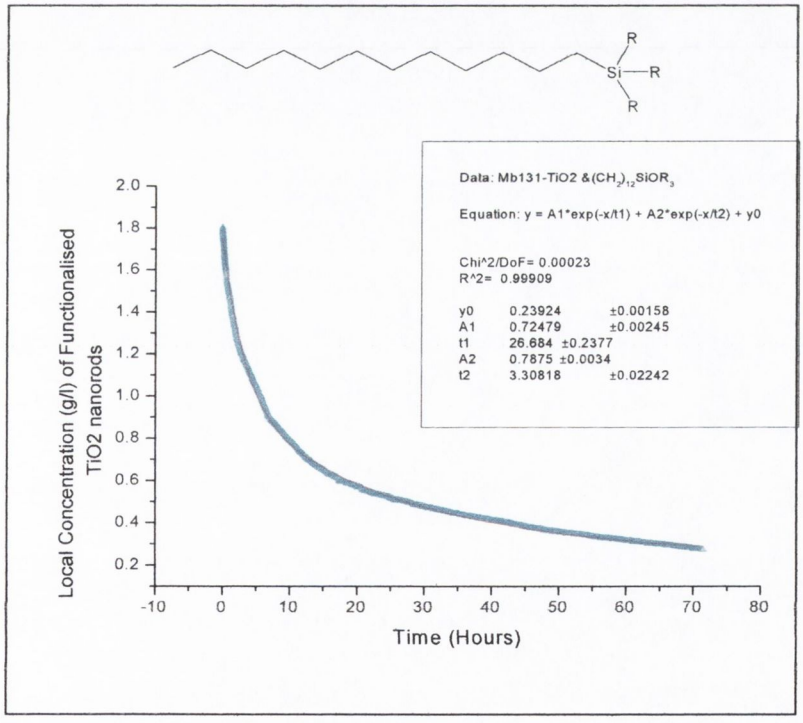

Figure 4.20 *Local concentration of Duodecyl- POSS functionalised TiO_2 the fit to the second order decay curve is almost a perfect match $R^2 = 0.99909$.*

From the sedimentation curve illustrated in figure 4.22 it is clear that the solubility increases as the concentration of polystyrene increases. The stable concentration of the dodecyl-functionalised titania nanorods in THF is 0.1 g/l. This increases up to 0.30 g/l with the addition of 2.52 mg of polystyrene. And further still to 0.5 g/l when the concentration of polystyrene is increased to 55 mg. the concentration of soluble material steadily increases as the concentration of polymer increases. When the concentration of polystyrene has increased to 10.29 g/l the amount of material in stable suspension is 0.42 g/l this represents a four fold increase in solubility (see also figure 4.21).

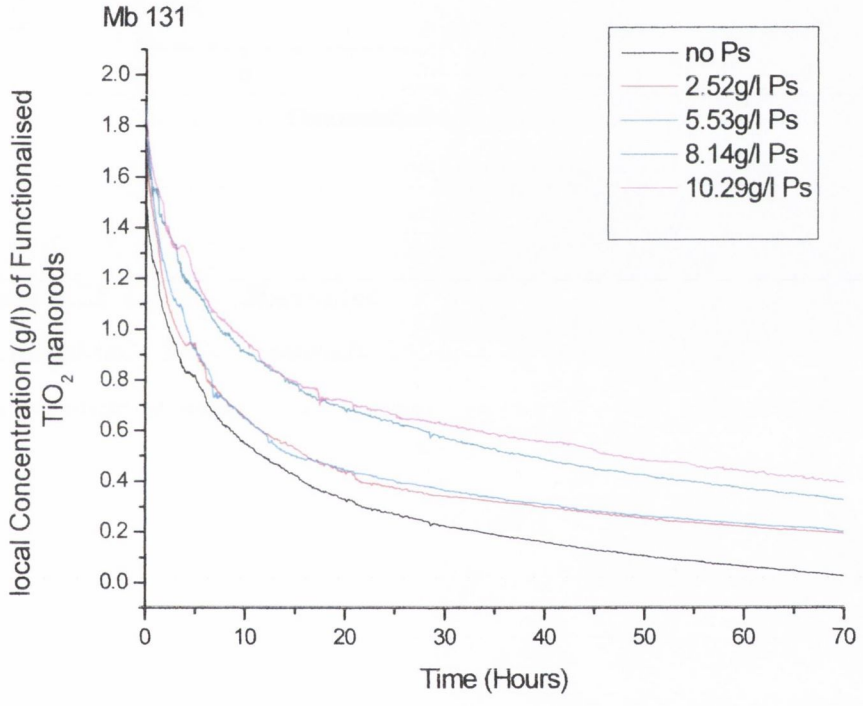

Figure 4.21 *Local concentration of dodecyl- functionalised TiO_2 nanorods as measured as a function of times any remaining non-soluble material falls out after about 70hours.*

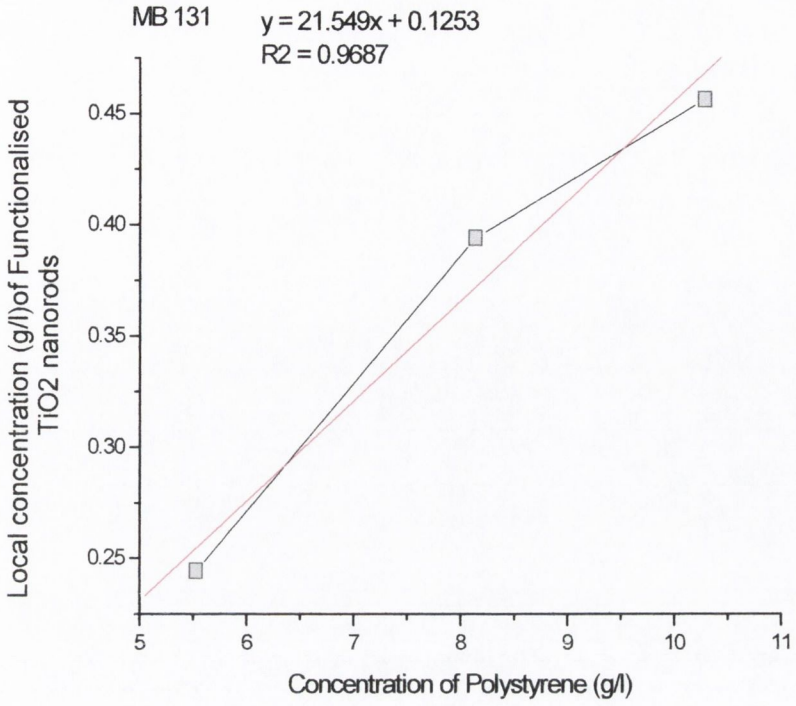

Figure 4.22 *Graph illustrating the increase in stability of dodecyl-functionalised TiO_2 nanorods the increase in stability with increasing concentration of polystyrene added.*

4.8 DSC testing

Prior to beginning of mechanical testing of the siloxane / titania hybrids, it was necessary to ensure that that the addition of the functionalised titania did not lead to crystallization in the sample, this was to eliminate the possibility that any strength increase would be due to a change in the morphology of the polymer rather than reinforcement due to the presence of the titania /siloxane material. However polystyrene by its nature tents to be an amorphous polymer and so not inclined to any amount of crystallization, and our results from the DSC showed this tendency unchanged

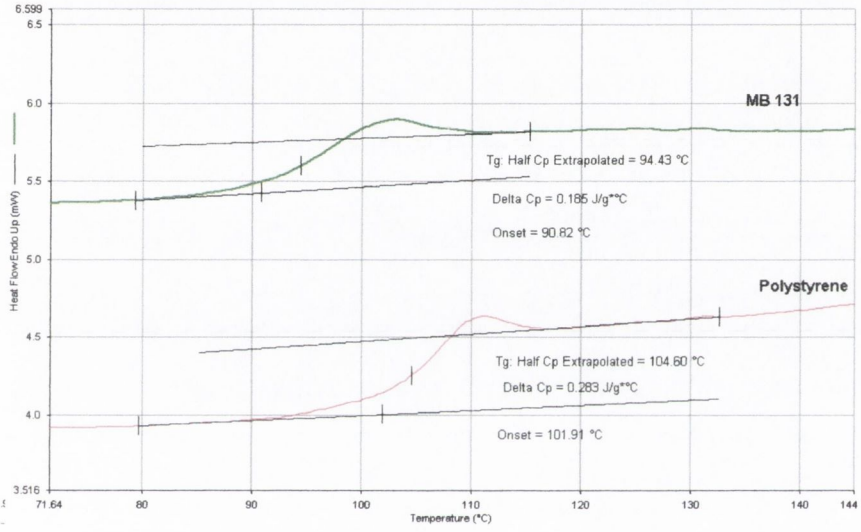

Figure 4.23 *DSC plots of 2% dodecyl-functionalised Titania sample with polystyrene and of polystyrene with no Titania additives. The sample shows no sign of crystallisation and there is little if any change in the glass transition temperature. All the Titania /siloxane composite samples showed analogous plots to the one above.*

4.9 Mechanical testing

In this part of the work, the functionalised TiO_2 nanorods were mixed with polystyrene in THF solution in an attempt to make new reinforced polymer composites. Polymer films were prepared using the layer by layer technique, which was described by Cadek et al [10] This involved making a solution of pure polymer and blending that by adding different amounts of functionalised nanotubes. This solution was then deposited on to Teflon disks, which are 3 cm in length. The polymer solution is dropped on to the disk 1 ml at a time and the solvent is allowed to evaporate this is then repeated four times in total. This resulted in a thin film on the disk that can be easily peeled off. This thin film was then cut into strips, which are analysed using the Zwick 100 tensile tester. Tensile measurements were carried out to evaluate the relationship between composite morphology and mechanical performance. The data was used to calculate Young's modulus (Y), ultimate tensile strength (σ_T) and toughness (T) values.

Selections of weight percentages were chosen for TiO_2 nanorods concentration: 0%, 1% and 2.5%. Previous research has shown that the use of higher concentrations of nanotubes results in the formation of aggregates of nanotubes that do not infer any mechanical strength increases, as they are not interacting efficiently with the polymer matrix.

The polymer used through out this work was polystyrene (MW: 280,000), this was chosen as it was soluble in THF and was compatible with the functionalised -Titania samples. Results of mechanical testing for initial pure polystyrene are shown in Table 4.3.

Table 4.3 Mechanical testing results for *pure* polystyrene.

Percentage TiO_2 composite	Young's Modulus [GPa]	Ultimate Tensile strength [MPa]	Toughness [KJ/m^3]
Polystyrene	19	23.0	0.5299

4.9.1 Mechanical testing of allyl – functionalised TiO_2.

Stress-strain curves and mechanical testing results for allyl-functionalised TiO_2 are presented in figure 4.23 and table 4.4 respectively. As we can see an addition of 1 % of allylic functionalised Titania nanorods resulted in almost 3 times increase in Young's modulus, 4.3 times increase in tensile strength and 4 times increase in toughness. It is important to notice that higher 2.5 % concentration of functionalised nanorods gave substantially less increase in mechanical properties. We believe the major reason for this is that the nanorods form aggregates which do not allow for adequate or reasonable stress transfer and also add defects to the composite material.

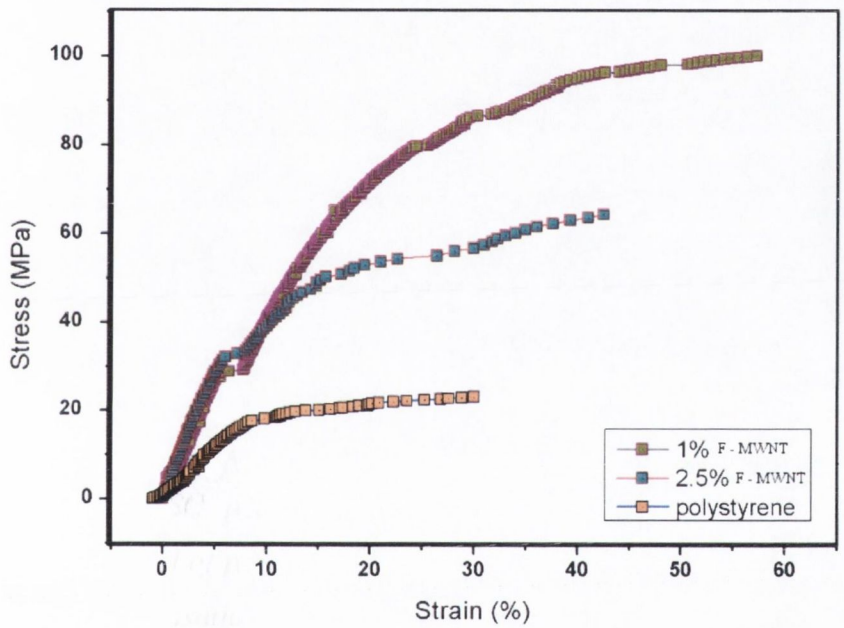

Figure 4.24 *Stress strain curve for allyl –functionalised titania –polystyrene.*

Table 4.4 Mechanical testing results for allyl –functionalised titania - polystyrene films.

Percentage TiO_2 composite	Young's Modulus [GPa]	Ultimate Tensile strength [MPa]	Toughness [KJ/m^3]
Polystyrene	1.9	23	0.5299
2.5%	5.3	64.3	1.48
1 %	5.7	100.1	2.3

4.9.2 Mechanical testing of propyl – Functionalised TiO_2.

Stress-strain curves and mechanical testing results for propyl-functionalised TiO_2 nanorods are shown in figure 4.24 and table 4.5 respectively. The addition of 1 % of propyl- functionalised tinania nanorods resulted in significant decline in Young's modulus, but gave 4.7 times increase in tensile strength and almost 4.3 times increase in toughness. Again higher concentration (2.5 %) did not demonstrate so significant increase in mechanical properties as lower 1 % addition due to the clustering of nanorods mentioned above.

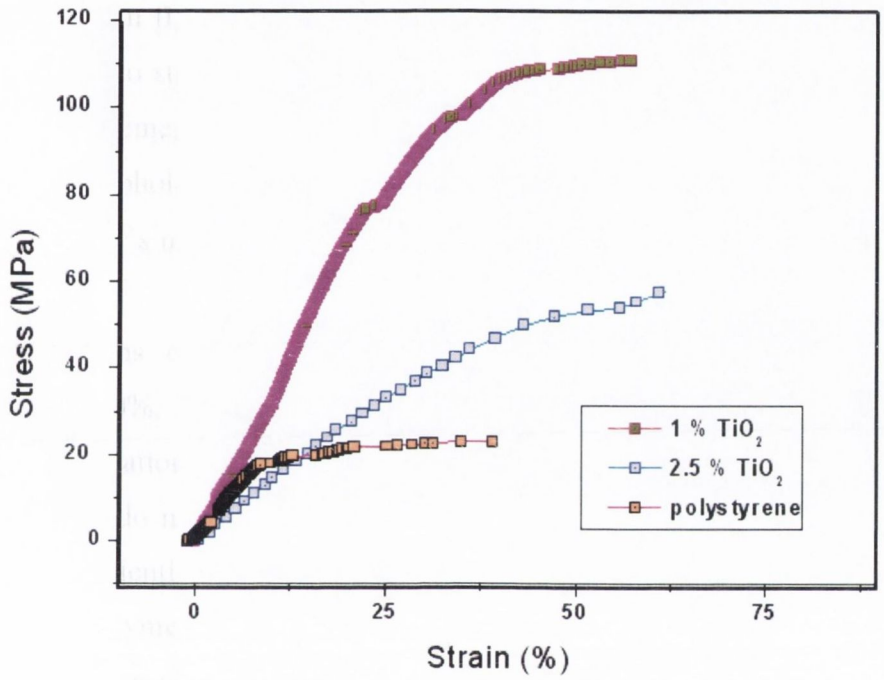

Figure 4.25 *Stress strain curve for propyl –functionalised –titania polystyrene films.*

Table 4.5 *Mechanical testing results for propyl –functionalised-titania polystyrene films*

Percentage TiO_2 composite	Young's Modulus [GPa]	Ultimate Tensile strength [MPa]	Toughness [KJ/m^3]
Polystyrene	1.95	23	0.5299
2.5%	1.21	67	1.54
1 %	0.46	110.4	2.53

4.9.3 Mechanical testing of hexyl – functionalised TiO_2

Stress-strain curves and mechanical testing results for hexyl-functionalised TiO_2 nanorods are shown in figure 4.25 and table 4.6 respectively. This time the addition of 1 % of hexyl-functionalised Titania nanorods barely changed the Young's modulus, but gave a 6.5 times increase in tensile strength and similarly a 6.5 times increase in toughness. Again the higher concentration (2.5 %) did not demonstrate such a significant increase in mechanical properties as lower 1 % addition presumably due to the clustering of nanorods mentioned above.

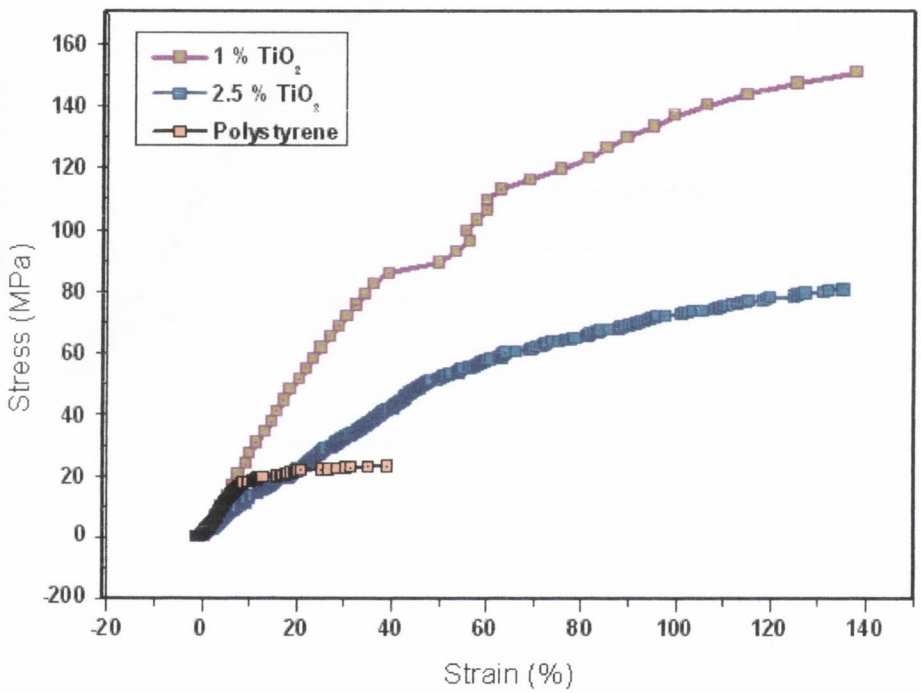

Figure 4.26 *Stress strain curve for hexyl –functionalised -titania polystyrene films.*

Table 4.6 *Mechanical testing results for hexyl –functionalised titania polystyrene films*

Percentage TiO_2 composite	Young's Modulus [GPa]	Ultimate Tensile strength [MPa]	Toughness [KJ/m^3]
Polystyrene	1.95	23	0.5299
2.5%	1.02	78.5	1.8
1 %	2.25	151	3.48

4.9.4 Mechanical testing of dodecyl – functionalised TiO_2

Stress-strain curves and mechanical testing results for dodecyl-functionalised TiO_2 nanorods are shown in figure 4.26 and table 4.7 respectively. The addition of 1 % of dodecyl -functionalised titania nanorods resulted in 2 times increase in Young's modulus and 4.8 times increase in tensile strength and in almost 5 times increase in toughness. Testing of the samples at higher concentration has not been performed due to the clustering of nanorods mentioned above.

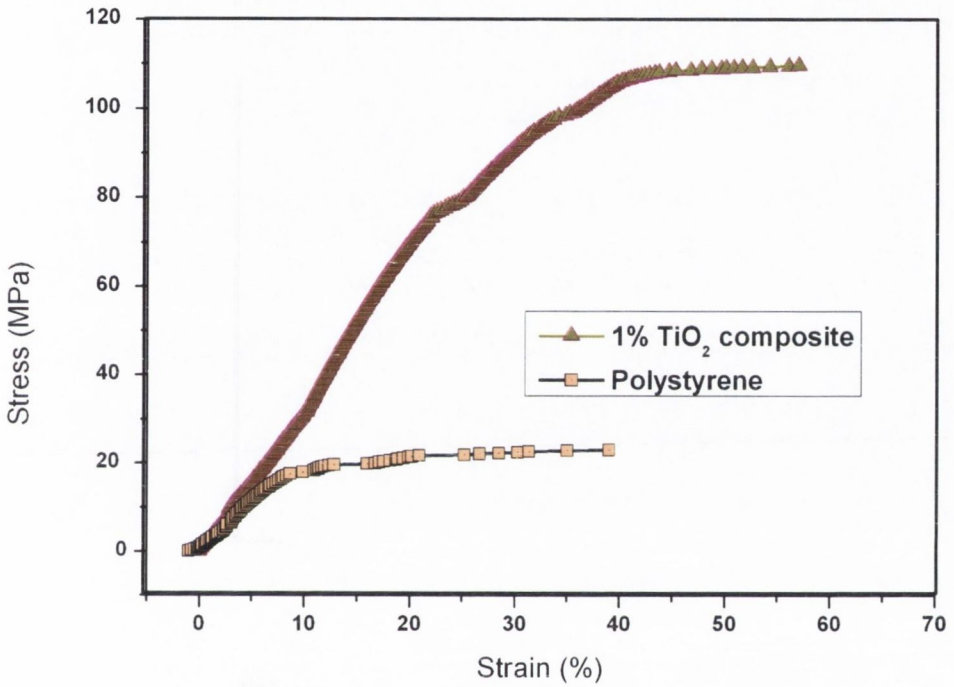

Figure 4.27 *Stress strain curve for dodecyl –functionalised -titania polystyrene films.*

Table 4.7 *Mechanical testing results for dodecyl – functionalised -titania polystyrene films*

Percentage TiO_2 composite	Young's Modulus [GPa]	Ultimate Tensile strength [MPa]	Toughness [KJ/m^3]
Polystyrene	1.95	23	0.5299
1 %	3.96	111	2.55

Results of measurements of ultimate tensile strength for different functionalities are compared in figures 4.27. It is evident that the greatest enhancement in tensile strength and toughness was achieved for hexyl-functionalised TiO_2 nanorods. Presumably 6 carbon chains provide the strongest interaction between the polymer matrix and TiO_2 surface resulting in the most efficient stress-stain transfer. Longer chains such as dodecyl might be aligned along the length of the nanorods without giving so strong interaction in the polymer matrix.

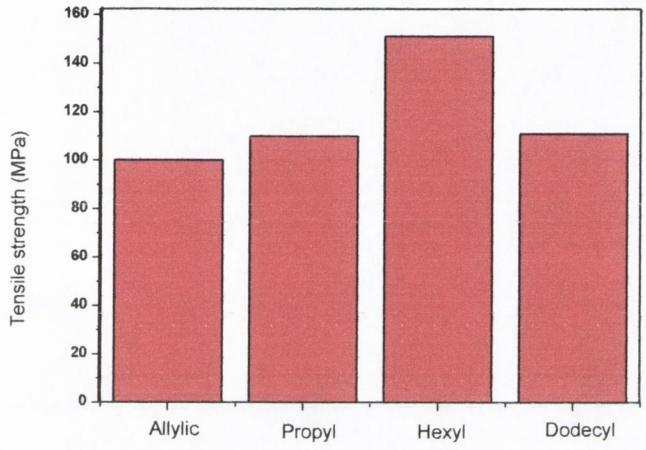

Figure 4.28 *Histogram showing the relationship between carbon chain length and Tensile strength for F – Titania.*

4.10. Conclusions

Thus we have demonstrated that TiO_2 nanorods can be effectively functionalised using appropriate trichloro- or triethoxisilanes. All functionalised TiO_2 nanorods demonstrated an increased solubility and stability in THF and polystyrene solutions in THF. It was found that concentration of functionalised TiO_2 nanorods increases linearly with an increase of polystyrene concentration in solution. This allowed the preparing of new polystyrene –TiO_2 nanorods composite films by solution casting techniques. New polymer composites demonstrated in very significant in mechanical characteristics. The 1 % addition of functionalized TiO_2 nanorods resulted in tremendous increases in tensile strength and toughness. However the concentrations of greater than one

volume percent of functionalized TiO_2 nanorods would not show such good degree of reinforcement. The major reason for this is that the functionalised nanorods form aggregates which do not allow for adequate or reasonable stress transfer and also add defects to the composite material. It was also found that the greatest enhancement in tensile strength and toughness was achieved for hexyl-functionalised TiO_2 nanorods. Hexyl chain provides the strongest interaction between the polymer matrix and TiO_2 surface resulting in the most efficient stress-stain transfer. Longer chains such as dodecyl are partially aligned along the length of the nanorods and do not provide so strong interaction with the polymer matrix.

4.10 References

1. Diebold, U. *Surf. Sci. Rep.* **2003**, *48*, 53.

2. Gratzel, M. *Nature* **2001**, *414*, 338.

3. Matsumoto, Y.; Murakami, M.; Shono, T.; Hasegawa, T.; Fukumura,T.; Kawasaki, M.; Ahmet, P.; Chikyow, T.; Koshihara, S.; Koinuma,H. *Science.* **2001,** *291*, 854.

4 .Huynh, W. U.; Dittmer, J. J.; Alivisatos, A. P. *Science.* **2002**, *295*,2425

5. Khan, S. U. M.; Sultana, T. *Sol. Energy Mater. Sol. Cells.* **2003**,*76*, 211.

6. Lakshmi, B. B.; Dorhout, P. K.; Martin, C. R. *Chem. Mater.* **1997**,*9*, 857. (b) Kasuga, T.; Hiramatsu, M.; Hoson, A.; Sekino, T.; Niihara, K. *Langmuir.* **1998**, *14*, 3160. (c) Zhang, X. Y.; Zhang, L. D.; Chen, W.; Meng,G. W.; Zheng, M. J.; Zhao, L. X. *Chem. Mater.* **2001**, *13*, 2511. (d) Kasuga, T.; Hiramatsu, M.; Hoson, A.; Sekino, T.; Niihara, K. *Ad*V. *Mater.* **1999**,*11*, 1307.

7. Pradhan, S. K.; Reucroft, P. J.; Yang, F.; Dozier, A. *J. CrystalGrowth.* **2003**, *256*, 83

8 .Pankove, J. I. *Optical Processes in Semiconductor*; Prentice Hall:New York, **1971**.

9 .Laudise, R. A.; Ballman, A. A. *J. Phys. Chem.* **1960**, *64*, 688. (b)Li, W. J.; Shi, E. W.; Zhong, W. Z.; Yin, Z. W. *J. Cryst. Growth.* **1999**,*203*, 186.

10. M. Cadek, J.N. Coleman, V. Barron, K. Hedicke, W.J. Blau, *Appl. Phys. Lett.*, **81,** 5123, (2002)]

11. Drucker D.C., *Introduction to mechanics of deformable solids*, McGraw-Hill, **1967.**

12. Shames I.H., Cozzarelli F.A., *Elastic and inelastic stress analysis,* Prentice-Hall, **1991**.

13. Beer F.P., Johnston E.R., et al, *Mechanics of Materials*, 3rd edition, McGraw-Hill, **2001**.

14. Popov, Egor P., *Engineering Mechanics of Solids*, Prentice Hall, Englewood Cliffs, N. J., **1990**.

Chapter 5

Nanotube composite materials

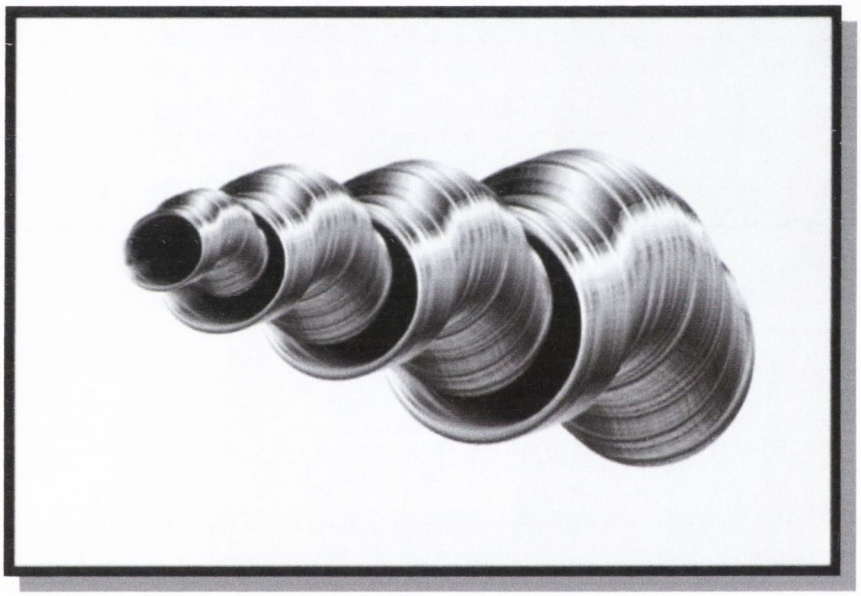

5.1 Introduction

Due to their novel structural, mechanical and electronic properties carbon nanotubes have been suggested for wide ranging applications in fields from chemical sensing to fibre reinforcement of plastics. Problems remain however in relation to their purity and process ability [1]. One particular difficulty; is that produced nanotubes are insoluble in almost all but the most aggressive of solvents. This issue has been partially addressed by the demonstration of stable, self-purifying dispersions of nanotubes in certain polymeric solutions [2]. However this solution is limited as it is non-trivial to predict the interaction of nanotubes with a given polymer and the number of polymers known to disperse nanotubes is small.

A simpler, more elegant solution is the controlled functionalisation of nanotubes. The ability to covalently bond chemical structures of choice in a controlled manner to nanotubes would allow the dispersion of the nanotubes in almost any solvent of choice. In addition it would greatly facilitate polymer-nanotube composite formation, as the interfacial polymer-nanotube interaction could be optimised for a wide range of polymers by varying the functionalities. However the benefits of simple controllable functionalisation would be much broader than this. Potential benefits could be imagined in many areas of science and technology from nanoelectronics, where covalently bonded molecular bridges could act as switching elements to plastics reinforcement, where interfacial stress transfer could be maximized by the covalent cross linking of the nanotubes.

Interaction of carbon nanotubes with appropriate siloxane precursors might result in new class of nanotube-polysiloxane composite materials. Thus main aim of this work is to develop novel carbon nanotube siloxane composites and investigate their properties.

5.2 Aims

First major objective of this part of our work was to prepare carbon nanotubes by arc-discharge method and purify them using methods that were reported previously. The next objective of this part of our work was to develop new

approaches for chemical functionalisation of carbon nanotubes using appropriate silane derivatives. An organometallic approach using BuLi is proposed for carbon nanotube modification with the subsequent binding of the lithiated nanotubes to appropriate halogen containing siloxane precursors. Next task of this work include the performing of sedimentation studies for functionalised carbon nanotubes in organic solvents to measure the solubility of the nanotubes in pure solvent and then with the addition of nanotubes and polymers in the solvent. DSC tests will be undertaken to analyse the thermal transitions of the nanotube polymer composites to see if the nanotubes affect the crystallinity of the polymers. Finally the next aim of this project was to prepare new ultra-strong polymer composite materials using chemically modified carbon nanotubes as additives and as a result provide an efficient bonding of nanotubes to the polymer matrix and good interfacial stress transfer. The preparation of new polymer composites is to be achieved by mixing the pure polymer with an optimal amount of polymer grafted carbon nanotubes in an appropriate organic solvent and by the preparation of films for nanotube-polymer composites. It was then planned to investigate the mechanical properties of the composites using Zwick-100 tensile tester.

5.3 Manufacture and Purification of carbon nanotubes

Multi-Walled Carbon Nanotubes were made using a Kratschmer-Huffmann Generator the basic design of which is shown in figure 4.1. Two graphite rods are used as the cathode and anode, between which arcing occurs when DC voltage power is supplied. A large quantity of electrons from the arc-discharge moves to the anode and collide into the anodic rod. Carbon clusters from the anodic graphite rod caused by the collision are cooled to low temperature and condensed on the surface of the cathodic graphite rod. The graphite deposits condensed on the cathode contain carbon nanotubes, nanoparticles, and clusters.

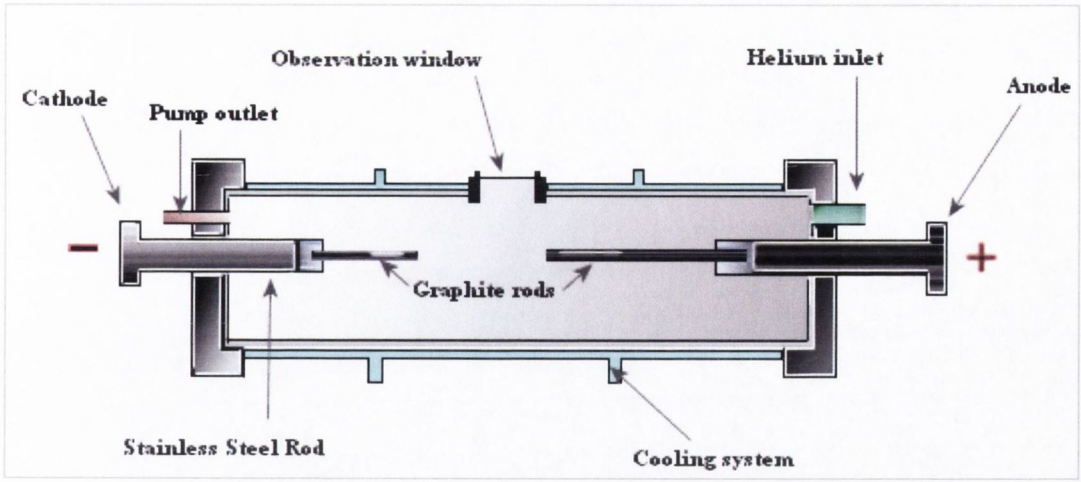

Figure 5.1 *Diagram illustrating a cross section of a Kratschmer-Huffmann Generator.*

The apparatus must be connected both to a vacuum line with a diffusion pump, and to a helium supply. The electrodes are two graphite rods, usually of high purity. Typically, the anode is a long rod approximately 6 mm in diameter and the cathode a much shorter rod 9 mm in diameter. Efficient cooling of the cathode has been shown to be essential in producing good quality nanotubes. The position of the anode should be adjustable from outside the chamber, so that a constant gap can be maintained during arc-evaporation. A voltage-stabilized DC power supply is normally used, and discharge is typically carried out at a voltage of 20 to 40 V and at a current in the range of 50 to 100 A. When a stable arc is achieved, the gap between the rods should be maintained at approximately 1 mm. The deposit was opened and the soft internal material was removed and divided into a fine powder. PPV (m-phenylenevinylene-co-2,5-dioctyloxy-p-phenylenevinylene) was produced using the Horner polycondensation. The PPV and toluene were mixed the resulting composite solution was further sonicated for 1 min using the sonic tip, and then for 2 hours in a low power (60W) sonic bath to ensure good dispersal and homogeneity. The solution was then left to settle for 48 hours to allow any impurities to sediment out. For each sample the resulting suspension was separated from the sediment by decantation.

The MWNT were retrieved from the polymer using Buckner filtration using a Teflon filter with a pore size of 0.45 microns over a sintered glass frit.

As functionalisation can lead to a breakdown in structure, this can also be detected in the TGA analysis. As the structural integrity of the nanotubes declines with functionalisation, the combustion temperature (as given by the derivative of the heating curve) also decreases. The greater the drop, the greater the structural corruption and therefore the greater the degree of functionalisation present in the bulk sample.

In addition to this, the derivative of TGA heating curve can also be use to determine the ratio of nanotubes to ligand /polymer present in the sample. This technique will be explained further in the section on sedimentation studies.

FTIR can also be useful in analysis of the bulk sample. The various stretches, bends, vibration and so on can help to clarify the type of bonding and functional groups present in the sample. As will be seen in the proceeding section on sedimentation of functionalised nanotubes, further proof of the presence of functionalities can be implied from the greatly increased stability of these samples in a polystyrene/THF solution. Raw non–functionalised nanotubes almost crash out after a minute where as those that have undergone processing can remain -in some cases-stable for weeks.

5.4 Characterisation methods of functionalised MWNT's.

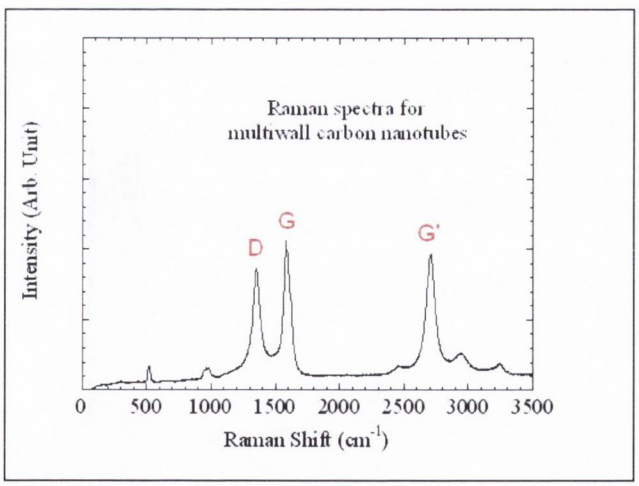

Figure 5.4 *Raman spectra showing the D, G and G' bands of functionalised multi walled nanotubes.*

Although individual or small clumps of functionalised nanotubes can be can be isolated using TEM or other forms of microscopy, such images do not necessary reflect the true nature of the entire bulk sample. Therefore other methods must be employed to ensure that the microscope imagery is a true reflection of the nature and degree of functionalisation. The first method available for bulk analysis is Raman spectroscopy. Figure 4.3 shows the three most characteristic peaks visible in the Raman spectra of multi walled nanotubes These peaks are called the D peak (~1330 cm^{-1}) the G peak (1581 cm^{-1}), and finally the G' peak (~1620 cm^{-1}). The G' band is due to a second order Raman scattering process related to sp^2 bonded carbons. The G band in the Raman spectra is that of sp^3 hybridised carbon it is a tangential C-C stretching mode. It is the area of graphitisation of the nanotube and from it, the degree of graphitisation can be estimated. Due to the structure of arc discharge nanotubes, which are perfectly straight and contain few if any sp^3 carbons, on the walls of the nanotube, the G band of these nanotubes is very large. Conversely, the *D* band is the dispersive disorder-induced band, which corresponds to the sp^2 bonded carbon atoms. By comparing the ratio of the intensity of the D band (I_D) with the intensity of the G band (I_G) the degree of functionalisation (I_D/I_G) can be estimated.

5.5 Reactions of MWNTS with pre-prepared compounds.

In all the following experiments in this section the catalytic Namur-COOH functionalised MWNTs were used. Under basic conditions the de-protonated carboxylic group will react with the amino to lose a proton to the amine group to form a ionic interaction between the two species as illustrated in figure 4.5 All amino containing molecules / MWNT composites have been prepared in the similar manner. Briefly; the MWNT has been dispersed in ethanol using ultra-sound. These were then stirred for 4-5 hours to ensure good dispersion .A solution of the various reactants in water/ethanol (50:50) was then added to the MWNTs.

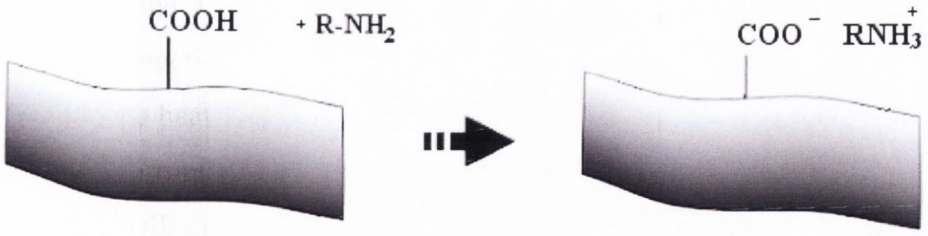

Figure 5.5 *Illustration showing siloxane reacting with the surface of the carboxylic functionalised catalytic MWNTs.*

The samples were stirred for twenty four hours in the presence of UV light (254 nm) for 24 hours. The products were washed with ethanol and dried under vacuum.

5.5.1 Reaction of Nanocycle MWNT and T_8NH_2 POSS

MWNT - T_8NH_2 composites have been prepared in the following manner. First MWNT have been dispersed in ethanol using ultra-sound. A solution of T_8NH_2 in water was added to the nanotubes and the mixture was stirred under UV radiation (254 nm) for 2 hours. The product was washed with ethanol and dried in vacuum. The MWNT/T_8NH_2 composites have been characterised by and TEM, TGA, IR and Raman spectroscopy. TEM images of MWNT/T_8NH_2 nanocomposites are shown in figure 5.6. According to these images there is a formation of POSS nanoparticles and POSS coating on carbon nanotubes. The IR spectra of this sample showed characteristic amido bands at 1658 cm^{-1} and 1706 cm^{-1}. The -COOH stretches were also clearly visible at 3604 cm^{-1} as were CH_2 stretches at 2860 cm^{-1}.

The Raman spectrum of the bulk material shows a sizable increase in intensity, from the initial nanotube sample, also visible is the appearance of the D' band with a slight shoulder. More significantly is that decrease in the G band, showing an increasing disorder of graphitic structure in the sample due to the chemical functionalisation.

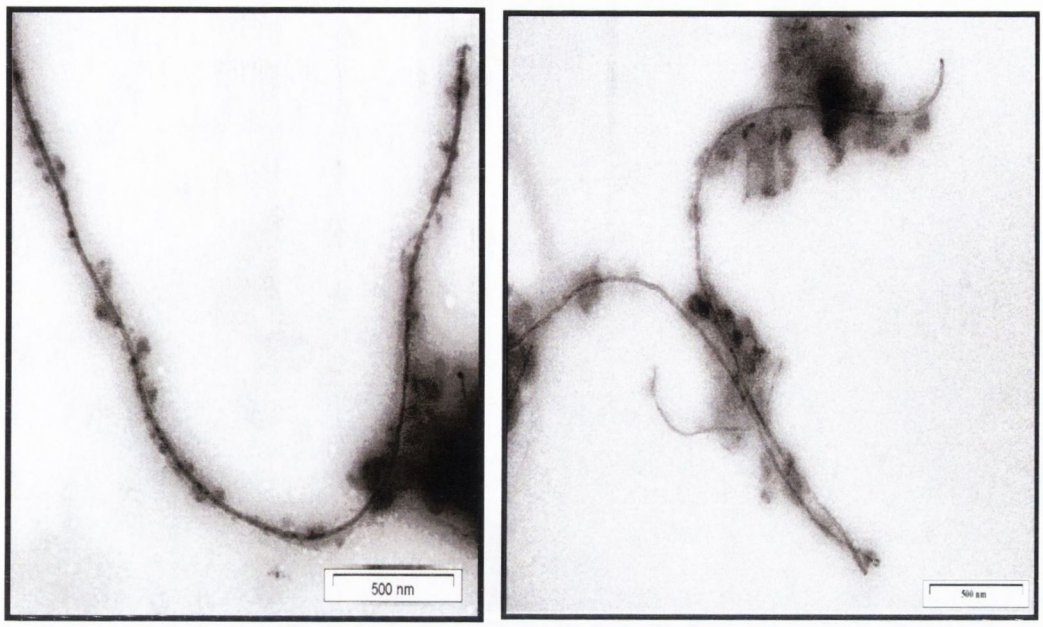

Figure 5.6 *TEM images showing the reaction of nanocycle nanotubes with T_8NH_2. This resulted with nanotubes being decorated by clusters of POSS nanoparticles.*

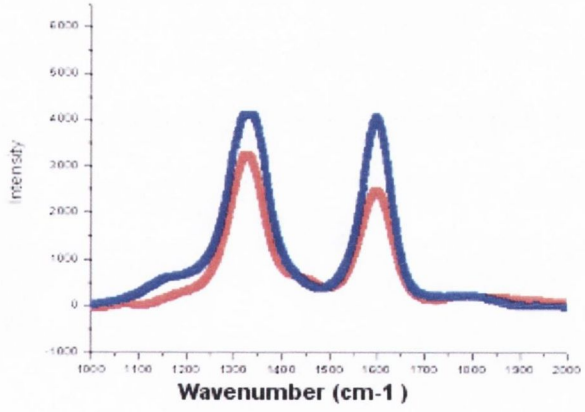

Figure 5.7 *Raman spectra of MWNT - T_8NH_2 composites.*

The functionalisation is also reflected in the TGA diagram as the derivative of the heat curve peak has shifted to a lower temperature 363 °C to compare with 546 °C for original nanotubes (figures 5.8 and 5.9).

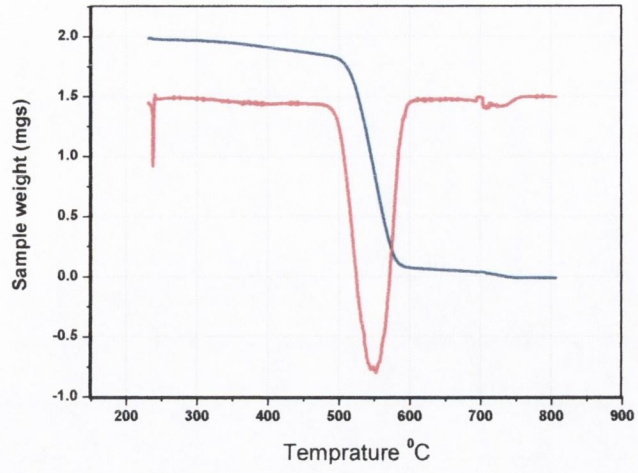

Figure 5.8 *TGA plots of initial multi-walled nanotubes.*

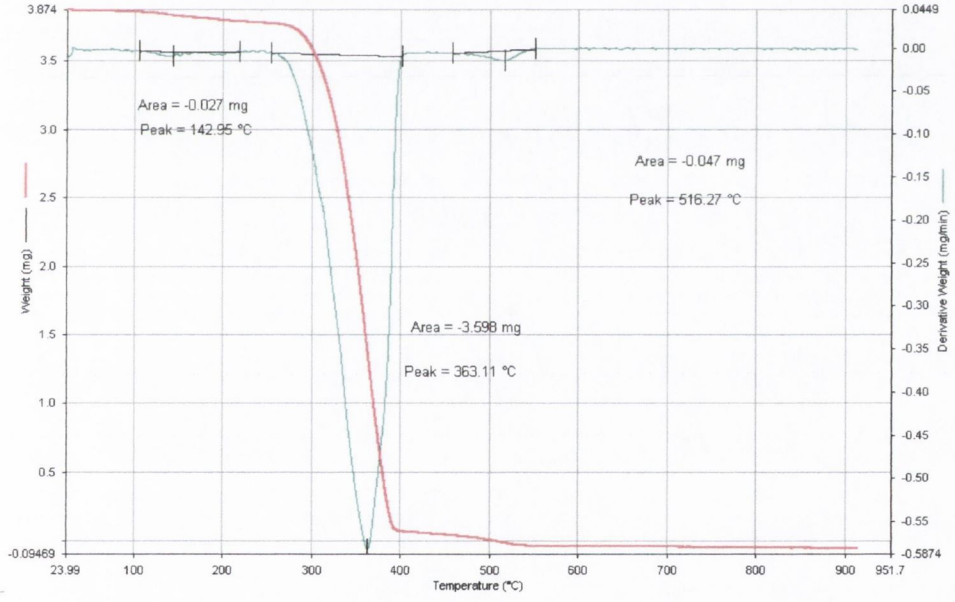

Figure 5.9 *TGA plot of F-MWNT.*

5.5.2 Reaction of Nanocycle MWNT with T_8NH_3 POSS

The treatment of MWNT with T_8NH_3Cl POSS was performed similarly to the preparation of MWNT - T_8NH_2 composites above. The products have been characterised by TEM, TGA, IR and Raman spectroscopy.

Figure 5.10 *TEM images of T_8NH_3Cl – MWNTs composites.*

The IR spectra of this sample showed characteristic amido bands 1658 cm^{-1} and 1706 cm^{-1}. The -COOH stretches again were also clearly visible at 3606cm^{-1} as were CH_2 stretches at 2866 cm^{-1}.

5.5.3 Reaction of Co/MgO MWNT with T_8NH_2. POSS

The similar reaction of Co/MgO multi-walled nanotubes with the T_8NH_2 gave dendrite-like aggregate of POSS nanoparticles covering the nanotubes as shown in Figure 5.13 shows that nanotubes are coated by POSS nanoparticles. In this case nanotubes serve as a backbone for the assemblies. The diameter of the nanotubes is around 40 nm. An average diameter of the POSS nanoparticles is 85 nm. As with the previous examples the IR spectrum showed the presence of CH_2 peaks at 2845 cm^{-1}, the amine group at 1678cm^{-1}, and a broad stretch of the carboxylic groups at 3325cm^{-1}. As can be seen from the Raman spectrum there is a slight increase in intensity of D band due to the chemical functionalisation.

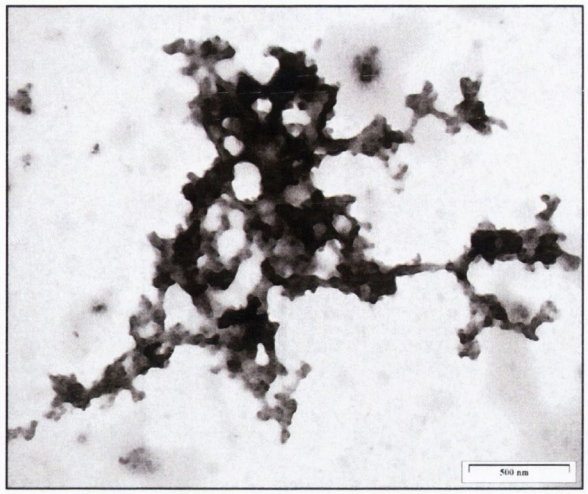

Figure 5.11 *TEM Image of Co/MgO MWNT T_8NH_2 POS*

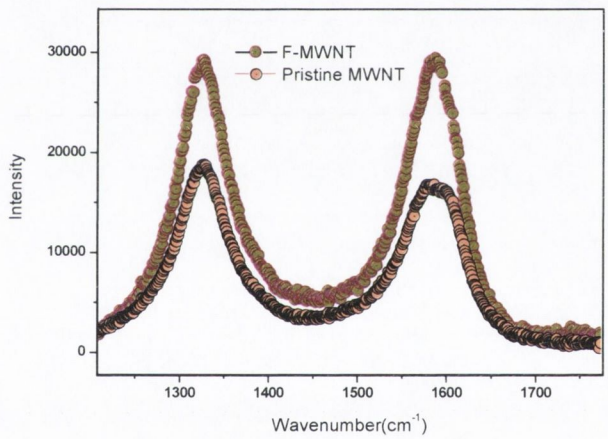

Figure 5.12 *Raman of bulk sample, lower curve pristine nanotubes upper curve f-MWNTs,*

The diameter of the nanotubes is around 40 nm. An average diameter of the POSS nanoparticles is 85 nm .As with the previous examples the IR spectrum showed the presence of CH_2 peaks at 2845 cm^{-1}, the amine group at 1678cm^{-1}, and a broad stretch of the carboxylic groups at 3325cm^{-1}. As can be seen from the Raman spectrum is a slight increase in intensity of D band due to the chemical functionalisation.

5.5.4 Reaction of Co/MgO MWNT with T_8NH_3. POSS

The treatment of Co/MgO MWNT with T_8NH_3Cl POSS was performed similarly to the preparation of MWNT - T_8NH_2 composites above. The product have been characterised by TEM, TGA, IR and Raman spectroscopy. IR spectrum showed the presence CH_2 peaks at 2855cm^{-1}, and a broad stretch of the carboxylic groups at 3320cm $^{-1}$, also clearly present was the Si-O-Si band at 1196 cm^{-1}, the amine group again appeared at 1678cm^{-1}.

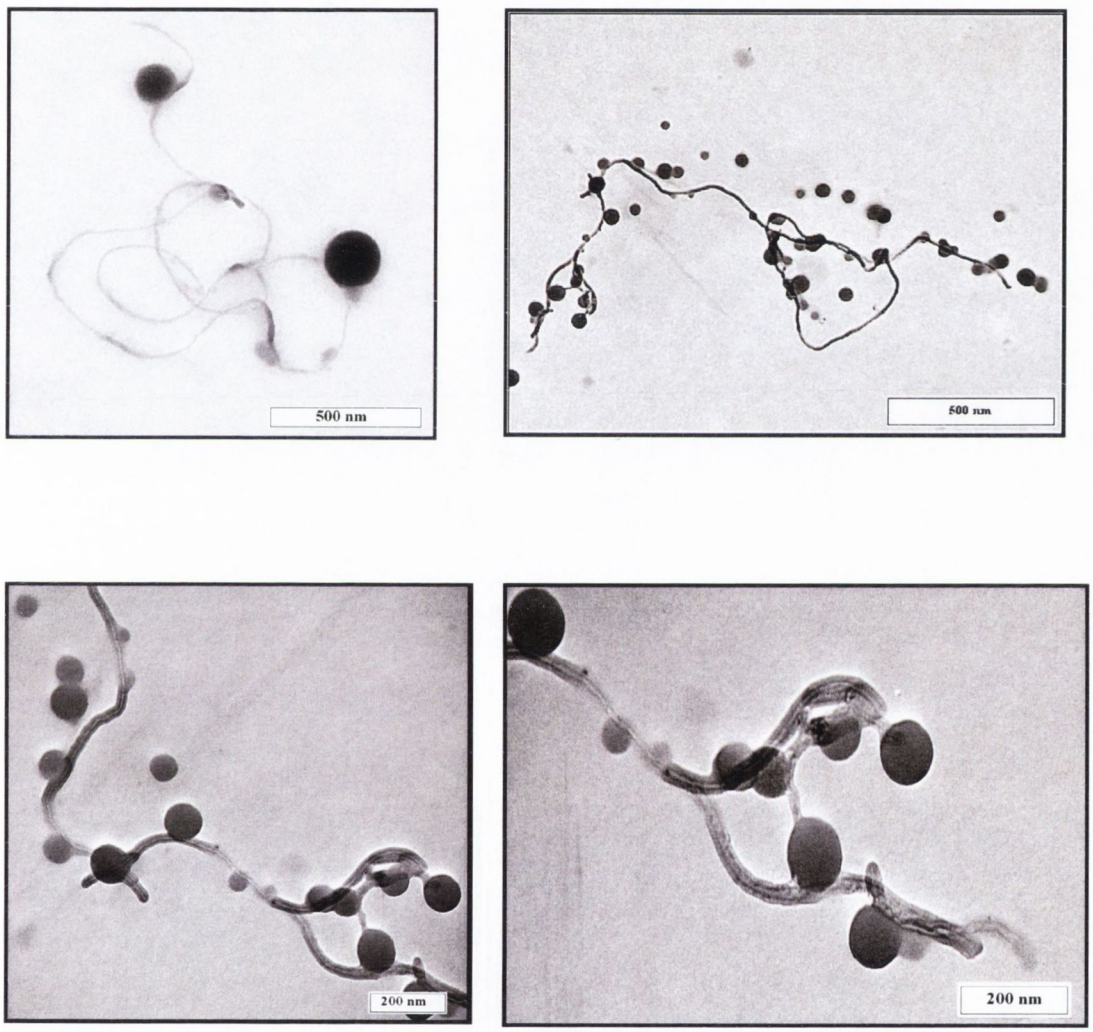

Figure 5.13 *Tem images of T_8NH_3 covered light in an even coating of POSS on top of which particles of the polymer have attached. These tend to form clusters near the tip of the nanotubes*

Close examination on the TEM images shows that the nanotubes have an even T_8NH_2POSS coating all along their length. . In addition to this the images clearly show that the nanotubes are also partially covered in spherical aggregates of POSS (average diameter of 160nm). These particles tend to form grape like clusters, particularly at the ends of the nanotubes

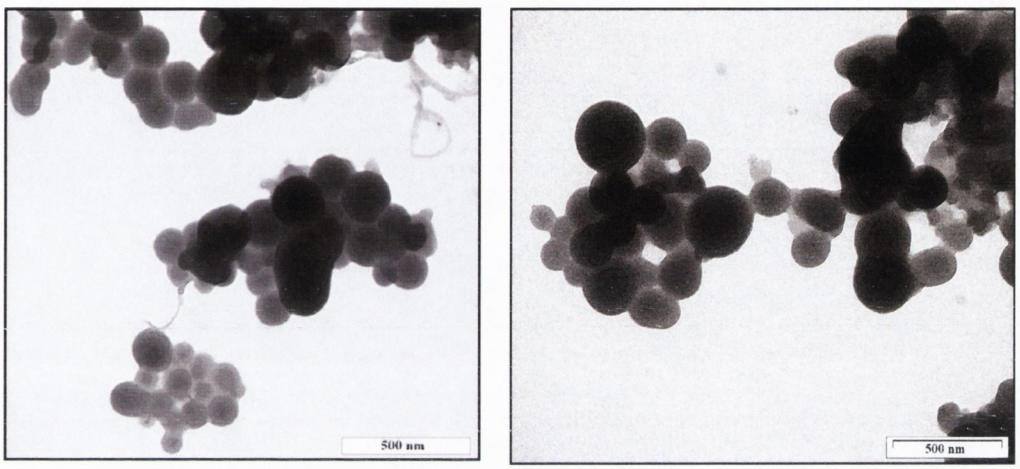

Figure 5.14 *Tem images of nanotubes covered in a heavy of coating of T_8NH_3 POSS.*

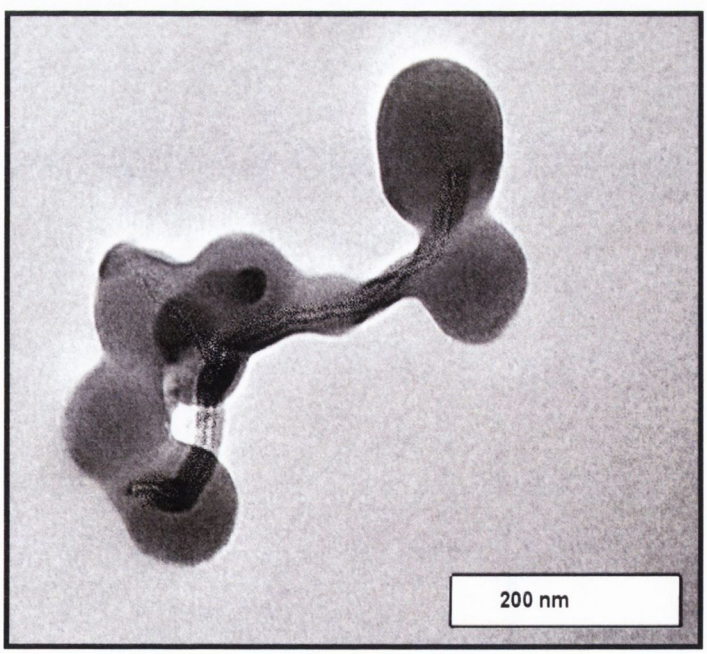

Figure 5.15 *TEM image showing a short nanotube fully encased in the POSS.*

The Raman spectrum clearly shows an increase in the D band, TGA analysis showed the combustion temperature to have dropped to 367 ^{O}C.

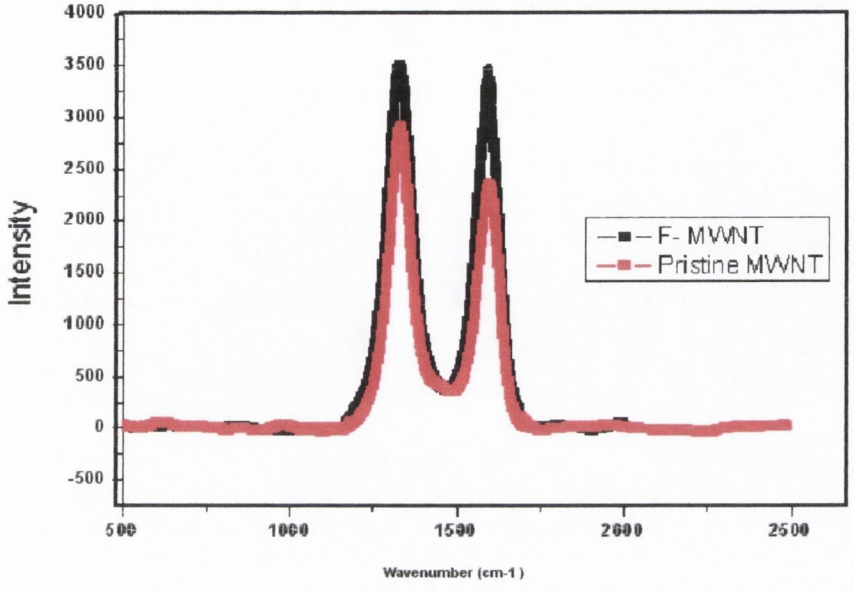

Figure 5.16 *Raman spectra of Co/MgO MWNT - T_8NH_3Cl composite.*

5.5.5 Reactions of lithiated MWNTs with siloxane precursors.

It has been reported that C_{60} can react with lithium alkyl and Grignard reagents giving alkylated metal fullerides *e.g.* $RC_{60}^{-}Li^{+}$ [6]. However, while these aspects of the organometallic chemistry of fullerenes have been quite well explored, the corresponding research on carbon nanotubes has not yet been developed. It is well known that nanotubes can contain many deviations from pure hexagonal structure. Examples of this are five membered rings required for positive closure at tips or kinks, and seven member rings required for negative curvature. Additionally the nanotube bodies can support combinations of five and seven membered rings known as the Stone-Wales defect [7]. These sites are potentially reactive due to the fact that these carbon atoms are under more sterical stress than the similar atoms in the graphitic planes, which means that they will react with lithium alkyls.

In this section we use this approach to metallate carbon nanotubes. Purified annealed CO-free MWNTs were reacted with BuLi in THF under argon at the

ambient temperature to give noticeably green solutions. The process involves a charge transfer from BuLi to the MWNT with the formation of extremely air and moisture sensitive adducts $(MWNT^{n-})Li^{+}_{n}$. After the treatment, the dispensability of the nanotubes in THF increases significantly (~ 40 % in solution). This is most likely due to the addition of the presence of butyl groups to the nanotubes.

We suggest that at low concentrations of BuLi, the metallation proceeds mainly at the tips and other non-hexagonal regions due to the steric stresses that the carbon atoms here are under. As the metallating reagent (lithium alkyl) is increased, these sites saturate resulting in the partial side-wall functionalisation. Additionally, depending on the electronic properties (*e.g.* metallic, semi conducting) of each nanotube, a partial or complete charge delocalisation might occur. This may result in some nanotubes being more susceptible to functionalisation with alkyl groups and Li atoms along the entire body of MWNT's.

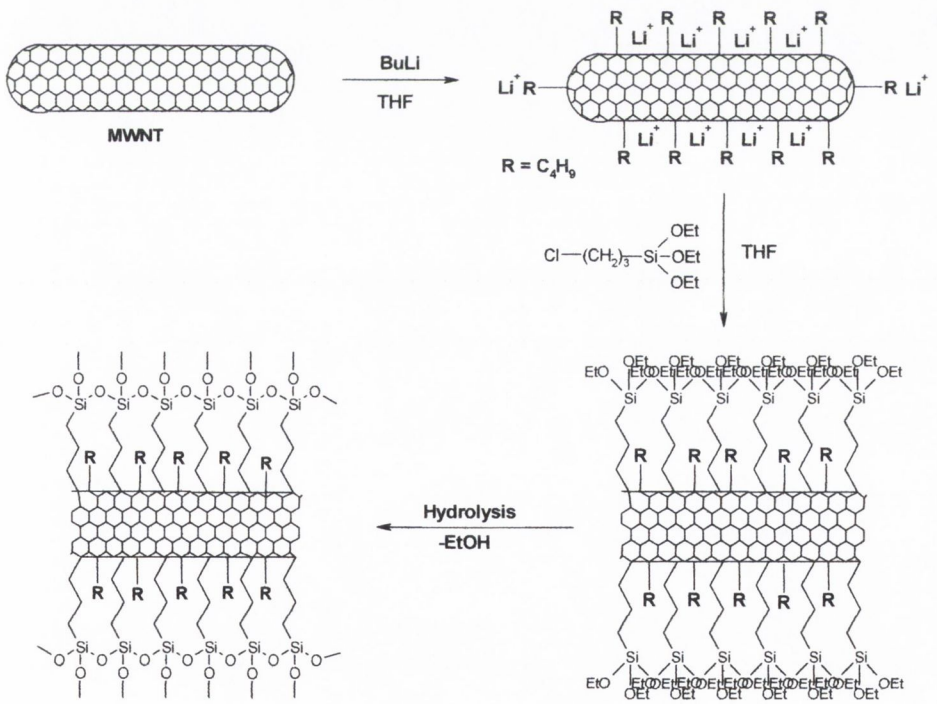

Scheme 5.1 *Illustration showing the general synthetic strategy adopted in this section of the work.*

In this section our strategy was to generate the coated nanotubes while simultaneously synthesising the Siloxane octamers. In this case we used purified arc discharge tubes, which had been treated initially with BuLi. These we reacted with $Cl(Prop)Si(OEt)_3$, in the hope of attaching the propyl group to the nanotubes with the elimination of LiCl This intermediate was then hydrolysed using the sol gel technique as normal as shown in scheme 5.1 The TGA-estimated siloxane content in the grafted MWNTs was between 64%-86% depending on the individual sample.

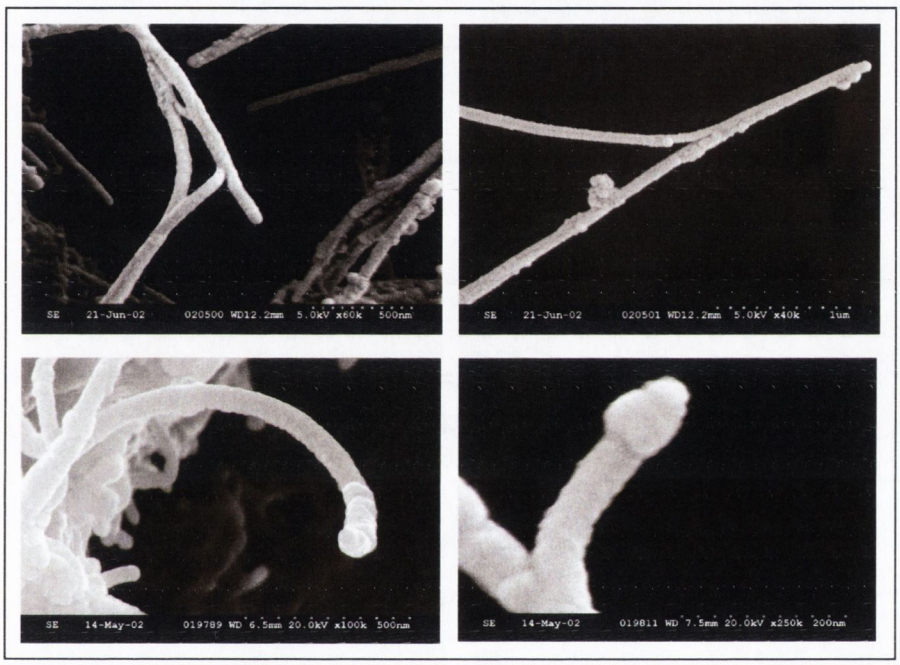

Figure 5.17 *SEM images of POSS coated Multi-walled nanotubes showing a tendency to concentrate on the tips rather than the edges, the upper samples are arc-discharge nanotubes and the lower images) are catalytic tubes, all samples were lithiated as outlined in the text.*

Under examination of these and similar samples we found that in some instances we had coated – not unsurprisingly - the nanotubes more so at the tip rather than at the sidewalls – as was expected.

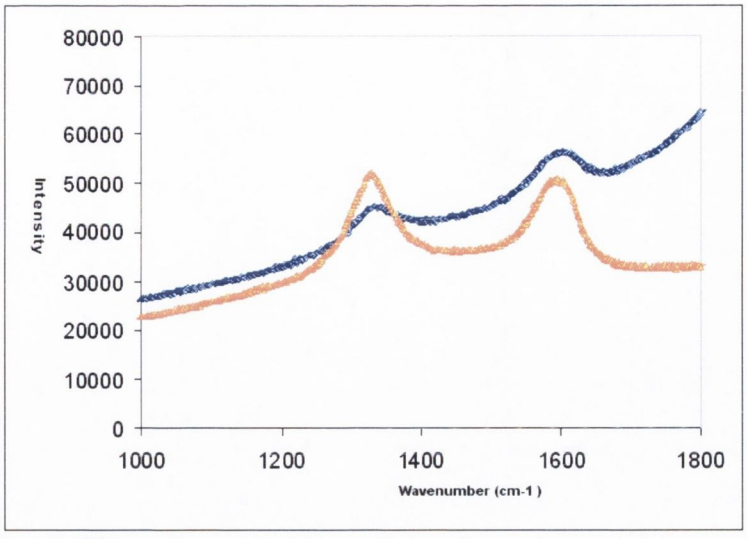

Figure 5.18 *Raman of the bulk sample, showing a clear decrease in the D band and increase in the G band.*

In another auxiliary experiment we decided to repeat the previous method using only highly pure nanotubes from Namur in Belgium .In addition we also allowed the reaction to proceed for a further 24 hours longer. The resulting sample shows again much evidence of nanotube coverage by POSS as in the previous cases. What was however totally unexpected was the presence of large macro sized objects found in some of these samples as shown in figure 5.19.

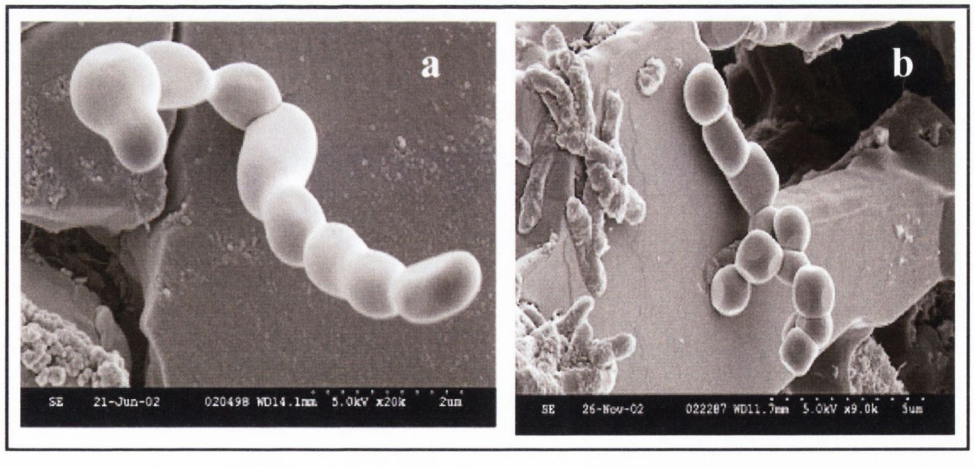

Figure 5.19 *SEM images of the macro sized particles, notice also the scale of image a compared to image b.*

When synthesised using BuLi in the absence of nanotubes the polymer has a solid morphology as can be seen in the background of Figure 5.19 it is only when nanotubes are introduced do we see these macro sized particles.

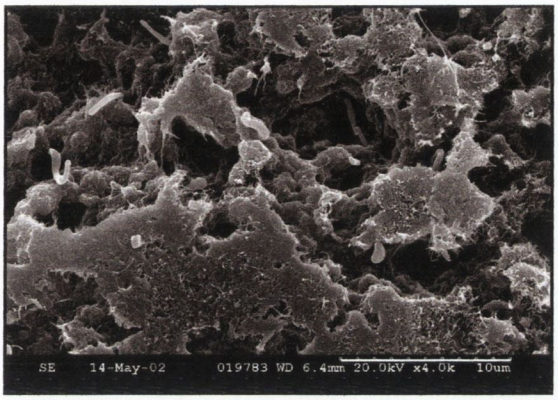

Figure 5.20 *TEM of the sample containing macro-sized objects.*

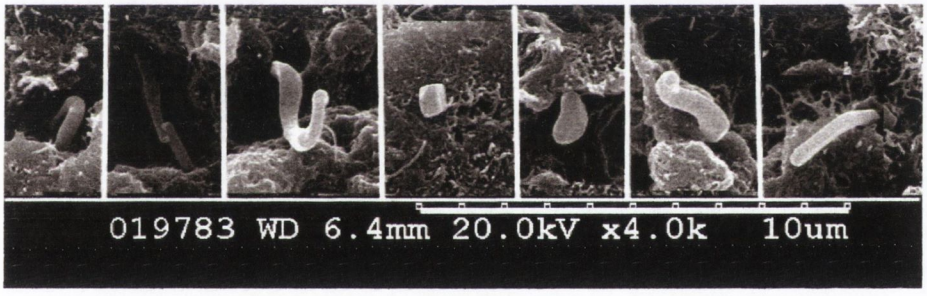

Figure 5.21 *TEM close up view of macro –sized clumps that began to appear in the samples.*

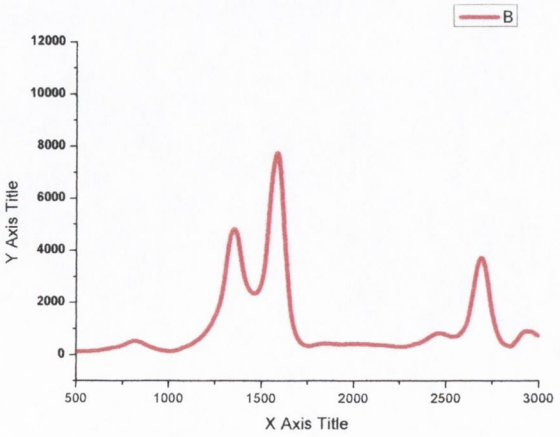

Figure 5.22 *Raman of bulk sample as can be seen the G band has increased*

dramatically in relation to the D band. This suggests a large amount of functionalisation present in the sample also notice the prominence of the D' band.

Upon closer inspection we can see a better view of these large masses.

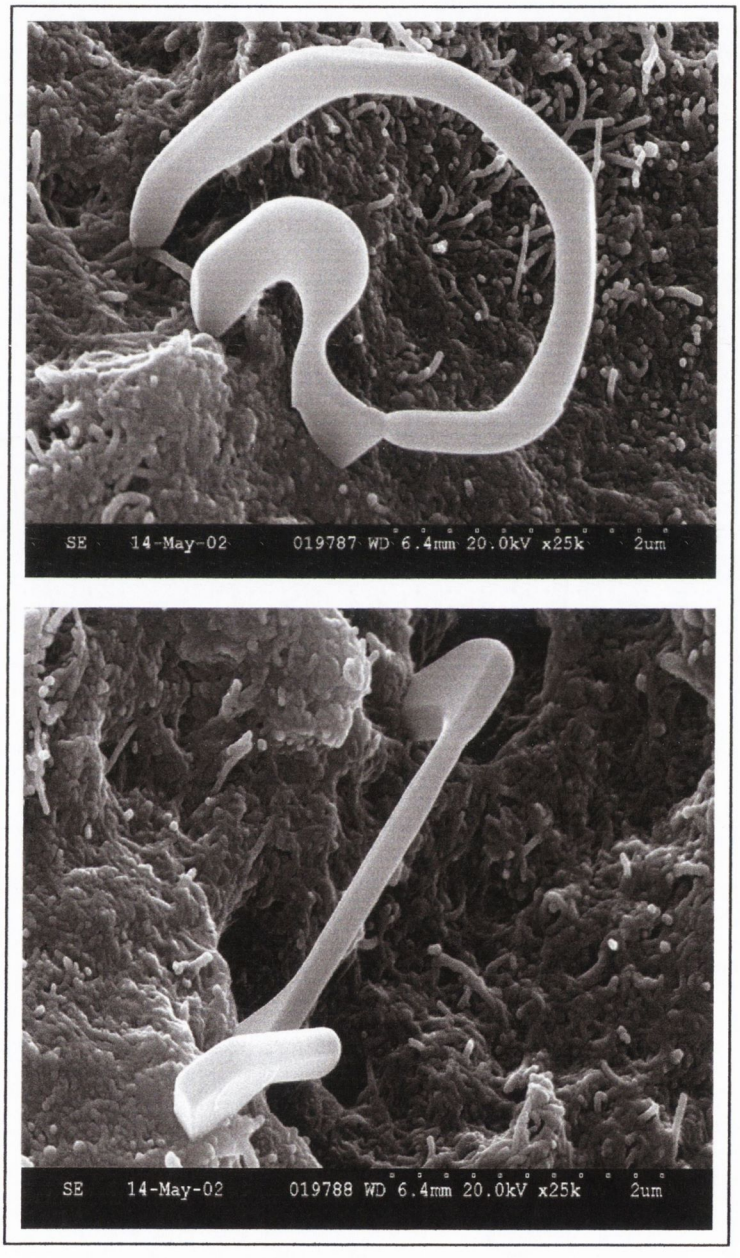

Figure 5.23 *SEM of the largest objects found in the lithiated samples.*

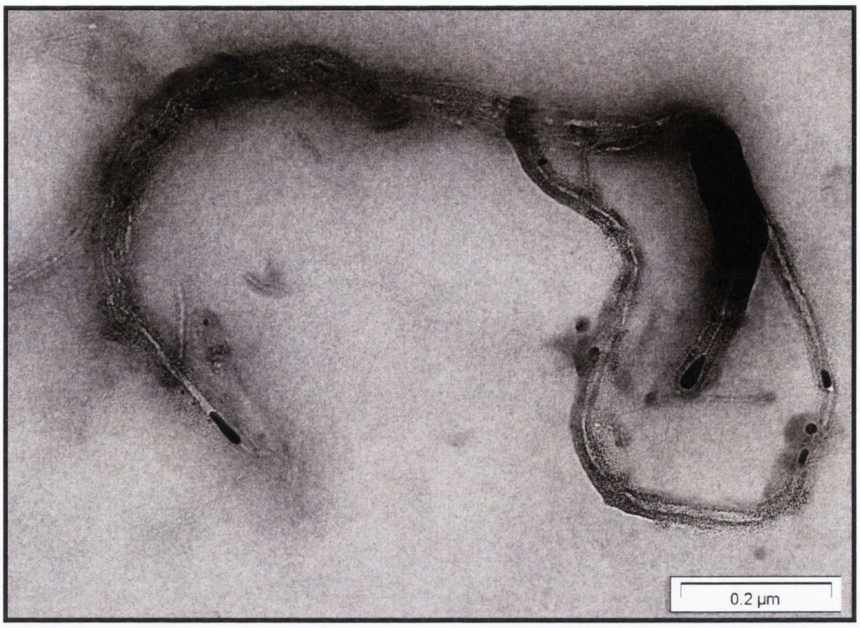

Figure 5.24 *TEM image of the same sample shown in figure 4.19, the POSS coating can be clearly distinguished covering the nanotubes, notice however that a section in the right hand corner is opaque. The thickness of the POSS layer making the beam impenetrable, notice also that in the left hand corner the nanotubes are clumped or "roped" together.*

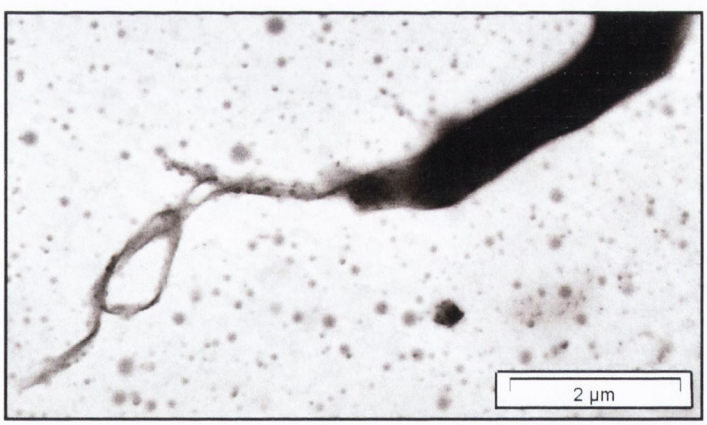

Figure 5.25 *TEM image of the same sample shown in figure 4.19 showing coarsely coated nanotube emerging from a larger aggregate. This large body is completely impervious to the electronic beam of the microscope.*

To ensure that these formations were not caused by salts formed during the reaction the sample was washed with water .SEM images after washing revealed that these formations were still present EDX studies also showed that the formations are composed mostly of Silicon and carbon.

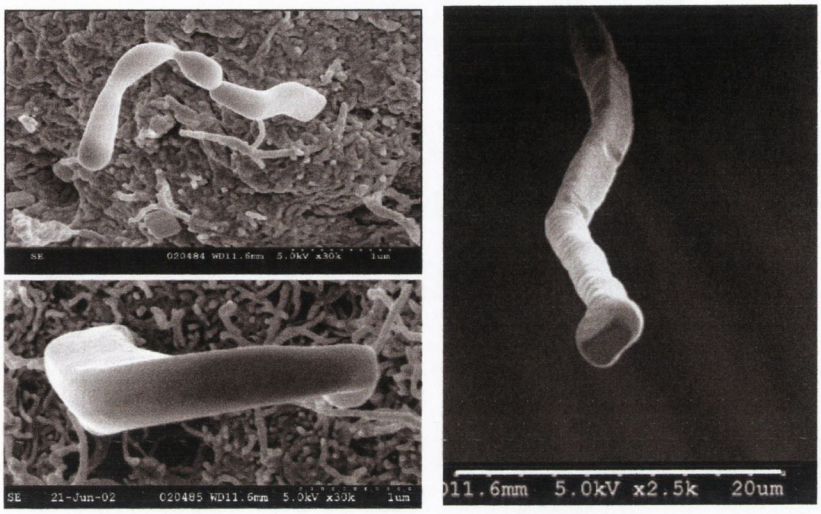

Figure 5.26 *SEM images of the samples after washing with water. The samples still contained these large objects.*

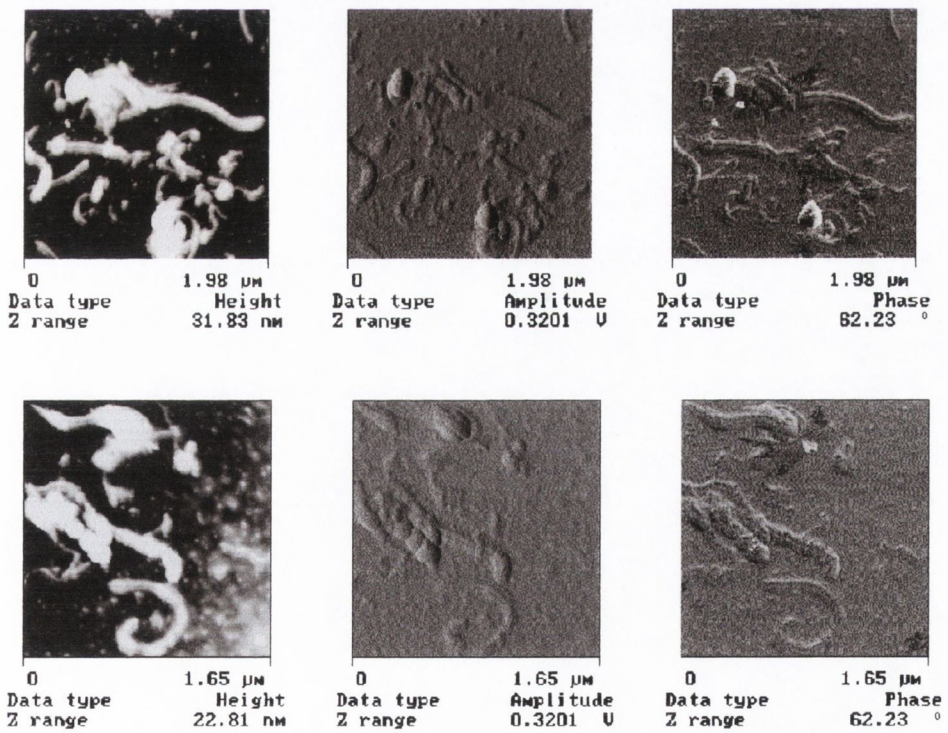

Figure 5.27 *AFM images showing the presence of the macro sized particles.*

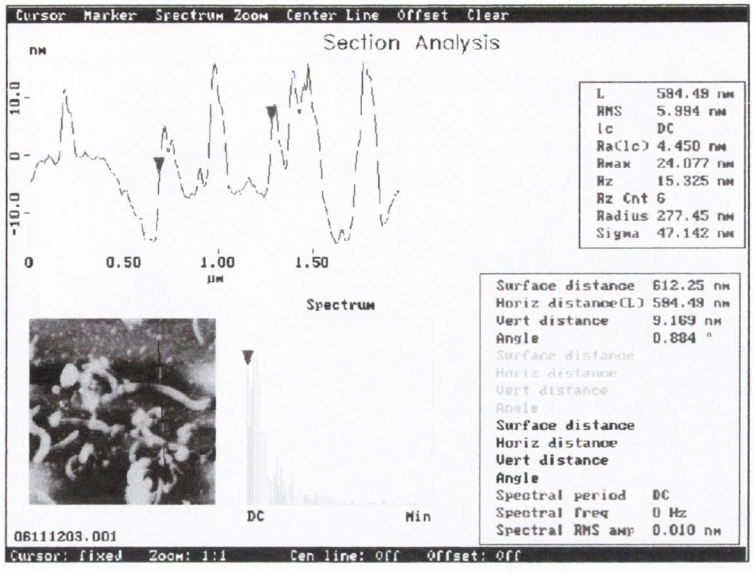

Figure 5.28 *AFM cross-section showing topography of the surface.*

5.6 Raman studies

Due to the success of the sedimentation studies described in the previous chapter the same functional groups were used to functionalise Multi-walled nanotubes, Raman spectroscopy used to check functionalisation.

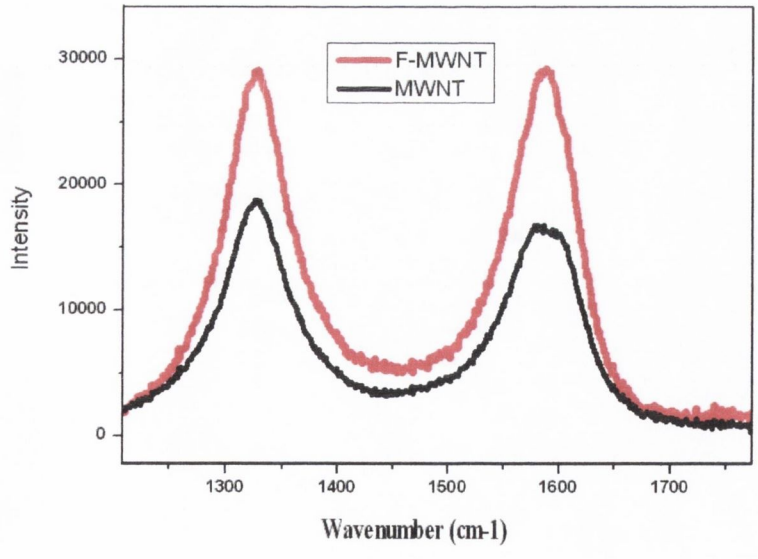

Figure 5.29 *Raman plot of Allylic F-MWNT.*

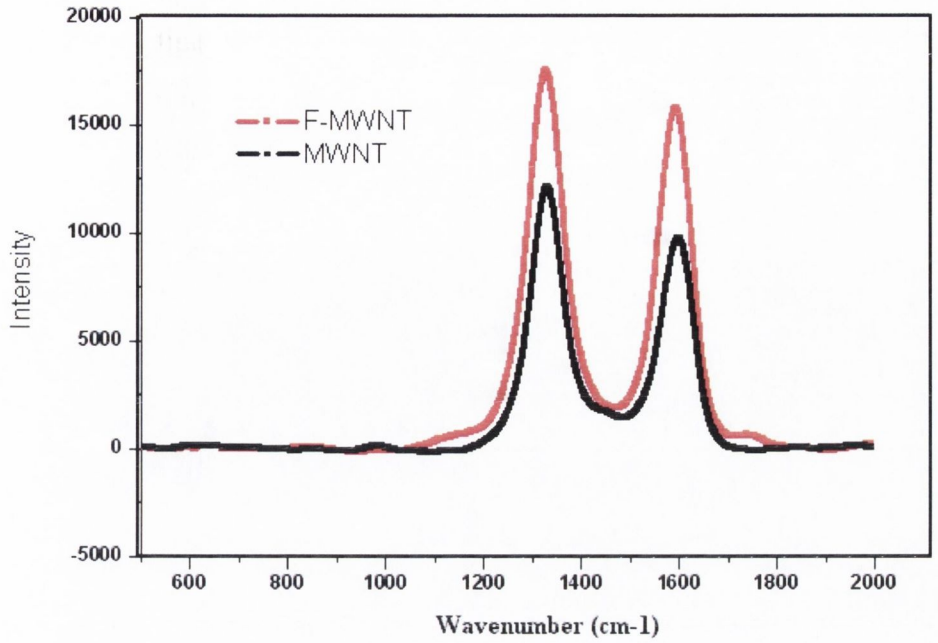

Figure 5.30 *Raman plot of Propyl F-MWNT*

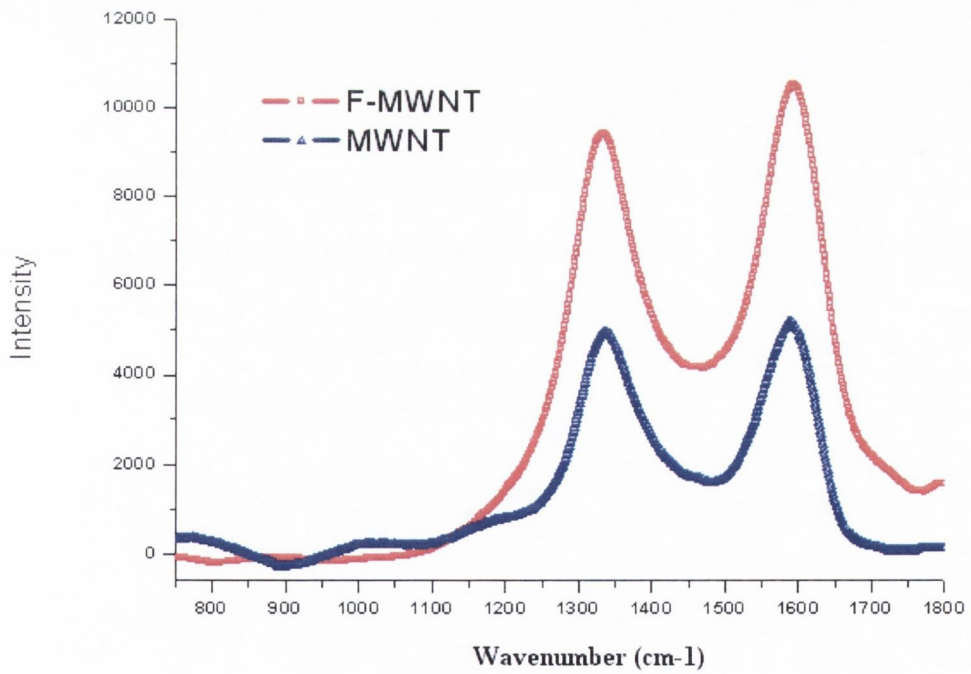

Figure 5.31 *Raman plot of hexyl F- MWNT*

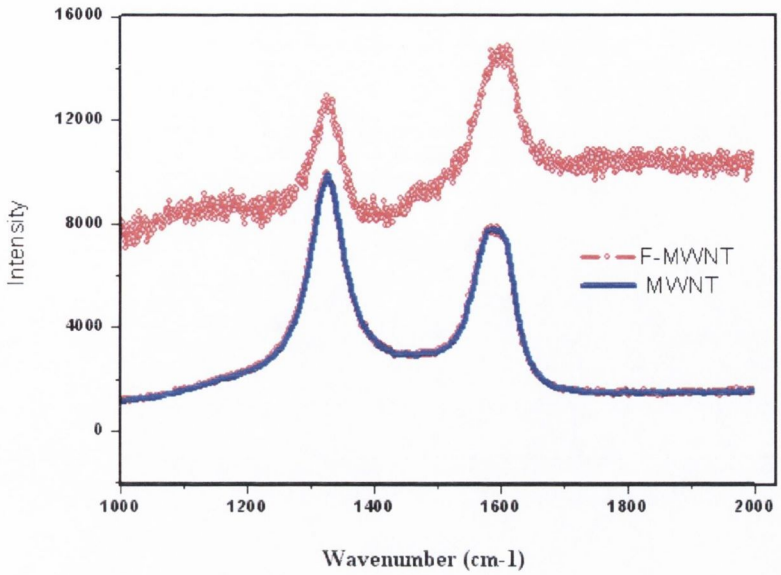

Figure 5.32 *Raman plot of Dodecyl F-MWNT.*

5.7 TGA and DSC studies of FMWNT.

As outlined in chapter four both TGA and DSC analysis was necessary to ensure that the addition of the functionalised MWNT did not lead to crystallization in the sample.

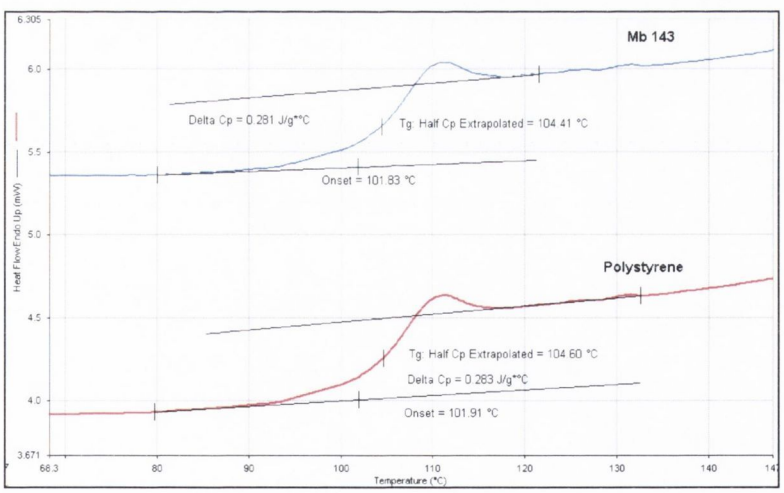

Figure 5.33 *DSC plots of 2% propyl-functionalised MWNT sample with polystyrene and of polystyrene with no MWNT additives. The sample shows no sign of crystallisation and there is little if any change in the glass transition*

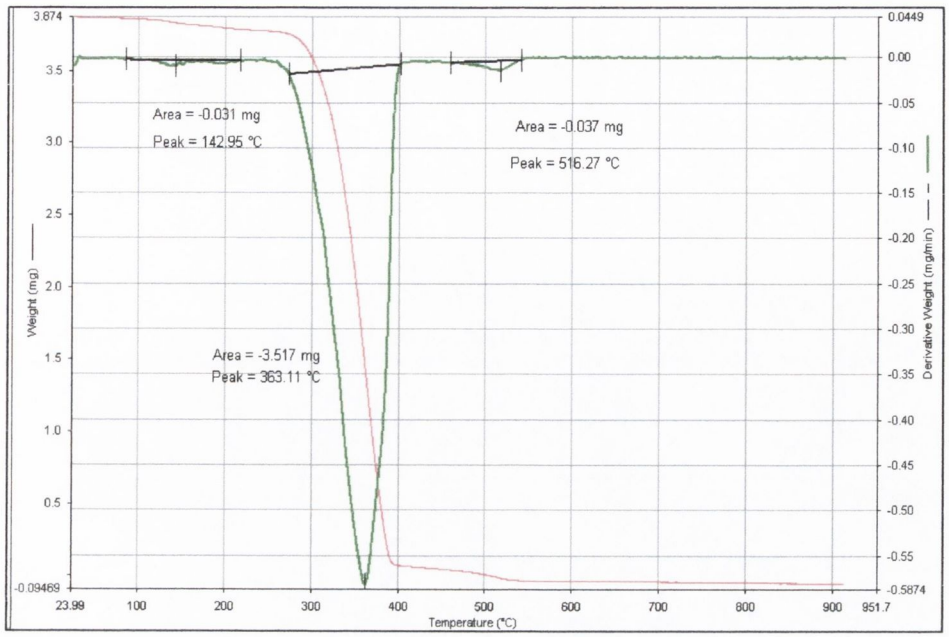

Figure 5.34 *TGA plot for Allylic F MWNT.*

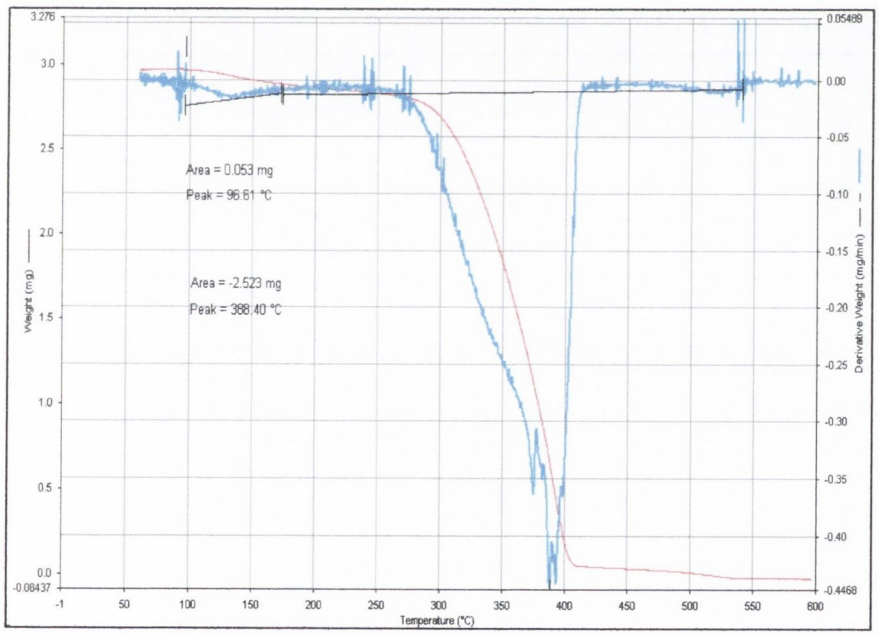

Figure 5.35 *TGA plot for Propyl - F -MWNT.*

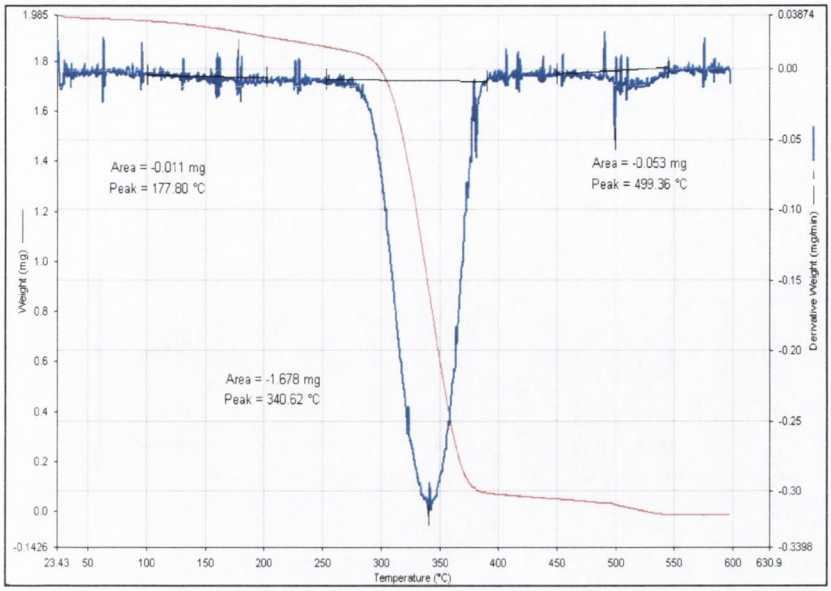

Figure 5.36 *TGA plot for hexyl - F -MWNT.*

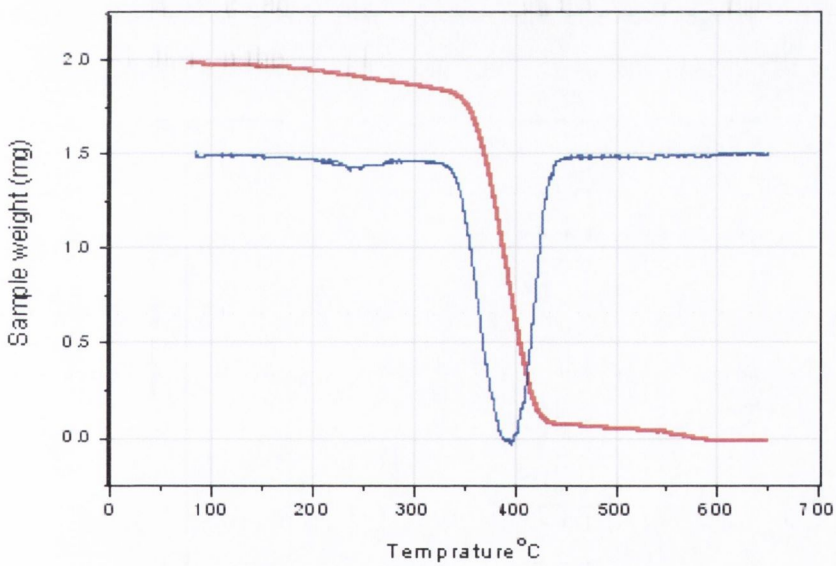

Figure 5.37 *TGA plot for Dodecyl - F -MWNT.*

From the TGA plots we can see that all four samples show a trop in the combustion temperature.

Table 5.1 *Combustion temperatures for the four F-MWNT samples used in the sedimentation studies and film reinforcement studies.*

Sample	**Combustion point**
Allyl – F- MWNT	352 °C
Propyl– F- MWNT	398 °C
Hexyl – F- MWNT	340 °C
Dodecyl – F- MWNT	397 °C

5.8 Sedimentation studies

Sedimentation studies were necessary to examine the solubility and stability of the siloxane functionalised nanotubes in THF. The THF was chosen as a solvent, because this solvent was most promising for the preparation of nanotube doped polystyrene films. Nanotubes would not normally be soluble in this solvent without functionalisation. A sample of nanotubes was taken and sonicated under the sonic tip for five minutes. This was then transferred as quickly as possible to a 1 cm quartz cuvette. The sample was then placed in a sedimentation machine and the transmitted light was recorded.

In figure 5.30 the rate at which propylsiloxy-functionalised nanotubes fall out of a THF solution is shown. The relatively stable concentration of functionalised nanotubes of 0.25 g/L have been reached at 45 hours.

5.8.1 Sedimentation of allyl functionalised MWNTs composite.

Sedimentation curve of allyl-functionalised MWNTs is illustrated in figure 5.38. The stable concentration of 0.35 g/l was reached after 25 hours. This implies that 39% of the initial weight contains MWNT that are functionalised sufficiently to remain stable for long periods.

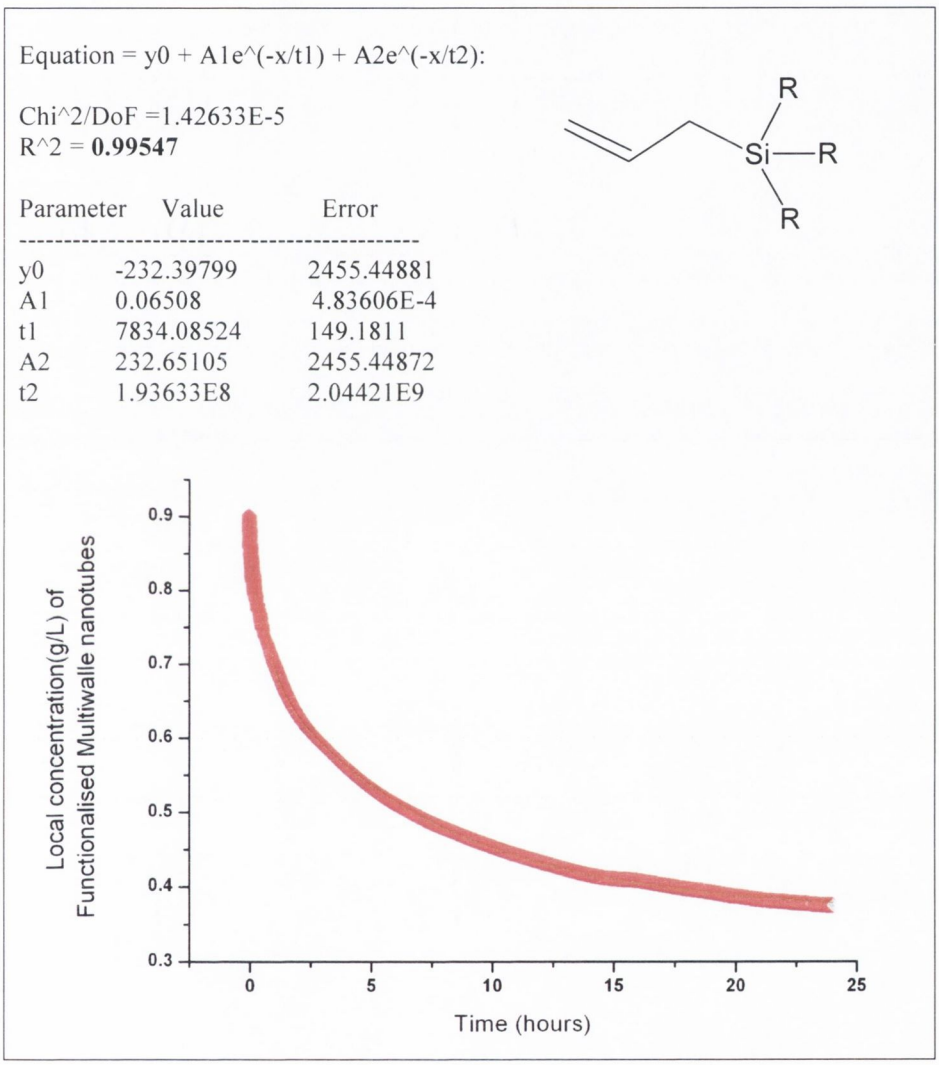

Figure 5.38 *Average Sedimentation curves for allyl- functionalised MWNTs composites.*

From the sedimentation curve illustrated in figure 5.39 it is clear that the solubility increases as the concentration of polystyrene increases. The stable

concentration of the F-MWNT in THF is 0.17 g/l. This increases up to 0.30g/l with the addition of 18.6 mg of polystyrene. And further still to 0.35g/l when the concentration of polystyrene is increased to 36.7 mg.

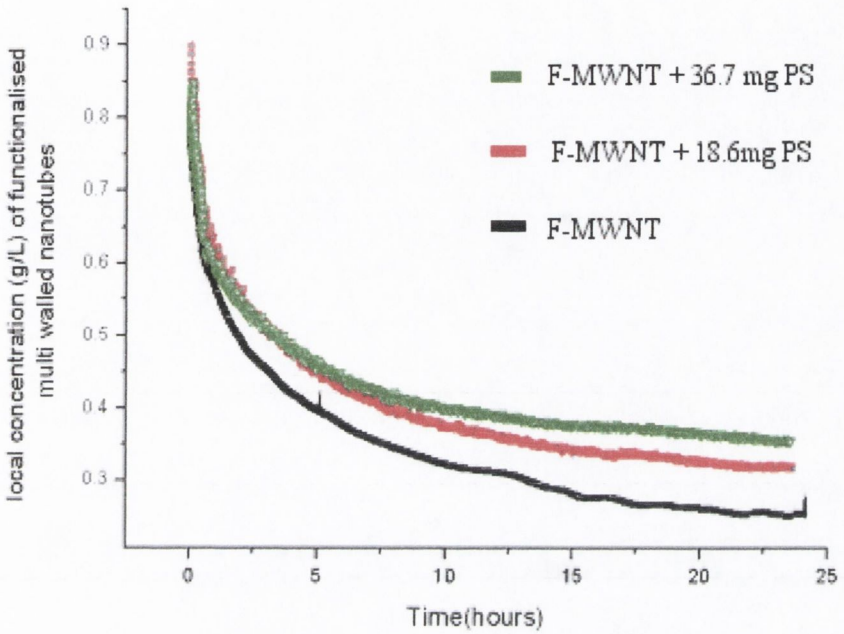

Figure 5.39 *Sedimentation curves for allyl- functionalised MWNTs composite.*

5.8.2 Sedimentation of propyl- functionalised MWNTs composite.

Sedimentation curve of propyl-functionalised MWNTs is shown in figure 5.40.

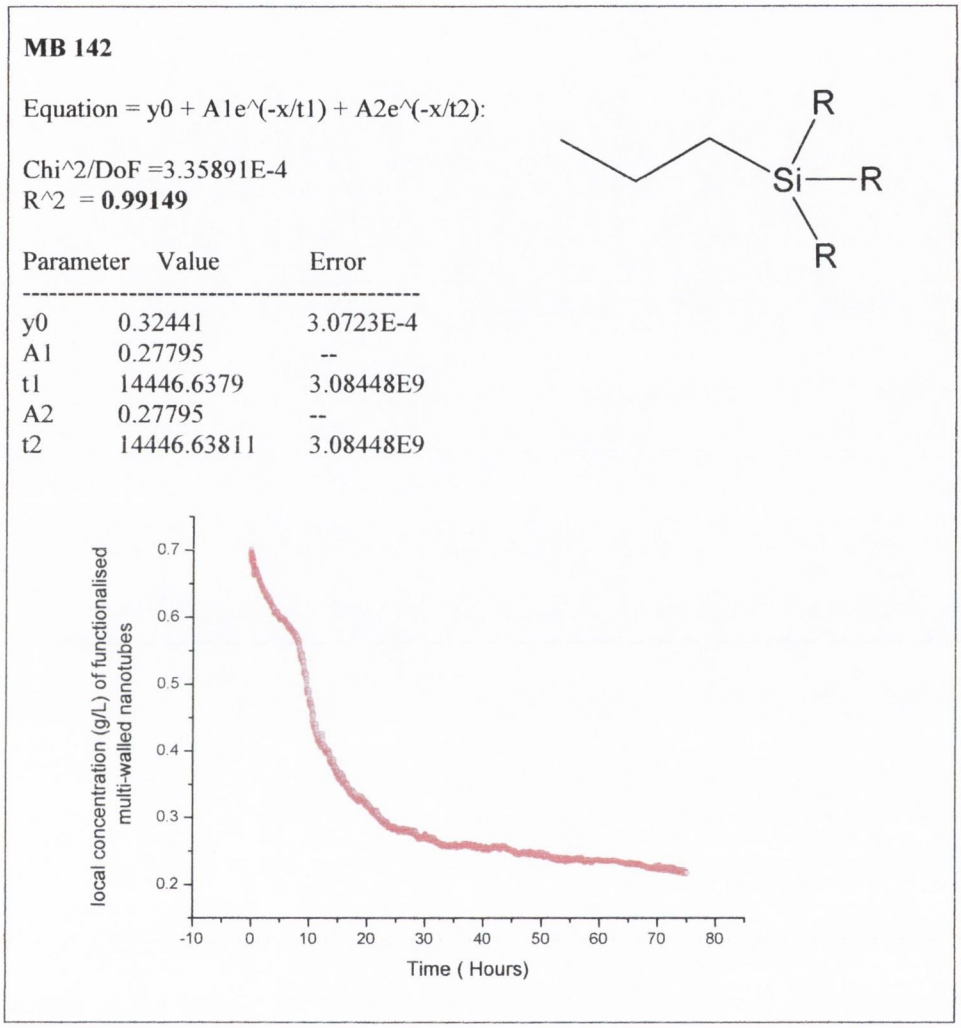

Figure 5.40 *Average sedimentation curve for sample propyl- functionalised MWNTs in polystyrene; the second order exponential decay fits closely to the shape of the curve.*

The sedimentation curve for propyl functionalised MWNT differs somewhat from that of the preceding allyl-functionalised MWNTs. In this case the material drops out quickly for the first 5-10 hours and then settles down to a stable concentration. Upon addition of polystyrene the rapid settling of the material begins now at 10 hours. Again however the stable concentration appears after

20 hours. The first addition of polystyrene however does not increase the stable concentration by the same proportion. The Propyl F-MWNT sample upon addition of 23.5 mg of polystyrene increases the stable concentration by a mere 6%. In contrast the addition of 18.7mg of polystyrene the stable concentration doubles. The presence of the double bond in the Allylic sample clearly reacts with the phenyl ring in the polystyrene.

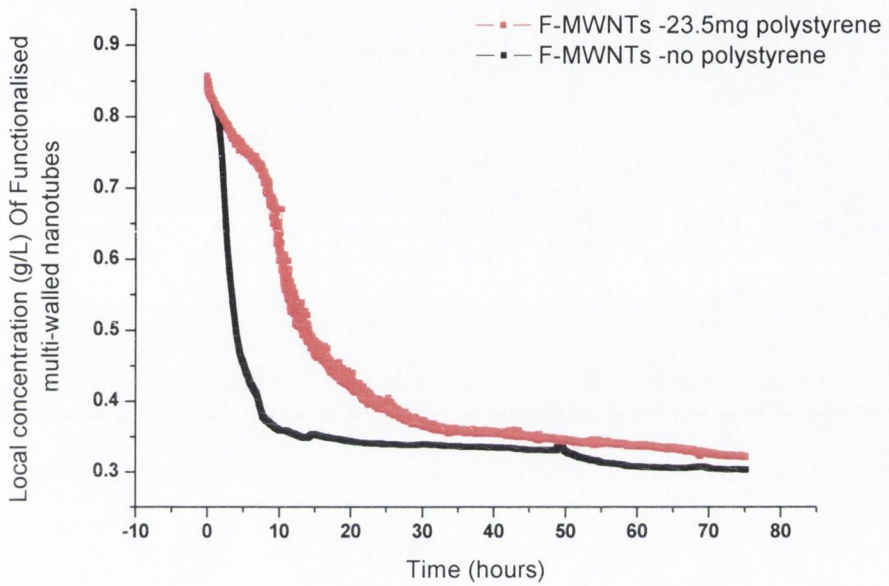

Figure 5.41 *Sedimentation curve of sample propyl- functionalised MWNTS after addition of polystyrene. The stable concentration is reached after 20 hours*

5.8.3 Sedimentation of hexyl- functionalised MWNTs composites.

The sedimentation curve of hexyl-functionalised MWNTs is shown in figure 5.42.

MB 141
Equation= y0 + A1e^(-x/t1) + A2e^(-x/t2):

Chi^2/DoF = 1.97167E-9
R^2 = 0.999429

Parameter	Value	Error
y0	0.02368	5.27951E-6
A1	0.00436	7.84852E-6
t1	7.2018	0.0458
A2	0.0018	1.01841E-5
t2	0.58857	0.00562

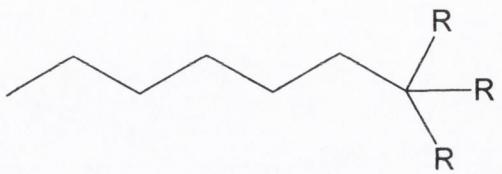

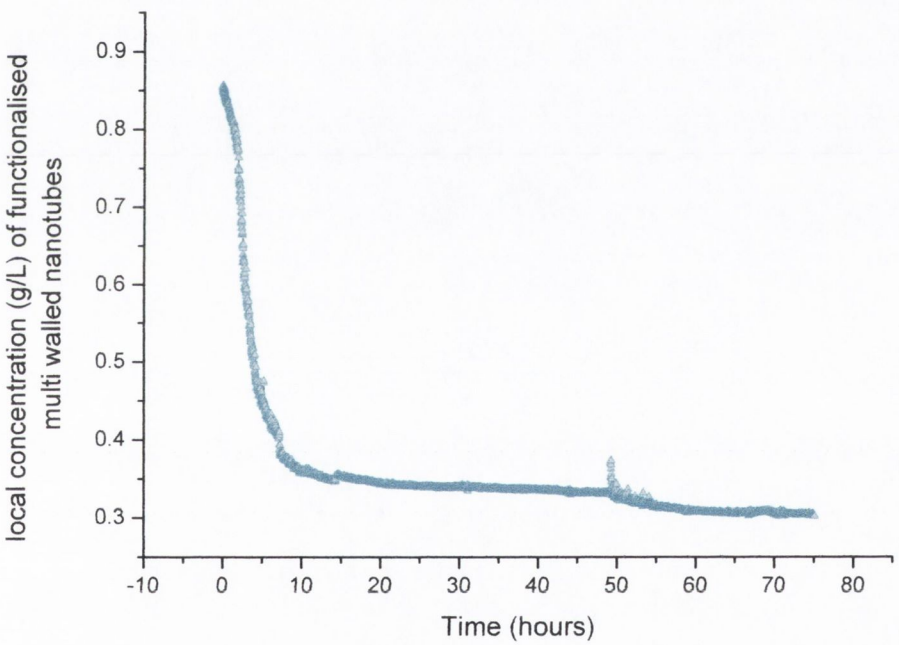

Figure 5.42 *Average sedimentation curve for sample Hexyl F-MWNT in polystyrene .The second order exponential decay fits very closely to the shape of the curve.*

In contrast to the two previous samples the addition of polystyrene does not affect the initial crashing out of the non –functionalised material, as was seen

previously. After 5 hours all the material that is going to fall out has done so, leaving the stable concentration thereafter. Although the graph only shows the system after 50 hours the polystyrene containing was left in the beams for a further 72 hours and the line had not altered. The stable concentration upon the addition of polystyrene increases by 50%. This is a greater increase than the Hexyl functionalised-MWNT sample, the hexyl group being three carbons longer are able to extend out into the polymeric chains this could give the sample enhanced stability in contrast to the three carbon sample

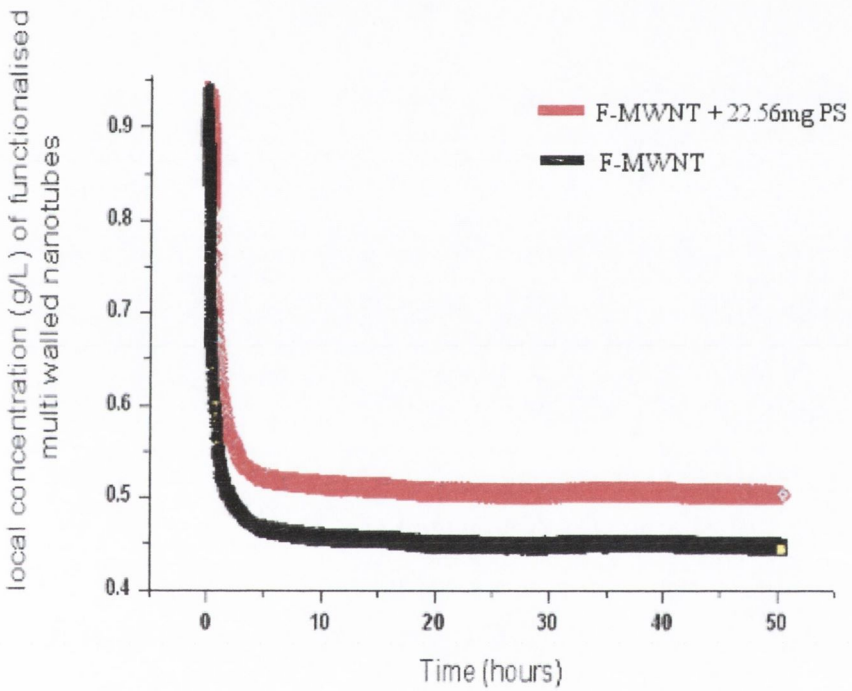

Figure 5.43 *Sedimentation curve for the hexyl- F-MWNT sample in polystyrene. The curve seems to be composed of two lines one parallel to the X axis representing the Y0 value and one parallel to the Y axis representing the A1 value*

5.8.4 Sedimentation of Dodeca- siloxane / lithiated Multi-walled nanotubes composite

The sedimentation curve of dodecyl-functionalised MWNTs is shown in figure 5.44.

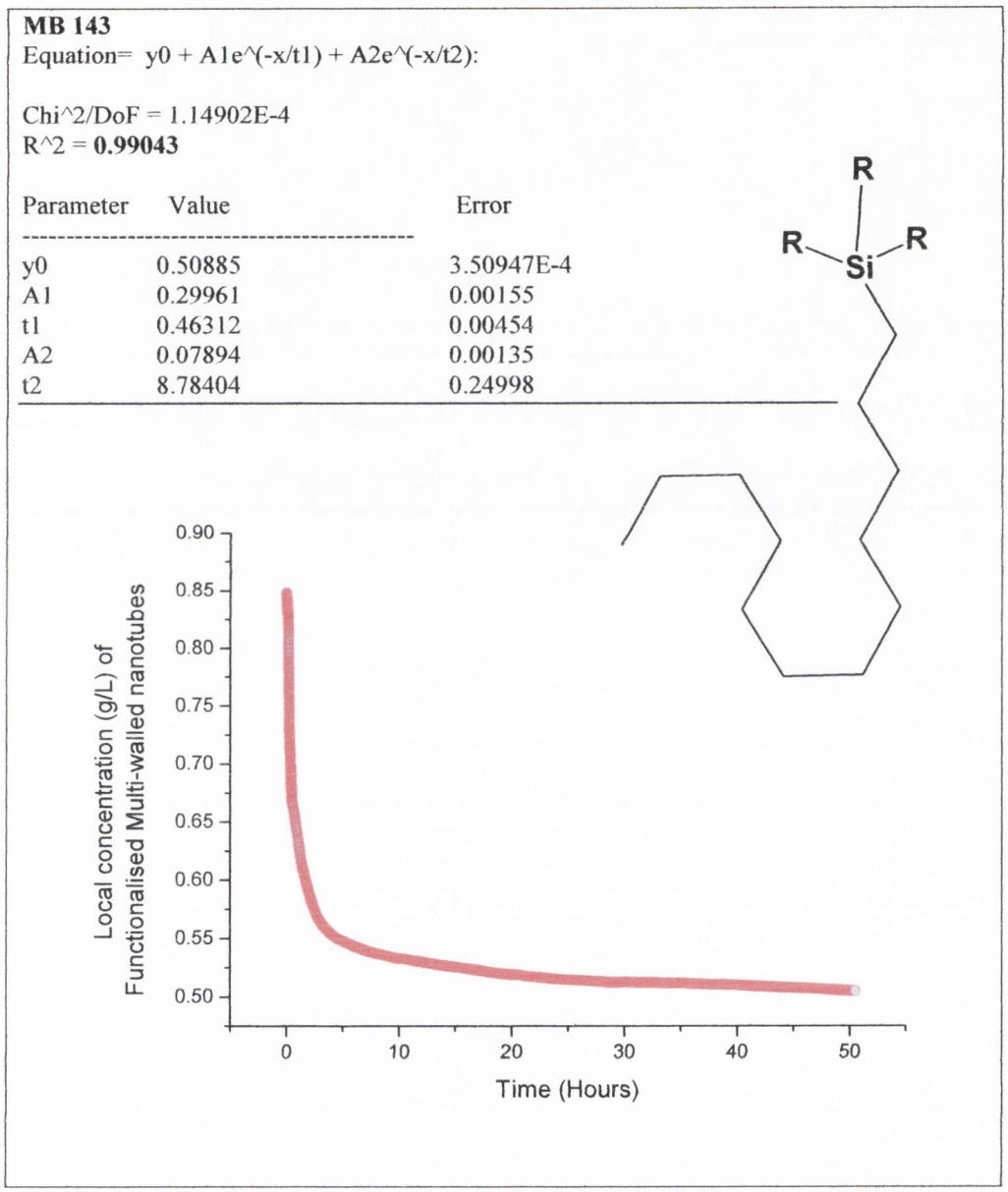

Figure 5.44 *Average sedimentation curve for sample dodecyl – F-MWNT in polystyrene the second order curve is almost an exact fit.*

As shown in figure 5.44 the stable concentration is reached after 25 hours from the shape of the curve clearly a large amount of material crashes out by 3-5

hours at 5 hours this begins to settle and by 20 hours has reached a completely stable state. Notice how ever that by 20 hours 55% of the original material still remains in suspension. This material showed very good long-term stability and remained *stable for over two months.*

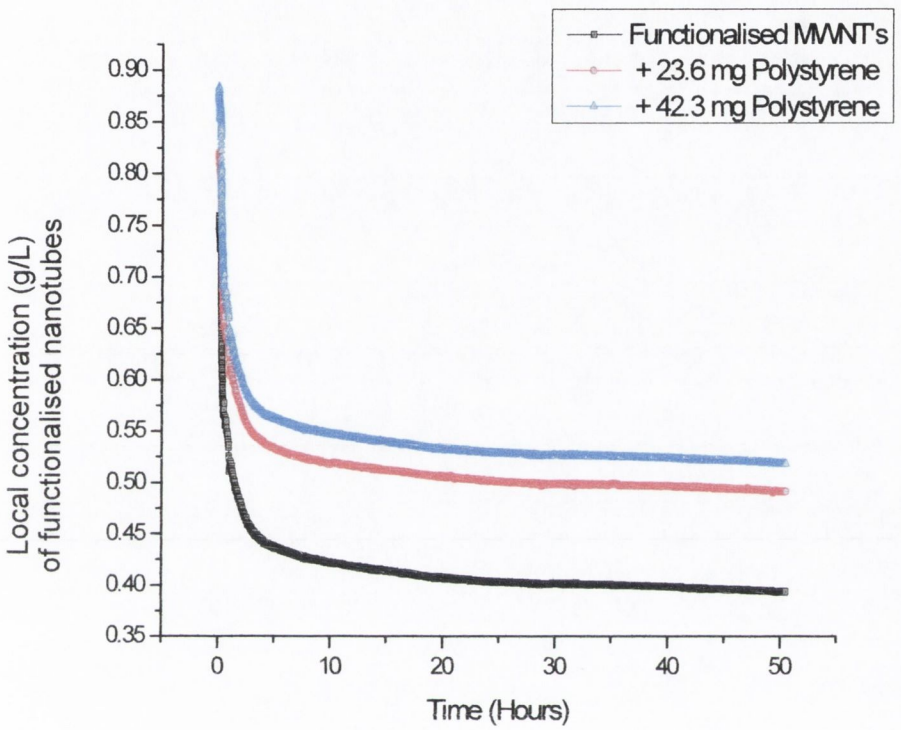

Figure 5.45 *Series sedimentation curve for sample Dodecyl- F-MWNT in polystyrene.*

From figure 5.45 we can easily see that the Dodecyl F-MWNTs have a stable concentration of 44.5 % of the initial weight added. Upon addition of 23.6 mg of polystyrene this increases 61 % of initial material a further increase to 65 % is achieved when the polystyrene is brought up to 42.3 mg. Of the four samples the is the largest proportional increase in stability upon introduction of polystyrene too the system

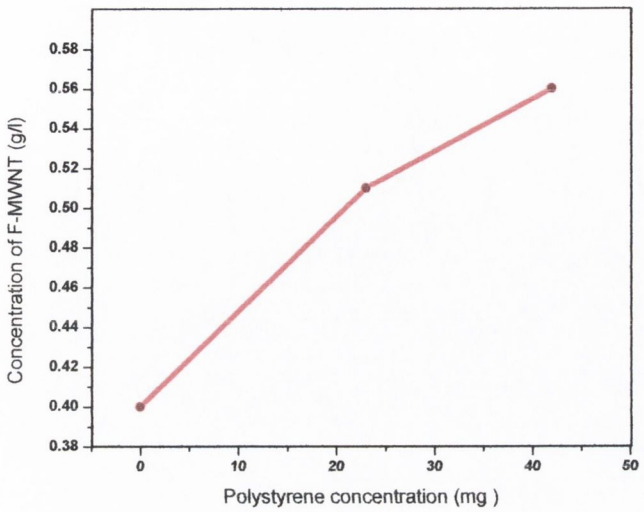

Figure 5.46 *Graph illustrating the increase of dodecyl F-MWNT concentration as polystyrene concentration increases.*

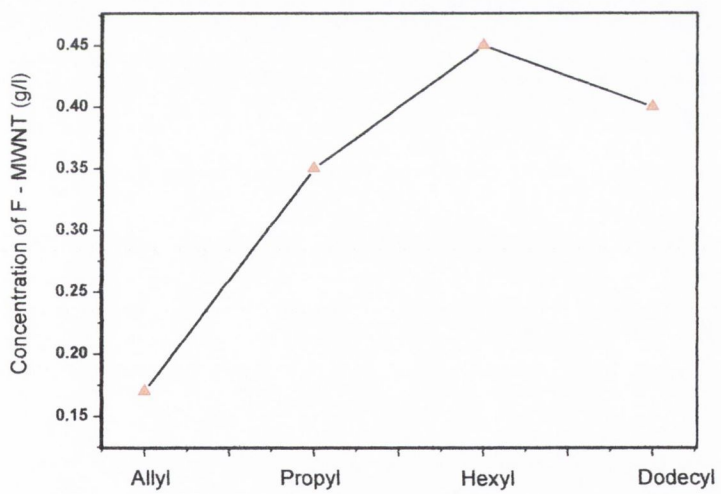

Figure 5.47 *Graph illustrating the increasing stability of F-MWNT in THF*

The concentration increases with length except in the C_{12} case.

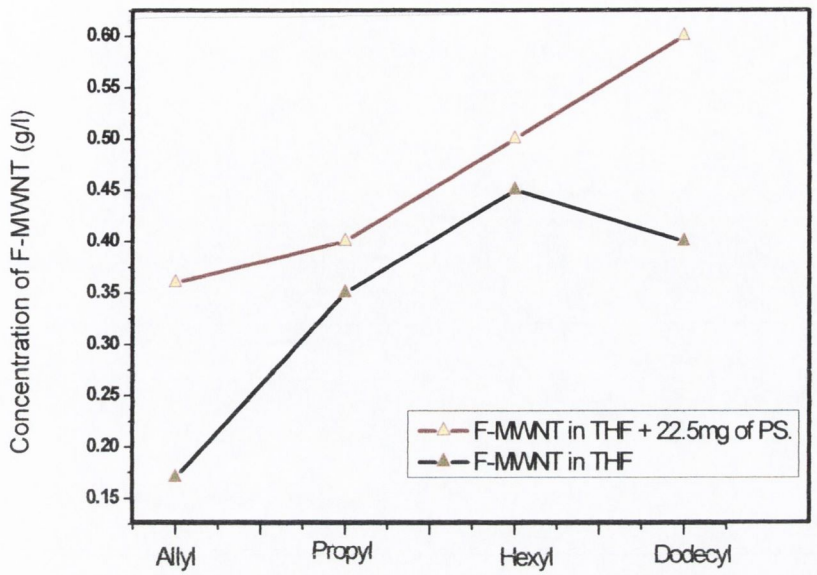

Figure 5.48 *Graph illustrating the increased solubility upon addition of 22.5 mg of Polystyrene, this contrast noticeably with the graph for F-MWNT in polystyrene only. Notice that the dodecyl has dramatically increased solubility in Polystyrene.*

From figure 5.48 we can see that the dodecyl F-MWNT in THF has less stability than that of hexyl F-MWNT. The dodecyl functionalised nanotubes however increase rapidly upon addition of the polystyrene. As illustrated in figure 5.44 the dodecyl chain has good potential for chain twisting and bending (due to the twelve carbon chains) these are twice as long as the hexyl chains and there fore can intertwine with the polystyrene leading to increased stability .The hexyl F-MWNT also have this ability, but this reduces again in the case of Propyl F-MWNT .The Allylic F-MWNT has of course no ability to twist but the double bond has good potential to interact with the phenyl groups of the polystyrene . This could account for the large increase seem for the F-Allylic sample upon addition of polystyrene to the system.

5.9 Mechanical testing

5.9.1 Film testing for Allylic F-MWNTs composites in Polystyrene.

Shown below in figure 5.49 is the stress strain curve for Allylic F-MWNTs composites in Polystyrene. As we can see an addition of 1% of allylic functionalised MWNT resulted in almost 4 times increase in Young's modulus, 3 times increase in tensile strength and almost 2.8 times increase in toughness. It is also important to notice that the higher 2.5 % concentration of functionalised nanorods gave substantially less increase in mechanical properties. We believe the major reason for this -as in the previous chapter on F-Titania- is that the nanorods form aggregates which do not allow for adequate or reasonable stress transfer and also add defects to the composite material.

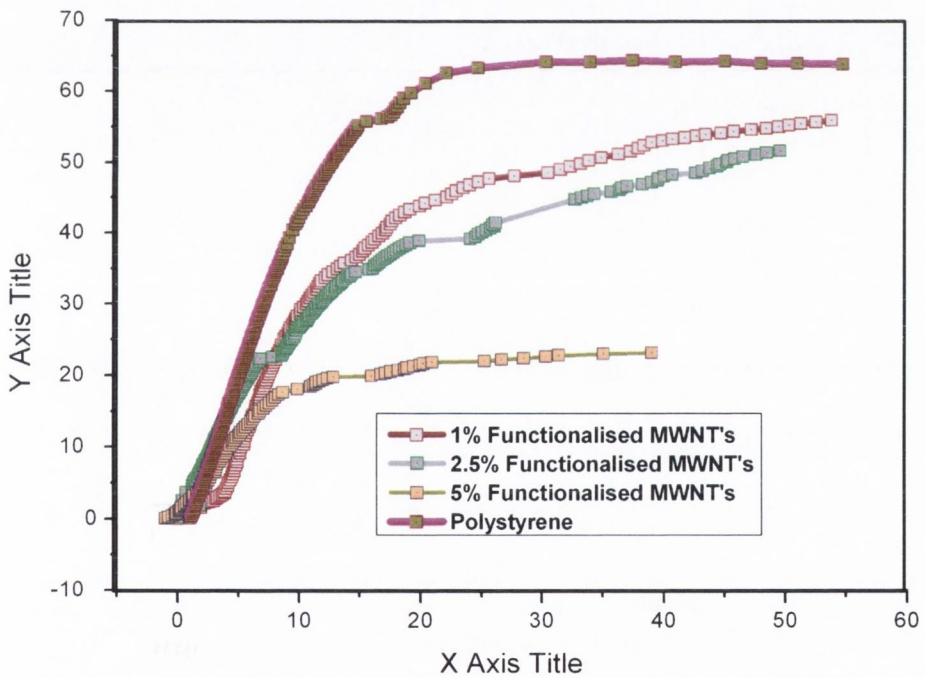

Figure 5.49 *Stress-strain curves for polystyrene films containing a range of allylic F-MWNTs volume fractions.*

Table 5.2 *Mechanical testing results for Allyl –F-MWNT polystyrene films*

Percentage F-MWNT composite	Young's Modulus [GPa}	Ultimate Tensile strength [MPa]	Toughness [KJ/m^3]
1%	0.463	64.3	1.48
2.5%	0.405	55.8	1.29
5 %	0.355	51.5	1.19
Polystyrene	0.195	23	0.5299

5.9.2 Film testing for Propyl F-MWNTs composites in Polystyrene.

Stress-strain curves and mechanical testing results for propyl-functionalised MWNT are shown in figure 5.50 and table 5.3 respectively. The addition of 1 % of propyl- F – MWNT resulted in a slight rise in Young's modulus, and gave a double increase in tensile strength and almost 2.5 times increase in toughness. Again higher concentration (2.5 % and 5 %) did not demonstrate so significant increase in mechanical properties as the lower 1 % addition due to the clustering of nanorods as mentioned previously.

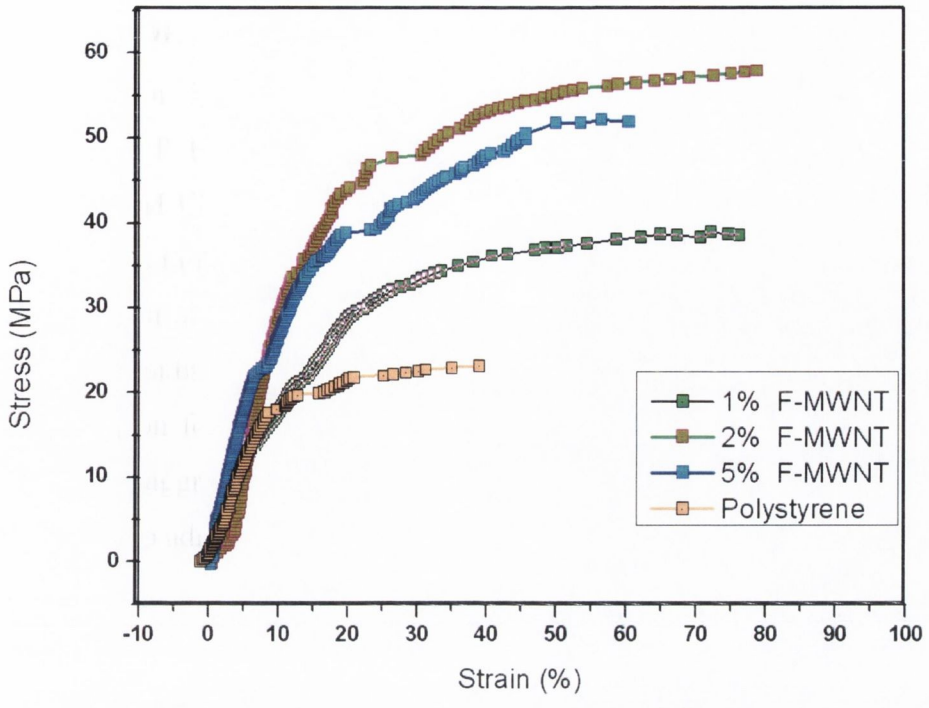

Figure 5.50 *Stress-strain curves for polystyrene films containing a range of -Propyl F-MWNTs volume fractions*

Table 5.3 *Mechanical testing results for Propyl –F-MWNT films*

Percentage F-MWNT composite	Young's Modulus [GPa}	Ultimate Tensile strength [MPa]	Toughness [KJ/m^3]
1%	0.41	57.8	1.33
2.5%	0.316	52.3	1.2
5%	0.12	38.9	0.94
Polystyrene	0.195	23	0.5299

5.9.3 Film testing for Hexyl- F-MWNTs composites in Polystyrene.

Stress-strain curves and mechanical testing results for hexyl-functionalised TiO_2 nanorods are shown in figure 5.51 and table 5.4 respectively.

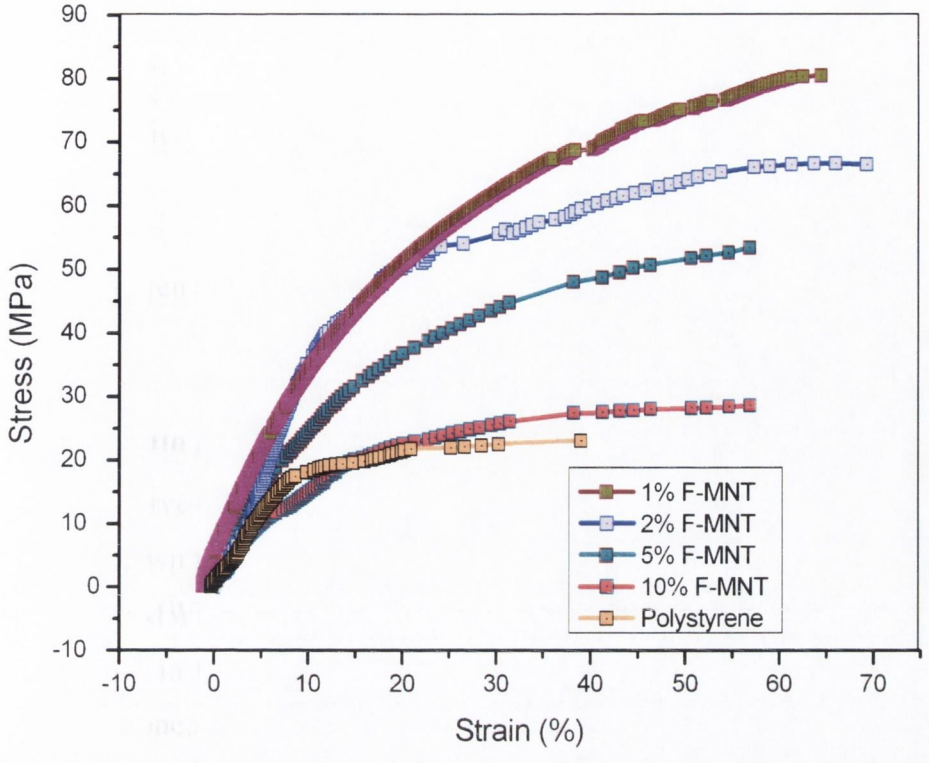

Figure 5.51 *Stress-strain curves for polystyrene films containing a range of hexyl F-MWNTs volume fractions*

This time the addition of 1 % of hexyl-F MWNT changed the Young's modulus by about 1.5 times but gave a 3 times increase in tensile strength and an impressive almost 3.5 times increase in toughness. Again higher concentration (2.5 %) did not demonstrate so significant increase in mechanical properties as lower 1 % addition again due to clustering.

Table 5.4 *Mechanical testing results for Hexyl –F-MWNT films*

Percentage F-MWNT composite	Young's Modulus [GPa}	Ultimate Tensile strength [MPa]	Toughness [KJ/m^3]
1%	0.32	80.3	1.85
2.5%	0.44	66.6	1.53
5%	0.227	53.3	1.23
10%	0.105	28.5	0.67
Polystyrene	0.195	23	0.5299

5.9.4 Film testing for dodecyl- F-MWNTs composites in polystyrene.

Stress-strain curves and mechanical testing results for are shown in figure 5.52 and table 5.5 respectively. The addition of 1 % of dodecyl-F MWNT resulted in a 2.5 times increase in Young's modulus and a 3.7% times increase in tensile strength and in almost 3.5 times increase in toughness. Testing of the samples at higher concentration has not been performed due to the clustering of nanorods mentioned above.

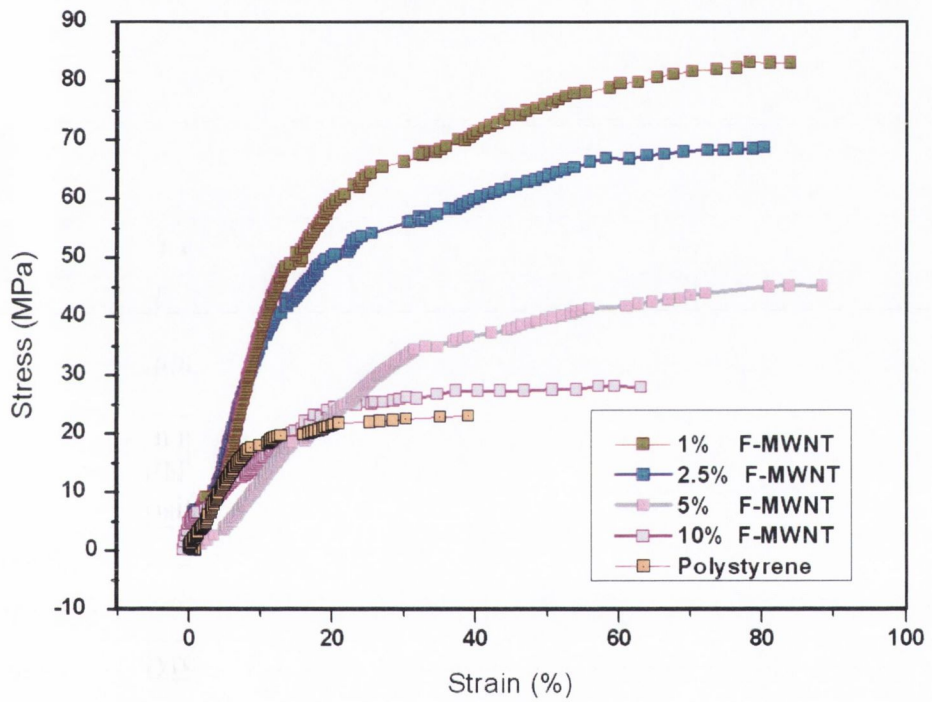

Figure 5.52 *Stress-strain curves for polystyrene films containing a range of Dodecyl F-MWNTs volume fractions*

Table 5.5 *Mechanical testing results for Dodecyl–F-MWNT films*

Percentage F-MWNT composite	Young's Modulus [GPa}	Ultimate Tensile strength [MPa]	Toughness [KJ/m^3]
1 %	0.493	83.0	1.9
2.5%	0.434	68.7	1.58
5%	0.114	45.1	1.04
10%	0.117	28.2	0.65
Polystyrene	0.195	23.0	0.5299

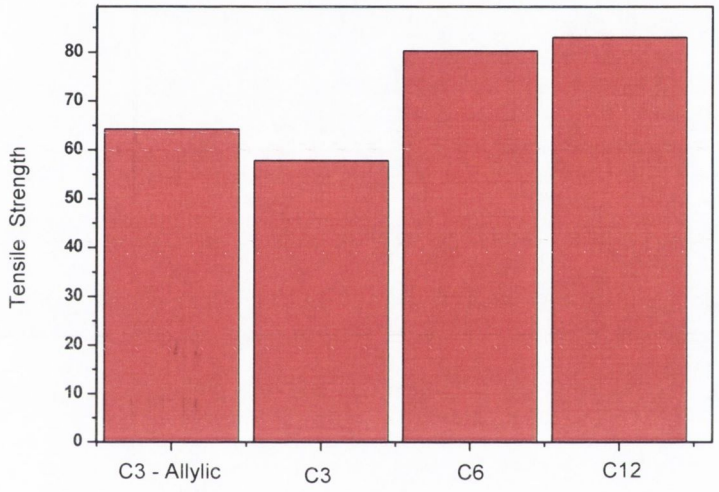

Figure 5.53 *Histogram showing the increase in UTS with increase in chain length. Both C-3 chains are lower than the higher lengths. The Allylic sample has higher UTS than the Propyl sample; this slight anomaly may be due to aromatic interactions between the double bond and the phenyl rings of the polystyrene. (All taken from the 1% values)*

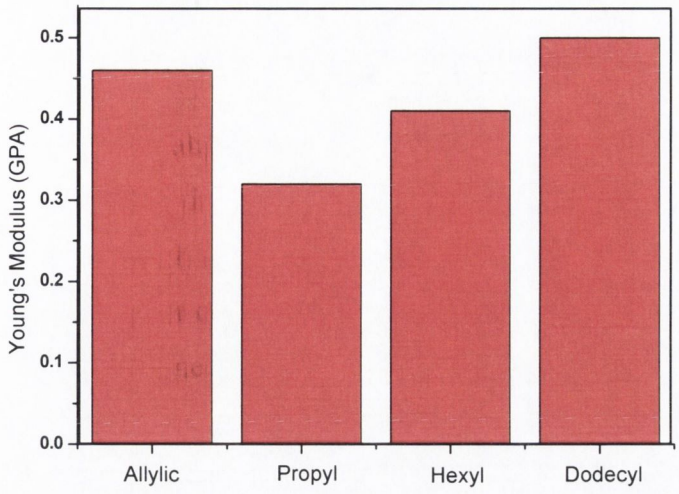

Figure 5.54 *Histogram showing the relationship between increase in Young's modulus and chain length, as was seen in the tensile stress relationship the Allylic sample has a greater value than expected for a three carbon chain. (All taken from the 1% values).*

From the mechanical testing it is clear that the addition of the smaller percentages of F-MWNT to the polystyrene lead to a greater enhancement in the Tensile strength and Toughness, The young's modulus of these samples also increases with the smaller percentages of F-MWNT, although compared to the increases of the other quantities, these are modest increases. The highest tensile strength was achieved for the longest (dodecyl) alkyl chain, because it provides the strongest interaction and as result the most efficient stress transfer between polymer matrix and nanotubes. The higher percentages of F –MWNT tend to disrupt the polymer matrix and therefore lower and weaken the films. Some of the 10% sample proved difficult to treat as they gave uneven lumpy films.

5.10 Conclusions

We have demonstrated that good quality MWNT can be produced by the arc-discharge method. These can be successfully purified using PPV, although not in usable quantities for research purposes. Catalytic nanotubes containing carboxylic functional groups can be successfully utilised to produce POSS functionalised- MWNT. This can be achieved by two methods, firstly by direct reaction with pre-prepared POSS molecules with amino functionalities, which interact with the acid groups on the MWNT surface. The second method involves the sintering of the catalytic MWNT to remove the carboxylic groups and then Lithiating these clean MWNT with BuLi. The lithiated MWNT can than be reacted with compounds of the formula R-$SiCl_3$ to yield functionalised MWNT. The *in situ* generation of POSS on the surface of MWNTS has lead to heavy POSS coatings to be formed. In some instances these coatings have formed macrosised objects.

These materials have being characterised by TEM, SEM IR and Raman spectroscopy, TGA and AFM. All functionalised nanotube composites showed an increase in the D band of the Raman plots and a decrease in the combustion temperature was seen in the TGA TEM and SEM images revealed heavy coating or POSS and IR spectra provided proof of covalent bonding in the sample produced by the use if BuLi.

Organometallic approaches using BuLi and appropriate trichlorosilanes have also been applied to functionalise MWNTs with allyl, propyl-, hexyl- and dodecyl functionalities. Sedimentation studies of all functionalised MWNTs in organic solvents have been performed to evaluate their solubility in the pure solvent as well as in the polymer solution in the solvent. Finally new polystyrene composite materials have been prepared using chemically modified MWNT as additives. Mechanical properties of the polymer composite films have been investigated by using a Zwick-100 tensile tester. These new polymer composites demonstrated a significant increase in Young's Modulus, tensile strength, toughness.

5.10 References

1. Chiu, P.W.; Duesberg, G.S.; Dettloaff-Weglikowska, U.; Roth, S. *Appl. Phys. Lett.* **2002,** *80*, 3811-3813

2. Saito, T.; Mutsushige, K.; Tanaka, K. *Physica B* **2002,** 1-4

3. Aizawa, M.; Shaffer, M.S.P. *Chem Phys. Lett.* **2003,** *368*, 121-124

4. Liu, L.; Zhang, S.; Hu, T.; Guo, Z.; Ye, C.; Dai, L.; Zhu, D. *Chem Phys. Lett.* **2002,** *359*, 191-195

5. Kelly, K.F.; Chiang, I.W.; Mickelson, E.T.; Hauge, R.H.; Margrave, J.L.; Wang, X.; Scuseria, G.E.; Radloff, C.; Halas, N.J.; *Chem Phys. Lett.* **1999,** *313*, 445-450

6. Hirsch, A. *Agnew. Chem. Int.* **2002,** *41*, 1853-1859

7. McCarthy, B.; Coleman, J.N., Czerw, R.; Dalton, A.B.; in het Panhuis, M.; Maiti, A.; Drury, A.; Bernier, P.; Nagy, J.B.; Lahr, B.; Byrne, H.J.; Carroll, D.L.; Blau, W.J. *J. Phys. Chem. B* **2002,** *106*, 2210-2216

Chapter 6

Experimental Section

6.1 General procedures

All manipulations on the preparation and handling of starting materials and subsequent products were all carried out under vacuum or argon by Schlenk techniques. Solvents were dried and distilled over sodium-potassium alloy under argon prior to use and then condensed into a reaction flask under vacuum shortly before use. The NMR spectra were recorded using a Bruker DPX 300 (^{1}H, 300 MHz) or a Varian – 400 (^{1}H, 400 MHz) instruments in C_6D_6, $CDCl_3$ or DMSO- d_6 at ambient temperature and referenced for ^{1}H internally to residual solvent peaks. IR spectra (500 – 4000 cm^{-1}) were recorded in "Nujol", using KBr discs and the Perkin Elmer instrument. (3-chloropropyl) triethoxysilane, (3-aminopropyl)triethoxysilane, allyltriethoxysilane and (3-mercaptapropyl)triethoxysilane were obtained from Aldrich. C_{60} and all nanotubes were obtained from the Physics department. The scanning electron microscopy (SEM) images of the samples were obtained using Hitachi S-4300 scanning electron microscope, which was operated at 5.0 kV. The transmission electron microscopy (TEM) images were taken on Hitachi H-7000. The TEM was operated at a beam voltage of 100 kV. Samples for TEM were prepared by deposition and drying of a drop of the powder dispersed in ethanol onto a formvar coated 400 mesh copper grid.

6.2 Experimental for Chapter 2

6.2.1 Synthesis of Octachloropropylsilsesquioxane (T_8Cl) (1)

Method A:

The mixture of (3-chloropropyl) triethoxysilane (20 ml, 83 mmol) with concentrated HCl (15 ml, 2.4 mol) in methanol (500ml) was heated under reflux for 35 hours. The solvent was removed in vacuum to give a white powdery product. The product was then washed several times with hexane and dried in vacuum giving white crystals (8.6 g, 79.8 %), which were found to have a melting point at 103°C. ^{1}H NMR (400 MHz, $CDCl_3$, 298K): δ 3.56 (s, 16H, CH_2Cl); 1.91 (s, 16H, CH_2), 0.83 (s, 16H, CH_2Si). ^{13}C NMR (125MHz, $CDCl_3$,

295K): δ 46.57 (CH_2), 25.98 (CH_2), 9.48 (CH_2). ^{29}Si NMR (99 MHz, $CH_3C_6H_5$, 295K): δ -65.23 (s). IR (KBr, cm^{-1}): 2954 (s), 2924 (s), 2854 (s), 1638 (m), 1459 (m), 1378 (w), 1260 (w); 1093 (w), 1022 (w), 799 (w), 599 (w), 480 (s).

Method B:

The mixture of (3-chloropropyl) triethoxysilane (20 ml, 83 mmol) with NaOH (0.166 ml, 4.15 mmol) in THF (50 ml) was heated under reflux for 22 hrs. The solvent was removed in vacuum to give a white powder precipitate. This product was washed several times with hexane and dried in vacuum to give white crystals (6.8 g, 63 %) which had a melting point at 104°C. ^{1}H NMR (400 MHz, $CDCl_3$, 298K): δ 3.55 (s, 16H, CH_2Cl); 1.85 (s, 16H, CH_2); 0.80 (s, 16H, CH_2Si). ^{29}Si NMR (99MHz, $CH_3C_6H_5$, 295K): δ –65.47 (m). IR (KBr, cm^{-1}): 2953 (s), 2924 (s), 2854 (s), 1637 (m),1459 (m), 1377 (w), 1311 (w),1240 (w), 1118 (m), 1090 (m), 1038 (w),864 (w), 799 (w), 722 (w), 626 (w).

6.2.2 Synthesis of Octaaminopropylsilsesquioxane (T_8NH_2)(2)

The hydrolytic condensation was performed in THF (50 ml) using (3-aminopropyl) triethoxysilane (20 ml, 0.88 mmol)? and NaOH (0.18 ml, 4.53 mmol) and was refluxed for 20 hrs. The solvent was removed in vacuum to give a white powder product. This product was washed several times methanol & dried in vacuum to give white granular crystals (7.9 g, 65%) which had a melting point at 160°C. ^{1}H NMR (400 MHz, d. $CDCL_3$ 298K): δ 3.69 (s, 32H, NH_2), 3.42 (quartet, 16H, CH_2-NH_2), 1.30 (t, 16H, CH_2), 1.30 (t, 16H, CH2), 0.88 (qui, 16H,CH_2Si). ^{29}Si NMR (99 MHz, $CDCL_3$295K): δ –65.5 (m). IR (KBr, cm^{-1}): 2955 (w), 2923 (w), 2853 (w), 1621 (m), 1446 (m), 1260 (w), 1212 (w), 1174 (w), 1127 (w), 1020 (m), 797 (w).

6.2.3 Synthesis of octa(3-aminopropyl)silsesquioxane octahydrochloride (T_8NH_3Cl) (3)

The hydrolytic condensation was performed in methanol (500 ml) using ((3- aminopropyl)triethoxysilane (20 ml , 0.08 mol) and concentrated HCl (15 ml). The mixture was heated under reflux and stirred for 2 days. After THF was added to the mixture giving a white precipitate. The product was washed with

THF and dried in the vacuum giving white solid (8.018 g, 97%) ^{1}H NMR (400 MHz, $CDCl_3$, 298K): δ 3.75 (t, 16H, CH_2Cl); 1.90 (qui, 16H, CH_2), 0.81 (t, 16H, CH_2Si). ^{29}Si NMR (99 MHz, $CHCl_3$, 295 K): -66.12(s),

6.2.4 Synthesis of octa(3-mercaptapropyl)silsesquioxane (T_8SH_8) (4)

The mixture of (3-mercaptopropyl) trimethoxysilane (5.0 g, 0.025mol) and concentrated HCl (4ml) in methanol (100ml) was refluxed for 24 hours. The top solvent layer was separated from the bottom oily layer which was dried under vacuum producing an oily product. (2.08g ,70% yield). ^{1}H NMR (400 MHz, $CDCl_3$, 298K): δ 3.54 (s, 0.5H, MeOH) 2.6 (br, 2H, S-CH_2) 1.7 (br, 2H, CH_2) 1.4 (t, 1H, SH) 0.77 (t, 2H, Si-CH_2). ^{13}C NMR (126 MHz, $CDCl_3$, 298K): δ 49.7 (CH_3-O), 27.1(CH_2), 26.9 (CH_2), 10.4 (CH_2). ^{29}Si NMR (99 MHz, $CHCl_3$, 295K): -64.5. IR (cm^{-1}): 3440 (br,w), 2929 (s), 2554 (m), 1452 (m), 1259 (s), 1106(s), 804 (s), 693(m).

6.2.5 Synthesis of Octa(allyl)silsesquioxane (T8allyl) (5)

A. Base catalysed hydrolytic condensation of allyltriethoxysilane

The mixture of allyltriethoxysilane (11ml, 0.049mol), tetrabutyl ammoniumhydroxide (5ml, 0.015moles), methanol (20ml) and distilled water (4ml) was heated under reflux for 24 hours. The white precipitate that formed was washed with hexane and dried under vacuum to give a white powdery product with the yield of 2.654g (86%) . ^{1}H NMR (400 MHz, $(CD_3)_2CO$, 298K): δ 5.77 (qui, 1H,), 4.93 (quartet, 2H,), 1.30 (qui, 16H, CH_2). ^{13}C NMR (126 MHz, $(CD_3)_2CO$, 298K): δ 131.8 (CH) 115.6 (CH_2) 19.4 (CH_2). ^{29}Si NMR (99 MHz, THF, 295K): δ -66. IR (KBr, cm^{-1}) 3079(s), 3003(s), 1808(w), 1634 (s), 1419 (m), 1391 (m), 1130 (br, s), 931 (s), 900 (s), 760(m), 631(m).

B: Acid catalysed hydrolytic condensation of allyltriethoxysilane (5)

The mixture of allyltriethoxysilane (5.5ml,.0245mol) ,concentrated HCl (5.5ml) and methanol (20ml) was heated under reflux for 24 hours giving colourless oily product (2.54g ,79%). Two layers appeared. The top methanol layer was decanted off. The bottom oily layer was removed and dried under vacuum to

remove solvent. ^{1}H NMR (400 MHz, $CDCl_3$, 298K): δ 5.77 (t, 1H, =C-H), δ 4.95 (quartet, 2H, $=CH_2$), 1.63 (qui, 2H, Si-CH_2). ^{13}C NMR (126MHz, $CDCl_3$, 298K): δ 131.8 (CH), 115.6 (CH_2), 19.4 (CH_2).^{29}Si NMR (99 MHz, CH3OH, 295K): δ –66.9(s). IR (cm^{-1}):3390 (br, w), 3070 (m), 2970 (m), 2890 (m), 1634 (s), 1419 (m), 1117 (s), 901 (s), 761 (s).

6.2.6 Synthesis of $Cp_8Si_8O_{12}$ (6)

Trichloro-cyclopenta-2,4-dienyl-silane ($CpSiCl_3$) was prepared from $SiCl_4$ and CpNa according to published procedure [1]. (21.9g, 0.11m) in 100 ml of THF was carefully hydrolysed by the drop wise addition of a solution of $(NH_4)_2CO_3$ (2.97g, 0.03m) solution in distilled water (70ml) at 0°C. The mixture was stirred at ambient temperature for one week. The product was extracted with diethyl ether and the organic layer was separated and dried with anhydrous magnesium sulphate. The solution was concentrated in vacuum. A pale yellow solid was precipitated. The precipitate was washed with diethyl ether and dried in vacuum to give 8.6 g (67% yield). ^{1}H NMR (400 MHz, $CDCl_3$, 22°C), 5.71 (40H, vbr, Cp, H-C=), 3.22 (10H, vbr, Cp, H-C-). ^{29}Si NMR (99MHz, $CDCl_3$, 22 °C) δ: –71.50 (s), -74.39 (s), –77.04 (s). IR (KBr, cm^{-1}): 2962(m), 1709(m), 1446 (m), 1261 (m), 1089(w sh), 845(w), 801 (w) 757(m), 431(w). MS (ESI TOF, CH_3CN-H_2O): 1171 $[M + H]^+$, 1002 $[M\text{-}3Cp + CN - H^+]^+$, 928 $[M - 4Cp + CH_3 - 3H^+]^+$, 780 $[M - 6Cp]^+$, 558 $[M – 2\ Cp + 2CH_3CN]^{2+}$, 484 $[M – 4Cp + CH_3CN + H_2O - 2H^+]^{2+}$. Cryoscopy in c-hexane: average (out of 5) M.w. 1193.

6.2.7 Synthesis of $PhCpSiCl_2$(7)

Freshly distilled cyclopentadiene monomer (30.46g, 0.41m) was added slowly to sodium sand (9.43g, 0.41m.) in THF (300ml). The mixture was stirred for 12 h until all sodium metal dissolved. Then the solution of CpNa in THF was added drop-wise to phenyltrichlorosilane (88.89g, 0.41m) at 0°C. The mixture was stirred for 24h and was allowed to stand overnight under argon. The mixture was filtered via canula and the filtrate was evaporated in vacuum to

give a creamy yellow oil (93g, 78 %). ^{1}HNMR (400 MHz, C_6D_6, 22°C) δ: 6.9 - 7.9 (6 H, br m, Ph) 5.24 –5.01 (5 H, br m, Cp). ^{13}C NMR (126MHz, $CDCl_3$, 298K) δ: 133.72 ,124.85, 67.43-65.36, 25.08, IR (KBr, cm^{-1}): 2954 and 1430 cm^{-1} (C-H str) ,1063 cm^{-1}.(Si-O-Si str) 1704(w), 1446(w), 1379(w), 1260, 1142(w), 568(w m).

6.2.8 Hydrolysis of $Cp(Ph)SiCl_2$ (8)

The $Cp(Ph)SiCl_2$ oil (93g) as prepared in section 6.2.8 above was diluted with freshly dried THF (50ml) and stirred for 2 h to achieve good dispersion. A solution of distilled water (10ml) and HCL (1ml, 1.0M) was then slowly added drop-wise via canula under argon atmosphere. The solution was then stirred at room temperature for 24 h and allowed to stand for a further 48 h. The solvent was removed in vacuum to give a strong orange/yellow precipitate (87g, 93%). ^{1}HNMR (400 MHz, C_6D_6, 22°C)δ: 6.9 - 7.9 (br m, 6 H, Ph) 5.24 – 5.01 (br m, 5 H, Cp), ^{29}Si NMR (99MHz, $CDCl_3$, 22 °C) δ -67,-75, -60, -40, -32, -20 ppm. IR (KBr, cm^{-1}): 2954 (m), 1709(m), 1430 (m), 1261 (m), 1063 (w sh), 865(w), 798 (w) 756(m), 4321 (w). MS (ESI TOF, CH_3CN): 1888 $[(PhCpSiO)_{10}\text{-}Ph\text{-}Cp]^+$,1762[-$(PhCpSiO)_9$-Cp,]$^+$,1685-$[(PhCpSiO)_9\text{-}Ph\text{-}Cp]^+$, 1153 $[(PhCpSiO)_6\text{-}Cp]^+$. Cryoscopy in c-hexane: average (out of 5) M.w.1875.

6.2.9 Synthesis of $(CpC_3H_6)_8Si_8O_{12}$ (9)

(3-Cyclopentadienylpropyl)triethoxysilane was prepared from (3-chloropropyl)-triethoxysilane (60.20 g,0.25 M) and CpNa in THF and was purified by vacuum distillation (b.p. 90–91°C/1 mm, 41 g, 61%). The hydrolytic condensation of (3-cyclopentadienylpropyl)triethoxysilane (20 g, 0.074 M) in acetone (170 ml) was performed by the addition of distilled water (25 ml),with the traces of conc. HCl (0.5 ml) at 0°C. The mixture was stirred at ambient temperature for one week. The solvent was removed in vacuum to give a pale yellow precipitate. The product was washed with hexane and dried in vacuum (6.94 g, 59%). Anal. Calc. for $C_{64}H_{88}Si_8O_{12}$: C, 60.38; H, 6.92. Found: C, 60.63; H, 6.98%. ^{1}H NMR (400 MHz, $CDCl_3$, 22°C) δ: 6.4–5.99 (32H, br m, Cp), 3.51 (8H, br m, Cp), δ

1.85–0.77 (48H,vbr m, CH_2). ^{29}Si NMR (99 MHz, CDCl3, 22°C) δ:68.51 (br s). IR (KBr, cm^{-1}): 2933(w), 1713(m),1455(m), 1383(w), 1155(w m), 1050(w), 799(w), 700(m), 467(w sh). MS (ESI TOF, CH_3CN): 1272$[M]^+$, 1207 $[M–Cp]^+$, 844 $[M\text{-}4CpC_3H_6]^+$. Cryoscopy in c-hexane: average (out of 5) M.w.1297.

6.3 Chapter 3

6.3.1 Oligomerisation of $Cp_{10}Si_{10}O_{15}$ (10)

$Cp_{10}Si_{10}O_{15}$ (8.2 g, 0.007 M) was stirrd in THF (150 ml) at ambient temperature for 2 h and then heated under reflux for 10 h. The mixture was then filtered and yellow precipitate was washed several times with diethyl ether and dried in vacuum to give 7.3 g of the product. ^{1}H NMR (400 MHz, DMSO-d_6, 22°C), 6.65- 5.45 (vbr, Cp+ Cp-dimer), 3.55 -1.7 (vbr, Cp Cp+ Cp-dimer). ^{29}Si NMR (99MHz, $CDCl_3$, 22 °C) δ: from –71.50 to –78.73 (br). MS (ESI TOF, CH_3CN): 1592.5 $[(T_{10})_3 –5Cp + 3H]^{2+}$, 1518 $[(T_{10})_4 –2Cp - H]^{3+}$, 1148.3 $[(T_{10})_3 –Cp - 2H]^{3+}$, 998 $[(T_{10})_3 – 8Cp + 5H]^{3+}$, 778 $[(T_{10})_2 –3H]^{3+}$.IR (KBr, cm^{-1}): 2954(w), 1650(w), 1594 (w), 1430 (m), 1089(w sh), 944(w), 737 (w) 714(m), 491(w). UV/ VIS (λ_{max}, nm): 208(br), 246(br).

Polymerisation of $[(CpC_3H_6)_8Si_8O_{12}]_n$ (11)

$Cp_{10}Si_{10}O_{12}$ (6.2 g, 0.048M) was stirred in THF (150ml) at ambient temperature for 2 h and then heated under reflux for 10 h. The solvent was removed in vacuum; the yellow-brown solid was washed several times with diethyl ether and dried in vacuum to give 5.3g of the product. ^{1}H NMR (400 MHz, DMSO-d_6, 22°C), δ: 6.61 -5.84 (ms, vbr, Cp+ Cp-dimer), 2.62 - 2.17 (ms, vbr, Cp+Cp-dimer), 1.87-0.90 (vbr m, CH_2). ^{29}Si NMR (99MHz, DMSO-d_6, 22 °C) δ: from -67.88 to -70.04 (br). IR (KBr, cm^{-1}):2976(w), 1704(w), 1446(w), 1379(w), 1260(w), 1142(w), 568(w).

Reaction of t-BuLi with FCPOSS T_8Cl. (12)

T_8Cl (0.17g) was dissolved in dry THF (20ml) and stirred under argon for 24 hours. BuLi in hexane (1ml) was slowly added drop wise and stirred overnight. The THF was remove under vacuum and the precipitate washed with dry hexane to remove un-reacted BuLi. The precipitate was dried under vacuum to (0.14g 82 **%** yield of the product). ^1H NMR (400 MHz, $CDCl_3$, 298K): δ 3.7 (brm,8H, CH_2 C) , 3.55(brm, CH_2) , 2.03 (CH_2), 1.88 (brm,8H, CH_2), 1.325 (brm,8H, CH_2) , 1.26 (CH_2) 1.04 (s,36H, CH_3), 0.89(brm,8H, CH_2 Si), 0.84 (brm,8H, CH_2 Si) . ^{13}C NMR (125MHz, $CDCl_3$, 295K): δ 46.57 (CH_2), 31.8 (CH_2), 31.1 (CH_2) 27.1 (CH_3) , 25.98 CH_2), 13.6(CH_2) MS ES (CH_3CN): 941.9 $[M\text{-}2Bu^t]^+$, 888.9 $[M\text{-}3Bu^t]^+$, 760 $[M\text{-}4Bu]^+$

6.3.2 Grignard synthesis compounds 13, 14 and 15

T_8Cl_8 (0.75g, 7.5x 10^{-5}m) mixed with NaI (0.15g) in dry acetone (20ml) was stirred under reflux for 24 hours. The solvent along with the un-reacted NaI was decanted off and the precipitate $T_8Cl_6I_2$ was washed with dry ether. 0.65g Yield 84%. Oven-dried magnesium turnings (0.00g 0.5.5 x 10^{-4} moles) and freshly distilled anhydrous diethyl ether (10 ml) were added to a flame dried 100 ml round-bottom flask, and stored under argon. $T_8Cl_6I_2$ (0.5g, 5.5x 10^{-5}m) mixed in dry Ether (20ml) was added slowly and the reaction began to initiate immediately with a precipitate clearly visible after five hours. The reaction was refluxed at 76°C for a further 24 hours. After reflux the solvent was removed under vacuum and the precipitate washed with DCM. After washing the precipitate was re-dissolved in dry ether and refluxed again for 24 hours .The sample was hydrolysed in air by drop wise addition of water (2ml). The precipitate was dried under vacuum to (0.140g,, 20% yield) the product. ^1H NMR (400 MHz, $CDCl_3$, 298K): δ 3.55 (t,8H, CH_2Cl) , 3.2 (t 2H, CH_2OH) , 1.9(brq ,CH_2) ,1.59 (s,OH), 0.8 (t, CH_2Si) .^{13}C NMR (125MHz, $CDCl_3$, 295K): δ46.66 (CH_2Cl), 25.8 (CH_2) ,12.9 (CH_2OH) , 8.9 (CH_2) ,0.5 (CH_2) .^{29}Si

NMR (99MHz, $CH_3C_6H_5$, 295K): δ –65.47 (vbr) MS ES (CH_3CN): 391[M-2(CH_2)3OH – 4$(CH_2)_3$I –2I] $^+$, 609[M-2I-$_{CH2}$]$^{++}$, 775 [M-2$(CH_2)_3$-2I – 2$(CH_2)_3$I]$^+$.. IR (KBr, cm^{-1}): 2954 (s2924 (s), 2854 (s), 1638 (m), 1459 (m), 1378 (w), 1260 (w); 1093 (w), 1022 (w), 799 (w), 587 (w), 482(s).

6.3.3 Reaction of T_8Cl_8 with $LiN[(Si(CH_3)_3)_2]$ (16)

Initially $HN[(Si(CH_3)_3)_2]$ (0.26g) was reacted with BuLi (1ml ,0.26mol THF(5 ml) under argon. Once the reaction was complete the solvent was removed under vacuum and the product - $LiN[(Si(CH_3)_3)_2]$ was stored under argon . T_8Cl_8 (0.15g; 1.4 x 10^{-4}mol) was dissolved in dry THF (25ml) and mixed with $LiN[(Si(CH_3)_3)_2]$ (0.19g , 1.15 x 10^{-5} mol) .The reaction was stirred for 36 hours. The solvent was removed under vacuum and the light brown precipitate washed with THF and hexane (0.258g , 78% yield) to give the product.^{1}H NMR (400 MHz, $CDCL_3$, 298K): δ 3.7 (t, 4H , CH_2) , 3.5 (t, 4H , CH_2-N) , 1.85 (brm,8H, CH_2), 1.33 (brm,8H, CH_2), 0.88 (brm,8H ,CH_2-Si), 0.82 (brm,8H, CH_2-Si) , 0.2 (s, 32H ,Si- CH_3) .^{13}C NMR (125MHz, CDCl3, 295K): δ 67(CH_2 -N) , 46 (CH_2) , 25.8 (CH_2) , 25.0 (CH_2) , 10 (CH_2) , 8.8 (CH_2) , 1.9 (CH_2) .^{29}Si NMR (99MHz, $CH_3C_6H_5$, 295K): δ –65.47 (sh m). –61(s). IR (KBr, cm-1): 2954 (s), 2854 (s), 1637 (m), 1459 (m), 1375 (w), (w); 1193 (str), 1022 (w), 799 (s), 587 (w), 482(s).

6.3.4 Reaction of T_8Cl_8 with lithiated ferrocene (17)

Ferrocene (1 g, 005 mol) THF (50 ml) were stirred under Argon and cooled to -10°C. t-BuLi (6.3 ml, 1.7 molar) was then added drop wise for 20 minutes. The mixture was stirred at -10°C for 1 hour and allowed to warm to room temperature. The solvent was removed by vacuum and the solid washed with

dry hexane (20ml) to remove any un-reacted BuLi,. The sample was dried under vacuum and dry THF (50ml) added. T_8Cl (0.7 g, 0.68mmol) was dissolved in THF, added to the prepared lithiated ferrocene and stirred for 12 hrs. The THF was removed by evaporation under vacuum, and diethyl ether added .A precipitate began to form, which was allowed to settle for 48 hrs. Both components were separated and dried under vacuum. Washing with diethyl ether, further purified the methanol soluble precipitate. After removing all solvent under vacuum, a light brown product was obtained in reasonable yield (0.17g, 89.5% Check it) .The ether layer was found to contain unreacted ferrocene. ^{1}H NMR (400 MHz, d. CH_3OH, 298K): δ 4.25 (t, 5H, Cp),4.18 (4H,Cp-C), 3.49 (t, 2H, CH_2), 3.2 (t,2H, CH_2) 1.98(qui,2H, CH_2), 1.87 (brm, 2H, CH_2), 1.3 (brm,2H, CH_2 -Si), 1.17 (qui, 2H, CH_2 -Si).

IR (KBr, cm^{-1}): 2953 (w), 2924 (w), 2854 (w), 1620 (m), 1460 (m), 1377 (w), 1308 (w), 1263 (w), 1211 (w), 1174 (w), 1107 (m), 1306 (m), 862 (w), 820 (w).

MS ES (CH3CN): 438[M-3(CH_2Fc)- CH_2]$^{++}$,761[M- CH_2Cl] $^{++}$.

6.3.5 Reaction of lithiated C_{60} with T_8Cl. (18)

C_{60} (.003g, $4x10^{-6}$ mol) mixed with BuLi (1ml) in THF (20ml) and stirred for 48 hours and allowed to settle . The solvent was removed under vacuum and the precipitate washed with two aliquots of dry hexane to remove excess BuLi . T_8Cl_8 (0.043 g) was dissolved in dry THF and added drop wise and stirred to the lithiated C_{60} under Argon. A dark brown precipitate formed after 24 hours. The solvent was removed and the precipitate washed with THF and hexane and dried in vacuum to give the product (0.028 g , 65 % yield).^{1}H NMR (400 MHz, $CDCl_3$, 298K): δ 3.5(t, CH_2), 3.4 (brm, CH_2) , 1.7(brm, CH_2), 1.4(brm, CH_2), 1.03 (t, CH_2) 0.8 (brm, CH_2 -Si), 0.3 (t, CH_3).^{13}C NMR (125MHz, $CDCl_3$, 295K): 145 (brm, C_{60}), 137(CH_2) , 67.2 (CH_2), 64.1(CH_2), 48 (brm, CH_2), 21(brm, CH_2), 14 (CH_2), 0.9 (CH_3).^{29}Si NMR (99MHz, $CH_3C_6H_5$, 295K): δ –65.47(vbr). MS ES (CH_3CN): 2386 [M-Bu^+- CH_2]$^+$, 1170 [M-2Bu^+]$^+$, 781[M-{(CH_2)$_3$-C_{60}}-Bu^+-(CH_2)$_3$Cl]$^{++}$.

6.3.6 Reaction C_{60} with $PhSiCl_3$ using BTMA catalyst

C_{60} (0.015g, $2.12x10^{-5}$mol) was dissolved in toluene (30ml) and Phenyltrichlorosilane (0.034g, $8.035x10^{-7}$mol) was added drop-wise under argon. The resulting mixture was shaken with water (10ml) until hydrolysis was complete. After removing the acidic aqueous layer and washing with water (20ml), 40% benzyltrimethylammonium hydroxide solution (0.05ml, $1.3x10^{-4}$m) was added. The mixture was then refluxed for 4 hr., allowed to stand for 4 days, refluxed for 24 hr., and then cooled and filtered. The resulting dark brown particles were found to be soluble in DMSO. The product was precipitated out from the DMSO by addition of diethyl ether. The light brown precipitate was left in contact with air for two weeks and was found to have complete solubility in water. The product was analysed using the Z scan technique and was found to give a third order non-linear optical response, indicating the presence of fullerene. ^{1}H NMR (400 MHz, $CDCl_3$, 298K): δ 7.4(brm, 5H,Ph); 4.49 (s, 3H, CH_3). ^{13}C NMR (125 MHz, $CDCl_3$, 295K): δ 133 (C_{60}), 130 (ortho-Ph), 129 (meta -Ph), 127 (para-Ph), 115(ipso-Ph), 51 (CH_3).

6.4 Experimental for Chapter 4

6.4.1 Reaction of TiO_2 nanorods and $(CH_2=CHCH_2)Si(OEt)_3$

6.4.2 TiO_2 nanorods (.06g) were placed under vacuum for one hour and then flushed with argon. Dry THF was then added via canula under argon .The resultant mixture was then stirred vigorously for 24 hours. $(CH_2=CHCH_2)$ $Si(OEt)_3$ (0.2ml, $9x10^{-4}$mol) was then added drop-wise using an insulin syringe. The mixture was stirred for 48 hours. Thereafter the solvent was removed under vacuum and the precipitate was washed with dry ether to remove any un-reacted Siloxane. (0.054g, 90% Yield)

6.4.3 Reaction of TiO_2 nanorods and $(C_3H_7)SiCl_3$

This reaction was prepared analogously to reaction 6.4.2 above using TiO_2 (0.32g) and $(C_3H_7)SiCl_3$ (0.15ml, $6.5x10^{-4}$ mol) with yield of (0.023g, 72%).

6.4.4 Reaction of TiO_2 nanorods and $C_6H_{13}SiCl_3$

This reaction was prepared analogously to reaction 6.4.2 above using TiO_2 (0.037g) and $C_6H_{13}SiCl_3$ (1.5 ml, $7.6x10^{-3}$ mol) with good yield (0.0285g ,76%).

6.4.5 Reaction of TiO_2 nanorods and silane $(C_{12}H_{25})SiCl_3$

This reaction was prepared analogously to reaction 6.5.1 above using TiO_2 (0.34μg) and silane $(C_{12}H_{25})SiCl_3$ (1.5 ml,$5.04x10^{-3}$ mol) with good yield (.0285g, 76%)

6.4.6 Sedimentation studies of functionalised TiO_2 with polystyrene

Sedimentation studies were carried out in THF for all functionalised TiO_2 nanorods without and with polystyrene. TiO_2 nanorods –of known weight - were placed in a sample tube, THF (10 mls), was added and sonicated using the sonic tip for 5 min. From this solution a 1 cm^3 cuvette was filled immediately after sonication. The cuvette was sealed with a cap and the cap was further sealed with para-film M ™ taking care not to obscure where the light emitters would transmit through. This was then immediately placed in the sedimentation machine and test time of 24 hrs was run with the frequency of the light emitting set to every 10 sec for the first hour and then this was changed to once every 30 sec for the remaining 23 hrs. The procedure was performed similarly with an addition of controlled amounts of polystyrene.

6.4.7 Preparation of polymer composite films

In all studies the Polystyrene (Mw = 280,000), obtained from Sigma-Aldrich was used as supplied. THF was used as the solvent in all cases. A stock

composite solution was made up by adding a mass fraction (1wt.-%), of the relevant functionalised Titania powder to the polymer solution. The solution was the sonicated for two hours in a sonic bath. Thereafter the samples were sonicated using a sonic tip (600W, 20%). A range of mass fractions was fabricated by blending this stock solution of pure polystyrene in the required concentrations.1ml of each solution was carefully syringed onto polished Teflon discs of 4cm diameter. The solvent was allowed to evaporate in a closed fumehood for two- four hours. The films were then peeled off the discs and cut into strips of 3mm x 10mm each, which were measured using a digital callipers. The average thickness was 0.3mm, which was measured using a low torque digital micrometer.

6.4.8 Mechanical testing of films

Tensile testing of the polymer films was carried out using a Zwick Z100 tensile tester. A 100 N load cell and a cross head speed of 0.5 mm/min were used to obtain stress strain curves. The diameter and thickness of each strip was measured before the strip was placed into the Zwick machine for mechanical testing. The measurements for diameter and thickness were inputted into the machine. The machine then stretched the sample until the sample broke.
In this way the Young's modulus and the tensile strength of the film can be measured. The process was repeated approximately three times for each film so an average strength could be measured. Each of the polymer-titania composites had their tensile strengths measured against that of the tensile strength of the initial pure polymer.

6.5 Experimental for Chapter 5

6.5.1 Reaction of multi-walled nanotubes and $(CH_2=CHCH_2)Si(OEt)_3$

Nanocyl multi-walled nanotubes were obtained from Nanocyl S.A® (0.35μg) were dried under vacuum for one hour and then placed under inert atmosphere .Dry THF was then added via canula under Argon .The resultant mixture was then stirred vigorously for 24 hours. BuLi in hexane (1ml?, mol?) was added to the mixture at 0°C and it was stirred under argon for 48 hrs. Then

the mixture was left for precipitation for 24 hrs. After settling the THF was decanted and the mixture was washed twice with dry hexane and once with dry diethyl ether, to remove any un-reacted BuLi Then new portion of dry THF was added to the mixture. (CH_2=$CHCH_2$) $Si(OEt)_3$ (0.2ml, $9x10^{-4}$mol) was then added drop wise via insulin syringe. The reaction was stirred for 76 hours. Thereafter the solvent was removed under vacuum and the dry precipitate washed with dry THF to remove any un-reacted siloxane. (0.29g ,85% yield). The product was characterised using IR, TGA and DSC. IR (KBr, cm^{-1}): 2924 (s), 2857 (s), 1651 (m), 1460 (s), 1377 (s), 1311 (w), 1154 (m), 1085 (w), 1021 (w), 945 (w), 890 (w), 722 (m), 427 (s).

6.5.2 Manufacture and Purification of carbon nanotubes

The MWNT soot used in this experiment was produced using the arc-discharge method in the physics department laboratory. The host polymer was poly (m-phenylenevinylene-co-2,5-dioctyloxy-p-phenylenevinylene)(PPV) produced using the Horner polycondensation method and was again obtained from the physics department. PPV and toluene were mixed to give a 16.7g/L solution. This solution was sonicated for 1 min using a high power sonic tip and then approximately 20mg of MWNTs soot from the same batch were added. The resulting composite solution was further sonicated for 1 min using the sonic tip, and then for 2 hours in a low power (60W) sonic bath to ensure good dispersal and homogeneity. The solution was then left to settle for 48 hours to allow any impurities to sediment out. For each sample the resulting suspension was separated from the sediment by decantation.

The MWNTs were retrieved from the polymer using Buckner filtration using a Teflon filter with a pore size of 0.45 microns over a sintered glass frit.10ml of the decanted solution was mixed thoroughly with toluene (250ml) and sonicated for 1 minute at low power (20%). The deep green/blue solution was then quickly filtered leaving a black residue of MWNTs on the filter paper and creating a yellow filtrate -indicating the presence of polymer and the absence of MWNTs. The residual PPV was then removed from the filtrate by repeated washing with toluene, until the emerging solvent showed a complete lack of yellow discolouring. The purified MWNT were then sonicated at low power

into ether, poured into a large Petri dish and allowed to dry in air. The dried MWNTs were then scraped off the dish, weighed and then were ready for synthesis. TEM was then used to check the purity.

6.5.3 Synthesis of lithiated MWNT's

Dry annealed MWNTs (1.5 mg) were sonicated under argon for 10 mins in dry THF, cooled to-10°C and n- BuLi (2 ml, 1.6 molar) was added drop wise over 20 mins. The mixture was stirred for 36h hours. The suspension was then allowed to settle and the THF solution was removed by canula filtration and the precipitate was washed with dry THF, (2x25 ml,) and then dry hexane, 2x25 ml. The sample was dried under vacuum for 24 hr. Lithiated nanotubes were stored in dry THF under Ar for further use.

6.5.4 Reaction of T_8Cl, with lithiated MWNTs

Lithiated MWNTs (2.5 mg) were treated with trichlorotriethoxysiloxane (0.01 g, 0.010 mmol) in THF and stirred for 48 hrs. The THF was decanted off and the nanotubes dried under vacuum. The product was characterised using IR, SEM and TEM. IR (KBr, cm^{-1}): 2924 (s), 2857 (s), 1651 (m), 1460 (s), 1377 (s), 1311 (w), 1154 (m), 1085 (w), 1021 (w), 945 (w), 890 (w), 722 (m), 427 (s).

6.5.5 Reaction of T_8NH_2 with MWNTs

MWNT (2 mg) in ethanol (15 ml) were sonicated for 15 minutes. A solution of T_8NH_2 (50 mg) in water (15 ml) was added and the mixture was stirred under UV radiation (254 nm) for 2 hours. The mixture was then left for precipitation for 12 hours. The solution was decanted from the precipitate. The product was washed with ethanol and dried in vacuum.

6.5.6 Reaction of lithiated MWNTs with (Chloropropyl)triethoxysilane.

Freshly prepared lithiated MWNTs ( ) in THF (20ml) were treated with (3-Chloropropyl)triethoxysilane (g?, mol?) under intensive stirring at 0°C. The mixture was stirred for 24 hrs. Then it was left for precipitation for another 24

hrs. THF solution was then decanted. The mixture was washed with dry THF. The solution hydrolysed by addition of THF and ammonium carbonate solution (5g.) with water (10 ml). The hydrolysed mixture was stirred for 72 hours, and then left for precipitation. After settling the THF layer was carefully decanted off. The precipitate was washed 3 times with distilled water followed by washing with diethyl ether and dried in vacuum for 1 day. The product was characterised using IR, SEM and TEM. IR (KBr, cm^{-1}): 2924 (s), 2857 (s), 1651 (m), 1460 (s), 1377 (s), 1311 (w), 1154 (m), 1085 (w), 1021 (w), 945 (w), 890 (w), 722 (m), 427 (s).

6.6 References

1 . Barker P.J., Davies A.G., Henriquez R, Nedelec J-Y. J. Chem. Soc. Perkin Trans. II. **1982,** 745 - 750Čermák J., Kvíčalová M, Blechta V., Čapka M., Bastl Z. J. Organomet. Chem. **1996**,50, 77 - 84

Chapter 7

Conclusions and future work

Chapter 7

7.1 Conclusions

We have demonstrated that chloride and amino functionalised octasilsesquioxanes can be produced at exceptionally higher yields compared to the literature. This was essentially achieved by the simple introduction of the heating the reaction mixture under reflux. This simple modification also allowed the preparation of both the chloride allyl and thiol octasilsesquioxanes quickly and with much higher yields. Octa(allyl)silsesquioxane was synthesised in high yield and very high purity via acid catalysed hydrolysis. It was found that base catalysed hydrolysis of the allyltriethoxysilane results in the formation of highly insoluble decallylsilsesquioxanes (T_{10}). Several new Cp-functionalized POSS have been prepared. This was achieved by using the sol-gel condensation process. This technique revealed that Cp-Si bond is very sensitive to acidic media and the process should be performed in the presence of bases such ammonium carbonate. These new POSS compounds could also be further modified into different metal-containing products by metallation of the free C_5H_5-groups. This can be a fundamentally new approach for the preparation of new controlled pore size materials.

Cp-functionalized POSS have been shown to be promising precursors for preparation on novel polymeric and oligomeric derivatives using Diels-Alder condensation reaction. This approach allowed preparing new nanoparticulate and nanoporous materials of controlled pore size. This could be a very promising method for the preparation of new controlled pore size metal-containing materials. Reactions of T_8Cl POSS with *t*-BuLi Li $N[(Si(CH_3)_3)_2]$ and lithiated ferrocene resulted in tetra *t*-Bu- $N[(Si(CH_3)_3)_2]$ - and ferrocenyl-substituted POSS derivatives respectively. In contrast reactions with NaI (trashalogenation) and lithiated fullerene resulted only in di-substituted species. Thus despite eight equivalents or an excess of the reagents was used to treat T_8Cl POSS, full substitution of all eight chlorine atoms have never been achieved. We believe that full substitution is impossible for two main reasons: sterical hinderance and limited solubility of the substituted species. The C_{60} –

siloxane composite demonstrated a third order non-linear optical response. This material might find a potential application in non- linear optical devices.

Titania nanorods have been successfully functionalized using appropriate triethoxy or trichloro- silane derivatives. Allyl- propyl-, hexyl- and dodecyl-functionalised TiO_2 nanorods composites have been prepared and characterized. These materials have shown an enhanced solubility in THF and even greater solubility in THF solution of polystyrene. It was observed that solubility of TiO_2 nanorods in THF increases with an increase of the alkyl chain length.

Further developments of the preparation of MWNTs using the Kratschmer Huffmann generator have been performed in this work. The conditions for synthesis of nanotubes were re-examined and optimised. The nanotubes were purified by a selection of popular purification techniques. The preferred purification technique was that using the polymer PPV. MWNTS were also functionalised with allyl-, propyl-, hexyl- and dodecyl- functionalities using a new organometallic approach. In this approach MWNTs have been lithiated with BuLi and then the lithiated nanotubes were treated with an appropriate triethoxy- or trichloro- silane derivatives. Similarly to functionalised TiO_2 nanorods alkyl functionalized carbon nanotubes demonstrated an increased solubility in THF and in THF solution of polystyrene. Again the solubility of nanotubes in THF increased with an increase of the alkyl chain length.

Both alkyl functionalised TiO_2 nanorods and carbon nanotubes were added to polystyrene in order to investigate their potential for this polymer reinforcement. We have found that the mechanical properties of alkyl-functionalised TiO_2 nanorods - or carbon nanotube - polymer composites strongly depend on the length of the alkyl chain and percentage of TiO_2 nanorods or nanotubes. The 1 % addition of functionalized TiO_2 nanorods or carbon nanotubes resulted in very significant increase in tensile strength, toughness. However, the concentrations of greater than one volume percent of these would not show such a good degree of reinforcement as lower 1 % concentration. The reason for this is that the nanorods and nanotubes form aggregates which do not allow for adequate or reasonable stress transfer and also add defects to the composite material. It was also found that the greatest enhancement in tensile strength and toughness was achieved for hexyl-functionalised TiO_2 nanorods. Hexyl chain provides the strongest interaction

between the polymer matrix and TiO_2 surface resulting in the most efficient stress-stain transfer. Longer chains such as dodecyl- are partially aligned along the length of the nanorods and do not provide so strong interaction with the polymer matrix.

In overall this project should contribute to the development of organometallic chemistry of POSS, TiO_2 and carbon nanotubes and application of novel nanotube derivatives for polymer composite reinforcement.

7.2 Future work

Chemistry and applications of functionalised POSS have a great potential. POSS are nanosized (1-2 nm) structures with controlled properties and dimensions. They can be potentially used as building blocks for new functional materials as nano-sized catalysts and drug carriers and as components for self-organising nanostructures.

The work involving Cp-functionalised POSS molecules could be expanded very easily. They could serve as new multifunctional ligands in organometallic chemistry. Cp-functionality can be easily metalated using alkali metals or BuLi. Then these derivatives can be reacted with various transition metals and main group elements giving new polymetallic structures with various properties. These compounds might find a potential application in catalysis, separation technologies and molecular electronics. The allyl functionalised POSS must also have a very rich organometallic chemistry and a broad range of potential applications.

Functionaslised POSS can also be used as building blocks for new nanostructured materials of controlled dimensions. They can be cross-linked into 3D assemblies by different chemical or physical processes. They also can be mixed with various metal or metal oxide nanoparticles to form ordered 1D or 2D arrays.

Functionalised TiO_2 nanorods seem to have a great potential for nanotechnology. Properties and applications of these nanocomposites have not still been explored. We have shown that functionalised TiO_2 nanorods can significantly reinforce polystyrene. These materials and approaches can also be

used for reinforcement of many other polymers. In addition TiO_2 nanorods pose insulating and semiconducting properties that might be important for nanoelectronics.

Finally functionalised carbon nanotubes have already been envisaged as components for nanoelectronics and additives for plastic reinforcement. Our metallorganic approaches have expanded chemistry and modification routes for nanotube functionalisation. This should allow preparation of new types of nanocomposite materials based on carbon nanotubes and functionalised POSS. These materials could have a broad range of applications in nanotechnology and materials science.

Appendix I

In order to fully understand the sedimentation of non-soluble phases in various dispersions we need to derive an equation to describe the local concentration of sedimenting particles as a function of time to do this we consider the sedimentation of solid particles under the following assumptions[1, 2, 3]. Firstly, the solid particles are small with respect to the sedimentation vessel and all have the same density, secondly, the constituents of the solution are incompressible, and finally that there is no mass transfer between the solid and the fluid phases during sedimentation. Under these circumstances the dynamic process of a particulate system can be described by field variables that must obey to the two local conservation equations for mass and linear momentum i.e.

$$\frac{\partial C}{\partial t} + \nabla(Cv_s) = 0 \qquad \text{Equation 1.}$$

$$\rho_S \frac{\partial}{\partial t}\left(Cv_s\right) + \rho_S \nabla\left(Cv_S^2\right) = -\nabla(Cp_f) - C\rho_s g + \beta\nabla C \qquad \text{Equation 2.}$$

Where C is the local concentration of the sedimenting phase under study, ρ_s is the solid component density; v_s is the velocity of the solid component; p_f is the fluid pressure, g is the acceleration due to gravity, β is related to the solid fluid interaction force and has the dimensions of a pressure. In addition we note that the fluid pressure obeys.

$$-\frac{\partial p_f}{\partial z} = \rho_l g \,. \qquad \text{Equation 3}$$

Solution of the above equations gives

$$\frac{\partial C}{\partial t} = \frac{-Cg\left(\rho_s - \rho_l\right)v_s - \rho_s C v_s \, dv_s/dt}{\left(\beta - p_f\right)} \qquad \text{Equation 4}$$

In order to eliminate v_s and dv_s/dt we need to consider Newton's second law. The forces acting on a single particle are gravity and the viscous drag force. Thus we can write

$$m\frac{dv_S}{dt} = mgb - fv_S$$ Equation 5

Where m is the mass per sedimentation particle, b is the buoyancy correction factor ($b=1-\rho_l/\rho_s$) and f is the frictional co-efficient as given by Stokes law.

Solving this equation gives

$$v_S = \frac{mgb}{f}\left(1 - e^{-\frac{f}{m}t}\right)$$ Equation 6

And as

$$\frac{dv_S}{dt} = gbe^{-\frac{f}{m}t}$$ Equation 7

We can estimate m and f from the known properties of the system. Using these quantities we can calculate, for this system, that the exponential term decays over the order of seconds. As this is a very short time compared to the timescale of the sedimentation experiment, the exponentials can be neglected. Integration of equation 4 then gives

$$C = C_n \exp\left[-\frac{g^2(\rho_S - \rho_l)mb}{f(\beta - p_f)}t\right] = C_n e^{-t/\tau}$$ Equation 8

Where C_n is a constant and

$$\tau = \frac{f(\beta - p_f)}{g^2(\rho_S - \rho_l)mb}$$

For spherical particles, $f = 6\pi\eta a$, where η is the solvent viscosity, a is the particle radius and $m = 4\rho_s\pi a^3/3$. This allows us to express the time constant as

$$\tau = \frac{9\eta(\beta - p_f)}{4g^2(\rho_S - \rho_l)^2 a^2}$$ Equation 9

However, in the case of cylindrical particles, the frictional co-efficient tends to be higher than for the spherical case. For a cylindrical particle of length, *l*, and radius *r*, the viscous drag is given by, $f = 6K\pi\eta a$, where *K* is a function of *l*/ *r* [4]. K tends to increase with aspect ratio, approaching 5 for aspect ratios of 1000. In addition

$m = \rho_s \pi r^2 l$ and $a = (3r^2 l/4)^{1/3}$. Equation 10

Thus the time constant for cylindrical particles is

$$\tau = \frac{6K\eta(\beta - p_f)3^{1/3}}{g^2(\rho_S - \rho_l)^2(2r^2 l)^{2/3}}$$ Equation 11

In a real dispersion there may be more than one distinct sedimenting phases. Each phase will be characterised by its own time constant and by the partial concentration of that phase. In addition there may be a soluble component. Thus the local time dependent concentration of dispersion with *n* insoluble phases and one soluble phase is described by the equation

$$C(t) = C_0 + \sum_n C_n e^{-t/\tau_n}$$ Equation 12

Where C_0 is the concentration of the soluble phase. In addition conservation of mass dictates that the total concentration, C_{Tot}, is given therefore given by

$$C_{Tot} = C_0 + \sum_n C_n$$ Equation 13

References

1. Garrido, F.; Concha,R.; Burger, R . *Int. J. Miner. Process.* **2003,** *72,* 57-74.

2. PW Atkins, Physical Chemistry, Fourth Edition, p961, Oxford University Press, **1992.**

3. M. Tory. ("Sedimentation of small particles in a viscous fluid", Southampton: 4. Computational Mechanics, **1996**.)

Huang Q.;Gao.L. *Chem. Lett.* **2003,** *32*,638-642.